National Library of Canada
Acquisitions and Bibliographic Services Branch
395 Wellington Street
Ottawa, Ontario
K1A 0N4

Bibliothèque nationale du Canada
Direction des acquisitions et des services bibliographiques
395, rue Wellington
Ottawa (Ontario)
K1A 0N4

Your file Votre référence

Our file Notre référence

NOTICE

The quality of this microform is heavily dependent upon the quality of the original thesis submitted for microfilming. Every effort has been made to ensure the highest quality of reproduction possible.

If pages are missing, contact the university which granted the degree.

Some pages may have indistinct print especially if the original pages were typed with a poor typewriter ribbon or if the university sent us an inferior photocopy.

AVIS

La qualité de cette microforme dépend grandement de la qualité de la thèse soumise au microfilmage. Nous avons tout fait pour assurer une qualité supérieure de reproduction.

S'il manque des pages, veuillez communiquer avec l'université qui a conféré le grade.

La qualité d'impression de certaines pages peut laisser à désirer, surtout si les pages originales ont été dactylographiées à l'aide d'un ruban usé ou si l'université nous a fait parvenir une photocopie de qualité inférieure.

Canada

On the Numerical Continuation of Nonhyperbolic Periodic Solutions in Ordinary Differential Equations

With Applications to a Two-Level Laser Model

A Ph.D. Thesis
submitted to the School of Graduate Studies and Research
in partial fulfillment of the requirements for
the degree of Doctor of Philosophy in Mathematics [1]

Klaus-Georg Nolte

Department of Mathematics
University of Ottawa
Ottawa, Ontario, Canada K1N 6N5

December 13, 1993

[1]The Ph.D. Program is a joint program with Carleton University, administered by the Ottawa-Carleton Institute of Mathematics and Statistics

ISBN 0-315-95963-0

UNIVERSITÉ D'OTTAWA
UNIVERSITY OF OTTAWA

Abstract

Based upon the combination of the pseudo-arclength continuation method, the Poincaré map and various defining equations, several systems of equations are constructed that trace nonhyperbolic periodic solutions of autonomous ordinary differential equations. A system that equally well continues a saddle-node, a period-doubling and a secondary Hopf bifurcation across a two-dimensional parameter space is presented first. Additional formulae are provided which, along with the continuation, completely characterize these codimension-one bifurcations and therefore lead to the detection of certain codimension-two bifurcations, in particular Takens–Bogdanov bifurcations, cusps, isola formation points or perturbed bifurcation points and degenerate period-doublings and degenerate secondary Hopf bifurcations. Secondly, systems are developed which continue these codimension-two bifurcations across a three-dimensional parameter space, thereby detecting certain codimension-three bifurcations of periodic orbits. The application of these ideas to a five-dimensional system describing a two-level laser leads to a variety of interesting bifurcations. A winged cusp, a swallow tail, two kinds of degenerate Takens–Bogdanov points and isola formation points for different codimension-one loops are found. Also, maximal bounds in a three-dimensional parameter domain for the existence of certain periodic solutions are given. Moreover, the coexistence of several attractors of the same and/or different topological structure is demonstrated. Finally, attractive tori are found in a systematic way and briefly discussed.

Statement of Originality

Below is a list of work I carried out in the framework of this thesis, which, to the best of my knowledge, constitutes an original contribution to the advancement of science:

1. implementations of computer algorithms that continue certain codimension-two bifurcations of periodic solutions in systems of ordinary differential equations,
2. numerical bifurcation analysis to detect and characterize certain codimension-three bifurcations of periodic solutions in systems of ordinary differential equations,
3. systematic search for attractive tori appearing in supercritical secondary Hopf bifurcations,
4. applications of these codes to a two-level laser model with detuning.

Für meine Eltern,

Werner und Anneliese

Acknowledgements

Well, after having spent countless hours crunching numbers in the computer room of the Department of Mathematics, after having produced an infinite amount of data, after having processed an endless pile of paper, and finally, after having written the introduction, I think it is about time to sit back, relax and say "Thanks!".

Without any doubt, the first one goes to my parents, Anneliese and Werner. If they had not made it possible for me to attend Secondary School and to receive higher education, if they had not supported me through my previous studies at Cologne University and at Bonn University — this thesis would not have been written.

Next, there is Privat Dozent Dr. Herbert Arndt of the Applied Mathematics Department at the University of Bonn (and, indirectly, Edward Lorenz). His suggested Diplom thesis "Über Attraktoren im Lorenz System" really got me into mathematics and encouraged me to go further.

At this point, I must mention the Stiftung Volkswagen in Hannover, Germany. Its generous two-year scholarship made it possible for me to continue my work at the University of Ottawa.

I am also most grateful to my supervising Professors Rémi Vaillancourt and Ivan L'Heureux. They gave me enough freedom to continue(!) research along a fascinating branch(!) of mathematics — continuation methods — and they patiently tried to bring physics a little closer to me. In addition, I am very much obliged to Rémi for introducing me to LaTeX, for letting me use his equipment to typeset this work and for incorporating all the bitmap and postcript figures. Ivan, on the other hand, deserves a special thank for reading my preliminary drafts, for pointing out numerous typos and for his suggestions regarding the fine structure of this thesis. Moreover, this thesis was partially supported by their NSERC grants OGP7691 and OGPIN029. Thanks again!

The government of Ontario had its impact too. It would have been much harder

to finish this thesis without the one-year OGS scholarship it granted to me.

Then there are all the nice people at the Department of Mathematics of the University of Ottawa. They all contributed, in one way or another, to a pleasant stay in Ottawa and the completion of this thesis.

I would also like to thank Profs. Eusebius Doedel of Concordia University in Canada, Rüdiger Seydel of Universität Ulm in Germany, Dirk Roose of Katholieke Universiteit Leuven in Belgium, and John Guckenheimer of Cornell University in the United States. They all spent a little but valuable time for brief yet helpful discussions.

Finally, a big thank you to my wife, Bettina and to my little daughter, Lisa. If they had not come to live with me in Ottawa — who knows? And I know, I should have spent more time on the playground! Thanks, Bettina and Lisa!

Contents

Chapter 1

Introduction

1.1 We Live in a Dynamic World?

Yes, we do! And there could not be any doubt about it. Peace and war, growth and birth, traffic and time, waves and weather, motion and machines, death and diseases,..., we constantly experience that, indeed, "we live in a dynamic world" [65].

1.1.1 Booming Nonlinear Dynamics

In the past years the theory of chaos and nonlinear dynamics in general has received a lot of attention throughout the various sciences.

Numerous new books at the introductory, advanced and research level, as well as new editions of previous releases, prove the enormous popularity of this theory. From the more mathematical point of view, we only mention [1], [2], [3], [14], [19], [18], [24], [26], [40], [48], [56], [66], [70], [60], [79], [80], [84], [98], [102], [111], [119], [128], [139], [143], [147], [163], [172], [177], [178], [186]. From the more applied side, we merely list [8], [17], [63], [95], [112], [114], [132], [138], [142], [162] [183]. A little bit more "search" would easily extend these lists to the hundreds of titles.

In addition, new journals and book series have been released, the primary task of which is the publication of scientific work related to chaos and nonlinear dynamics. Again, we only indicate the tip of an iceberg by mentioning a few of them: *International Journal of Bifurcation and Chaos in Applied Science and Engineering, Chaos, Journal of Nonlinear Science, Chaos Solitons & Fractals, Nonlinearity, Nonlinear Science Today, Physica D, Cambridge Nonlinear Science Series, Advanced Series in Nonlinear Dynamics.*

The number of papers, articles, reports seems to approach infinity. In [13] alone, one finds more than 2200 references! It truly looks like a "nonlinear" (exponential) publicatgion growth.

Furthermore, this huge interest has also been demonstrated by the increasing number of related conferences, seminars, workshops and meetings with corresponding proceedings. Additionally, several "Centres for Nonlinear Dynamics" and "Dynamical Systems Groups" have been established at universities and research centres throughout the world.

"Bilder der Wissenschaften" ($\approx$ "The Nature of Things") in German TV and the popular German magazines "GEO" ($\approx$ "National Geographic Magazine") and "Spektrum der Wissenschaften" ($\approx$ "Scientific American") devoted special issues to this topic as well.

Furthermore, there are experiments to introduce parts of this theory at the secondary-school level [99] and I, myself, taught a one-week "minicourse" on chaos and fractals to high-school students.

Indeed, chaos and nonlinear dynamics seem to have become a new science [58]. No wonder that periodic solutions of nonlinear dynamical systems, being an essential ingredient of this theory, profit from this boom.

A simple but nevertheless essential reason for all these activities undoubtably lies hidden in the simple quotes "we live in a dynamic world" [65] and "this world is nonlinear" [58].

1.1.2 Dynamics and Numerics

"The Dynamics of Numerics and the Numerics of Dynamics" was the title of a conference held at the University of Bath from July 31st to August 2nd 1990; this title clearly emphasizes the interplay between numerical methods and nonlinear phenomena. In fact, it is fair to say that chaos owes much of its popularity to advances in computing technology. More powerful computers let us attack more complex problems; formulae manipulating languages replace extremely tedious and manually unmanageable algebraic simplifications, arithmetics and transformations and advanced graphical displays provide insight into very complicated structures, patterns, and solutions of nonlinear equations. Besides that, user-friendly softwares for cheaper, yet better, microcomputers enable a growing group of users to pursuie computer-aided analyses of their own dynamical system. Here, we do not even mention all the soft-

ware that is related to "Julia sets", "Fatou sets", and "Mandelbrot sets", or simply to "fractals" in general.

Moreover, many of the results and successes related to nonlinear dynamics would not have been achieved without advances in the numerical methods themselves, as frequently only a combined analytical and numerical approach has led to progress [101], [100]. This refers, in particular, to periodic solutions. Simply put, these results and successes come with just the right amount of theory so as to leave interesting questions to be answered numerically.

"Real life" problems are almost always too sophisticated to allow deep analytical insight. Consider again periodic solutions of nonlinear dynamical systems. Even though, in the two-dimensional case, the Poincaré–Bendixson theorem [7], [27], [66] provides an existence proof in certain cases, the question of existence and uniqueness in the general case remains open. Hilbert's 16th problem has not been solved analytically — but, in [93], was approached numerically! Moreover, the search for periodic solutions can be arbitrarily difficult if higher dimensions, "strongly nonlinear right-hand sides", coupled partial differential equations, stochastic forcing, delayed arguments, dependencies on parameters, discontinuous vector fields, ..., are involved. And certainly, Hopf's theorem [7], [66], [186], [81], would not be that renowned, if numerically we were not able to compute eigenvalues, to integrate differential equations, to iterate Newton's method, and graphically to display, that is to "see", a periodic solution.

1.2 Motivation

Periodic solutions are important in several respects. It has been shown, for instance, that transitions from stationary or periodic behaviour to quasiperiodic or chaotic motion frequently follow certain general patterns,all of which presume periodic solutions. Period-doubling cascades obeying Feigenbaum's law, homoclinic and heteroclinic connections, different types of intermittency, Hopf–Landau and Ruelle–Takens pictures — periodic solutions are throughout essential parts of these scenarios, see [18]. Only to include a very recent paper dealing with this topic we mention [59]. A complete understanding of these mechanisms could possibly explain transitions from a periodic to a chaotic heartbeat [112] or from laminar to turbulent flows and flames [181], [82], [121]. The meaning is obvious!

Furthermore, periodic solutions have been found as building blocks of "strange attractors" [173], [133]. Once again, it is their existence, uniqueness and topological structure that can help shed light onto these exceedingly complicated structures.

Attractive periodic solutions are important since they enable us to predict the time asymptotic behaviour of a model. One needs only think of the weather or population oscillations or economic quantities. On the contrary, unstable periodic solutions are practically unobservable. But they can gain stability and become attractive when "continued" with respect to the parameters of the model. Since these parameters are frequently based upon measurements (and hence are inaccurate) or may be known only approximately, or, even worse, must be chosen completely at random, it is important to know how much one can modify these parameters without changing the qualitative structure of the solutions (or, vice versa, how much one has to "perturb" them to observe qualitatively different solution behaviour). This important question occurs in all areas of science:

1. from glycolytic models [106] to railway dynamics [148],
2. from optical systems [32], [33], [54], [55], [51] to computer graphics [73],
3. from reaction-diffusion systems [34] to robotics [113],
4. from acoustics [110] to the rolling motions of ships [53],
5. from Taylor vortices [125] to the human brain [142],
6. ....

1.3 Goals and Mathematical Tools

1.3.1 Goals of this Thesis

One aim of this thesis is to answer the above question in the case of periodic solutions of autonomous ordinary differential equations. Ultimately, we want to compute boundary curves or manifolds in higher dimensional parameter space which characterize a given input periodic orbit in terms of existence, stability and type of (local) bifurcation. Since these problems cannot be solved analytically, we shall develop several algorithms that continue codimension-one and codimension-two bifurcations of periodic solutions across a two-dimensional, respectively three-dimensional, parameter

space. Explicitly, we shall follow saddle-nodes, period-doublings and secondary Hopf bifurcations but also cusps, transcritical bifurcation points, isola formation points and Takens–Bogdanov bifurcations, and, finally, degenerate period-doublings and secondary Hopf bifurcations. We emphasize that we refer here to nontrivial periodic solutions which do not bifurcate off from equilibria branches in a Hopf bifurcation.

Then, applying these methods to a two-level laser model proposed in [54], [55], we also aim to extend these authors' bifurcation results from equilibria to periodic solutions. In particular, we shall systematically search for (and find!) supercritical secondary Hopf bifurcations leading to attractive invariant curves. Furthermore, we want to detect certain codimension-three bifurcations and classify the dynamics in a neighbourhood of the corresponding "organizing centre".

1.3.2 Mathematical Tools

To accomplish this task, various numerical algorithms will be designed first and then applied in practice. The main idea is to use a combined continuation and optimization approach: by varying a first parameter of the model, the given input periodic orbit is continued until a critical parameter value, where it bifurcates or, more generally, a specific auxiliary condition becomes fulfilled. The same idea is then applied again. By freeing a second parameter, we may now augment the original system by additionally imposing the defining equation for the encountered degeneracy, respectively the auxiliary condition, and continue until a higher order degenerate bifurcation occurs or an additional auxiliary condition is satisfied. In this way we may find higher and higher order degenerate bifurcations and optima with respect to an increasing number of parameters.

These algorithms will contain as their principal parts the Poincaré map method to locate a fixed point (representing a periodic orbit) and the pseudo-arclength parametrization along the solution manifold to realize the continuation concept. The occurring nonlinear systems will be solved by Newton's method. However, when continuing cusps, degenerate period-doublings or secondary Hopf bifurcations, we shall present and use another approach based upon numerical differentiation, the secant predictor and updated Jacobian matrices. The numerical integration of all differential equations will be performed by means of ISML standard software.

Naturally, this thesis will strongly be oriented in a numerical direction.

1.4 Related Work and Main Results

Neither our goals nor our methods to achieve them are new! Several existing continuation packages go beyond the mere analysis of equilibria and continue periodic solutions, even nonhyperbolic ones. Again without claiming any completeness, we would like to mention here the codes and packages: PEFLOQ [6], AUTO [42], BIFOR2 [72], DERPER [75], BISTAB [107], DERPAR[103], BIFPACK [164], PATH [89], PHASER [102], PITCON [152], INSITE [140], and the more recent PLTMG [15], CHAOS SIMULATIONS [22], CANDYS/QA [47], SYMCON [57], PHASE PLANE [45], CHAOS [11], DSTOOL [12], MACMATH [78], KAOS [68], LINLBF [97], CONEX [160] and DYNAMICS [188].

However, all of these codes (including ours!) are limited with respect to the order of the corresponding degeneracy or codimension of the bifurcation. We are not aware of any algorithm that automatically(!) traces a codimension-four bifurcation, while the package [97], for instance, still manages to follow certain codimension-three bifurcations of equilibria. Because of the much greater numerical effort involved when treating periodic solutions of flows, most packages, such as [160] for instance, go "only" as far as automatically continuing codimension-one bifurcations. In this context we emphasize the word "automatically". Any code that can trace a branch of equilibria in an ordinary differential equation, i.e. continue a solution of $f(x, \lambda) = 0$, is, at least theoretically, also capable of computing a curve of degenerate periodic solutions by constructing suitable functions f. This is what our codes already do. Even though they require a considerable amount of input (first, second and third variational equations as well as certain derivatives of the generating vector field with respect to parameters and, of course, an initial solution), they automatically trace and analyze some higher order degenerate periodic solutions.

Moreover, we would like to point out that, when continuing fixed points of the "theoretically nice" Poincaré map, one may encounter additional, special problems that simply do not exist if the diffeomorphism was not derived from a continuous flow. For instance, the periodic solution may shrink to an equilibrium or its period may tend to infinity. Our codes, a main result of this thesis, can handle several of these difficulties automatically and we believe they are therefore superior to the ones that are not specifically designed for the continuation of Poincaré maps.

Those who expect a new theorem should not be too disappointed. The application

of our codes to Haken's laser model compensates with the detection of a variety of interesting codimension-three bifurcations involving only periodic solutions, among them several kinds of degenerate cusps (including a "winged cusp") and isola formation points for closed loops of lower codimension bifurcations. We shall also present a "swallow tail" of periodic solutions. By systematically continuing secondary Hopf bifurcations and computing the stability coefficient "a", we also detected, for the first time, attractive two-tori in this model. In fact, we strongly conjecture the existence of attractive, "doubled" two-tori and attractive three-tori. Hence, we largely widened the known spectrum of attractors in this particular model by the finding of quasiperiodic ones.

Even though these tori seem to exist only in a narrow interval and are quite small in diameter, they might grow in different parameter directions and gain more physical significance.

In summary we can certainly say that our results extend the ones known from [54], [55] far beyond mere equilibria knowledge.

1.5 Thesis Structure

After providing the basic and fundamental mathematical definitions and theorems in Chapter 2, we proceed by introducing the concept of bifurcations in Chapter 3. Numerous examples will be given that distinguish among several cases. We also state Hopf's theorem for flows and maps, Sotomayor's theorem for a saddle-node bifurcation and related results for a transcritical bifurcation, pitchfork bifurcation and period-doubling bifurcation. In fact, we shall prove the last ones in Chapter 5.

In Chapter 4, we briefly describe the physical model to which we shall apply our algorithms.

Chapter 5 constitutes the heart of the thesis. Based upon Chapters 2 and 3, we present the pseudo-arclength continuation method and the Poincaré map method. Furthermore, we explain certain degeneracy conditions, show how to formulate them mathematically and how to detect the corresponding bifurcations during continuation.

The remaining chapters are devoted to applications of our codes to the model presented in Chapter 4. Numerous results will be presented. In Chapter 6, we start with some periodic solutions and one-parameter continuations of them. Thereby

we detect saddle-node-, period-doubling- and secondary Hopf bifurcations. These in turn will be continued, in Chapter 7, across a two-dimensional parameter space. Additionally, during this continuation, each of these bifurcations will be completely characterized in terms of the stability and direction of the participating branches of periodic solutions and invariant curves (in case of a secondary Hopf bifurcation). This will enable us to find a variety of codimension-two bifurcations. Several of these will be continued in the last chapter, Chapter 8, leading to the detection of some codimension-three bifurcations. Our results will mostly be presented in the form of figures. For easy reference, Figs. 6.1 to 6.8 of Chapter 6, Figs. 7.1 to 7.25 of Chapter 7, and Figs. 8.1 to 8.20 of Chapter 8 are collected at the end of the thesis under the heading "Figures". However, Fig. 5a and Figs. 7a to 7f are found in Chapters 5 and 7, respectively, where they are referred to.

Finally, in our conclusion, we shall briefly present some systems which, we believe, could be useful in extending our work to detecting global bifurcations.

1.6 Caution – Numerics!

The basic assumption of all bifurcation theorems — namely the existence of a certain solution satisfying some degenerate condition — in our particular case, it can only be verified by means of computers. Therefore, when interpreting our results, no matter how carefully obtained, one must not forget that they are mainly based upon numerical methods. Consequently, caution is necessary!

However, whenever possible, we used the state-of-the-art IMSL subroutines to support our codes. In particular, we used the DIVPRK subroutine to integrate all the occurring differential equations with an error tolerance $\approx 10^{-8}$. Also, Newton's method was said to have converged to a solution (x_0, λ_0) of $f(x, \lambda) = 0$ if both the norm of the increment $(dx, d\lambda)$ and the norm of $f(x_0, \lambda_0)$ satisfied the inequalities: $\|(dx, d\lambda)\|_2 < 10^{-12}$ and $\|f(x_0, \lambda_0)\|_2 < 10^{-12}$. These operations, and in fact, the whole code, were carried out in double precision. We also experimented with different integration routines and error tolerances — our results, however, seemed to be rather unaffected by them.

Nevertheless, one does not have any warranty that, after convergence has occurred, the algorithms indeed remained on the same solution branch and did not jump, unnoticed, to a "similar" but different, nearby, one. Furthermore, even if the codes

proceeded along one and the same solution branch, we cannot be sure, that they did not skip over relevant details, for instance bifurcations, along that branch.

We would also like to mention that in the same way as mere graphical results are dangerous to interpret, so are endless number listings alone. It is simply too easy to overlook valuable detailed information along the solution branch by using just one way to present the output data. Combining both ways, we therefore critically inspected and compared graphical with numerical outputs and (sometimes re-) interpreted the results. We find this strategy to be an unrenounceable part of continuation methods.

But, let us quote E. J. Doedel [43] "one must be a believer" and C. Sparrow [173] "people who live in glass houses should not throw stones".

Chapter 2

Mathematical Basis

This chapter summarizes the standard definitions and fundamental results that form the mathematical basis of the subsequent analysis. This theory is well known and most of the theorems are at least stated (if not proven) in almost every advanced textbook on calculus, ordinary differential equations or nonlinear dynamics. In particular we would like to mention here [7], [10], [27], [41], [71], [74], and the more modern literature on dynamical systems and bifurcations as for instance [18], [23], [66], [25], [70], [79], [81], [102], [120], [143], [147], [178], [186]. The proofs will therefore be omitted.

2.1 The Implicit Function Theorem

From calculus we state the implicit function theorem. Even though there exists a more general version of it for the Banach-space case, the finite dimensional form is sufficient for our purpose. For a proof of this theorem see [41].

Theorem 2.1.0.1 *Let $F(x,\lambda) = F(x_1, x_2, \ldots, x_n, \lambda)$ be a vector-valued function defined in an open set $G \subset \mathbb{R}^n \times \mathbb{R}$, $F : G \longrightarrow \mathbb{R}^n$. Assume further that F has continuous first derivatives in a neighbourhood of (x_0, λ_0), where (x_0, λ_0) is a point in G such that:*

$$F(x_0, \lambda_0) = 0, \qquad \det\left(\frac{\partial F}{\partial x}(x_0, \lambda_0)\right) \neq 0. \tag{2.1.1}$$

Then there exists a δ-neighbourhood $U_\delta(x_0)$ of x_0 in $\mathbb{R}^n$ and an ϵ-neighbourhood $I = (\lambda_0 - \epsilon, \lambda_0 + \epsilon)$ of λ_0 in $\mathbb{R}$ such that, for any $\lambda \in I$, there is a unique solution $x = x(\lambda)$ of:

$$F(x,\lambda) = F(x(\lambda),\lambda) = 0 \tag{2.1.2}$$

in U. Furthermore, the vector-valued function $x = x(\lambda)$ has continuous first derivatives in I.

2.2 Results on Ordinary Differential Equations

We are concerned here with nonlinear, autonomous, parameter dependent, deterministic, ordinary differential equations governed by sufficiently smooth vector fields:

$$\dot{x} = f(x, \lambda) \tag{2.2.1}$$

with $f : \mathbb{R}^n \times \mathbb{R}^p \longrightarrow \mathbb{R}^n$. For fixed $\lambda = \lambda_0$ we sometimes use the simpler notation $\dot{x} = f(x)$, and then $f : \mathbb{R}^n \longrightarrow \mathbb{R}^n$.

2.2.1 Existence, Uniqueness and Smoothness of Solutions

The question of existence, uniqueness and smoothness of solutions to equation (2.2.1) is settled by the subsequent theorem, a proof of which can be found in [7], [71], [74], [27].

Theorem 2.2.1.1 *For every $x \in \mathbb{R}^n$ and $\lambda \in \mathbb{R}^p$ there exists a unique solution (or trajectory) $\phi(t, x, \lambda)$ of (2.2.1) satisfying:*

$$\frac{d}{dt}\phi(t, x, \lambda) = f(\phi(t, x, \lambda), \lambda) \tag{2.2.2}$$

with initial condition $\phi(0, x, \lambda) = x$. If $f \in C^r(\mathbb{R}^n \times \mathbb{R}^p, \mathbb{R}^n)$, then this solution is a C^r-function of (t, x, λ). Furthermore, this solution exists for $t \in (t^-_{x,\lambda}, t^+_{x,\lambda})$ which constitutes its maximal interval of existence.

Next we state the "transport theorem", that expresses the rate of change of a volume that varies with a flow.

Theorem 2.2.1.2 *Consider the differential equation $\dot{x} = f(x)$ and let $K \subset \mathbb{R}^n$ be compact. Define $t^-_K := \max_{x \in K}\{t^-_x\}$ and $t^+_K := \min_{x \in K}\{t^+_x\}$ and for every $t \in (t^-_K, t^+_K)$ let $V(t) := \mathrm{vol}_n(\phi(t, K)) := \int_{\phi(t,K)} dx_1 \wedge dx_2 \wedge \cdots \wedge dx_n = \int_{\phi(t,K)} dx$ be the n-dimensional volume of $\phi(t, K)$. Then:*

$$\frac{dV}{dt}(t) = \int_{\phi(t,K)} \mathrm{div}\, f \, dx \tag{2.2.3}$$

describes the rate of change of the volume $V(t)$ varying with the flow governed by the vector field f.

A proof of this theorem can be found in [7]. Note that a (constant) negative divergence of f implies an exponential contraction of any initial volume V_0:

$$V(t) = V_0 e^{(\operatorname{div} f)t}. \tag{2.2.4}$$

However, it does not follow that V_0 shrinks in all directions. In fact, a combined expanding and contracting flow is possible and can lead to so-called "strange attractors", see [3], [161], [173].

2.2.2 Results on Equilibria

We now present some results about equilibria (x_0, λ_0) of the vector field f satisfying $f(x_0, \lambda_0) = 0$ in (2.2.1). Therefore, we make first the concept of stability, attraction and hyperbolicity precise.

Definition 2.2.2.1 An equilibrium (x_0, λ_0) of the vector field f in (2.2.1) is said to be *stable* if, given $\epsilon > 0$, there is a $\delta = \delta(\epsilon) > 0$ such that any solution $\phi(t, x, \lambda_0)$ with $\|x - x_0\|_2 < \delta$ implies $\|\phi(t, x, \lambda_0) - x_0\|_2 < \epsilon$ for all $t > 0$. The equilibrium (x_0, λ_0) is said to be *asymptotically stable* if it is stable and *attractive*, that is, there is a $\delta_0 > 0$ such that $\|x - x_0\|_2 < \delta_0$ implies $\|\phi(t, x, \lambda_0) - x_0\|_2 \to 0$. Finally, the equilibrium (x_0, λ_0) is called *unstable* if it is not stable. The equilibrium (x_0, λ_0) is called *hyperbolic*, if all the eigenvalues of $\frac{\partial f}{\partial x}(x_0, \lambda_0)$ have nonzero real parts. Otherwise the equilibrium is called *nonhyperbolic*.

Note that stability and attraction assume the existence of solutions $\phi(t, x, \lambda_0)$ for all positive times if $\|x - x_0\|$ is only sufficiently small.

A first major theorem involving equilibria is provided by the following linearization principle from [71]:

Theorem 2.2.2.1 *If the equilibrium (x_0, λ_0) of (2.2.1) is hyperbolic, then there is a homeomorphism h defined on some neighbourhood $U(x_0)$ locally taking trajectories $\phi(t, x, \lambda_0)$ of (2.2.1) to solutions of the system:*

$$\dot{z} = \frac{\partial f}{\partial x}(x_0, \lambda_0) z, \tag{2.2.5}$$

i.e. to the system governed by the linear part of f about the equilibrium.

This theorem asserts that in the hyperbolic case the linear and nonlinear systems behave locally qualitatively in the same way.

The proof of the next theorem, concerning stability, is based on the previous one. Again we refer to [7], [27], [71] or [74].

Theorem 2.2.2.2 *If the spectrum* $\sigma = \sigma\left(\frac{\partial f}{\partial x}(x_0, \lambda_0)\right)$ *lies strictly in the left-hand half of the complex plane, then the equilibrium* (x_0, λ_0) *of* (2.2.1) *is locally asymptotically stable. Conversely, if there is an eigenvalue in the spectrum with positive real part, then* (x_0, λ_0) *is unstable.*

Note that this theorem does not allow any conclusion about the stability of (x_0, λ_0) if the corresponding eigenvalue with greatest real part is on the imaginary axis. In fact, in [7] there are two examples satisfying these assumptions, where, in the first one, the nonhyperbolic equilibrium is asymptotically stable while it is unstable in the second one. In order to distinguish among these possibilities we must consider higher order terms of the vector field f. Furthermore, attraction and stability are independent. Indeed, there are known phase portraits showing an unstable but attractive equilibrium — again we refer to [7].

For convenience let us now introduce the following abbreviated notation:

$$f_x^0 := \frac{\partial f}{\partial x}(x_0, \lambda_0)$$

and in particular for future references:

$$f_\lambda^0 := \frac{\partial f}{\partial \lambda}(x_0, \lambda_0)$$

$$f_{x\lambda}^0 := \frac{\partial^2 f}{\partial x \partial \lambda}(x_0, \lambda_0)$$

$$f_{xx}^0 := \frac{\partial^2 f}{\partial x^2}(x_0, \lambda_0)$$

$$f_{\lambda\lambda}^0 := \frac{\partial^2 f}{\partial \lambda^2}(x_0, \lambda_0)$$

and so on for the higher derivatives.

A central role is played by so-called "invariant manifolds":

Definition 2.2.2.2 Let (x_0, λ_0) be a fixed point of (2.2.1) and $U(x_0) \subset \mathbb{R}^n$ be a neighbourhood of x_0. Then:

1. $W^s_{\rm loc}(x_0) := \{x \in U(x_0) | \phi(t,x,\lambda_0) \in U(x_0), \lim_{t\to\infty} \phi(t,x,\lambda_0) = x_0\}$ is called the *local stable manifold* of x_0.

2. $W^u_{\rm loc}(x_0) := \{x \in U(x_0) | \phi(t,x,\lambda_0) \in U(x_0), \lim_{t\to-\infty} \phi(t,x,\lambda_0) = x_0,\}$ is called the *local unstable manifold* of x_0.

3. $W^s(x_0) := \bigcup_{t\le 0} \phi(t, W^s_{\rm loc}(x_0), \lambda_0)$ is called the *global stable manifold* of the equilibrium (x_0, λ_0).

4. $W^u(x_0) := \bigcup_{t\ge 0} \phi(t, W^u_{\rm loc}(x_0), \lambda_0)$ is called the *global unstable manifold* of the equilibrium (x_0, λ_0).

The following results on existence of invariant manifolds, stability of nonhyperbolic equilibria and approximation of the centre manifold are based upon this terminology. The proofs can be found in [23].

Theorem 2.2.2.3 *Suppose the differential equation* (2.2.1) *with* $f \in C^p$ *has the equilibrium* (x_0, λ_0). *Define* $\sigma = \sigma(f^0_x)$ *to be the spectrum of* f^0_x *and:*

$$\sigma_s := \{\mu \in \sigma(f^0_x) | \Re(\mu) < 0\}, \tag{2.2.6}$$

$$\sigma_u := \{\mu \in \sigma(f^0_x) | \Re(\mu) > 0\}, \tag{2.2.7}$$

$$\sigma_c := \{\mu \in \sigma(f^0_x) | \Re(\mu) = 0\}, \tag{2.2.8}$$

and let $E^s(x_0)$, $E^u(x_0)$ *and* $E^c(x_0)$ *be the generalized eigenspaces to* σ_s, σ_u *and* σ_c, *respectively. Then there exist global stable and unstable* C^p*-manifolds* $W^s(x_0)$ *and* $W^u(x_0)$ *tangent to* $E^s(x_0)$ *and* $E^u(x_0)$, *respectively, in* x_0. *Furthermore there exists a* C^{p-1}*-centre manifold* $W^c(x_0)$ *tangent to* $E^c(x_0)$ *in* x_0. *These manifolds are invariant under the flow.*

For fixed $\lambda = \lambda_0$ we now shift the equilibrium to the origin and introduce a new basis. Confining ourselves to the physically more interesting case with $\sigma_u = \emptyset$, we may consider equation (2.2.1) momentarily rewritten as:

$$\dot{x} = Bx + k(x,y) \tag{2.2.9}$$

$$\dot{y} = Cy + g(x,y). \tag{2.2.10}$$

Here the matrix $B \in L(\mathbb{R}^m, \mathbb{R}^m)$ has m eigenvalues on the imaginary axis and the matrix $C \in L(\mathbb{R}^{n-m}, \mathbb{R}^{n-m})$ has $n-m$ eigenvalues with negative real parts and the

functions k and g vanish together with their first derivatives at $(0,0)$. The centre manifold $W^c(0)$, being tangent at the origin to $E^c(0)$ which is the subspace defined by $y = 0$, admits a local representation: $W^c(0) = \{(x,y) | \quad y = h(x)\}$. Now let:

$$\dot{x} := Bx + k(x, h(x)) \tag{2.2.11}$$

be the projection of the flow from $W^c(0)$ onto $E^c(x_0)$. Then the following stability results holds:

Theorem 2.2.2.4 *If $0 \in \mathbb{R}^m$ is an asymptotically stable (unstable) fixed point of* (2.2.11), *then $0 \in \mathbb{R}^n$ is also an asymptotically stable (unstable) fixed point of* (2.2.9), (2.2.10).

That the centre manifold $h(x)$ can actually be computed to arbitrary order is the contents of the next theorem:

Theorem 2.2.2.5 *For any differentiable function $h^* : \mathbb{R}^m \longrightarrow \mathbb{R}^{n-m}$ let the differential operator $\mathcal{N}(h^*)$ be defined as:*

$$\mathcal{N}(h^*)(x) := h^*_x(x)\Big(Bx + k(x, h^*(x))\Big) - Ch^*(x) - g(x, h^*(x)). \tag{2.2.12}$$

Suppose $h^*(x)$ satisfies $h^*(0) = h^*_x(0) = 0$ and $\mathcal{N}(h^*)(x) = \mathcal{O}(\|x\|^r)$ for some $r > 1$ as $\|x\| \to 0$. Then it is true that:

$$h(x) = h^*(x) + \mathcal{O}(\|x\|_2^r) \tag{2.2.13}$$

for $\|x\|_2 \to 0$.

We now introduce the concept of periodic solutions.

2.2.3 Results on Periodic Solutions

Definition 2.2.3.1 The solution $\phi(t, x_0, \lambda_0)$ of (2.2.1) is called *T-periodic* with $T > 0$ if $\phi(T, x_0, \lambda_0) = x_0$ and $\phi(t, x_0, \lambda_0) \neq x_0$ for $0 < t < T$.

In order to study the stability of a periodic solution, we slightly generalize definition 2.2.2.1.

Definition 2.2.3.2 A subset $M \subseteq \mathbb{R}^n$ is called *stable* if, for every neighbourhood U of M and every $x_0 \in M$, there is a neighbourhood V of x_0 with $\phi(t, x, \lambda_0) \in U(M)$ for all $t \geq 0$ and all $x \in V(x_0)$. M is called *asymptotically stable* if it is stable and there is a $\delta_0 > 0$ such that $\|x - x_0\|_2 < \delta_0$ implies $\|\phi(t, x, \lambda_0) - M\|_2 \to 0$. The subset M is called *unstable* if it is not stable. In particular, the periodic solution $\phi(t, x_0, \lambda_0)$ is *stable, asymptotically stable* or *unstable* if its *orbit*:

$$\gamma := \{\phi(t, x_0, \lambda_0) | \quad 0 < t \leq T\} \tag{2.2.14}$$

is a stable, asymptotically stable or unstable subset of $\mathbb{R}^n$.

Remark 2.2.3.1 Note that unlike the equilibria case, we did not define the term "attractive" for a general subset $M \subseteq \mathbb{R}^n$. Indeed, there exists no commonly accepted definition. Even though most attempts to characterize a so-called "strange attractor" in principle coincide, they still differ in subtleties. However, in the cases we are mostly concerned with, M is either a closed curve or a single point and the ambiguities vanish. We could equally well have defined a periodic orbit to be attractive if for each $x_0 \in \gamma$ there is a $\delta_0 > 0$ such that $\|x - x_0\|_2 < \delta_0$ implies $\|\phi(t, x, \lambda_0) - \gamma\|_2 \to 0$. Asymptotic stability of γ would then be equal to stability plus attraction.

The following Floquet theory provides an essential tool to determine the stability of the periodic orbit γ. Consider therefore the equation for its first variation:

$$\dot{z} = f_x(\phi(t, x_0, \lambda_0), \lambda_0) z. \tag{2.2.15}$$

For its solution we have, see [27]:

Theorem 2.2.3.1 *Every fundamental matrix $U(t)$ of (2.2.15) can be written as $U(t) = Q(t)e^{tB}$ with $Q(t)$ a regular and T-periodic matrix and $B \in L(\mathbb{R}^n, \mathbb{R}^n)$. In particular, with $U(0) = \mathrm{id}$, it follows: $U(T) = Q(T)e^{TB} = e^{TB}$.*

Definition 2.2.3.3 The eigenvalues δ_j of the fundamental matrix $U(T)$ of (2.2.15) with $U(0) = \mathrm{id}$ are called the *Floquet multipliers* of the T-periodic solution $\phi(t, x_0, \lambda_0)$ or of the T-periodic orbit γ.

Since $U(T)$ is regular, none of the δ_j equals 0. It can further be shown [7], [26] that $+1$ is always an eigenvalue of $U(T)$ with corresponding eigenvector being tangent to the flow across x_0. Hence, renumbering the Floquet multipliers, we can define $\delta_1 := +1$ which we call the trivial Floquet multiplier. Furthermore, the δ_j are independent of the particular point $x_0 \in \gamma$. Again we refer to the book [26].

Definition 2.2.3.4 The T-periodic orbit γ is called *hyperbolic* if $+1$ is an algebraically simple Floquet multiplier of γ.

The moduli of the nontrivial δ_j tell us something about the stability of γ as the following theorem shows [27]:

Theorem 2.2.3.2 *The hyperbolic T-periodic orbit γ is asymptotically stable if and only if:*

$$\|\delta_j\| < 1 \quad \text{for } j \neq 1 \ (\text{with } \delta_1 = 1). \tag{2.2.16}$$

On the other hand, if $\|\delta_k\| > 1$ for some k, then γ is unstable.

An essential part of this thesis is based upon the so-called *Poincaré map* "S". In oder to define it well, we first need the following result [74]:

Theorem 2.2.3.3 *Consider equation (2.2.1) with $f \in C^r$. Let $x_1 := \phi(T, x_0, \lambda_0)$, $T > 0$, and H_1 be a hyperplane containing x_1 and being transversal to the flow across x_1. Then there exists an open neighbourhood V of x_0 in $\mathbb{R}^n$ and a unique C^r-map $\tau : V(x_0) \times \{\lambda_0\} \to \mathbb{R}$ such that:*

$$\phi(\tau(x, \lambda_0), x, \lambda_0) \in H_1 \ \text{ for all } \ x \in V(x_0) \tag{2.2.17}$$

with $\tau(x_0, \lambda_0) = T$.

For our purpose, we choose $x_1 = \phi(T, x_0, \lambda_0) = x_0$. That is, $x_1 = x_0$ belongs to a T-periodic orbit γ. Using theorem 2.2.3.3 we can now define:

Definition 2.2.3.5 Let γ be a T-periodic orbit. For any $x_{\text{orig}} := x_0 \in \gamma$ and any hyperplane H containing x_{orig} and being transversal to the flow across it, the Poincaré map "S" is firstly defined as:

$$S : V(x_{\text{orig}}) \cap H \times \{\lambda_0\} \longrightarrow H \tag{2.2.18}$$

$$x \mapsto S(x, \lambda_0) := \phi(\tau(x, \lambda_0), x, \lambda_0). \tag{2.2.19}$$

Using a continuity argument, we now generalize this definition by only demanding x_{orig} to be sufficiently close to a point $x_0 \in \gamma$. Choosing H perpendicular to the flow

across x_{orig} by requiring its normal to be $f(x_{\text{orig}}, \lambda_0)$, shifting the origin to x_{orig} and introducing new coordinates in H we now redefine the Poincaré once more to:

$$S : H^* \times \{\lambda_0\} \longrightarrow \mathbb{R}^{n-1} \tag{2.2.20}$$

$$\overline{x} \mapsto S(\overline{x}, \lambda_0) := U^T\Big\{\phi(\tau(x, \lambda_0), x, \lambda_0) - x_{\text{orig}}\Big\} \tag{2.2.21}$$

with

$$\overline{x} = U^T(x - x_{\text{orig}}) \Leftrightarrow x = U\overline{x} + x_{\text{orig}}, \tag{2.2.22}$$

H^* a neighbourhood of $0 \in \mathbb{R}^{n-1}$ and $U \in L(\mathbb{R}^{n-1}, \mathbb{R}^n)$ an orthonormal transformation matrix introducing a new basis in H. To obtain U we simply extend span $\left\{\frac{f(x_{\text{orig}}, \lambda_0)}{\|f(x_{\text{orig}}, \lambda_0)\|}\right\}$ by some vectors $v_1, v_2, \ldots v_{n-1} \in \mathbb{R}^n$ to form an orthonormal basis of $\mathbb{R}^n$ and put the v_j in the j-th column of U. Strictly speaking, the map $S = S_U$ depends on the matrix U which is not unique. However, in the original variables this distinction is unnecessary. We remark further that, once the return plane H^* has been choosen in this way, one may define $S(\overline{x}, \lambda)$ for $x = U\overline{x} + x_{\text{orig}} \in V(x_{\text{orig}}) \cap H$ and λ in a sufficiently small neighbourhood of λ_0, since the flow will remain transversal to H under small perturbations in λ.

It is precisely this last definition that will be used over and over again.

Remark 2.2.3.2 Note that if $x_{\text{orig}} = x_0 \in \gamma$, $x_0 \in \mathbb{R}^n$, it carries over to the fixed point $\overline{x}_0 := 0 \in \mathbb{R}^{n-1}$ of S, that is, $S(0, \lambda_0) = 0$. On the other hand, if $x_{\text{orig}} \notin \gamma$, then the point $x_0 \in \gamma \cap H$, $x_0 \in \mathbb{R}^n$ and sufficiently close to x_{orig}, carries over to the fixed point $\overline{x}_0 = U^T(x_0 - x_{\text{orig}})$ close to the origin in $\mathbb{R}^{n-1}$.

From theorem 2.2.3.3 and straightforward differentiation of $S(\overline{x}, \lambda_0)$ with respect to $\overline{x}$ we have next:

Theorem 2.2.3.4 *The Poincaré map $S : H^* \longrightarrow \mathbb{R}^{n-1}$ is a local diffeomorphism with derivative:*

$$S_{\overline{x}}(\overline{x}, \lambda_0) = U^T\Big\{f\Big(\phi(\tau(x, \lambda_0), x, \lambda_0), \lambda_0\Big)\frac{\partial \tau}{\partial x}(x, \lambda_0) + \frac{\partial \phi}{\partial x}(\tau(x, \lambda_0), x, \lambda_0)\Big\}U. \tag{2.2.23}$$

The proof of the following result can be found in [26].

Theorem 2.2.3.5 *Let γ be a periodic orbit and $x_0 \in \gamma$. Then the nontrivial Floquet multipliers are precisely the eigenvalues of the linearized Poincaré map (2.2.23), evaluated at the fixed point $(\overline{x}_0, \lambda_0)$.*

Hence, we have essentially eliminated the "trivial" direction tangential to the flow. Note also that for the decrease in dimension we have to pay with the three quantities:

$$\tau(x_0, \lambda_0), \quad \frac{\partial \tau}{\partial x}(x_0, \lambda_0), \quad \frac{\partial \phi}{\partial x}(\tau(x_0, \lambda_0), x_0, \lambda_0), \tag{2.2.24}$$

that are in general not analytically available and must be computed numerically. Another way to view the Poincaré map lies in recognizing the fact that this formulation decouples the generally unknown return time $\tau(x, \lambda_0)$ and period T of a periodic orbit γ from the space coordinates x.

2.3 General Theorems for Maps

Now that we have seen how a periodic solution gives rise to a diffeomorphism, we need to include some general results about sufficiently smooth maps:

$$F : \mathbb{R}^n \times \mathbb{R}^p \longrightarrow \mathbb{R}^n \tag{2.3.1}$$

$$x \mapsto F(x, \lambda). \tag{2.3.2}$$

2.3.1 Results on Fixed Points of Maps

Analogously to the case for flows, we first define:

Definition 2.3.1.1 Let the orbit γ of $x_0 \in \mathbb{R}^n$ under (2.3.2) be the set of points:

$$\gamma := \{x_{i+1} | i \in \mathbb{Z} \text{ with } x_{i+1} := F(x_i, \lambda_0)\}, \tag{2.3.3}$$

and denote by $F^n(x, \lambda_0)$ the n-th forward iterate of F:

$$F^n(x, \lambda_0) := \overbrace{F\Big(F(F(F \cdots (x, \lambda_0), \lambda_0), \lambda_0), \lambda_0\Big)}^{n-times}. \tag{2.3.4}$$

The point (x_0, λ_0) is called a *fixed point* of (2.3.2) if $F(x_0, \lambda_0) = x_0$. A fixed point (x_0, λ_0) is said to be *stable* if, given $\epsilon > 0$, there is a $\delta = \delta(\epsilon) > 0$ such that $\|x - x_0\|_2 < \delta$ implies $\|F^n(x, \lambda_0)) - x_0\|_2 < \epsilon$ for all $n > 0$. The fixed point (x_0, λ_0) is said to be *asymptotically stable* if it is stable and *attractive*, that is, there is a $\delta_0 > 0$ such that $\|x - x_0\|_2 < \delta_0$ implies $\|F^n(x, \lambda_0) - x_0\|_2 \to 0$. The fixed point (x_0, λ_0) is called *unstable* if it is not stable. Finally the fixed point (x_0, λ_0) is called *hyperbolic* if all the eigenvalues of $F_x(x_0, \lambda_0) = F_x^0$ have modulus different from 1 and it is called *nonhyperbolic* if it is not hyperbolic.

Note that every point $x \in \mathbb{R}^n$ creates a unique orbit as long as F is invertible. Under additional smoothness assumptions on F and its inverse, the map F is a (local) diffeomorphism, as, for instance, the Poincaré map S.

Again in agreement with the case for flows, there exists a version of Hartman's linearization theorem for diffeomorphisms and by using it one can prove the following stability result, see [66]:

Theorem 2.3.1.1 *Let $F : \mathbb{R}^n \longrightarrow \mathbb{R}^n$ be a diffeomorphism. The hyperbolic fixed point x_0 is then asymptotically stable if and only if the spectrum of F_x^0 lies strictly in the unit circle. If there is an eigenvalue of F_x^0 with modulus greater than 1, then x_0 is unstable.*

Remark 2.3.1.1 Similar to the case for flows, this theorem does not apply in the nonhyperbolic case. Here one needs again to consider higher order terms. Recall further that equilibria of flows with associated eigenvalus on the imaginary axis constitute a special situation. In the case of periodic solutions this critical condition is replaced by nontrivial Floquet multipliers on the unit circle. Again it is this occurrence that indicates a potential change in the (local) qualitative solution structure.

Invariant manifolds for diffeomorphisms are defined in very much the same way as for flows:

Definition 2.3.1.2 Let x_0 be a fixed point under the diffeomorphism $F : \mathbb{R}^n \longrightarrow \mathbb{R}^n$ and $U(x_0) \subset \mathbb{R}^n$ be a neighbourhood of x_0. Denoting by $F^n(x)$ the n-th forward iterate of F, respectively by $F^{-n}(x)$ the n-th backward iterate of F, we define:

1. $W^s_{\text{loc}}(x_0) := \{x \in U(x_0) | \lim_{n\to\infty} F^n(x) = x_0, F^n(x) \in U(x_0)\}$ is called the *local stable manifold* of x_0.

2. $W^u_{\text{loc}}(x_0) := \{x \in U(x_0) | \lim_{n\to\infty} F^{-n}(x) = x_0, F^{-n}(x) \in U(x_0)\}$ is called the *local unstable manifold* of x_0.

3. $W^s(x_0, \lambda_0) := \bigcup_{n=0}^{n=+\infty} F^{-n}(W^s_{loc}(x_0))$ is called the *global stable manifold* of x_0.

4. $W^u(x_0, \lambda_0) := \bigcup_{n=0}^{n=+\infty} F^n(W^u_{loc}(x_0))$ is called the *global unstable manifold* of x_0.

Not surprisingly, the results on invariant manifolds for flows carry over to the case for maps in an obvious way. For details we refer to [23], [120].

Theorem 2.3.1.2 *Suppose the diffeomorphism $F \in C^r$ has the fixed point x_0. Devide the spectrum $\sigma(F_x^0)$ into:*

$$\sigma_s := \{\mu \in \sigma(F_x^0) | \mid \mu \mid < 1\} \tag{2.3.5}$$

$$\sigma_u := \{\mu \in \sigma(F_x^0) | \mid \mu \mid > 1\} \tag{2.3.6}$$

$$\sigma_c := \{\mu \in \sigma(F_x^0) | \mid \mu \mid = 1\} \tag{2.3.7}$$

and let $E^s(x_0)$, $E^u(x_0)$, $E^c(x_0)$ be the generalized eigenspaces to σ_s, σ_u, σ_c, respectively. Then there exist global stable and unstable C^r-manifolds $W^s(x_0)$ and $W^u(x_0)$ tangent to $E^s(x_0)$ and $E^u(x_0)$, respectively, in x_0. Furthermore there exists a C^{r-1}-centre manifold $W^c(x_0)$ tangent to $E^c(x_0)$ in x_0.

In order to state a stability result for the nonhyperbolic case, we adopt the above procedure for flows. Keeping $\lambda = \lambda_0$ fixed, shifting x_0 to the origin and introducing new coordinates, we consider equation (2.3.2) momentarily rewritten as:

$$x_{n+1} = Bx_n + K(x_n, y_n) \tag{2.3.8}$$

$$y_{n+1} = Cy_n + G(x_n, y_n). \tag{2.3.9}$$

Here the matrix $B \in L(\mathbb{R}^m, \mathbb{R}^m)$ has m eigenvalues on the unit circle, the matrix $C \in L(\mathbb{R}^{n-m}, \mathbb{R}^{n-m})$ has $n-m$ eigenvalues inside the unit circle and the functions K and G vanish along with their first derivatives. Again the centre manifold $W^c(0)$ admits locally a representation $W^c(0) = \{(x,y)|y = H(x)\}$. Now let:

$$x_{n+1} := Bx_n + K(x_n, H(x_n)) \tag{2.3.10}$$

be the reduced map on $y = H(x)$. Then the following stability result holds [23]:

Theorem 2.3.1.3 *If $x_0 = 0 \in \mathbb{R}^m$ is an asymptotically stable (unstable) fixed point of* (2.3.10), *then $x_0 = 0 \in \mathbb{R}^n$ is also an asymptotically stable (unstable) fixed point of* (2.3.8), (2.3.9).

An appoximation theorem for $H(x)$ can also be found in [23]:

Theorem 2.3.1.4 *For any differentiable function $H^* : \mathbb{R}^m \to \mathbb{R}^{n-m}$ let the operator $\mathcal{N}(H^*)$ be defined as:*

$$\mathcal{N}(H^*)(x) := H^*\Big(Bx + K(x, H^*(x))\Big) - CH^*(x) - G(x, H^*(x)). \tag{2.3.11}$$

Suppose further that $H^*(x)$ *satisfies* $H^*(0) = H_x^*(0) = 0$ *and* $\mathcal{N}(H^*)(x) = \mathcal{O}(\|x\|^r)$ *for some* $r > 1$ *as* $\|x\| \to 0$. *Then it is true that:*

$$H(x) = H^*(x) + \mathcal{O}(\|x\|_2^r) \tag{2.3.12}$$

as $\|x\|_2 \to 0$.

2.3.2 Results on Periodic Orbits of Maps

Definition 2.3.2.1 If there are $k > 1$ distinct points $x_{j+1} := F(x_j)$ for $j = 0, 1, \ldots, k-1$ (with $x_0 = x_k$) then γ is called a *periodic orbit of period* k (or a k*-cycle*).

Remark 2.3.2.1 If x_j belongs to a k-cycle, we can reduce the problem of determining its (non-) hyperbolicity and stability by considering its k-th forward iterate:

$$F^*(x) := F^k(x) := \overbrace{F\Big(F(F(\cdots(x))\Big)}^{k \text{ times}}, \tag{2.3.13}$$

since each x_j carries over to a fixed point of F^*. Using the chain rule we find the eigenvalues of the linear part of $F^*(x_j)$ by realizing that:

$$F_x^*(x_j) = F_x(F^{k-1}(x_0)) \cdot F_x(F^{k-2}(x_0)) \cdots F_x(F(x_0)) \cdot F_x(x_0). \tag{2.3.14}$$

Chapter 3

Bifurcations

It should be apparent by now that equilibria with eigenvalues on the imaginary axis and periodic orbits with nontrivial Floquet multipliers on the unit circle play a distinctive role. They signal possible changes in the (local) qualitative solution structure. If, in a one-parameter family of vector fields, an eigenvalue attains the value zero, or a nontrivial Floquet multiplier reaches the value $+1$, then the implicit function theorem 2.1.0.1 does not apply anymore. Typically the equilibria branch or, in case of periodic solutions, the corresponding periodic orbit branch then bends around or splits into two or more distinguished branches. Also, if a pair of complex conjugate eigenvalues crosses the imaginary axis, then the solution branch typically continues to exist. But it could have gained or lost stability. Similarly, if a pair of complex conjugate Floquet multipliers (or a single -1 multiplier) crosses the unit circle, then, generically, the branch continues to exist as a function of the parameter but the periodic orbits can change from asymptotically stable to unstable ones (or vice versa).

These observations lead us to the concept of bifurcations. Should our definition be broad enough to include so-called "global bifurcations", we would have to introduce structural stability before, see [66]. However, since we deal here mostly with local phenomena and in order to keep the definition sufficiently general to cover a broad spectrum of phenomena, we can make life a little easier and define:

Definition 3.0.2.2 A *most general (local) bifurcation point* $(x_0, \lambda_0) \in \mathbb{R}^n \times \mathbb{R}^p$, respectively $(\overline{x}_0, \lambda_0) \in \mathbb{R}^{n-1} \times \mathbb{R}^p$, for the general equation $g(x, \lambda) = 0$ satisfies the following conditions:

1. either the flow associated with the vector field g has an equilibriun at (x_0, λ_0), i.e. $g(x_0, \lambda_0) = 0$, with a corresponding eigenvalue of $g_x(x_0, \lambda_0)$ on the imaginary

axis, or

2. the flow associated with the vector field g has a nonhyperbolic periodic orbit across x_0 for $\lambda = \lambda_0$. That is, the resulting Poincaré map with $x_{\text{orig}} = x_0$ satisfies $S(0, \lambda_0) = 0$ and its linear part $S_x(0, \lambda_0)$ has an eigenvalue on the unit circle (the periodic orbit then has a nontrivial Floquet multiplier on the unit circle).

This definition allows some noteworthy peculiarities. For instance:

Example 3.0.2.1 The flow governed by:

$$\dot{x} = f(x, \lambda) = \lambda - x^3 \tag{3.0.1}$$

obeys for each λ a unique equilibrium given by $x = x(\lambda) = \lambda^{1/3}$. Even though $(x_0, \lambda_0) = (0, 0)$ is a (most general) bifurcation point, the solution structure does not change in a neighbourhood of $\lambda_0 = 0$. The equilibria remain asymptotically stable throughout. However, this picture is immediately destroyed if we slightly perturb $f(x, \lambda)$. Then either the bifurcation point disappears or the solution curve develops an S-shape due to the creation of two more equilibria.

Example 3.0.2.2 The differential equation:

$$\dot{x} = f(x, \lambda) = (x - \lambda)^2 \tag{3.0.2}$$

has all of its equilibria on the straight line $x = x(\lambda) = \lambda$. In contrary to example (3.0.2.1) though, every point along this line constitutes a (most general) bifurcation point. But the qualitative behaviour remains again unchanged in a neighbourhood of each of them. The equilibria remain unstable throughout (they attract from only one side). This time a small perturbation has an even greater impact. Adding a small $\epsilon > 0$ to f makes all of the equilibria disappear, while subtracting an $\epsilon > 0$ generates two parallel lines of equilibria: $x^{\epsilon}_{1,2}(\lambda) = \pm\sqrt{\epsilon} + \lambda$. While the upper line consists of unstable equilibria, the lower one contains asymptotically stable ones. In particular, neither line contains a bifurcation point.

3.1 The Saddle-Node Bifurcation

As an important example of a bifurcation point, let us define a saddle-node point, a phenomenon that can occur in both flows and maps.

Definition 3.1.0.3 Let the function $G : \mathbb{R}^n \times \mathbb{R} \to \mathbb{R}^n$ be defined as either:

$$G(x, \lambda) := g(x, \lambda) \tag{3.1.1}$$

in case we are treating zeros of an arbitrary vector field g (and in particular equilibria of flows associated with g), or as:

$$G(x, \lambda) := F(x, \lambda,) - x \tag{3.1.2}$$

in case we are concerned with fixed points of arbitrary maps F (and in particular of Poincaré maps S extracted from flows induced by g). Suppose there is a solution (x_0, λ_0) of $G(x, \lambda) = 0$ such that G_x^0 has only the algebraically simple eigenvalue 0 on the imaginary axis. Call the corresponding right eigenvector v and left eigenvector w. Then (x_0, λ_0) is called a (*general*) *saddle-node point* (or "*fold*", or "*turning point*" or "*limit point*"), if it also satisfies the inequation:

$$w^T G_\lambda^0 \neq 0. \tag{3.1.3}$$

If (x_0, λ_0) additionally satisfies the condition:

$$w^T G_{xx}^0 vv \neq 0, \tag{3.1.4}$$

then it is called a *quadratic* (or "*nondegenerate*" or "*typical*" or "*generic*") *saddle-node point.* Furthermore, if (x_0, λ_0) satisfies (3.1.3) but not (3.1.4), then (x_0, λ_0) is called a *cubic saddle-node point* (or "*hysteresis point*"), if it satisfies:

$$w^T \left(G_{xxx}^0 vv + 3G_{xx}^0 z \right) v \neq 0, \tag{3.1.5}$$

where z is the unique solution of: $G_x^0 z = -G_{xx}^0 vv$ with $z \perp v$.

Going one step further, we define (x_0, λ_0) to be a *quartic saddle-node point*, if it satisfies (3.1.3), but violates (3.1.4) and (3.1.5) and therefore satisfies:

$$w^T \left(G_{xxxx}^0 vvv + 6G_{xxx}^0 vz + 4G_{xx}^0 y \right) v + w^T 3G_{xx}^0 zz \neq 0, \tag{3.1.6}$$

where z is the unique solution of: $G_x^0 z = -G_{xx}^0 vv$ with $z \perp v$, and further y is the unique solution of: $G_x^0 y = -G_{xxx}^0 vvv - 3G_{xx}^0 vz$ with $y^T v = \|z\|_2^2$.

The importance of a saddle-node point is clear from the following theorem due to Sotomayor, see [66]:

Theorem 3.1.0.1 *Consider the equation $G(x,\lambda)=0$ and assume the point (x_0,λ_0) is a quadratic saddle-node point for it according to definition* 3.1.0.3.

Then there exists a smooth curve of solutions to $G(x,\lambda)=0$ crossing (λ_0,x_0) and being tangent to the hyperplane $H=(x,\lambda_0)$. This solution curve lies locally on one side of H. Either for $\lambda>\lambda_0$ there are no solutions and then for $\lambda<\lambda_0$ there are two (hyperbolic) solutions or there are two (hyperbolic) solutions for $\lambda>\lambda_0$ and no solution for $\lambda<\lambda_0$.

Also, the set of all one-parameter equations $G(x,\lambda)=0$ satisfying $G(x_0,\lambda_0)=0$ with only 0 as an algebraically simple eigenvalue of G_x^0 on the imaginary axis and satisfying additionally the above conditions (3.1.3) *and* (3.1.4) *is dense and open in the space of all one-parameter C^∞-functions with a root at (x_0,λ_0) and with an associated 0 eigenvalue of G_x^0. According to the definition of G these solutions are then either equilibria of flows or fixed points of maps. In particular, if F is a Poincaré map, then the fixed points correspond to periodic orbits.*

In other words, if the continuation of a root (x_0,λ_0) in an arbitrary one-parameter vector field $G(x,\lambda)$ meets an eigenvalue 0 of the associated derivative $G_x(x,\lambda)$, then this bifurcation will typically be a quadratic saddle-node of roots of $G(x,\lambda)$. There are two possibilities for the exceptional cases to occur:

1. either we are simply extremely lucky and one, or even several, of the imposed conditions for a quadratic saddle-node bifurcation are violated, or

2. the vector field itself is not arbitrary but inherits some kind of atypical structure (like symmetry or the existence of a so-called trivial solution branch) which is independent of λ and simply forbids a quadratic saddle-node from occurring.

However, without further restrictions on G we must generically vary another of the λ coordinates in order to encounter an (algebraically) double 0 eigenvalue or to achieve equality in one of the conditions (3.1.3) or (3.1.4). Furthermore, these exceptional cases can always be perturbed into quadratic saddle-nodes. Hence, in some sense, such a bifurcation is then composed of quadratic saddle-nodes.

Remark 3.1.0.2 The above theorem 3.1.0.1 does not address stability. While it is true that for $x\in\mathbb{R}$ the solution branch changes stability when bending around a

quadratic(!) saddle-node point (x_0, λ_0), this does no longer need to be the case in higher dimensions. Depending on the location of the other eigenvalues of G_x^0, the solution branch may then either loose or gain stability or remain unstable.

Example 3.1.0.3 The standard example of a quadratic saddle-node bifurcation is provided by:

$$f(x, \lambda) = x^2 - \lambda. \tag{3.1.7}$$

The equilibria lie on $\lambda = \lambda(x) = x^2$ and they become unstable when the parabola bends around the quadratic saddle-node point $(x_0, \lambda_0) = (0, 0)$ and x becomes positive.

Example 3.1.0.4 Notice that in the above particular example 3.0.2.1 the eigenvalue $-3\lambda^{2/3}$ does not transversally cross the imaginary axis at the bifurcation value $\lambda_0 = 0$ but only touches it and then becomes negative again. This kind of behaviour is certainly atypical. In terms of the theorem, we see that condition (3.1.4) is violated, but (3.1.3) and (3.1.5) hold: $(0, 0)$ is a cubic saddle-node. Also, the vertical tangent along the solution manifold of $f(x, \lambda) = \lambda - x^3 = 0$ at the bifurcation point $(x_0, \lambda_0) = (0, 0)$ (the imaginary axis) can be perturbed into one with a negative slope. Thereby we would create two quadratic saddle-nodes marking the bounds of an interval with three equilibria — in other words, a hysteresis loop. In very much the same way, the vertical tangent can be perturbed into one with positive slope such that (3.0.2.1) does not possess any bifurcation point.

Example 3.1.0.5 According to definition 3.1.0.3, none of the equilibria in example 3.0.2.2 is a saddle-node point. Nevertheless, considering $f^*(x, \lambda, \epsilon) = (x - \lambda)^2 + \epsilon$ makes it clear that the whole line $x = x(\lambda) = \lambda$ simultaneously undergoes a saddle-node bifurcation if ϵ is decreased across 0.

3.2 The Transcritical Bifurcation

Now we strengthen our assumptions on the most general bifurcation point by additionally requiring that the inequation (3.1.3) is not satisfied. Then, as the following two examples illustrate, we may or may not have two distinct branches crossing each other.

Example 3.2.0.6 The equation:

$$f(x,\lambda) = x^2 + \lambda^2 = 0 \tag{3.2.1}$$

has trivially the unique solution $(x_0, \lambda_0) = (0,0)$ violating condition (3.1.3). However, a perturbation $x^2 + \lambda^2 - \epsilon = 0$ will yield a small circle of solutions with two saddle-nodes at $(x,\lambda) = (0, \pm\sqrt{\epsilon})$. Checking the location of the eigenvalues along the circle, we immediately see that the upper semicircle is unstable while the lower one constitutes a branch of asymptotically stable solutions. Hence there is an exchange of stability at the saddle nodes. For obvious reasons, the bifurcation point (x_0, λ_0) is appropriately called an "*isola formation point*" or "*hermite*". For more information we refer here to [92] and [105].

Example 3.2.0.7 Consider now:

$$f(x,\lambda) = x^2 - \lambda^2 = 0. \tag{3.2.2}$$

Again condition (3.1.3) is violated at the solution $(x_0, \lambda_0) = (0,0)$. It is easy to check that there are exactly two distinct equilibrium branches $x_{1,2}(\lambda) = \pm\lambda$ intersecting each other at a nonzero angle and exchanging stability at (x_0, λ_0). Furthermore both branches have a well defined derivative $\frac{dx_{1,2}}{d\lambda}(0) = \pm 1$. That means both branches transversally cross the hyperplane $H = (x, 0)$ and exist on both sides of $\lambda_0 = 0$. In [81] this feature is called a "two-sided bifurcation".

However, a perturbation $x^2 - \lambda^2 + 2\epsilon = 0$ destroys this picture and creates the two hyperbolas $x^{\epsilon}_{1,2}(\lambda) = \pm\sqrt{\lambda^2 - 2\epsilon}$ with two saddle-nodes at $(x,\lambda) = (0, \pm\sqrt{2\epsilon})$. Similarly to 3.2.0.6 the hyperbolas exchange stability at their saddle-nodes such that the lower parts retain stability. On the other hand, subtracting 2ϵ from f makes the solution manifold not contain any bifurcation at all.

Remark 3.2.0.3 Notice that both examples 3.2.0.6 and 3.2.0.7 satisfy condition (3.1.4) while they both violate condition (3.1.3). Yet their qualitative behaviour differs drastically. In order to distinguish among these cases, one clearly needs more information about the underlying function f — for instance, if the saddle-nodes of the perturbed systems "open towards each other" or "away from each other" or whether there exists at least one ("trivial") solution branch from which another one can bifurcate.

Before giving a precise definition of a transcritical bifurcation, we need some more terminology used to characterize an assumed "trivial" solution branch. Consider therefore the equation $G(x,\lambda)=0$ with $G:\mathbb{R}^n\times\mathbb{R}\longrightarrow\mathbb{R}^n$ sufficiently smooth. The *general solution manifold*, M_{gen}, of $G(x,\lambda)=0$ is then defined as:

$$M_{\text{gen}}:=\{(x,\lambda)\in\mathbb{R}^n\times\mathbb{R}|G(x,\lambda)=0\}, \tag{3.2.3}$$

while the *regular solution manifold*, M_{reg}, of $G(x,\lambda)=0$ is defined as:

$$M_{\text{reg}}:=\{(x,\lambda)\in\mathbb{R}^n\times\mathbb{R}|G(x,\lambda)=0 \text{ and } \operatorname{rank}[G_x(x,\lambda)\ \ G_\lambda(x,\lambda)]=n\}. \tag{3.2.4}$$

M_{reg} is a 1-dimensional, differentiable manifold in $\mathbb{R}^n\times\mathbb{R}$ without boundary. Suppose now $G(x_0,\lambda_0)=0$ and the point (x_0,λ_0) lies along a smooth branch of solutions. We can then parametrize this particular branch, for instance using arclength parametrization:

$$G(x(s),\lambda(s))=0, \tag{3.2.5}$$

$$\|\dot{x}(s)\|_2^2+|\dot{\lambda}(s)|^2=1, \tag{3.2.6}$$

where the dot denotes $\frac{\partial}{\partial s}$ and with $(x(0),\lambda(0))=(x_0,\lambda_0)$. This particular branch transversally crosses the hyperplane $H=(x,\lambda_0)$ if and only if:

$$\dot{\lambda}(0)\neq 0. \tag{3.2.7}$$

Then the solutions along this branch exist (locally) on both sides of λ_0.

Definition 3.2.0.4 Let the function $G(x,\lambda)$ be defined as in (3.1.1), (3.1.2). Suppose there is a solution (x_0,λ_0) of $G(x,\lambda)=0$ such that G_x^0 has only the algebraically simple eigenvalue 0 on the imaginary axis with right eigenvector v and left eigenvector w. Furthermore, assume that (x_0,λ_0) lies along a smooth branch of solutions that is parametrized by its arclength as in (3.2.5) and (3.2.6) with $\dot{\lambda}(0)\neq 0$.

Then (x_0,λ_0) is called a *nondegenerate* (or "*typical*" or "*generic*") *transcritical bifurcation point* (or "*point with stability exchange*" or "*perturbed bifurcation point*"), if it also satisfies the equation:

$$w^TG_\lambda^0=0 \tag{3.2.8}$$

and the inequations:

$$w^T\left(G_{xx}^0\dot{x}(0)+G_{x\lambda}^0\dot{\lambda}(0)\right)v\neq 0, \tag{3.2.9}$$

$$\text{and } w^TG_{xx}^0vv\neq 0. \tag{3.2.10}$$

The dynamics near a transcritical bifurcation point are described by:

Theorem 3.2.0.2 *Let the function $G(x,\lambda)$ be defined as in (3.1.1), (3.1.2) and suppose it has a transcritical bifurcation point at (x_0,λ_0) according to definition 3.2.0.4.*

Then there exist two distinct smooth solution branches of $G(x,\lambda)=0$ across (x_0,λ_0) and both transversally cross the hyperplane $H=(x,\lambda_0)$.

In case all other eigenvalues of G_x^0 have negative real parts, respectively those of $G_x^0+\mathrm{id}$ are within the unit circle, then the two branches exchange their stability.

A proof of this theorem will follow in Chapter 5.

If the function G admits the trivial solution branch $x=x(\lambda)=0$, then we have $(\dot{x}(0),\dot{\lambda}(0))=(0,\pm 1)$ along it, and (3.2.9) becomes the more popular condition: $w^T G_{x\lambda}^0 v \neq 0$, see [66], [186], [143], [102]. In example 3.2.0.7 however, we must check condition (3.2.9). At $(x_0,\lambda_0)=(0,0)$ we find $(\dot{x}(0),\dot{\lambda}(0))=(\pm 1/\sqrt{2},\pm 1/\sqrt{2})$ for the branch $x=x(\lambda)=\lambda$. This gives in (3.2.9) the value $\pm\sqrt{2}\neq 0$. Since all other conditions are satisfied as well, we recover the transcritical bifurcation. Of course, had we initially choosen the branch $x=x(\lambda)=-\lambda$, we would have found the same result.

3.3 The Pitchfork Bifurcation

We continue by assuming that both inequations (3.1.3) and (3.1.4) are violated. Then we may still have two distinct branches transversally crossing each other, but the "nontrivial" one may now exist (locally) on only one side of λ_0.

Example 3.3.0.8 Both problems:

$$f_1(x,\lambda)=x\lambda-x^3=0 \quad \text{and} \quad f_2(x,\lambda)=x\lambda+x^3=0 \tag{3.3.1}$$

have the trivial solution $x=x(\lambda)=0$ loosing stability when λ is increased passed 0. In addition, f_1 admits the parabola $\lambda=\lambda(x)=x^2$ "opening to the right", while f_2 allows the parabola $\lambda=\lambda(x)=-x^2$ "opening to the left". In contrary to example 3.2.0.7, these second branches, the parabolas, exist on only one side of $\lambda_0=0$.

While the parabola contains only stable solutions for f_1, it contains only unstable solutions for f_2. In particular, the solutions along these parabolas retain their stability, respectively instability.

Adding a small amount $2\epsilon x^2$ to f_1 transforms at first the parabola towards $x_\epsilon(\lambda) = \epsilon \pm \sqrt{\epsilon^2 + \lambda}$. This has the effect of perturbing (x_0, λ_0) into a transcritical bifurcation point which can now be perturbed further into two quadratic saddle-nodes. In very much the same way can f_2 be "unfolded" into quadratic saddle-nodes. Similar to remark 3.2.0.3, equality in the above conditions (3.1.3) and (3.1.4) alone here does not determine the character of (x_0, λ_0). Because of its geometrical picture, this phenomena is called a "pitchfork bifurcation", a "supercritical" one for f_1 and a "subcritical" one for f_2.

Let us be precise:

Definition 3.3.0.5 Let the function $G(x, \lambda)$ be defined as in (3.1.1), (3.1.2). Suppose there is a solution (x_0, λ_0) of $G(x, \lambda) = 0$ such that G_x^0 has only the algebraically simple eigenvalue 0 on the imaginary axis. Call the corresponding right eigenvector v and left eigenvector w. Furthermore, assume that (x_0, λ_0) lies along a smooth branch of solutions that is parametrized by its arclength as in (3.2.5), (3.2.6) with $\dot{\lambda}(0) \neq 0$.

Then the point (x_0, λ_0) is called a *quadratic* (or "*nondegenerate*" or "*typical*" or "*generic*") *pitchfork bifurcation point* (or "symmetry-breaking bifurcation point"), if it also satisfies the following four conditions:

$$w^T G_\lambda^0 = 0, \tag{3.3.2}$$

$$w^T \left(G_{xx}^0 \dot{x}(0) + G_{x\lambda}^0 \dot{\lambda}(0) \right) v \neq 0, \tag{3.3.3}$$

$$w^T G_{xx}^0 vv = 0, \tag{3.3.4}$$

$$w^T \left(G_{xxx}^0 vv + 3 G_{xx}^0 p \right) v \neq 0, \tag{3.3.5}$$

with p a particular solution of $G_x^0 p = -G_{xx}^0 vv$.

If the function G is an odd function of $x \in \mathbb{R}$, then it satisfies $G_{xx}^0 = 0$ at $(0,0)$ and it admits the trivial solution branch. Along this branch we find again $(\dot{x}(0), \dot{\lambda}(0)) = (0, 1)$ and we recover the more familiar conditions $G_{x\lambda}^0 \neq 0$ and $G_{xxx}^0 \neq 0$, see [66], [186], [143], [102].

Based upon definition 3.3.0.5 we have:

Theorem 3.3.0.3 *Let the function $G(x, \lambda)$ be defined as in* (3.1.1), (3.1.2) *and suppose it has a pitchfork bifurcation point at (x_0, λ_0) according to definition* 3.3.0.5.

Then there exist two distinct smooth solution branches of $G(x,\lambda) = 0$ *across* (x_0,λ_0). *One of them , "*C_1*", transversally crosses the hyperplane* $H = (x,\lambda_0)$, *while the other one ,"*C_2*", has quadratic tangency with it and lies (locally) on one side of it. If the quotient:*

$$\frac{w^T\left(G^0_{xxx}vv + 3G^0_{xx}p\right)v}{w^T(G^0_{xx}\dot{x}(0) + G^0_{x\lambda}\dot{\lambda}(0))v}\dot{\lambda}(0) > 0, \tag{3.3.6}$$

then C_2 *exists for* $\lambda < \lambda_0$, *while* C_2 *exists for* $\lambda > \lambda_0$ *in case the quotient* (3.3.6) *is negative.*

In case all the other eigenvalues of G^0_x *have negative real parts, respectively those of* $G^0_x + \mathrm{id}$ *lie inside the unit circle, then we have a stability result. If:*

$$\frac{w^T(G^0_{xx}\dot{x}(0) + G^0_{x\lambda}\dot{\lambda}(0))v}{w^Tv}\dot{\lambda}(0) < 0, \tag{3.3.7}$$

then C_1 *gains stability when* λ *increases passed* λ_0 *while it looses stability in case the quotient* (3.3.7) *is positive. Furthermore, if:*

$$\frac{w^T\left(G^0_{xxx}vv + 3G^0_{xx}p\right)v}{w^Tv} > 0, \tag{3.3.8}$$

then C_2 *contains unstable solutions (and exists on that side of* λ_0 *where* C_1 *is stable, while* C_2 *contains stable solutions (and exists on that side of* λ_0 *where* C_1 *is unstable, if the quotient* (3.3.8) *is negative.*

Again we defer the proof of this theorem to Chapter 5.

Example 3.3.0.9 As an example involving a non-odd function, consider:

$$f(x,\lambda) = (x - \lambda^2 - \lambda)(x^2 - \lambda) = 0. \tag{3.3.9}$$

We find $(\dot{x}(0),\dot{\lambda}(0)) = (\pm 1/\sqrt{2}, \pm 1/\sqrt{2})$ at $(x_0,\lambda_0) = (0,0)$ along the solution branch $x = x(\lambda) = \lambda^2 + \lambda$. Since $G^0_{xx} = 0$, the conditions reduce to $G^0_{xxx} \neq 0$ and $G^0_{x\lambda} \neq 0$, which can easily be checked. The resulting pitchfork has its "middle tooth" non-linearly bended upward. Concerning stability, we find that points on the parabola $x = x(\lambda) = \lambda^2 + \lambda$ become stable when λ increases passed $\lambda_0 = 0$ while points along the second parabola $\lambda = \lambda(x) = x^2$ remain unstable. Hence we have a subcritical pitchfork bifurcation.

3.4 Potential Bifurcation Points and Strict Bifurcation Points

Depending on the higher derivatives of G evaluated at a root (x_0, λ_0) satisfying $G(x_0, \lambda_0) = 0$, we encounter increasingly higher degeneracies. These, in turn, may or may not result in distinct solution branches crossing at (x_0, λ_0). Let us give some more examples and a concluding definition.

Example 3.4.0.10 The function:

$$f(x, \lambda) = (x - \lambda)(x^2 + \lambda^2) \tag{3.4.1}$$

has all of its equilibria along the single line $x = x(\lambda) = \lambda$ not showing any "anomalies". Nevertheless the point $(0,0)$ is a bifurcation point violating condition (3.1.3). If we consider the equation $f(x, \lambda) = 0$ as a cubic polynomial in x with coefficients depending on λ though, we realize that for $\lambda_0 = 0$ an exceptional case occurs — the root $x = 0$ has multiplicity three. We can perturb the second factor $(x^2 + \lambda^2)$ of f in such a way that it will develop an additional closed loop of zeros of f about $(0,0)$. This loop (or isola) crosses the other solution branch $x = x(\lambda) = \lambda$ in two transcritical or pitchfork bifurcations, and f then admits three distinct equilibria in a neighbourhood of λ_0.

Example 3.4.0.11 The vector field:

$$f(x, \lambda) = x^2 - \lambda^4 \tag{3.4.2}$$

has all of its equilibria along the two parabolas $x = x(\lambda) = \pm\lambda^2$ which agree to first order at the bifurcation point $(0,0)$ that violates (3.1.3). From a mere geometrical point of view, it should be clear that there are perturbations of f that obey two transcritical bifurcation points or that do not show any bifurcation points at all.

Example 3.4.0.12 As a final example, consider:

$$f(x, \lambda) = x^2 - \lambda^3. \tag{3.4.3}$$

This time, the curve of equilibria $x = x(\lambda) = \pm\lambda^{3/2}$ looses differentiability at the bifurcation point $(0,0)$ where condition (3.1.3) is once again not satisfied. It develops here a "cusp". Now subtracting $\epsilon\lambda^2$, $\epsilon > 0$, makes the curve intersect itself at the now

transcritical bifurcation point $(0,0)$, thereby creating a little loop just left of it. The perturbation $-\lambda^2(\epsilon_1+\epsilon_2)+\epsilon_1\epsilon_2\lambda$, on the other hand, creates an isola of equilibria by detaching the loop from the main curve and "smoothing" the cusp to a saddle-node. This phenomena is sometimes called a "cusp supported isola".

No doubt we could continue with examples inheriting higher and higher degeneracies: "swallow tails", "butterflies", "double isolas", figure 8's", "winged cusps" would be next. In fact, in [86] a systematic hierarchy is proposed. But, firstly, we would soon run out of appropriate names and, secondly, the equations become quickly too complex to allow easy analytical insight.

However, in Chapter 5 we shall elaborate on these ideas and presented examples. In particular, we shall explain the meaning of the above conditions (3.1.3), (3.1.4), (3.1.5), (3.1.6) and derive conditions to distinguish among the various degenerate saddle-nodes we have encountered. For now let us define:

Definition 3.4.0.6 Let the function $G(x,\lambda)$ be defined as in (3.1.1), (3.1.2) and assume $G(x_0,\lambda_0)=0$. If

$$\dim([G_x^0 \;\; G_\lambda^0]) = k+1 \;\text{ and }\; \dim\Big(([G_x^0 \;\; G_\lambda^0])^T\Big) = k, \tag{3.4.4}$$

then the point (x_0,λ_0) is called a *potential bifurcation point*. In case $k=1$, it is called a *simple potential bifurcation point*. Finally, if there are two or more distinct branches across (x_0,λ_0), this point is called a *strict bifurcation point*.

In particular, we see that the above transcritical bifurcation in example 3.2.0.7 and pitchfork bifurcation in example 3.3.0.8 provide (simple) strict bifurcations.

3.5 The Period-Doubling

Next we introduce a period-doubling point. In contrast to a saddle-node point, this phenomenon can only occur in maps (and in particular in Poincaré maps). It does not possess a counterpart in the equilibrium theory for flows.

Consider the function $G := F \circ F - \mathrm{id}$. It has a root at (x_0,λ_0) if (x_0,λ_0) is a fixed point of F. Now, if -1 is an algebraically simple eigenvalue of F_x^0, then 0 is an algebraically simple eigenvalue of G_x^0. Furthermore, if F does not possess the eigenvalue $+1$, then the implicit function theorem 2.1.0.1 guarantees a unique

smooth curve of fixed points across (x_0, λ_0) that can be parametrized by λ. Then, in particular, $\dot{\lambda}_0 \neq 0$ when we use the arclength parametrization (3.2.5), (3.2.6) along this fixed point branch. This implies, for the function G, a smooth solution branch across (x_0, λ_0) with $\dot{\lambda}_0 \neq 0$. But since:

$$w^T G^0_\lambda = w^T \left((F^0_x + \mathrm{id}) F^0_\lambda \right) = 0, \tag{3.5.1}$$

we see that (x_0, λ_0) is a simple potential bifurcation point for G. Finally, we also have:

$$w^T G^0_{xx} vv = w^T \Big(F^0_{xx}(F^0_x v)(F^0_x v) + F^0_x (F^0_{xx} vv) \Big) = 0. \tag{3.5.2}$$

Hence, G satisfies (3.3.2) and (3.3.4) in definition 3.3.0.5 of a pitchfork bifurcation. Indeed we now define:

Definition 3.5.0.7 Let (x_0, λ_0) be a fixed point of the map $F : \mathbb{R}^n \times \mathbb{R} \longrightarrow \mathbb{R}^n$ such that F^0_x has only the simple eigenvalue -1 on the unit circle with corresponding right eigenvector v and left eigenvector w. Assume further that the unique fixed point branch containing (x_0, λ_0) is parametrized using its arclength as in (3.2.5), (3.2.6) with $(\dot{x}(0), \dot{\lambda}(0)) = (\dot{x}_0, \dot{\lambda}_0)$ and $\dot{\lambda}(0) \neq 0$. Then define the map G to be the second iterate of F minus the identity: $G(x, \lambda) := F(F(x, \lambda), \lambda) - x$. Suppose now G satisfies the following (nondegenerate or typical) conditions:

$$\begin{aligned} 0 \;&\neq\; w^T \left((G^0_{xx} \dot{x}_0 + G^0_{x\lambda} \dot{\lambda}_0) v \right. && (3.5.3) \\ &=\; -w^T \Big(F^0_{xx}(F^0_x \dot{x}_0) + F^0_{xx} \dot{x}_0 + F^0_{xx} F^0_\lambda \dot{\lambda}_0 + 2F^0_{x\lambda} \dot{\lambda}_0 \Big) v, && (3.5.4) \end{aligned}$$

and:

$$\begin{aligned} 0 \;&\neq\; w^T \Big(G^0_{xxx} vv + 3G^0_{xx} p \Big) v && (3.5.5) \\ &=\; w^T \Big(F^0_{xxx}(F^0_x v)(F^0_x v)(F^0_x v) + 3F^0_{xx}(F^0_{xx} vv)(F^0_x v) \Big) && (3.5.6) \\ &\quad + w^T \Big(F_x(F^0_{xxx} vvv) + 3F^0_{xx}(F^0_x p)(F^0_x v) + 3F^0_x (F^0_{xx} pv) \Big), && (3.5.7) \end{aligned}$$

with p a particular solution of :

$$G^0_x p = -G^0_{xx} vv. \tag{3.5.8}$$

Then the point (x_0, λ_0) is called a *quadratic* (or "*nondegenerate*" or "*typical*" or "*generic*") *period-doubling point* or ("*flip*").

The behaviour of the system in a neighbourhood of a period-doubling point is described by the following theorem:

Theorem 3.5.0.4 *Consider the map* (2.3.2). *Assume further that* (x_0, λ_0) *is a quadratic period-doubling point for it according to definition* 3.5.0.7.

Then there exists a smooth curve of fixed points of F *crossing* (x_0, λ_0) *that can locally be parametrized by* λ. *In addition, there is a unique smooth branch of (hyperbolic) 2-periodic orbits of* F *crossing* (x_0, λ_0), *tangent to the hyperplane* $H = (x, \lambda_0)$ *and locally on one side of it.*

The doubled orbits occur (locally) for $\lambda < \lambda_0$, *if:*

$$\frac{w^T\left(G^0_{xxx}vv + 3G^0_{xx}p\right)v}{w^T\left(G^0_{xx}\dot{x}_0 + G^0_{x\lambda}\dot{\lambda}_0\right)v}\dot{\lambda}_0 > 0, \tag{3.5.9}$$

while they appear for $\lambda > \lambda_0$ *in case the quotient in* (3.5.9) *is negative.*

In case all other eigenvalues of F^0_x *lie inside the unit circle, we have a stability result for the fixed points and 2-periodic orbits:*

For increasing λ *across* λ_0 *the fixed points gain stability, if:*

$$\frac{w^T\left(G^0_{xx}\dot{x}_0 + G^0_{x\lambda}\dot{\lambda}_0\right)v}{w^Tv}\dot{\lambda}_0 < 0, \tag{3.5.10}$$

while they loose stability in case the quotient (3.5.10) *is positive.*

The doubled orbits will be asymptotically stable (and exist on that side of λ *where the fixed points are unstable), if:*

$$\frac{w^T\left(G^0_{xxx}vv + 3G^0_{xx}p\right)v}{w^Tv} < 0, \tag{3.5.11}$$

while they will be unstable (and exist on that side of λ *where the fixed points are asymptotically stable) if the quotient in* (3.5.11) *is positive.*

Once again, the proof will follow from results in the next chapter.

Example 3.5.0.13 In one dimension the above quotients simplify enormously:

$$F(x, \lambda) = 1 - \lambda x^2 \tag{3.5.12}$$

undergoes a period-doubling at $(x_0, \lambda_0) = (2/3, 3/4)$. We compute: $G^0_{xx} = 0$, $G^0_{xxx} = -27/4$, $G^0_{x\lambda} = 2$ and $(\dot{x}(0), \dot{\lambda}(0)) = (\mp - 2/\sqrt{85}, \pm 9/\sqrt{85})$. With $w = v = p = 1$ we then easily confirm a supercritical period-doubling, i.e. the fixed point looses its stability to an emanating branch of 2-periodic orbits that exist (locally) for $\lambda > 3/4$.

Example 3.5.0.14 Consider the map:

$$F(x,\lambda) = x^2 + \lambda x - 1 \tag{3.5.13}$$

with a fixed point branch $x(\lambda) = \frac{1}{2}\left(-\lambda + 1 - \sqrt{(\lambda-1)^2+4}\right)$. For $\lambda_0 = 1$ the fixed point attains the value $x_0 = -1$ and $F_x^0 = -1$. However, while condition (3.5.3) holds, condition (3.5.5) is violated. Again notice that the eigenvalue $1 - \sqrt{(\lambda-1)^2+4}$ along the fixed point branch does not transversally cross -1. In contrary, -1 is a local maximum of the eigenvalue, so that the fixed points remain unstable in a neighbourhood $I_0(1) \setminus \{1\}$.

One can also easily check, that $(-1,\lambda) \mapsto (-\lambda,\lambda)$ belongs to a 2-periodic orbit γ that, for $\lambda = 1$, coincides with the fixed point. Using remark 2.3.2.1 we see that γ is asymptotically stable in $I_1 = (1-\sqrt{2}, 1+\sqrt{2}) \setminus \{1\}$, where, at $\lambda = 1 \pm \sqrt{2}$, the eigenvalue -1 signals a possible further period-doubling (or quadrupling). We emphasize that γ exists on both sides of $\lambda_0 = 1$, that it is not tangent to the hyperplane $H = (x, \lambda_0)$ and that there are three solution branches for $G(x,\lambda) = (F \circ F - \mathrm{id})(x,\lambda) = 0$ across the bifurcation point $(x_0,\lambda_0) = (-1,1)$.

Remark 3.5.0.4 We would like to point out the similarities between this degenerate period-doubling and the transcritical bifurcation. In view of 3.2.0.7 it should not be too surprising that we can perturb $F \circ F - \mathrm{id}$ so that we arrive at either no bifurcation at all or at two opposed pitchforks (pitchforks "opening away from each other"). Furthermore, a comparison with 3.2.0.6 makes it plausible that there should also exist a degenerate period-doubling where the 2-periodic orbits form an isola that shrinks to a point and finally disappears at the bifurcation point. We would then be left with only one solution branch across (x_0,λ_0). In fact, later on we shall provide such an example. Eventually, going another step further, one can imagine that both types of degenerate period-doublings coalesce and create a "doubly-degenerate period-doubling" with only two distinct solution branches — a smooth fixed point branch and a 2-periodic one exhibiting a cusp as in example 3.4.0.12. Unfortunately though, even in one dimension it is a challenging problem to find an explicit expression for f that inherits this type of bifurcation. However, we believe that the map $(x,\lambda) \to F(x,\lambda) := x(1 + \lambda^3 + 2^{2/3}3\lambda + 2^{1/3}3\lambda^2) + \lambda x^3$ provides a good start for an analysis in this direction as the eigenvalue $1 + \lambda^3 + 2^{2/3}3\lambda + 2^{1/3}3\lambda^2$ along the trivial fixed point $x(\lambda) = 0$ crosses -1 nontransversally with only second order contact.

3.6 The Hopf Bifurcation

Let us continue by assuming a pair of complex conjugate eigenvalues, μ_0, $\overline{\mu_0}$, on the imaginary axis in case of an equilibrium of a flow. As long as there is no 0 eigenvalue, the implicit function theorem 2.1.0.1 still guarantees a unique solution branch $x = x(\lambda)$ of $f(x, \lambda) = 0$. But, if $\mu(\lambda)$, $\overline{\mu(\lambda)}$ transversally cross the imaginary axis, then periodic solutions can bifurcate into phase space. Such a bifurcation is called a *Hopf bifurcation* or *Poincaré-Andronov-Hopf bifurcation*. The theorem below, due to Hopf [77], gives the necessary details.

However, in order to state the Hopf theorem for equilibria in a most suitable form, we first apply centre manifold theory and consider the vector field (2.2.1) restricted on it. If $\pm i\omega$, with $\omega \neq 0$, are the only eigenvalues on the imaginary axis, the resulting system is now two-dimensional. Transforming it by an additional smooth change of coordinates into its normal form, see [66], and expressing the result in polar coordinates, we may then assume a system of the form:

$$\dot{r} = (d\lambda + ar^2)r \tag{3.6.1}$$

$$\dot{\theta} = \omega + c\lambda + br^2 \tag{3.6.2}$$

where a, b, c, d are constant coefficients.

Theorem 3.6.0.5 *Let the differential equation* (2.2.1) *with* $\lambda \in \mathbb{R}$ *be given. Suppose there is an equilibrium* (x_0, λ_0) *satisfying the following conditions:*

1. *The spectrum of* f_x^0 *has only one simple pair of pure imaginary eigenvalues* $\mu_{1,2} = \pm i\omega$, *with* $\omega \neq 0$, *on the imaginary axis. (Then the equilibrium, and hence its eigenvalues* $\mu_{1,2}$, *vary smoothly with* λ : $\mu_{1,2} = \mu_{1,2}(\lambda) := \Re(\mu(\lambda)) + i\Im(\mu(\lambda))$ *and* $\mu_{1,2}(\lambda_0) = \pm i\omega$.)

2. $\frac{dRe(\mu)}{d\lambda}(\lambda_0) := d \neq 0$.

Then the Taylor expansion of degree 3 *of the system restricted on its centre manifold, brought into normal form and expressed in polar coordinates, is given by* (3.6.1), (3.6.2). *Furthermore, if in* (3.6.1) $a \neq 0$, *then there exists a (locally) unique branch of hyperbolic periodic solutions* $\gamma = \gamma(\lambda)$ *tangent to the parabola* $\lambda = -ar^2/d$. *Moreover, suppose that all other eigenvalues of* f_x^0 *have negative real parts. If* $a < 0$, *then these periodic orbits are asymptotically stable. In case* $d < 0$, *they appear for* $\lambda < \lambda_0$,

while, in case $d > 0$, they appear for $\lambda > \lambda_0$. If, on the other hand, $a > 0$, then these periodic orbits are unstable. In case $d < 0$, they appear for $\lambda > \lambda_0$ and, in case $d > 0$ they appear for $\lambda < \lambda_0$.

Note that even in two-dimensional systems the reduction and transformation of the original vector field into the form (3.6.1) generally involves tremendous calculations. However, assuming the system is given in the form:

$$\dot{x} = -\omega y + k(x,y) \tag{3.6.3}$$

$$\dot{y} = \omega x + g(x,y), \tag{3.6.4}$$

then in [66] one finds the following formula for the "stability coefficient" a:

$$\begin{aligned} a = & \frac{1}{16}\left\{k^0_{xxx} + k^0_{xyy} + g^0_{xxy} + g^0_{yyy}\right\} + \frac{1}{16\omega}\left\{k^0_{xy}\left(k^0_{xx} + k^0_{yy}\right)\right\} \\ & + \frac{1}{16\omega}\left\{-g^0_{xy}\left(g^0_{xx} + g^0_{yy}\right) - k^0_{xx}g^0_{xx} + k^0_{yy}g^0_{yy}\right\}. \end{aligned} \tag{3.6.5}$$

Example 3.6.0.15 Examples of (subcritical) Hopf bifurcations are, for instance, provided by the famous Lorenz equations (see, for instance, [117], [52], [76], [133], [134], [173]):

$$\begin{aligned} \dot{x} &= \sigma(y - x) \\ \dot{y} &= rx - y - xz \\ \dot{z} &= xy - bz \end{aligned} \tag{3.6.6}$$

where σ, r and b are parameters. It is well known [120] that the symmetric equilibria branches $(x_{\text{br}}, y_{\text{br}}, z_{\text{br}}) := (\pm c_{\text{br}}, \pm c_{\text{br}}, r-1)$ with $c_{\text{br}} := \sqrt{b(r-1)}$ undergo a subcritical Hopf bifurcation at $r = r_H := \frac{\sigma(\sigma+b+3)}{\sigma-b-1}$ for $\sigma = 10$ and $b = 8/3$. In fact, in [182] it is proven that the function $r_H(\sigma, b)$ always leads to a subcritical Hopf bifurcation in the physical parameter range $\sigma > b + 1$ and $b > 0$. For pictures showing the numerically computed unstable periodic orbits surrounding the equilibria we refer to [173].

Example 3.6.0.16 An example for a supercritical Hopf bifurcation is furnished by:

$$\ddot{x} - \lambda\dot{x} + x + \dot{x}^3 = 0. \tag{3.6.7}$$

After introducing $y := \dot{x}$, we can rewrite this system as a two-dimensional one. For λ increasing past $\lambda_0 := 0$, a stable and attractive periodic orbit appears surrounding the origin. For more information and pictures we refer to [180].

For a degenerate Hopf bifurcation, one (or even several) of the following conditions:

1. μ_1 is of multiplicity > 1,
2. there are other eigenvalues on the imaginary axis different from $\mu_{1,2}$,
3. the "stability coefficient" a is equal to 0,
4. the "direction coefficient" d is equal to 0,

hold, and we refer to examples presented in [66].

3.7 The Secondary Hopf Bifurcation

Let us end this chapter by considering the analog of the above theorem 3.6.0.5 in case of smooth maps $x \mapsto F(x, \lambda)$. Hence let $x_0 = F(x_0, \lambda_0)$ and assume that F_x^0 has only a pair of complex conjugate eigenvalues $\delta_{1,2} = e^{\pm ic}$, with $c \neq k\pi$, on the unit circle. If there are no other eigenvalues of modulus 1 then we may consider the map now restricted on its two-dimensional centre manifold. As a first consequence, there exists a smooth branch of fixed points $x = x(\lambda)$ with $x_0 = x(\lambda_0)$. Under the further assumptions that

$$\frac{d}{d\lambda}(|\delta(\lambda)|) \text{ at } \lambda = \lambda_0 := d \neq 0 \tag{3.7.1}$$

and

$$\delta^k \neq 1 \quad \text{for } k = 1, 2, 3, 4, \tag{3.7.2}$$

a normal form theorem for maps applies, see [66], and we may assume now that F, expressed in polar coordinates, is given by:

$$r \mapsto r + rd(\lambda - \lambda_0) + ar^3 \tag{3.7.3}$$

$$\theta \mapsto \theta + c + br^2 + \text{ higher order terms} \tag{3.7.4}$$

where a, b, c are further constant coefficients.

The Hopf theorem for maps (or Naimark-Sacker theorem or secondary Hopf theorem in case of a Poincaré map) then states, see [66]:

Theorem 3.7.0.6 *Let the above conditions on the map F hold and assume that the coefficient $a \neq 0$. Then there is (locally) a unique branch of simple closed curves*

which are invariant under F. Suppose now that F_x^0 has no other eigenvalues of unit length. If $a < 0$, then these invariant curves are (locally) attractive and in case $d < 0$ they appear for $\lambda < \lambda_0$, while they appear for $\lambda > \lambda_0$ in case $d > 0$. If, on the other hand, $a > 0$, then these invariant curves are repelling. In case $d < 0$ they appear for $\lambda > \lambda_0$, while they appear for $\lambda < \lambda_0$ in case $d > 0$.

Again it should be clear that in particular the calculation of "the stability coefficient" a requires a substantial amount of theoretical and numerical work — the more if the map F is actually a Poincaré map extracted from a higher dimensional vector field. Nevertheless, if the system has indeed been transformed and restricted to its centre manifold and is given by:

$$x_{n+1} = \cos(c)x_n - \sin(c)y_n + k(x_n, y_n) \tag{3.7.5}$$

$$y_{n+1} = \sin(c)x_n + \cos(c)y_n + g(x_n, y_n), \tag{3.7.6}$$

then in [185], [66] one finds the following formula for a:

$$a = -\Re\left\{\frac{(1-2\delta)\overline{\delta}^2}{1-\delta}\xi_{11}\xi_{20}\right\} - \frac{1}{2}|\xi_{11}|^2 - |\xi_{02}|^2 + \Re\left\{\overline{\delta}\xi_{21}\right\} \tag{3.7.7}$$

with:

$$\xi_{20} = \frac{1}{8}\left\{\left(k_{xx}^0 - k_{yy}^0 + 2g_{xy}^0\right) + i\left(g_{xx}^0 - g_{yy}^0 - 2k_{xy}^0\right)\right\} \tag{3.7.8}$$

$$\xi_{11} = \frac{1}{4}\left\{\left(k_{xx}^0 + k_{yy}^0\right) + i\left(g_{xx}^0 + g_{yy}^0\right)\right\} \tag{3.7.9}$$

$$\xi_{02} = \frac{1}{8}\left\{\left(k_{xx}^0 - k_{yy}^0 - 2g_{xy}^0\right) + i\left(g_{xx}^0 - g_{yy}^0 + 2k_{xy}^0\right)\right\} \tag{3.7.10}$$

and

$$\xi_{21} = \frac{1}{16}\left\{\left(k_{xxx}^0 + k_{xyy}^0 + g_{xxy}^0 + g_{yyy}^0\right) + i\left(g_{xxx}^0 + g_{xyy}^0 - k_{xxy}^0 - k_{yyy}^0\right)\right\}. \tag{3.7.11}$$

Let us provide examples of a supercritical secondary Hopf bifurcation and a supercritical Naimark-Sacker bifurcation (it is quite difficult to produce a "convincing" picture of an unstable invariant curve surrounding an attractive fixed point).

Example 3.7.0.17 The flow of the piecewise-linear differential equation:

$$\begin{aligned} \dot{x} &= -\lambda f(y-x) \\ \dot{y} &= -f(y-x) - z \\ \dot{z} &= y \end{aligned} \tag{3.7.12}$$

with $f(u) := -au + \frac{1}{2}(a+b)(|u+1| - |u-1|)$ exhibits a supercritical secondary Hopf bifurcation for $a = 0.07$, $b = 0.1$ and $\lambda_0 \approx 1.0$. For pictures showing the stable periodic orbit at $\lambda = 0.5$ and the attractive two-torus at $\lambda = 2.0$ we refer to [26]. We note that the bifurcation value for λ is not given precisely — a hint on the complexity of the necessary calculations.

A supercritical Naimark-Sacker bifurcation involving a two-dimensional map can be found in [66]:

Example 3.7.0.18 Consider the map:

$$\begin{aligned} x &\mapsto y \\ y &\mapsto \lambda y(1-x). \end{aligned} \tag{3.7.13}$$

For $\lambda_0 = 2$ the linear part of the equilibrium $(\frac{\lambda-1}{\lambda}, \frac{\lambda-1}{\lambda})$ has eigenvalues $\delta_{1,2} = e^{\pm i\pi/3}$. In this "simple" example the calculations leading to the coefficients a and d can be performed exactly. The results $d = 1 \neq 0$ and $a = \frac{\sqrt{3}-7}{4} < 0$ imply the existence of an attractive invariant closed curve surrounding the unstable fixed point $(x, y) = (\frac{1}{2}, \frac{1}{2})$. For diagrams showing this behaviour we refer to [180].

The difficulties, even in the construction of "artificial" examples of degenerate secondary Hopf or Naimark-Sacker bifurcations with additional eigenvalues on the unit circle, are mostly due to the fact that one necessarily needs higher dimensions. Then one is quickly led to nonlinear algebraic systems that can no longer be solved analytically. Already in two dimensions this fact is of course true in order for $a = 0$ or $d = 0$ to hold. In fact, we do not know of any explicit model which has, firstly, been rigorously proven to undergo a degenerate secondary Hopf bifurcation, and, secondly, been fully analyzed in a neighbourhood of λ_0. However, in a subsequent chapter we shall provide examples of Poincaré maps where numerical results indicate a 0 direction coefficient d.

We emphasize that these problems still lack complete and thoroughly satisfactory understanding. In particular when, in this connection, "global" bifurcations are to be considered as well, one is frequently confined to numerical experiments and conjectures based upon their results, see [66], [109], [49], [67], [88], [96].

Chapter 4

The Model

In this chapter we introduce the particular physical model that will serve as an example in order to demonstrate the performance of our various algorithms.

The model arises in laser optics. It describes a unidirectional (ring) cavity filled with a medium of homogeneously broadened two-level atoms and driven by an external coherent optical signal. Considering only the single mode case, applying the plane-wave approximation and taking the mean-field limit, one simplifies the Maxwell-Bloch equations and reduces them to, see [54], [55]:

$$\begin{aligned} \frac{dz}{dt} &= -k[(1+i\Theta)z - Y + 2cp] \\ \frac{dp}{dt} &= zD - (1+i\Delta)p \\ \frac{dD}{dt} &= -\gamma[(z^*p + zp^*)/2 + D - \sigma]. \end{aligned} \tag{4.0.1}$$

Here $z = z_1 + i\,z_2$ and $p = p_1 + i\,p_2$ are the complex valued output field and the atomic polarization, and D is the normalized real valued population difference between the 2 atomic levels. The parameter Y represents the normalized amplitude of the external field — it is assumed to be real and positive. $\sigma = -1$ corresponds to an active medium, while $\sigma = 1$ corresponds to a passive one (or optical bistability). Furthermore, γ stands for the longitudinal decay rate and k is the cavity linewidth (both quantities are assumed to be rescaled by the transverse relaxation rate $\gamma_\perp$). If the frequencies of the external field, the cavity and the atoms are denoted by ω_o, ω_c and ω_a, then the two detuning parameters Δ and Θ are defined as:

$$\Delta := \frac{(\omega_a - \omega_o)}{\gamma_\perp} \text{ and } \Theta := \frac{(\omega_c - \omega_o)}{k\gamma_\perp}. \tag{4.0.2}$$

Finally, c is called the "cooperativity parameter". In the case $\sigma = 1$, it acts as a bistability parameter. Then the unique equilibrium branch:

$$\begin{aligned} Y &= |z_s|\Big\{[1 + \frac{2c\sigma}{1+\Delta^2+|z_s|^2}]^2 + [\Theta - \frac{2c\Delta\sigma}{1+\Delta^2+|z_s|^2}]^2\Big\}^{1/2} \\ D_s &= \frac{(1+\Delta^2)\sigma}{1+\Delta^2+|z_s|^2} \\ p_s &= \frac{(1-i\,\Delta)z_s\sigma}{1+\Delta^2+|z_s|^2} \end{aligned} \tag{4.0.3}$$

develops into an S-shape in the $Y, |z_s|$ plane for c exceeding a critical value $c_{\text{crit}} = c_{\text{crit}}(\Delta, \Theta)$, [55]. Let us separate the real and imaginary part of (4.0.1). Then we arrive at the model $\dot{x} = f(x, \lambda)$ with:

$$\begin{aligned} \dot{x}_1 &= -k(x_1 - \Theta x_2 - Y + 2cx_3) \\ \dot{x}_2 &= -k(x_2 + \Theta x_1 + 2cx_4) \\ \dot{x}_3 &= x_1x_5 - x_3 + \Delta x_4 \\ \dot{x}_4 &= x_2x_5 - \Delta x_3 - x_4 \\ \dot{x}_5 &= -\gamma(x_1x_3 + x_2x_4 + x_5 - \sigma) \end{aligned} \tag{4.0.4}$$

and $x := (z_1, z_2, p_1, p_2, D) \in \mathbb{R}^5$, and $\lambda := (Y, \Delta, \Theta, c, k, \gamma) \in \mathbb{R}^6$ and $\sigma = \pm 1$. We remark that the vector field f is analytic and only "mildly" nonlinear.

It is interesting to note that the particular choice of $\lambda = (0, 0, 0, c, k, \gamma, -1)$ splits the system (4.0.4) into an uncoupled three-dimensional one equivalent to the famous Lorenz equations [117], [54]. Then, having the immense richness in the bifurcation structure of the latter system in mind, for example [173], [133], [134], [52], one should not be too surprised when finding related results in (4.0.4). However, the three-parameter Lorenz equations, one of the most extensively studied nonlinear systems of ordinary differential equations, even today still poses many open questions that cannot be answered with mathematical rigour. A fortiori, we therefore cannot expect a thorough and satisfactory understanding of the seven parameter laser system (4.0.4). In fact, this system is far from being fully understood, [54], [55].

We would also like to mention that it has not been proven that every trajectory in the laser system exists for all positive times nor that it remains bounded. However, this is true for the Lorenz equations, and the results in [54], [55] and our numerical experience strongly indicates it in the case of system (4.0.4) as well.

As a further remark, we note that the vector field governing (4.0.4) is dissipative, i.e. its divergence is negative: $\operatorname{div} f = -2k - 2 - \gamma < 0$, independently of x and the other parameters $Y, \Delta, \Theta, c, \sigma$. Applying the transport theorem 2.2.1.2, we see that any volume in $\mathbb{R}^5$ shrinks exponentially with the flow. Of course, it does not follow that each direction contracts. But every equilibrium point (periodic orbit) possesses a stable manifold of dimension at least one (two). Furthermore, while in the dissipative Lorenz equations the three-dimensional phase space prohibits an attractive two-torus, in case of the laser system the negative divergence alone does not contradict such an attractor from occurring. Attractive two-tori and three-tori may very well exist in a five-dimensional phase space.

In order to compare our results with the ones in [54], [55], we confine ourselves from now on to the optical bistability case, that is $\sigma = 1$. Moreover, we exclusively chose $k = 0.5$ and $\gamma = 2$ and, with the exception of Figs. 6.7 and 6.8, $c = 500$. There is nothing special about these values though — they merely enable a comparison with the results presented in Figs. 3a,..., 3e in [54]. The remaining three components of λ, i.e. Y, Δ, Θ, will still give more than enough parameter space to explore.

The equilibria behaviour of (4.0.4) has been extensively studied for the physical interesting parameter range ($10 \prec c < 10^3, 10^{-2} < \gamma < 2, 10^{-2} < k < 10$) and Δ, Θ from 0 to the "tens" in [54], [55]. In particular, for $\sigma = 1$ and a wide range of the remaining parameters, the occurring Hopf bifurcations were classified into sub- and supercritical ones. To distinguish among the cases the stability coefficient a was computed and, based upon a change of its sign, degenerate Hopf bifurcations of codimension two were detected. A similar analysis was carried out for the saddle-nodes of equilibria. Again, based upon verifying a degeneracy in the remaining conditions, codimension-two bifurcations involving hysteresis points and additional eigenvalues of f_x^0 on the imaginary axis were found. The numerical observations concerning the distribution of these bifurcations in parameter space let these authors then suggest and speculate where chaotic behaviour is more likely to occur and how its existence may be affected by changing a relevant parameter. However, their results neither include periodic orbits nor allow any conclusion about them.

At this point we would also like to confirm a finding in [55], namely that the domains of attraction may have very complicated boundaries and that slight, in fact very slight, changes in the initial conditions may lead the trajectory to a different attractor, see here our Figs. 7.12, 7.13 and 7.14.

The deepest systematic study with respect to multi-codimension bifurcations of an equilibrium was probably done in [32], [33]. Under special assumptions on the detuning parameters ($\Delta = -\Theta$), using centre manifold theory, tedious calculations, "MAPLE" and yet extensive numerical work to find the zeros of polynomials of degree ≤ 27, these authors were able to compute a codimension-four bifurcation point. Here a cubic saddle-node coalesces with a degenerate Hopf bifurcation point. Such an "organizing centre" is an important point, since in its close vicinity one might expect a rich variety of qualitatively distinct behaviour including chaotic motion, [66].

Leaving the equilibria, we must say that only little is known about periodic solutions and time dependent attractors — even less if their corresponding branches are not connected to equilibria via a Hopf bifurcation. In [54], [55] the brute force approach, see Subsection 5.5.1, reveals the mere existence of attractive periodic orbits and seemingly strange attractors. But a systematic study of their intervals of existence (with respect to a parameter) and of their bifurcations is still lacking.

Even though the routes to chaos via successive period-doublings as well as intermittence have been observed, an attractive invariant torus has not been detected. Also, the question concerning coexisting attractors is in no way settled. In fact, in [54], [55] the coexistence of an attractive periodic orbit and a stable equilibrium is characterized as "interesting". We quote further from [55] "it is a great surprise that one may find three attractors apart from that of the stationary solution", and "... a striking property of the system (4.0.4); namely, a stable pulsation can exist even if no instability of the stationary solution occurs".

Besides these stimulating comments, we were also motivated to choose this particular model to test our codes, since, at least in certain important circumstances, it is also sufficiently realistic to admit an experimental comparison (and indeed verification!) of theoretically and numerically obtained results, [115], [135], [116]. This, in turn, may lead to immediate practical use in the design of optical bistable devices.

Finally, system (4.0.4) is of more theoretical importance, since it proves to be another suitable example demonstrating the richness in the bifurcation structure of nonlinear dynamical systems.

Chapter 5

Continuation Methods and Bifurcations

"Bifurcation theory is a method for finding interesting solutions to nonlinear equations by tracking dull ones and waiting for them to loose stability", [179] — this is precisely what this chapter is about. We outline some general ideas of continuation methods and describe in detail the pseudo-arclength continuation method to "track a dull" (in the sense of "known") solution of a parameter dependent equation. Then we explain how to detect, accurately approach and characterize certain bifurcations. This involves, in particular, stability analysis and the determination of tangents to "interesting" (in the sense of "new") bifurcating solution branches. As a particular case, we then introduce the Poincaré map method to find and follow periodic orbits in autonomous ordinary differential equations. The chapter concludes by discussing some schemes concerning branch switching and step length control.

Consider the equation $f(x,\lambda) = 0$ with $f : \mathbb{R}^n \times \mathbb{R}^p \longrightarrow \mathbb{R}^n$ sufficiently smooth and assume a known solution (x_0, λ_0) to it. Introducing $y = (x,\lambda) \in \mathbb{R}^{n+p}$ we also sometimes simplify the notation and consider $f(y) = 0$ with $y_0 = (x_0, \lambda_0)$ the known (initial) solution. The function f could be a flow generating vector field as in (2.2.1) or, in case we are concerned with maps (2.3.2), in particular Poincaré maps, see definition 2.2.3.5, it could also describe its fixed points or 2-periodic orbits by setting $f := F - \mathrm{id}$, respectively $f := F \circ F - \mathrm{id}$. However, for the subsequent analysis this is irrelevant.

The regular solution manifold:

$$M_{\mathrm{reg}} := \{(x,\lambda) \in \mathbb{R}^n \times \mathbb{R}^p | f(x,\lambda) = 0 \text{ and } \mathrm{rank}[f_x(x,\lambda)\ f_\lambda(x,\lambda)] = n\} \qquad (5.0.1)$$

is then a p-dimensional, differentiable manifold in $\mathbb{R}^n \times \mathbb{R}^p$ without boundary. In general though, M_{reg} is only a strict subset of the general solution manifold:

$$M_{\text{gen}} := \{(x, \lambda) \in \mathbb{R}^n \times \mathbb{R}^p | f(x, \lambda) = 0\}. \tag{5.0.2}$$

Assuming that the initial solution $y_0 = (x_0, \lambda_0)$ is in M_{reg}, continuation methods try to approximate that connected component of M_{gen} containing $y_0 = (x_0, \lambda_0)$. In case $p = 1$ this reduces to calculating sequences of points $y_N = (x_N, \lambda_N), N = 1, 2, 3 \ldots$, along one (or several) one-dimensional solution paths that will in general intersect each other.

Even though the vast majority of continuation software packages treat this latter case $p = 1$, there has been some progress in case of higher dimensional solution manifolds, see [150], [5]. However, for the purpose of this chapter it is sufficient to consider from now on the case $p = 1$.

In what follows, we will closely follow the ideas outlined in [4], [26], [42], [90], [91], [104], [149], [163], [165]. The interested reader may find more specific information in the papers in [107], [108], [126], [127], [153] and [170]. Hence we are concerned here with solving:

$$f(y) = f(x, \lambda) = 0 \tag{5.0.3}$$

with $f : \mathbb{R}^n \times \mathbb{R} \longrightarrow \mathbb{R}^n$ a sufficiently smooth function of $y = (x, \lambda) \in \mathbb{R}^{n+1}$.

Definition 5.0.0.8 If a solution $y_0 = (x_0, \lambda_0)$ of (5.0.3) satisfies $\text{rank}[f_x^0] = n$, then $y_0 = (x_0, \lambda_0)$ is called a *strongly regular solution.* If $\text{rank}[f_x^0 \; f_\lambda^0] = n$, then the solution $y_0 = (x_0, \lambda_0)$ is called a *regular solution.* A connected subset of M_{reg} is called a *regular solution path* (or "*regular branch*" or "*regular curve*") if all of its points are regular.

Note that every strongly regular solution is also a regular solution. Also, a saddle-node point, see definition 3.1.0.3, satisfies, in particular, $\dim \text{null}[f_x^0] = 1$ and $f_\lambda^0 \notin \text{Range}[f_x^0]$, so that it still corresponds to a regular solution point. We see that in the regular case the implicit function theorem 2.1.0.1 applies, and we can parametrize the unique solution branch across (x_0, λ_0) either as a function of λ (in the strongly regular case) or as a function of some other component of the vector x (in the regular but not strongly regular case). After possibly interchanging this particular component of x with λ, let us momentarily assume a parametrization in terms of λ: $x = x(\lambda)$.

The following problem arises then: how to proceed from $y_0 = (x_0, \lambda_0)$ in order to efficiently compute different points $y_N = (x_N, \lambda_N)$, for $N = 1, 2, \ldots$, along the same regular solution path and how to detect possible bifurcations.

One "trivial" idea would simply be: take a "small" ϵ, fix $\lambda_N := \lambda_0 + N\epsilon$, use Newton's method with initial guess $x_N := x_{N-1}$ to solve $f(x_N, \lambda_N) = 0$ for x_N and iterate this process for $N = 1, 2, 3, \ldots$. However, without changing the parametrization, this method obviously fails at all most general bifurcation points, in particular at regular saddle-node points. Also, the convergence of Newton's method relies on a sufficiently close initial guess, and, as it will turn out soon, one can predict the next solution x_N much better than by simply taking the previous one, x_{N-1}.

5.1 The Pseudo-Arclength Continuation

To be able to follow a regular branch around a saddle-node point we do not fix λ at all but treat it as an additional variable. Since we then have n equations in $(n+1)$ unknowns, we need to impose one more condition on the next solution point y_{N+1}. One way to do this is by requiring $y_{N+1} = (x_{N+1}, \lambda_{N+1})$ to lie in a hyperplane perpendicular to the tangent line along the solution branch in the current point $y_N = (x_N, \lambda_N)$ and "close" to it. To be specific, let $(x(s), \lambda(s))$ be the arclength parametrization (3.2.5), (3.2.6) of the regular solution branch:

$$f(x(s), \lambda(s)) = 0 \tag{5.1.1}$$

with:

$$\|\dot{x}(s)\|_2^2 + |\dot{\lambda}(s)|^2 = 1, \tag{5.1.2}$$

and $y(0) = (x(0), \lambda(0)) = y_N = (x_N, \lambda_N)$ the previous solution and the "dot" denoting derivative with respect to the arclength "s". With $\dot{y}_N = \dot{y}(0) = (\dot{x}(0), \dot{\lambda}(0)) = (\dot{x}_N, \dot{\lambda}_N)$, the (normalized) tangent at the previous point, the additional condition can then be formulated as:

$$< x_{N+1} - x_N, \dot{x}_N > + (\lambda_{N+1} - \lambda_N)\dot{\lambda}_N - \delta s = 0, \tag{5.1.3}$$

where δs is a fixed but "small" increment in the arclength parameter s. Hence, we predict the new solution $y_{N+1} = (x_{N+1}, \lambda_{N+1})$ in the direction of the tangent to the current solution at distance δs from the previous one $y_N = (x_N, \lambda_N)$:

$$x_{N+1}^0 \approx x_N + \delta s \dot{x}_N \quad \text{and} \quad \lambda_{N+1}^0 \approx \lambda_N + \delta s \dot{\lambda}_N, \tag{5.1.4}$$

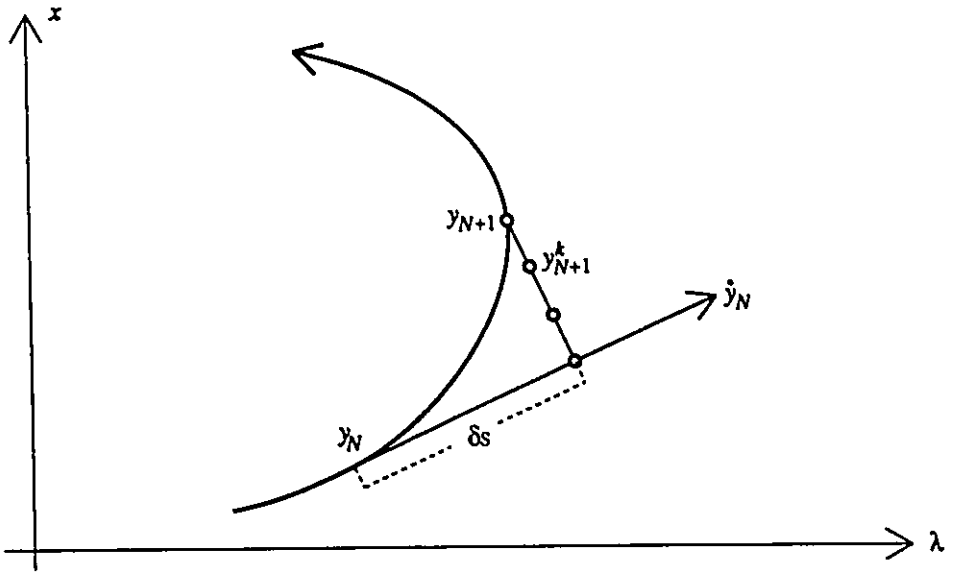

Figure 5a: The pseudo-arclength continuation method.

see Fig. 5a. For obvious reasons some authors refer to this type of predictor as "Euler predictor". It agrees to first order with the solution, see [16]. Hence, to find the next point $y_{N+1} = (x_{N+1}, \lambda_{N+1})$, the pseudo-arclength continuation method solves the augmented system $g(y_{N+1}) = 0$:

$$f(x_{N+1}, \lambda_{N+1}) = 0 \tag{5.1.5}$$

$$< x_{N+1} - x_N, \dot{x}_N > + (\lambda_{N+1} - \lambda_N)\dot{\lambda}_N - \delta s = 0 \tag{5.1.6}$$

for y_{N+1} with an initial guess for a corrector scheme given by (5.1.4). It remains to compute the tangential direction $\dot{y}_N = (\dot{x}_N, \dot{\lambda}_N)$. By differentiating (5.1.1) with respect to s we find at first:

$$f_x(x(s), \lambda(s))\dot{x}(s) + f_\lambda(x(s), \lambda(s))\dot{\lambda}(s) = 0. \tag{5.1.7}$$

At $s = 0$, equation (5.1.7) reduces to the homogeneous linear system:

$$f_x^N \dot{x}_N + f_\lambda^N \dot{\lambda}_N = 0. \tag{5.1.8}$$

Since $\text{rank}[f_x^N \; f_\lambda^N] = n$, the system (5.1.8) together with the normalization:

$$\|\dot{x}_N\|_2^2 + |\dot{\lambda}_N|^2 = 1 \tag{5.1.9}$$

has the solutions $\pm\dot{y}_N = \pm(\dot{x}_N, \dot{\lambda}_N)$, unique up to orientation.

In summary, the pseudo-arclength continuation method consists essentially of the following steps:

1. Choose a steplength δs and the proper orientation of the normalized current tangent vector $\dot{y}_N = (\dot{x}_N, \dot{\lambda}_N)$.

2. Predict the next solution point $y_{N+1} = (x_{N+1}, \lambda_{N+1})$ by performing an initial guess $y^0_{N+1} = (x^0_{N+1}, \lambda^0_{N+1})$:

$$x^0_{N+1} \approx x_N + \delta s \dot{x}_N \quad \text{and} \quad \lambda^0_{N+1} \approx \lambda_N + \delta s \dot{\lambda}_N. \tag{5.1.10}$$

3. Correct the predicted values $y^0_{N+1} = (x^0_{N+1}, \lambda^0_{N+1})$, for instance by Newton's method:

$$\begin{pmatrix} x^k_{N+1} \\ \lambda^k_{N+1} \end{pmatrix} = \begin{pmatrix} x^{k-1}_{N+1} \\ \lambda^{k-1}_{N+1} \end{pmatrix} - \begin{pmatrix} \delta^{k-1}_x \\ \delta^{k-1}_\lambda \end{pmatrix}, \tag{5.1.11}$$

where $(\delta^{k-1}_x, \delta^{k-1}_\lambda) =: z$ solves $A^{k-1}z = b^{k-1}$ with A^{k-1} defined as:

$$\begin{pmatrix} f_x(x^{k-1}_{N+1}, \lambda^{k-1}_{N+1}) & f_\lambda(x^{k-1}_{N+1}, \lambda^{k-1}_{N+1}) \\ \dot{x}_N & \dot{\lambda}_N \end{pmatrix} \tag{5.1.12}$$

and b^{k-1} defined as:

$$\begin{pmatrix} f(x^{k-1}_{N+1}, \lambda^{k-1}_{N+1}) \\ < x^{k-1}_{N+1} - x_N, \dot{x}_N > + (\lambda^{k-1}_{N+1} - \lambda_N)\dot{\lambda}_N - \delta s \end{pmatrix}. \tag{5.1.13}$$

Now, after $y_{N+1} = (x_{N+1}, \lambda_{N+1})$ has been found by employing Newton's method, then $\dot{y}_{N+1} = (\dot{x}_{N+1}, \dot{\lambda}_{N+1})$, the tangential direction at $(x_{N+1}, \lambda_{N+1}) = y_{N+1}$, solves in particular:

$$f^{N+1}_x \dot{x}_{N+1} + f^{N+1}_\lambda \dot{\lambda}_{N+1} = 0. \tag{5.1.14}$$

But, fortunately, the matrix $[f^{N+1}_x \; f^{N+1}_\lambda]$ is readily available since it simply constitutes the upper $(n \times n+1)$ submatrix of the latest Jacobian matrix (5.1.12) in the iteration process to find $y_{N+1} = (x_{N+1}, \lambda_{N+1})$. This is certainly a very convenient feature of the pseudo-arclength continuation method since the additional cost to find the next predictor remains low.

A little caution must be taken, however, when choosing the sign in the next tangent $\pm\dot{y}_{N+1} = \pm(\dot{x}_{N+1}, \dot{\lambda}_{N+1})$. Since we want to preserve the initially chosen orientation along the branch, it is natural to choose the sign such that the next tangent vector always encloses an angle θ with the previous one satisfying $0 \leq \theta \leq \pi/2$. The

package AUTO in [42] for instance fulfills this condition by normalizing $\dot{y}_{N+1}$ with respect to $\dot{y}_N$: $< \dot{x}_{N+1}, \dot{x}_N > + \dot{\lambda}_{N+1}\dot{\lambda}_N = 1$. Of course, after the proper orientation has been found in this way, one must rescale $\dot{y}_{N+1} = (\dot{x}_{N+1}, \dot{\lambda}_{N+1})$ to make it of unit length.

As a simple consequence of this method we state:

Corollary 5.1.0.1 *The pseudo-arclength continuation method works along any regular solution path provided the steplength δs is sufficiently small. In particular, it does follow the unique solution branch across a saddle-node.*

Proof: Let (x_N, λ_N) be a solution point on a regular solution path that has been computed with Newton's method. Assume that the matrix: $\begin{pmatrix} f_x^N & f_\lambda^N \\ \dot{x}_N & \dot{\lambda}_N \end{pmatrix}$ is singular. Then, in particular, there is a $(v, w) \in \mathbb{R}^n \times \mathbb{R}$, $\|v\|_2^2 + w^2 = 1$, such that $< \dot{x}_N, v > + \dot{\lambda}_N w = 0$. Also, the tangent vector $(\dot{x}_N, \dot{\lambda}_N)$ satisfies: $f_x^N \dot{x}_N + f_\lambda^N \dot{\lambda}_N = 0$. Regularity implies therefore that (v, w) agrees with $(\dot{x}_N, \dot{\lambda}_N)$ up to a possibly different sign. But then:

$$0 = < \dot{x}_N, v > + \dot{\lambda}_N w = \pm(\|v\|^2 + w^2) = \pm 1 \tag{5.1.15}$$

yielding a contradiction. Hence the above matrix is regular. The Jacobian matrix in the next step from $(x_N, \lambda_N) \longrightarrow (x_{N+1}, \lambda_{N+1})$ is now: $\begin{pmatrix} f_x^{N+1} & f_\lambda^{N+1} \\ \dot{x}_N & \dot{\lambda}_N \end{pmatrix}$ and it will remain regular if δs is choosen sufficiently small. □

5.2 General Continuation Methods

The above mentioned features (1), (2), (3) of pseudo-arclength continuation are the principal elements of virtually all other methods: choose a steplength, predict and correct towards the next solution. It would be exaggerated however to claim that, independently of the specific problem under investigation, these three steps remain unchanged. In fact, there exists a variety of related methods, where these steps are specially designed to adapt to individual problems.

Let us now briefly outline how one can alter the above steps in order to adjust to a specific problem.

5.2.1 General Predictors

Suppose for instance that not only the Jacobian matrix but also the second partial derivatives of f are easily available. Then, by differentiating (5.1.7) we find:

$$\begin{aligned} 0 &= f_{xx}(x(s),\lambda(s))\dot{x}(s)\dot{x}(s) + 2f_{x\lambda}(x(s),\lambda(s))\dot{x}(s)\dot{\lambda}(s) + f_{\lambda\lambda}(x(s),\lambda(s))\dot{\lambda}^2(s) \\ &\quad + f_x(x(s),\lambda(s))\ddot{x}(s) + f_\lambda(x(s),\lambda(s))\ddot{\lambda}(s). \end{aligned} \tag{5.2.1}$$

Evaluating this expression at $s = 0$ and rearranging terms we get:

$$f_x^N\ddot{x}_N + f_\lambda^N\ddot{\lambda}_N = -f_{xx}^N\dot{x}_N^2 - 2f_{x\lambda}^N\dot{x}_N\dot{\lambda}_N - f_{\lambda\lambda}^N\dot{\lambda}_N^2. \tag{5.2.2}$$

If y_N is regular, then the general solution to (5.2.2) now reads:

$$\begin{pmatrix} \ddot{x}_N \\ \ddot{\lambda}_N \end{pmatrix} = \begin{pmatrix} \ddot{x}_p \\ \ddot{\lambda}_p \end{pmatrix} + \alpha \begin{pmatrix} \ddot{x}_{\text{hom}} \\ \ddot{\lambda}_{\text{hom}} \end{pmatrix}. \tag{5.2.3}$$

Here $(\ddot{x}_p, \ddot{\lambda}_p)$ denotes a particular solution of the underdetermined inhomogeneous linear system (5.2.2) and $(\ddot{x}_{\text{hom}}, \ddot{\lambda}_{\text{hom}})$ its homogeneous counterpart. Note that the right-hand side of (5.2.2) is a known quantity once the tangent $\dot{y}_N = (\dot{x}_N, \dot{\lambda}_N)$ has been found according to (5.1.8), (5.1.9). Furthermore, the homogeneous part can conveniently be choosen as $(\ddot{x}_{\text{hom}}, \ddot{\lambda}_{\text{hom}}) = (\dot{x}_N, \dot{\lambda}_N)$ as it also solves (5.1.8), (5.1.9). Now, by differentiating (5.1.2) and evaluating the result at $s = 0$ we have:

$$< \dot{x}_N, \ddot{x}_N > + \dot{\lambda}_N\ddot{\lambda}_N = 0, \tag{5.2.4}$$

so that $\alpha = - < \dot{x}_N, \ddot{x}_p > - \dot{\lambda}_N\ddot{\lambda}_p$. If we use $(\dot{x}_N, \dot{\lambda}_N)$ and $(\ddot{x}_N, \ddot{\lambda}_N)$, then the predictor:

$$x_{N+1}^0 \approx x_N + \delta s\,\dot{x}_N + \frac{(\delta s)^2}{2}\ddot{x}_N \quad \text{and} \quad \lambda_{N+1}^0 \approx \lambda_N + \delta s\,\dot{\lambda}_N + \frac{(\delta s)^2}{2}\ddot{\lambda}_N \tag{5.2.5}$$

will be of order 2.

Of course, the additionally imposed equation (5.1.3) for the next solution $y_{N+1} = (x_{N+1}, \lambda_{N+1})$ becomes a little more complicated. Let $\gamma(s)$ with $\gamma(0) = y_N = (x_N, \lambda_N)$ denote the parametrized curve that agrees in y_N up to second order with the parametrized solution branch $(x(s), \lambda(s))$. For a given increment δs, one must first find $s^* = s^*(\delta s)$ such that the arclength from (x_N, λ_N) along $\gamma(s)$ to $\gamma(s^*)$ equals δs. This can easily be done since the resulting integral is analytically solvable; in this case equation (5.1.3) becomes:

$$< y_{N+1} - y_N - s^*\dot{y}_N - \frac{(s^*)^2}{2}\ddot{y}_N, \dot{y}_N + s^*\ddot{y}_N >= 0. \tag{5.2.6}$$

Unfortunately, the availability of the Jacobian matrix (and, even more, of the second derivatives) depends on the nature of f. Even worse, their evaluation consumes easily and frequently 90% or more of the overall costs (regarding computing time and storage). If one merely continues an equilibrium branch of (2.2.1), then the second order predictor approach is still a manageable choice. But if f is not given in a "nice" analytic form, but contains integrals, differential equations, derivatives of some other function..., then, in most cases, it will be very difficult and expensive to evaluate its second derivatives. Finally, even though higher order predictors do allow a larger steplength δs, one does not want δs to be too large in order not to skip over relevant details along the branch. They are therefore rarely encountered in practice.

Another method is based upon evaluating the secant between the last two computed points y_N and y_{N-1}. Approximating the normalized tangential direction by the normalized secant across these points leads to the predictor:

$$y_{N+1}^0 \approx y_N + \delta s(y_N - y_{N-1}). \tag{5.2.7}$$

An orientation of this scheme is naturally provided by the order in which the last two solutions y_N and y_{N-1} have been computed. If we understand $\dot{y}_N = (\dot{x}_N, \dot{\lambda}_N)$ to be such a normalized secant vector, then the extra condition (5.1.3) remains unchanged. To start this method, one must first find a second solution y_1. If $y_0 = (x_0, \lambda_0)$ is strongly regular, this can be achieved by using the trivial predictor $x_1^0 \approx x_0$ and then correcting to solve $f(x_1, \lambda^*) = 0$ with $\lambda^* := \lambda_0 + \epsilon$, ϵ "small" and fixed. Finally, we note that one can generalize the secant scheme to predict the next solution point based upon extrapolating several of the last computed points.

However, the secant predictor, also of order 1, and the tangent predictor provide probably the most widely used schemes in continuation methods.

5.2.2 General Correctors

Since the corrector's duty is to solve an $(n+1)$-dimensional equation $g(y) = 0$, we refer here mostly to the literature about solving nonlinear systems of equations, for example [36], [83], [136], [137] and [146]. If the Jacobian matrix $g_y(y)$ is easily available and relatively inexpensive to evaluate, then, as already pointed out, Newton's method will generally do a fine job. If, on the other hand, some partial derivatives are not available or too costly to evaluate, then one can approximate these derivatives by numerical differentiation.

Also, instead of evaluating the Jacobian matrix at each iteration, one can keep it constant and retain its value from the first iteration. This idea yields the "Chord method".

Another approach would be to update the Jacobian matrix g_y^k at each iteration towards y_{N+1} according to Broyden's scheme [21]:

$$g_y^{k+1} = g_y^k + \frac{\left[g(y_{k+1}) - g(y_{k+1}) - g_y^k(y^{k+1} - y^k)\right]\ (y^{k+1} - y^k)^T}{\|y^{k+1} - y^k\|_2^2}, \tag{5.2.8}$$

see also [37]. Other approaches finally split the Jacobian into two matrices, the first one of which can be (inexpensively) evaluated and the latter one is not available, see [36]. In connection with continuation methods, damped Newton iterations have also been applied [16]. Here one uses only a certain δ multiple of the Newton increment. This idea turns out to be implicitly connected with the choice δs of the steplength along the branch.

Lastly we would like to mention that we obtained surprisingly good results for some specific problems by taking as an initial approximation for the Jacobian matrix in the next step the final one, with Broyden's scheme (5.2.8) updated, from the last step. This method worked very well along regular branches, in particular around saddle-nodes. However, this success is probably intrinsically related to the special nature of our function $g(y)$, since the sequence g_y^k in (5.2.8) does not necessarily converge, see [36].

As a final remark, let us emphasize again that, if we do not apply Newton's method, we no longer have the tangent as a convenient and immediate byproduct and must use other predictors.

5.3 Characterizing Bifurcations

This section provides some tools to detect, locate and characterize a bifurcation point.

5.3.1 Detecting Bifurcations

Assume $y_N = (x_N, \lambda_N) \in \mathbb{R}^{n+1}$ is a potential bifurcation point of order $k > 0$ with a tangential direction $\dot{y}_N = (\dot{x}_N, \dot{\lambda}_N)$ along an otherwise regular and smooth part of the one-dimensional general solution manifold M_{gen} of equation (5.0.3). Then let $\text{null}[f_y^N] = \text{null}[f_x^N\ f_\lambda^N] = \text{span}\{\phi_0, \phi_1, \phi_2, \ldots, \phi_k\}$ with $\phi_i \in \mathbb{R}^{n+1}$ and $\text{null}([f_y^N]^T) =$

$\text{null}([f_x^N\ f_\lambda^N]^T) = \text{span}\{\psi_1, \psi_2, \psi_3, \ldots, \psi_k\}$ with $\psi_i \in \mathbb{R}^n$. Without loss of generality, we may assume that the ϕ_i, ψ_i are normalized and:

$$\phi_0 = \dot{y}_N = \begin{pmatrix} \dot{x}_N \\ \dot{\lambda}_N \end{pmatrix} \text{ and } \phi_1 = \begin{pmatrix} \rho \in \mathbb{R}^n \\ \phi_1(n+1) \end{pmatrix}. \tag{5.3.1}$$

That is, ϕ_0 corresponds to the direction of the assumed smooth branch across $y_N = (x_N, \lambda_N)$, while the other basis vectors of $\text{null}[f_x^N\ f_\lambda^N]$ and $\text{null}([f_x^N\ f_\lambda^N]^T)$ remain as yet arbitrary.

The tangent $\dot{y}_N$ of every (possibly other) smooth solution branch across y_N now satisfies (5.1.8) and hence:

$$\dot{y}_N = \dot{y}_N(\alpha) = \sum_{i=0}^{k} \alpha_i \phi_i \tag{5.3.2}$$

with coefficients α_i to be to determined. Putting (5.3.2) into (5.2.2), using $\psi_i^T f_y^N = 0$, and imposing the "nonzero" condition $\alpha_0^2 + \alpha_1^2 \cdot \alpha_k^2 = 1$ upon $\dot{y}_N$, we arrive at the "Algebraic Bifurcation Equation" $Q(\alpha) = 0$, $Q : \mathbb{R}^{k+1} \longrightarrow \mathbb{R}^{k+1}$, in detail:

$$Q(\alpha) := \begin{pmatrix} \psi_1^T f_{yy}^N \dot{y}_N(\alpha)\dot{y}_N(\alpha) \\ \psi_2^T f_{yy}^N \dot{y}_N(\alpha)\dot{y}_N(\alpha) \\ \vdots \\ \psi_k^T f_{yy}^0 \dot{y}_N(\alpha)\dot{y}_N(\alpha) \\ \sum_{i=0}^{k} \alpha_i^2 - 1 \end{pmatrix} = 0 \tag{5.3.3}$$

Equation (5.3.3) must necessarily be satisfied for every smooth solution branch across the bifurcation point y_N. Note that $\dot{y}_N$ in (5.3.2) is in general not normalized, since the ϕ_i do not necessarily form an orthonormal basis. But, once a solution $\alpha \neq 0$ of (5.3.3) has been found, we can always rescale the corresponding tangent such that $\|\dot{y}_N\|_2 = 1$.

To obtain sufficient conditions, we quote from [85]:

Theorem 5.3.1.1 *If $\alpha \in \mathbb{R}^{k+1}$ fulfills the algebraic bifurcation equation* (5.3.3) *and in addition the "isolated root condition":*

$$\det\left(\frac{\partial Q}{\partial \alpha}(\alpha)\right) \neq 0, \tag{5.3.4}$$

then there exists a unique smooth solution branch of (5.0.3) *across y_N with tangential direction* (5.3.2). □

It is now easy to see that the Jacobian matrix g_y^N in the pseudo-arclength continuation method necessarily becomes singular at a potential bifurcation point y_N. Of course, its determinant does not necessarily have to transversally cross 0 (i.e. has a simple root), see the examples involving secondary Hopf bifurcations at strong resonance in Chapter 7, Subsection 7.4.2.

From [85] we now have that the pseudo-arclength continuation will "jump" over y_N from y_{N-1} if $\alpha = (1, 0, 0, \ldots, 0)$, corresponding to the tangent $\dot{y}_N = \phi_0$, satisfies condition (5.3.4) and the steplength δs is sufficiently small, i.e. the predictor based upon $\dot{y}_{N-1}$ is within "the convergence cone" of Newton's method. Hence, monitoring the sign of the determinant of the Jacobian matrix:

$$g_y^N = \begin{pmatrix} f_y(y_N) \\ \dot{y}_{N-1} \end{pmatrix} = \begin{pmatrix} f_x^N & f_\lambda^N \\ \dot{x}_{N-1} & \dot{\lambda}_{N-1} \end{pmatrix} \tag{5.3.5}$$

within the continuation will at least detect those potential bifurcation points $y_N = (x_N, \lambda_N)$ where its corresponding determinant changes sign. This "test function", namely the determinant of the Jacobian matrix, is probably the most widely used one. Depending on the specific problem, and in particular on its size, one can alternatively solve for the smallest eigenvalue or check for rank deficiency. Another idea is presented in [168].

On the other hand, if this determinant only touches 0 (i.e. has a higher order root), then one clearly needs a more sophisticated test — for example, one involving the derivative of the determinant with respect to arclength.

Anyway, once a test function has indicated that a potential bifurcation point has been enclosed, one can use the secant scheme, the bisection method, or the regula falsi method to approach it more accurately.

5.3.2 Recognizing Simple Strict Bifurcation Points

Let us confine ourselves now to simple potential bifurcation points, that is $k = 1$. We may then rewrite the algebraic bifurcation equation (5.3.3) as:

$$0 = \begin{pmatrix} \psi_1^T f_y^N (\alpha\phi_0 + \beta\phi_1)^2 \\ \alpha^2 + \beta^2 - 1 \end{pmatrix} = \begin{pmatrix} c_{11}\alpha^2 + 2c_{12}\alpha\beta + c_{22}\beta^2 \\ \alpha^2 + \beta^2 - 1 \end{pmatrix}, \tag{5.3.6}$$

with $c_{ij} := \psi_1^T f_{yy}^N \phi_{i-1}\phi_{j-1}$ or, upon using notation (5.3.1):

$$c_{11} = \psi_1^T \left(f_{xx}^N \dot{x}_N \dot{x}_N + 2 f_{x\lambda}^N \dot{x}_N \dot{\lambda}_N + f_{\lambda\lambda}^N \dot{\lambda}_N \dot{\lambda}_0 \right) \tag{5.3.7}$$

$$c_{12} = \psi_1^T \left(f_{xx}^N \dot{x}_N \rho + f_{x\lambda}^N \dot{\lambda}_N \rho + f_{x\lambda}^N \dot{x}_N \phi_1(n+1) + f_{\lambda\lambda}^N \dot{\lambda}_N \phi_1(n+1) \right) \tag{5.3.8}$$

$$c_{22} = \psi_1^T \left(f_{xx}^N \rho\rho + 2 f_{x\lambda}^N \rho\phi_1(n+1) + f_{\lambda\lambda}^N \phi_1(n+1)\phi_1(n+1) \right). \tag{5.3.9}$$

The isolated root condition (5.3.4) now reads:

$$\det \begin{pmatrix} 2\alpha c_{11} + 2\beta c_{12} & 2\alpha c_{12} + 2\beta c_{22} \\ 2\alpha & 2\beta \end{pmatrix} \neq 0. \tag{5.3.10}$$

Note that if dim null$[f_x^N] = 1$, then $f_\lambda^N \in$ Range$[f_x^N]$ and we may choose $\psi_1 = \psi = w$ the left eigenvector of f_x^N corresponding to the eigenvalue 0.

By our assumption of at least one solution branch, the one we are currently continuing, with direction $\dot{y}_N$ across y_N and our particular choice of $\phi_0, \phi_0 = \dot{y}_N$, we see that the coefficients $(\alpha, \beta) = (\alpha_1, \beta_1) = (1, 0)$ must satisfy (5.3.6) and therefore:

$$c_{11} = 0. \tag{5.3.11}$$

Consequently (α_1, β_1) fulfills the isolated root condition (5.3.10) if and only if:

$$c_{12} \neq 0. \tag{5.3.12}$$

Putting (5.3.11) in (5.3.6) we further have:

$$\beta(2c_{12}\alpha + c_{22}\beta) = 0. \tag{5.3.13}$$

Hence, if $c_{12} \neq 0$ holds, then a unique second, distinct (up to orientation), real solution of the algebraic bifurcation equation (5.3.11) exists with:

$$(\alpha, \beta) = (\alpha_2, \beta_2) = \left(\frac{-c_{22}}{\sqrt{c_{22}^2 + 4c_{12}^2}}, \frac{2c_{12}}{\sqrt{c_{22}^2 + 4c_{12}^2}} \right), \tag{5.3.14}$$

and it is straightforward to show that (α_2, β_2) satisfies the isolated root condition (5.3.10) as well. We thus recognize y_N as a strict bifurcation point with precisely two emanating branches with distinct tangents across it. The condition (5.3.12) is therefore sometimes called a "strict bifurcation condition for simple bifurcation from another (trivial) branch". In the case $\dot{\lambda}_N \neq 0$, we may choose $\phi_1 = (v^T, 0)^T$, where v is the right eigenvector corresponding to the eigenvalue 0 of f_x^N, and $\psi_1 = w$ since dim null$[f_y^N] = 2$ and $f_\lambda^N \in$ Range$[f_x^N]$. Then formulae (5.3.8), (5.3.12) reduce to:

$$c_{12} = w^T \left(f_{xx}^N \dot{x}_N + f_{x\lambda}^N \dot{\lambda}_N \right) v \neq 0, \tag{5.3.15}$$

which is essentailly the bifurcation condition given in [29].

Now, the Jacobian matrix g_y^N, being singular, has a one-dimensional nullspace since by definition each nullvector of g_y^N is necessarily contained in the span of $\{\phi_0, \phi_1\}$ and perpendicular to ϕ_0. Under the more stringent condition that 0 is also an algebraically simple eigenvalue of g_y^N, we now proceed to prove that the pseudo-arclength continuation method has indeed the power to locate such a bifurcation point.

Theorem 5.3.2.1 *Suppose y_N is a simple potential bifurcation point along the otherwise regular and smooth solution branch "C" with $c_{12} \neq 0$ (hence a strict bifurcation point). If additionally $\kappa(0) = \kappa_0 = 0$ is an algebraically simple eigenvalue of g_y^N, then the determinant of $g_y(y)$ does transversally cross 0 along C at the solution $y = y_N$.*

Proof: Since 0 is an algebraically simple eigenvalue of g_y^N, we may consider the parametrized eigenvalue-eigenvector relation:

$$g_y(y(s))\Phi(s) = \kappa(s)\Phi(s) \quad \text{and} \quad \|\Phi(s)\|_2 = 1 \tag{5.3.16}$$

in a neighbourhood of $s = 0$ along C. Differentiating (5.3.16) with respect to s and evaluating the result at $s = 0$ yields:

$$g_{yy}^0 \dot{y}_N \Phi(0) + g_y^N \dot{\Phi}(0) = \dot{\kappa}_0 \Phi(0) + \kappa_0 \dot{\Phi}(0). \tag{5.3.17}$$

Using $\kappa(0) = \kappa_0 = 0$, $\dot{y}_N = \phi_0$ and multiplying (5.3.17) from the left with the left nullvector of g_y^N, $(\psi_1, 0)$, we arrive at:

$$(\psi_1^T, 0) g_{yy}^N \phi_0 \Phi(0) = (\psi_1^T, 0)\dot{\kappa}_0 \Phi(0). \tag{5.3.18}$$

Now, $\Phi(0)$, being in $\text{span}\{\phi_0, \phi_1\}$ with additionally $\Phi(0) \perp \phi_0$ and $\|\Phi(0)\|_2 = 1$ can readily be expressed as: $\Phi(0) = \frac{1}{\sqrt{1-c^2}}\phi_1 - \frac{c}{\sqrt{1-c^2}}\phi_0$ with $c := \phi_1^T \phi_0 \neq \pm 1$. Noting that $(\psi_1^T, 0)\Phi(0) \neq 0$ since 0 is a simple root of $\det(g_y^N)$, and using $c_{11} = 0$, we conclude:

$$\begin{aligned} \dot{\kappa}_0 &= \frac{(\psi_1^T, 0) g_{yy}^N \phi_0 \Phi(0)}{(\psi_1^T, 0)\Phi(0)} = \frac{(\psi_1^T, 0)\left(\frac{-c}{\sqrt{1-c^2}} g_{yy}^N \phi_0 \phi_0 + \frac{1}{\sqrt{1-c^2}} g_{yy}^N \phi_0 \phi_1\right)}{(\psi_1^T, 0)\Phi(0)} \\ &=: \frac{\left(\frac{-c}{\sqrt{1-c^2}} c_{11} + \frac{1}{\sqrt{1-c^2}} c_{12}\right)}{(\psi_1^T, 0)\Phi(0)} = \frac{\frac{1}{\sqrt{1-c^2}} c_{12}}{(\psi_1^T, 0)\Phi(0)} \neq 0. \quad \square \end{aligned} \tag{5.3.19}$$

For completeness we quote a related result from [85]:

Theorem 5.3.2.2 *If the determinant of $g_y(y(s))$ changes sign at $s = 0$ along a smooth and otherwise regular solution branch, then $y(0)$ is a strict bifurcation point.*

If now $c_{12} = 0$, then several other higher order degeneracies may occur. For instance, the current branch may have lost its smoothness, see example 3.4.0.12. But the possibility of two distinct smooth solution branches having the same tangent also exists, see example 3.4.0.10. Finally, $f := F \circ F - \mathrm{id}$ in example 3.5.0.14 shows that there may also be three solution branches across y_N. Indeed, this example even inherits $c_{11} = c_{12} = c_{22} = 0$, and one must include higher order derivatives of f to conclude anything about possible emanating branches. The algebraic bifurcation equation (5.3.6) then becomes a homogeneous cubic polynomial typically giving rise to one or three distinct directions. In fact, this technique will be applied later in the context of degenerate period-doublings.

We emphasize again that simple potential bifurcation points are not generic in one-parameter problems. It is even more unlikely to encounter an accompanying coefficient c_{12} being 0 and still less likely the coincidence of both accompanying coefficients c_{12} and c_{22} being 0.

5.3.3 Stability

Now that we have seen how to detect bifurcations and how to find the directions of the emanating branches, we would certainly like to know something about the stability along them. Suppose, momentarily, that the vector field f generates a flow as in (2.2.1) or is related to maps (2.3.2) either by $f := F - \mathrm{id}$ or $f := F \circ F - \mathrm{id}$. Then we have:

Corollary 5.3.3.1 *Let $y_N = (x_N, \lambda_N)$ with tangential direction $\dot{y}_N = (\dot{x}_N, \dot{\lambda}_N)$ and $\kappa(0) = \kappa_0 = 0$ as an algebraically simple eigenvalue of f_x^N be a point along an otherwise regular part of the smooth solution branch and let* $\mathrm{null}[f_x^N] = \mathrm{span}\{v\}$ *and* $\mathrm{null}([f_x^N]^T) = \mathrm{span}\{w\}$.

Then the "crossing speed" of the critical eigenvalue 0 with respect to arclength in the direction $\dot{y}_N$ equals:

$$\dot{\kappa}_0 = \frac{w^T(f_{xx}^N \dot{x}_N + f_{x\lambda}^N \dot{\lambda}_N)v}{w^T v}. \tag{5.3.20}$$

Proof: Differentiate the eigenvalue-eigenvector relation:

$$f_x(x(s), \lambda(s))v(s) = \kappa(s)v(s) \quad \text{and} \quad \|v(s)\|_2 = 1 \tag{5.3.21}$$

with respect to arclength and evaluate the result at $s = 0$ to obtain:

$$(f_{xx}^N \dot{x}_N + f_{x\lambda}^N \dot{\lambda}_N)v + f_x^N \dot{v}_N = \dot{\kappa}_0 v + \kappa_0 \dot{v}_N. \tag{5.3.22}$$

Since $w^T v \neq 0$, we may now solve (5.3.22) for $\dot{\kappa}_0$ and recover (5.3.20). □

Hence, if all the remaining eigenvalues of f_x^N have negative real parts, respectively those of F_x^N are within the unit circle, and $\dot{\kappa}_0 > 0$, then the branch looses stability while it gains stability in case $\dot{\kappa}_0 < 0$. Of course, for the branch we are currently continuing, we may simply have checked the eigenvalues of $f_x(x(s))$ along it. However, formula (5.3.20) holds equally well for all possible emanating branches if (x_N, λ_N) is a simple potential bifurcation point, i.e. additionally $f_\lambda^N \in \text{Range}[f_x^N]$.

The question can be rather delicate, if $\dot{\kappa}_0 = 0$ along one branch. One way to attack these stability problems involves differentiating (5.3.21) twice. After lengthy calculations, one can find an expression for $\ddot{\kappa}_0$, which, in case it is different from 0 and all the remaining eigenvalues of f_x^N have negative real parts, respectively those of F_x^N are within the unit circle, implies a change of stability along that branch. Let us formulate the result in:

Theorem 5.3.3.1 *Let the point $y_N = (x_N, \lambda_N)$ with tangential direction $\dot{y}_N = (\dot{x}_N, \dot{\lambda}_N)$ be a simple potential bifurcation point along an otherwise regular part of the smooth solution branch. Assume further $\kappa(s)$ is an algebraically simple eigenvalue of $f_x(y(s))$ satisfying $\kappa(0) = \kappa_0 = \dot{\kappa}_0 = 0$ with $\text{null}[f_x^N] = \text{span}\{v\}$ and $\text{null}([f_x^N]^T) = \text{span}\{w\}$.*

Then formula (5.3.29) *below, with* (5.3.27), (5.3.30), (5.3.31) and (5.3.34), *gives an expression for $\ddot{\kappa}_0$. In particular, if all the other eigenvalues of f_x^N have negative real parts, respectively those of F_x^N are within the unit circle, and $\ddot{\kappa}_0 < 0$, then the branch is (locally) stable, while it is (locally) unstable in case $\ddot{\kappa}_0 > 0$.*

Proof: First of all, let us choose the second nullvector ϕ_1 of f_y^N in (5.3.1) orthonormal to the first one: $\phi_0 = \dot{y}_N = (\dot{x}_N^T, \dot{\lambda}_N)$. This is not an essential assumption, it merely facilitates the notion of an occurring linear system.

We differentiate (5.3.21) a second time to obtain:

$$\begin{aligned} \dot{\kappa}(s)v(s) + \kappa(s)\dot{v}(s) \;&=\; \Big(f_{xx}(x(s),\lambda(s))\dot{x}(s) + f_{x\lambda}(x(s),\lambda(s))\dot{\lambda}(s)\Big)v(s) \\ &\quad + f_x(x(s),\lambda(s))\dot{v}(s) \end{aligned} \tag{5.3.23}$$

and:

$$< \dot{v}(s), v(s) >= 0. \tag{5.3.24}$$

Of course, $v(0) = v$, $\dot{v}(0) = \dot{v}_0$ and $\ddot{v}(0) = \ddot{v}_0$. As $\kappa_0 = \dot{\kappa}_0 = 0$, it follows from (5.3.23) evaluated at $s = 0$:

$$f_x^N \dot{v}_0 = -\left(f_{xx}^N \dot{x}_N + f_{x\lambda}^N \dot{\lambda}_N\right) v_0. \tag{5.3.25}$$

Since $\text{null}[f_x^N] = \text{span}\{v\}$, we have next:

$$\dot{v}_0 = c_0 v_0 + p_0 \tag{5.3.26}$$

where p_0 is a particular solution of the linear inhomogeneous system (5.3.25) and c_0 is a constant yet to be determined. But, putting this into condition (5.3.24) for $s = 0$, we readily have: $c_0 = - < v, p_0 >$, so that:

$$\dot{v}_0 = - < v, p_0 > v + p_0. \tag{5.3.27}$$

Now we differentiate (5.3.23) once more, evaluate the result at $s = 0$ and use $\kappa_0 = \dot{\kappa}_0 = 0$ to get:

$$\begin{aligned} \ddot{\kappa}_0 v &= \left(f_{xxx}^N \dot{x}_N \dot{x}_N + 2 f_{xx\lambda}^N \dot{x}_N \dot{\lambda}_N + f_{xx}^N \ddot{x}_N + f_{x\lambda\lambda}^N \dot{\lambda}_N \dot{\lambda}_N + f_{x\lambda}^N \ddot{\lambda}_N\right) v \\ &\quad + 2\left(f_{xx}^N \dot{x}_N + f_{x\lambda}^N \dot{\lambda}_N\right) \dot{v}_0 + f_x^N \ddot{v}_0. \end{aligned} \tag{5.3.28}$$

Upon multiplying (5.3.28) from the left with $w = w_0 = w(0)$, we compute:

$$\begin{aligned} \ddot{\kappa}_0 &= \frac{w^T\left(f_{xxx}^N \dot{x}_N \dot{x}_N + 2 f_{xx\lambda}^N \dot{x}_N \dot{\lambda}_N + f_{x\lambda\lambda}^N \dot{\lambda}_N \dot{\lambda}_N + f_{xx}^N \ddot{x}_N + f_{x\lambda}^N \ddot{\lambda}_N\right) v}{w^T v} \\ &\quad + \frac{2 w^T\left(f_{xx}^N \dot{x}_N + f_{x\lambda}^N \dot{\lambda}_N\right) \dot{v}_0}{w^T v}. \end{aligned} \tag{5.3.29}$$

Hence, it remains to determine $\ddot{y}_N = (\ddot{x}_N, \ddot{\lambda}_N)$. From (5.2.2) we obtain:

$$\ddot{y}_N = (\ddot{x}_N, \ddot{\lambda}_N) = c_1 \phi_0 + c_2 \phi_1 + p_2, \tag{5.3.30}$$

where $\phi_0 = \dot{y}_N = (\dot{x}_N, \dot{\lambda}_N)$ and $\{\phi_0, \phi_1\}$ our basis of $\text{null}[f_y^N]$ — remember that, contrary to the hypothesis of (5.2.2), in the current setting the nullspace of $[f_y^N]$ is two-dimensional. Using (5.2.4), and $< \phi_0, \phi_1 >= 0$ in (5.3.30), we obtain:

$$c_1 = - < \phi_0, p_2 > . \tag{5.3.31}$$

Now we differentiate equation (5.2.1) once more and evaluate the result at $s = 0$:

$$\begin{aligned} 0 &= f_x^N \frac{d^3 x}{ds^3}(0) + f_\lambda^N \frac{d^3 \lambda}{ds^3}(0) + f_{xxx}^N (\dot{x}_N)^3 + 3 f_{xx\lambda}^N \dot{x}_N \dot{x}_N \dot{\lambda}_N + 3 f_{x\lambda\lambda}^N \dot{x}_N \dot{\lambda}_N \dot{\lambda}_N \\ &\quad + f_{\lambda\lambda\lambda}^N (\dot{\lambda}_N)^3 + 3 f_{xx}^N \dot{x}_N \ddot{x}_N + 3 f_{x\lambda}^N \dot{x}_N \ddot{\lambda}_N + 3 f_{x\lambda}^N \ddot{x}_N \dot{\lambda}_N + 3 f_{\lambda\lambda}^N \dot{\lambda}_N \ddot{\lambda}_N. \end{aligned} \tag{5.3.32}$$

Without loss of generality, we now assume that the coordinates of the particular solution p_2 of the linear inhomogeneous equation (5.2.2) satisfy:

$$p_2(n+1) = 0; \tag{5.3.33}$$

this is possible as dim null$[f_x^N \ f_\lambda^N] = 2$. Then, upon multiplying (5.3.32) from the left with w^T and substituting (5.3.30), we find after elementary rearrangements:

$$\begin{aligned} c_2 \ = \ & \frac{-w^T\left(f_{xxx}^N \dot{x}_N \dot{x}_N \dot{x}_N + 3f_{xx\lambda}^N \dot{x}_N \dot{x}_N \dot{\lambda}_N + 3f_{x\lambda\lambda}^N \dot{x}_N \dot{\lambda}_N \dot{\lambda}_N\right)}{3w^T f_{yy}^N \phi_0 \phi_1} \\ & - \frac{w^T\left(f_{\lambda\lambda\lambda}^N \dot{\lambda}_N \dot{\lambda}_N \dot{\lambda}_N + 3c_1 f_{yy}^N \phi_0 \phi_0 + 3f_{yy}^0 p_2 \phi_0\right)}{3w^T f_{yy}^N \phi_0 \phi_1}. \end{aligned} \tag{5.3.34}$$

□

In certain cases formulas (5.3.27), (5.3.29), (5.3.31), (5.3.34) may drastically simplify, and for the sub- and supercritical pitchfork bifurcations in example 3.3.0.8, we easily find $\ddot{\kappa}_0 = +4$ indicating unstable solutions or $\ddot{\kappa}_0 = -4$ showing that the branch is stable.

The proof of theorem 5.3.3.1 contains much more valuable information in case $\dot{\lambda}_N = 0$, i.e. the current branch touches the hyperplane $H = \{(x, \lambda_N) | \ \lambda = \lambda_N\}$:

Corollary 5.3.3.2 *Suppose $y_N = (x_N, \lambda_N)$, with tangent vector $\dot{y}_N = (\dot{x}_N, \dot{\lambda}_N)$ and $\kappa_0 = 0$ as an algebraically simple eigenvalue of f_x^N, is a simple potential bifurcation point along an otherwise regular part of the solution branch. Let* null$[f_x^N] =$ span$\{v\}$ *and* null$([f_x^N]^T) =$ span$\{w\}$. *If additionally $\dot{\lambda}_N = 0$, then:*

$$\phi_1(n+1) \neq 0 \ \text{ and } \ \ddot{\lambda}_N = c_2 \phi_1(n+1) \tag{5.3.35}$$

with c_2 as in (5.3.34).

Proof: Firstly, $\dot{\lambda}_N = 0$ implies $\dot{x}_N = v$ and therefore $\phi_0 = (v^T, 0)$. Furthermore, since $\{\phi_0, \phi_1\}$ is orthonormal and 0 is simple, $\phi_1(n+1) \neq 0$. Secondly, formula (5.3.35) follows then immediately from (5.3.30) and (5.3.33). □

If $\frac{d^n \lambda}{ds^n}(0) = 0$, then one can, of course, continue the above procedure and derive an expression for $\frac{d^{n+1}\lambda}{ds^{n+1}}(0)$. However, the formulae become quickly very complicated, since they require derivatives of f of the order $(n+2)$. But should f be given in a "nice" analytical form, then one could possibly attack this problem with symbolic manipulation software as in [9], [145]. However, such an approach is also limited as pointed out in [50].

5.4 Applications to Specific Bifurcations

We now apply the previous results to the most common bifurcations. This will amount to explaining the quantities in their respective definitions and proving the resulting theorems 3.1.0.1, 3.2.0.2, 3.3.0.3 and 3.5.0.4.

5.4.1 Applications to Saddle-Nodes

Suppose the point $y_N = (x_N, \lambda_N)$ is a saddle-node bifurcation point. Then $\dot{y}_N = (\dot{x}_N, \dot{\lambda}_N) = (v, 0)$ and $w^T f_\lambda^N \neq 0$ since $f_\lambda^N \notin \text{Range}[f_x^N]$, and from (5.2.2) it follows:

$$\ddot{\lambda}_N = \frac{-w^T f_{xx}^N vv}{w^T f_\lambda^N}. \tag{5.4.1}$$

and by conditions (3.1.3), (3.1.4) in definition 3.1.0.3 we see that the branch across a quadratic saddle-node has a well defined nonzero curvature. That is, the branch has quadratic contact with the hyperplane $H = (x, \lambda_N)$ and remains (locally) on one side of it. More precisely, if $\ddot{\lambda}_N > 0$, then the branch exists for $\lambda > \lambda_N$ (it"opens to the right"), while in case $\ddot{\lambda}_N < 0$ it exists for $\lambda < \lambda_N$ (it "opens to the left"). Concerning its stability, from (5.3.20) we immediately have:

$$\dot{\kappa}_0 = \frac{w^T f_{xx}^N vv}{w^T v}. \tag{5.4.2}$$

Again, we see that condition (3.1.4) in definition 3.1.0.3 plus the assumed simplicity of the $+1$ eigenvalue imply a quadratic saddle-node to be one with a well defined transversal crossing of the critical eigenvalue (compare this with examples 3.0.2.1, 3.1.0.4). Consequently, the branch changes stability at a quadratic saddle-node if all other eigenvalues have negative real parts, respectively are inside the unit circle. Hence for a quadratic saddle-node we have: $\dot{\kappa}_0 = 0 \Leftrightarrow \ddot{\lambda}_N = 0$.

Let us also consider a saddle-node point with $\dot{\lambda}_N = \ddot{\lambda}_N = 0$. Multiplying relation (5.3.32) from the left with w^T leads to:

$$\frac{d^3\lambda}{ds^3}(0) = \frac{-w^T \left(f_{xxx}^N vv + 3 f_{xx}^N \ddot{x}_N \right) v}{w^T f_\lambda^N}, \tag{5.4.3}$$

where $\ddot{x}_N$ is the unique solution of $f_x^N \ddot{x}_N = -f_{xx}^N vv$ with $\ddot{x}_N^T v = 0$. A branch across a cubic saddle-node point does therefore cross the hyperplane $H = (x, \lambda_N)$ with third

order contact. In this case we find from (5.3.29) for the second derivative of the parametrized eigenvalue:

$$\ddot{\kappa}_0 = \frac{w^T \left(f^N_{xxx} vv + f^N_{xx} \ddot{x}_N + 2 f^N_{xx} \dot{v}_0 \right) v}{w^T v}. \tag{5.4.4}$$

But with $\dot{\lambda}_N = \ddot{\lambda}_N = \kappa_0 = \dot{\kappa}_0 = 0$, it follows from (5.2.2), (5.3.22) with $\dot{x}_N = v$, $v\dot{v}_0 = 0$ and $v\ddot{x}_N = 0$ that:

$$\ddot{x}_N = \dot{v}_0. \tag{5.4.5}$$

Using this in (5.4.4), we arrive at:

$$\ddot{\kappa}_0 = \frac{w^T \left(f^N_{xxx} vv + 3 f^N_{xx} \ddot{x}_N \right) v}{w^T v}, \tag{5.4.6}$$

and therefore: $\ddot{\kappa}_0 = 0 \Leftrightarrow \frac{d^3\lambda}{ds^3}(0) = 0$.

In very much the same way, condition (3.1.6) in definition 3.1.0.3 for a saddle-node bifurcation assures that a quartic saddle-node bifurcation does not cross H but bounces back from it after having fourth-order contact with it. Furthermore we have: $\frac{d^3\kappa}{ds^3}(0) = 0 \Leftrightarrow \frac{d^4\lambda}{ds^4}(0) = 0$.

5.4.2 Applications to Transcritical Bifurcations

Suppose now that in corollary 5.3.3.1 the point $y_N = (x_N, \lambda_N)$ is a transcritical bifurcation point. Then, since $\dot{\lambda}_N \neq 0$, we can conveniently choose $\phi_1 = (v^T, 0)$ and $\psi_1 = w$. The coefficients (5.3.7), (5.3.8), (5.3.9) of the algebraic bifurcation equation become:

$$c_{11} = w^T (f^N_{xx} \dot{x}_N \dot{x}_N + 2 f^N_{x\lambda} \dot{x}_N \dot{\lambda}_N + f^N_{\lambda\lambda} \dot{\lambda}_N \dot{\lambda}_N) = 0, \tag{5.4.7}$$

$$c_{12} = w^T (f^N_{xx} \dot{x}_N + f^N_{x\lambda} \dot{\lambda}_N) v, \tag{5.4.8}$$

$$c_{22} = w^T f^N_{xx} vv. \tag{5.4.9}$$

Hence, we observe that conditions (3.2.9) and (3.2.10) in definition 3.2.0.4 are equivalent to $c_{12} \neq 0$ and $c_{22} \neq 0$. But $c_{12} \neq 0$ and theorem 5.3.1.1 imply that there are exactly two distinct solution branches across $y_N = (x_N, \lambda_N)$. Furthermore, corollary 5.3.3.1 shows that this condition also implies a transversal crossing of the critical eigenvalue along the current branch "C_1" with tangent $\dot{y}_N = (\dot{x}_N, \dot{\lambda}_N)$:

$$\dot{\kappa}_0 = \frac{w^T (f^N_{xx} \dot{x}_N + f^N_{x\lambda} \dot{\lambda}_N) v}{w^T v} = \frac{c_{12}}{w^T v} \neq 0. \tag{5.4.10}$$

From (5.3.2) and (5.3.14) we find next that the tangential direction of the emanating branch "C_2" equals: $\alpha_2\dot{\lambda}_N = \frac{\pm c_{22}}{\sqrt{c_{22}^2+4c_{12}^2}}\dot{\lambda}_N \neq 0$, so that both branches transversally cross the hyperplane $H = (x, \lambda_N)$.

We can also prove now that the two branches C_1 and C_2 indeed exchange their stability (if all other eigenvalues have negative real parts or lie inside the unit circle). Without loss of generality, let therefore $\dot{\lambda}_N > 0$. In order for C_2 to cross the hyperplane $H = (x, \lambda_N)$ in the same direction as C_1 we must choose the $\alpha_2 > 0$ in (5.3.14). Then, for the branch C_2, corollary 5.3.3.1 gives:

$$\dot{\kappa}_0 = \frac{w^T\left(f_{xx}^N(\alpha_2\dot{x}_N + \beta_2 v) + f_{x\lambda}^N\alpha_2\dot{\lambda}_N\right)v}{w^T v}. \tag{5.4.11}$$

Now we solve (5.3.13) for β_2 and put the result in (5.4.11) to find:

$$\dot{\kappa}_0 = -\alpha_2\frac{w^T(f_{xx}^N\dot{x}_N + f_{x\lambda}^N\dot{\lambda}_N)v}{w^T v} = -\alpha_2\frac{c_{12}}{w^T v} \neq 0 \tag{5.4.12}$$

which is of different sign as the corresponding formula (5.4.10) for C_1. Hence, if C_1 is stable (unstable) for $\lambda < \lambda_N$, then C_2 is unstable (stable) for $\lambda < \lambda_N$ and they exchange their stability when crossing λ_N.

This proves all the assertions of theorem 3.2.0.2.

5.4.3 Applications to Pitchforks

Assume now that in corollary 5.3.3.1 $y_N = (x_N, \lambda_N)$ is a pitchfork bifurcation point. Our choice of $\phi_1 = (v^T, 0)^T$ as a first basis element of null$[f_x^N \;\; f_\lambda^N]$ leads then to $c_{11} = c_{22} = 0$ and $c_{12} = w^T(f_{xx}^N\dot{x}_N + f_{x\lambda}^N\dot{\lambda}_N)v$ as in (5.4.8).

Again, condition (3.3.3) in definition 3.3.0.5 together with corollary 5.3.3.1 assure that the critical eigenvalue transversally crosses 0, respectively $+1$, along the branch C_1 with tangent $\dot{y}_N = (\dot{x}_N, \dot{\lambda}_N)$, namely:

$$\dot{\kappa}_0 = \frac{w^T(f_{xx}^N\dot{x}_N + f_{x\lambda}^N\dot{\lambda}_N)v}{w^T v} = \frac{c_{12}}{w^T v} \neq 0. \tag{5.4.13}$$

Let us proceed by proving that the critical eigenvalue along the branch C_2 does not transversally cross 0, respectively $+1$. But $c_{22} = w^T f_{xx}^N vv = 0$ implies readily that $(\alpha_2, \beta_2) = (0, 1)$ for C_2 corresponding to the tangential direction $(v^T, 0)^T$ along it. The use of corollary 5.3.3.1 for this tangent yields:

$$\dot{\kappa}_0 = \frac{w^T(f_{xx}^N v + f_{x\lambda}^N 0)v}{w^T v} = \frac{c_{22}}{w^T v} = 0. \tag{5.4.14}$$

Of course C_2 could still change stability if $\ddot{\kappa}_0 = 0$ and $\frac{d^3\kappa}{ds^3} \neq 0$, but we shall show next that the condition:

$$c^* := w^T \left(f^N_{xxx} vv + 3 f^N_{xx} p_0 \right) v \neq 0, \tag{5.4.15}$$

with p_0 a particular solution of $f^N_x p_0 = -f^N_{xx} vv$ in definition 3.3.0.5 for a pitchfork bifurcation, leads to $\ddot{\kappa}_0 \neq 0$.

We therefore apply theorem 5.3.3.1 with $\phi_0 = \dot{y}_N = (v^T, 0)$ and with $\phi_1 = (\dot{x}^T_N, \dot{\lambda}_N)$. That is, ϕ_0 is tangent to C_2 while ϕ_1 is tangent to C_1. Next, we remark that, in the current setting with $\dot{\lambda}_N = 0$ along C_2, the vector p_2 (see theorem 5.3.3.1) can be chosen such that $p_2 = (p_0^T, 0)^T$ with p_0 a particular solution of the inhomogeneous system:

$$f^N_x p_0 = -f^N_{xx} vv. \tag{5.4.16}$$

Now, in contrary to the choice of ϕ_1 in theorem 5.3.3.1, generally ϕ_1 is not perpendicular to ϕ_0. As a result, the coefficients c_1, c_2 in (5.3.30) depend linearly on each other, and (5.3.31) changes to $c_1 = -c_2 < v, \dot{x}_N > - < \phi_0, p_2 >$. However, as $\phi_0(n+1) = 0$, equation (5.3.30) leads to:

$$\ddot{\lambda}_N = c_2 \dot{\lambda}_N \tag{5.4.17}$$

for the branch C_2 — remember that $\dot{\lambda}_N \neq 0$ along C_1. Using this and once again $c_{22} = w^T f^N_{xx} vv = 0$, formula (5.3.34) simplifies to:

$$c_2 = \frac{-w^T \left(f^N_{xxx} vv + 3 f^N_{xx} p_0 \right) v}{3 w^T f^N_{yy} \phi_0 \phi_1} = \frac{-c^*}{3 w^T f^N_{yy} \phi_0 \phi_1}. \tag{5.4.18}$$

Putting this quantity into (5.3.30), we find from (5.3.29) with $w^T f^N_{xx} vv = 0$:

$$\begin{aligned} \ddot{\kappa}_0 &= \frac{w^T \left(f^N_{xxx} v^3 + c_2 f^N_{yy} \phi_0 \phi_1 + 3 f^N_{xx} p_0 v \right)}{w^T v} = \\ &= \frac{2 w^T \left(f^N_{xxx} vv + 3 f^N_{xx} p_0 \right) v}{3 w^T v} = -\frac{2c^*}{3 w^T v} \neq 0, \end{aligned} \tag{5.4.19}$$

by condition (3.3.5) in definition 3.3.0.5 for a pitchfork bifurcation. We have proven that, generically, the branch C_2 does not change stability — the critical eigenvalue touches 0, respectively +1, and then bounces back.

Finally, theorem 3.3.0.3 addressed the question: on which side of $H = (x, \lambda_N)$ does the branch C_2 exist? With $\phi_0 = (v^T, 0)$ as above and $\phi_1 = (\dot{x}_N, \dot{\lambda}_N)$ the direction along C_1, we recall (5.4.17): $\ddot{\lambda}_N = c_2 \dot{\lambda}_N$ with c_2 as in (5.4.18). We must show that:

$$\dot{\lambda}_N \dot{\kappa}_0 > 0 \text{ implies } \ddot{\lambda}_N \ddot{\kappa}_0 < 0, \tag{5.4.20}$$

$$\text{and } \dot{\lambda}_N\dot{\kappa}_0 < 0 \text{ implies } \ddot{\lambda}_N\ddot{\kappa}_0 > 0 \tag{5.4.21}$$

where the first derivatives refer to the branch C_1 and the second derivatives to the branch C_2. But, by (5.4.17), (5.4.18), (5.4.19) and (5.4.13) we find:

$$\ddot{\lambda}_N = \frac{-\dot{\lambda}_N c^*}{3c_{12}} = \frac{-\dot{\lambda}_N\ddot{\kappa}_0 w^T v}{2c_{12}} = \frac{-\dot{\lambda}_N\ddot{\kappa}_0}{2\dot{\kappa}_0} \neq 0, \tag{5.4.22}$$

and the above assertions (5.4.20) and (5.4.21) can be read off from this equation. This proves all of the assertions of theorem 3.3.0.3.

5.4.4 Applications to Period-Doublings

Recall that, by definition, a period-doubling bifurcation of the map $F(x,\lambda)$ is a pitchfork bifurcation of $f(x,\lambda) := F \circ F - x$.

Let us first express the crossing speed of the eigenvalue -1 in terms of λ:

Corollary 5.4.4.1 *Suppose $F(x_N,\lambda_N) = x_N$ and -1 is a simple eigenvalue of F_x^N with right eigenvector v and left eigenvector w. Assume further that F_x^N has no other eigenvalues of modulus* 1. *Then:*

$$\frac{dk}{d\lambda}(\lambda_N) =: k_\lambda^N = \frac{w^T\left(F_{xx}^N\left[(F_x^N - \mathrm{id})^{-1}(-F_\lambda^N)\right] + F_{x\lambda}^N\right)v}{w^T v}. \tag{5.4.23}$$

Proof: By the implicit function theorem 2.1.0.1 we can parametrize the unique solution branch across $y_N = (x_N,\lambda_N)$ in terms of λ and consider:

$$0 = F(x(\lambda),\lambda) - x(\lambda) \tag{5.4.24}$$

$$\text{and } k(\lambda)v(\lambda) = F_x(x(\lambda),\lambda)v(\lambda), \tag{5.4.25}$$

with $k(\lambda_N) = -1$, $\|v(\lambda)\|_2^2 = 1$ and $v(\lambda_N) = v$. Differentiating (5.4.24) and (5.4.25) with respect to λ yields:

$$-F_\lambda^N = (F_x^N - \mathrm{id})x_\lambda^N \tag{5.4.26}$$

$$k_\lambda^N v + k(\lambda_N)v_\lambda^N = (F_{xx}^N x_\lambda^N + F_{x\lambda}^N)v + F_x^N v_\lambda^N. \tag{5.4.27}$$

We can now solve (5.4.26) for x_λ^N, since $(F_x^N - \mathrm{id})$ is regular. Putting this solution into (5.4.27) we can then solve for k_λ^N and recover (5.4.23). □

Notice that in the case $n = 1$, this formula reduces to $k_\lambda^N = \frac{1}{2}F_{xx}^N F_\lambda^N + F_{x\lambda}^N$, which, when set different from 0, gives one of the nondegenerate conditions given in [66].

Corollary 5.4.4.2 Assume, in addition to the hypothesis of corollary 5.4.4.1, that $k_\lambda^N = 0$. Then $k_{\lambda\lambda}^N := \frac{d^2k}{d\lambda^2}(\lambda_N)$ equals:

$$k_{\lambda\lambda}^N = \frac{w^T\left(F_{xxx}^N x_\lambda^N x_\lambda^N + 2F_{xx\lambda}^N x_\lambda^N + F_{x\lambda\lambda}^N + F_{xx}^N x_{\lambda\lambda}^N\right)v + 2\left(F_{xx}^N x_\lambda^N + F_{x\lambda}^N\right)v_\lambda^N}{w^T v}, \tag{5.4.28}$$

with x_λ^N as in (5.4.26), $x_{\lambda\lambda}^N$ as in (5.4.29) and v_λ^N from (5.4.30).

Proof: Differentiating (5.4.25) again, using $k(\lambda_N) = -1$, $k_\lambda^N = 0$ and $w^T F_x^N = -w^T$, we readily recover (5.4.28), with x_λ^N from (5.4.26). The quantity $x_{\lambda\lambda}^N$ can further be found by considering the second derivative of (5.4.26). Then it follows that:

$$-\left(2F_{x\lambda}^N x_\lambda^N + F_{\lambda\lambda}^N + F_{xx}^N x_\lambda^N x_\lambda^N\right) = (F_x^N - \mathrm{id})x_{\lambda\lambda}^N \tag{5.4.29}$$

with regular $(F_x^N - \mathrm{id})$. At last, v_λ^N can be found by rearranging (5.4.27):

$$(F_x^N + \mathrm{id})v_\lambda^N = -\left(F_{xx}^N x_\lambda^N + F_{x\lambda}^N\right)v, \quad \text{with } v_\lambda^N \perp v, \tag{5.4.30}$$

arising from differentiating $\|v(\lambda)\|_2^2 = 1$. □

Consider now the function $f(x,\lambda) := F(F(x,\lambda),\lambda)) - x$ with $f(x_N,\lambda_N) = 0$.

Lemma 5.4.4.1 *$f(x,\lambda)$ has a simple potential bifurcation point at (x_N,λ_N).*

Proof:

$$f_x^N v = F_x(F(x_N,\lambda_N),\lambda_N)F_x^N v - v = (F_x^N)^2 v - v = 0 \tag{5.4.31}$$

and

$$w^T f_\lambda^N = w^T F_x^N F_\lambda^N + w^T F_\lambda^N = -w^T F_\lambda^N + w^T F_\lambda^N = 0. \tag{5.4.32}$$

Hence $\dim \mathrm{null}[f_y^N] = 2$ with $y_N = (x_N,\lambda_N)$. □

Since the fixed point branch "C_1" across (x_N,λ_N) crosses $H = (x,\lambda_N)$ transversally, it has a tangential direction with $\dot\lambda_N \neq 0$. Again let $\mathrm{span}\{\phi_0,\phi_1\}$ with $\phi_0 = (\dot x_N^T,\dot\lambda_N)^T$ and $\phi_1 = (v^T,0)^T$ be a basis of $\mathrm{null}[f_y^N]$.

As expected, we then find for the coefficients of the algebraic bifurcation equation (5.3.6):

$$c_{11} = w^T\left(f_{xx}^N \dot x_N \dot x_N + 2w^T f_{x\lambda}^N \dot x_N \dot\lambda_N + f_{\lambda\lambda}^N \dot\lambda_N \dot\lambda_N\right) = 0, \tag{5.4.33}$$

$$c_{12} = w^T\left(f_{xx}^N \dot x_N + f_{x\lambda}^N \dot\lambda_N\right)v, \tag{5.4.34}$$

$$c_{22} = w^T f_{xx}^N vv = w^T\left(f_{xx}^N(f_x^N v)f_x^N + f_x^N f_{xx}^N v\right)v = w^T f_{xx}^N vv - w^T f_{xx}^N vv = 0. \tag{5.4.35}$$

Remembering that the fixed point branch C_1 is in particular a solution of $f(x,\lambda) = 0$, we have $(\alpha_1,\beta_1) = (1,0)$ and $(\alpha_2,\beta_2) = (0,1)$ as the solutions to the algebraic bifurcation equation. Since, by definition of a period-doubling bifurcation, $c_{12} \neq 0$, we consequently find a second distinct branch "C_2" of solutions to f that corresponds to 2-periodic solutions to F. This branch has quadratic contact with H (its tangent equals $(v^T,0)^T = \phi_1$) and it exists (locally) on one side of it.

Of course we can express the crossing speed of the eigenvalue -1 along C_1 (5.4.23) in terms of the arclength. From corollary 5.3.3.1 we find again:

$$\dot{\kappa}_0 = \frac{w^T(f^N_{xx}\dot{x}_N + f^N_{x\lambda}\dot{\lambda}_N)v}{w^Tv} = \frac{c_{12}}{w^Tv} = k^N_\lambda \dot{\lambda}_N \neq 0. \tag{5.4.36}$$

Let us consider the stability of the 2-periodic orbits. We apply corollary 5.3.3.1 to $f(x,\lambda)$ along the branch of the doubled periodic orbits, i.e. $\phi_0 = \dot{y}_N = (\dot{x}_N,\dot{\lambda}_N) = (v^T,0)^T$. Hence, corollary 5.3.3.1immediately gives us that $\dot{\kappa}_0 = 0$ and we can apply theorem 5.3.3.1. An inspection of the linear systems to be solved for p_0 and p_2 again shows that, in our particular case, namely $\dot{\lambda}_0 = 0$, we can choose p_2 in (5.3.33) as $p_2 = (p_0^T,0)^T$. As in (5.4.18), the quantity c_2 becomes:

$$c_2 = \frac{-w^T\left(f^N_{xxx}vv + 3f^N_{xx}p_2\right)v}{3w^T(f^N_{yy}\phi_0\phi_1)}, \tag{5.4.37}$$

and, putting it into (5.3.30), we find from (5.3.29) with $v_0 = \dot{x}_N = v$ and $w^T f^N_{xx}vv = 0$:

$$\begin{aligned}\ddot{\kappa}_0 &= \frac{w^T\left(f^N_{xxx}v^3 + c_2 f^N_{yy}\phi_0\phi_1 + 3f^N_{xx}p_2v\right)}{w^Tv} \\ &= \frac{2w^T\left(f^N_{xxx}vv + 3f^N_{xx}p_2\right)v}{3w^Tv} = \frac{2c^*}{3w^Tv}.\end{aligned} \tag{5.4.38}$$

Thus we recover the familiar formula (5.4.19).

Not surprisingly, we also find for $n = 1$ that $c^* \neq 0$ becomes $-2F^N_{xxx} - 3(F^N_{xx})^2 \neq 0$, which constitutes the second nondegenerate condition in [66].

To be complete, the direction of the 2-periodic orbits is found by corollary 5.3.3.2 applied to $f(x,\lambda)$. It gives again: $\ddot{\lambda}_N = c_2\dot{\lambda}_N = -\frac{c^*}{3c_{12}}$. To summarize, we have proven all the assertions of theorem 3.5.0.4.

5.4.5 Applications to Degenerate Period-Doublings

Now we consider the case of a degenerate period-doubling in the sense that $c_{12} = 0$. The algebraic bifurcation equation (5.3.6) for $f = F \circ F - \mathrm{id}$ does not give any

information since all of its coefficients are zero. However, we do know that the fixed point branch C_1 with tangential direction $\phi_0 = \dot{y}_N = (\dot{x}_N, \dot{\lambda}_N)$ is a solution to $f(x,\lambda) = 0$, and that $\dim \text{null}[f_x^N \;\; f_\lambda^N] = 2$. Hence let $\{\phi_0, \phi_1\}$ be a basis for $\text{null}[f_x^N \;\; f_\lambda^N]$ with $\phi_1 = (v^T, 0)$. This can still be done as $\dot{\lambda}_N \neq 0$ and 0 is an algebraically simple eigenvalue of f_x^N.

We apply the by now familiar ideas and differentiate $f(x(s), \lambda(s)) = 0$ three times with respect to arclength to obtain:

$$\begin{aligned} 0 \;=\; & f_{xxx}^N \dot{x}_N \dot{x}_N \dot{x}_N + 3 f_{xx\lambda}^N \dot{x}_N \dot{x}_N \dot{\lambda}_N + 3 f_{x\lambda\lambda}^N \dot{x}_N \dot{\lambda}_N \dot{\lambda}_N + f_{\lambda\lambda\lambda}^N \dot{\lambda}_N \dot{\lambda}_N \dot{\lambda}_N \\ & + 3 f_{xx}^N \dot{x}_N \ddot{x}_N + 3 f_{x\lambda}^N \dot{\lambda}_N \ddot{x}_N + 3 f_{x\lambda}^N \dot{x}_N \ddot{\lambda}_N + 3 f_{\lambda\lambda}^N \dot{\lambda}_N \ddot{\lambda}_N \\ & + f_x^N \frac{d^3 x}{ds^3}(0) + f_\lambda^N \frac{d^3 \lambda}{ds^3}(0). \end{aligned} \tag{5.4.39}$$

From $c_{11} = c_{12} = c_{22} = 0$ we conclude that:

$$0 \;=\; w^T \left(f_{xx}^N \dot{x}_N \dot{x}_N + 2 f_{x\lambda}^N \dot{x}_N \dot{\lambda}_N + f_{\lambda\lambda}^N \dot{\lambda}_N \dot{\lambda}_N \right) \tag{5.4.40}$$

$$0 \;=\; w^T \left(f_{xx}^N \dot{x}_N + f_{x\lambda}^N \dot{\lambda}_N \right) v \tag{5.4.41}$$

$$0 \;=\; w^T f_{xx}^N v v. \tag{5.4.42}$$

It follows that there are $z_0, z_1, z_2 \in \mathbb{R}^n$ such that:

$$\begin{aligned} f_x^N z_0 &= f_{xx}^N v v \\ f_x^N z_1 &= f_{xx}^N \dot{x}_N v + f_{x\lambda}^N \dot{\lambda}_N v \\ f_x^N z_2 &= f_{xx}^N \dot{x}_N \dot{x}_N + 2 f_{x\lambda}^N \dot{x}_N \dot{\lambda}_N + f_{\lambda\lambda}^N \dot{\lambda}_N \dot{\lambda}_N. \end{aligned} \tag{5.4.43}$$

For any other smooth branch with tangent $(\dot{x}_i, \dot{\lambda}_i)$ let, as usual:

$$\begin{pmatrix} \dot{x}_i \\ \dot{\lambda}_i \end{pmatrix} = \alpha \begin{pmatrix} v \\ 0 \end{pmatrix} + \beta \begin{pmatrix} \dot{x}_N \\ \dot{\lambda}_N \end{pmatrix} \tag{5.4.44}$$

The equation for $(\ddot{x}_i, \ddot{\lambda}_i)$ arises from the second derivative of $f(x(s), \lambda(s)) = 0$:

$$f_x^N \ddot{x}_i + f_\lambda^N \ddot{\lambda}_i = -(f_{xx}^N \dot{x}_i \dot{x}_i + 2 f_{x\lambda}^N \dot{x}_i \dot{\lambda}_i + f_{\lambda\lambda}^N \dot{\lambda}_i \dot{\lambda}_i). \tag{5.4.45}$$

Replacing $(\dot{x}_i, \dot{\lambda}_i)$ with (5.4.44) and using (5.4.43) lead to:

$$f_x^N \ddot{x}_i + f_\lambda^N \ddot{\lambda}_i = -(\alpha^2 f_x^N z_0 + 2\alpha\beta f_x^N z_1 + \beta^2 f_x^N z_2). \tag{5.4.46}$$

Hence:

$$\begin{pmatrix} \ddot{x}_i \\ \ddot{\lambda}_i \end{pmatrix} = \alpha_c \begin{pmatrix} v \\ 0 \end{pmatrix} + \beta_c \begin{pmatrix} \dot{x}_N \\ \dot{\lambda}_N \end{pmatrix} - \begin{pmatrix} \alpha^2 z_0 + 2\alpha\beta z_1 + \beta^2 z_2 \\ 0 \end{pmatrix}. \tag{5.4.47}$$

Now we put (5.4.44) and (5.4.47) into (5.4.39). After multiplication from the left with w^T and subsequent elementary algebraic manipulations and upon using (5.4.40), (5.4.41), (5.4.42) again, we see that α_c, β_c drop out and we are left we a homogeneous cubic polynomial:

$$0 = c_{aaa}\alpha^3 + 3c_{aab}\alpha^2\beta + 3c_{abb}\alpha\beta^2 + c_{bbb}\beta^3, \tag{5.4.48}$$

where:

$$c_{aaa} = w^T \int_{xxx}^N vvv - 3w^T \int_{xx}^N z_0, \tag{5.4.49}$$

$$c_{aab} = w^T \left(\int_{xxx}^N vv\dot{x}_N + \int_{xx\lambda}^N vv\dot{\lambda}_N - 2\int_{xx}^N vz_1 - \int_{xx}^N z_0\dot{x}_N - \int_{x\lambda}^N z_0 \right), \tag{5.4.50}$$

$$\begin{aligned} c_{abb} &= w^T \left(\int_{xxx}^N v\dot{x}_N\dot{x}_N + 2\int_{xx\lambda}^N v\dot{x}_N\dot{\lambda}_N \right) \\ &\quad + w^T \left(\int_{x\lambda\lambda}^N v\dot{\lambda}_N\dot{\lambda}_N - \int_{xx}^N vz_2 - 2\int_{xx}^N \dot{x}_N z_1 - 2\int_{x\lambda}^N z_1\dot{\lambda}_N \right) \end{aligned} \tag{5.4.51}$$

and:

$$\begin{aligned} c_{bbb} &= w^T \left(\int_{xxx}^N \dot{x}_N\dot{x}_N\dot{x}_N + 3\int_{xx\lambda}^N \dot{x}_N\dot{x}_N\dot{\lambda}_N + 3\int_{x\lambda\lambda}^N \dot{x}_N\dot{\lambda}_N\dot{\lambda}_N \right) \\ &\quad + w^T \left(\int_{\lambda\lambda\lambda}^N \dot{\lambda}_N\dot{\lambda}_N\dot{\lambda}_N - 3\int_{xx}^N \dot{x}_N z_2 - 3\int_{x\lambda}^N z_2\dot{\lambda}_N \right). \end{aligned} \tag{5.4.52}$$

Hence we may consider:

$$0 = c_{aaa}\alpha^3 + 3c_{aab}\alpha^2\beta + 3c_{abb}\alpha\beta^2 + c_{bbb}\beta^3 \tag{5.4.53}$$

$$0 = \alpha^2 + \beta^2 - 1 \tag{5.4.54}$$

as the algebraic bifurcation equation for this particular degenerate case. Fortunately, we know one solution of this system, namely $(\alpha_0, \beta_0) = (0, 1)$ corresponding to the direction of the fixed point branch. Putting this into (5.4.53) we find: $c_{bbb} = 0$. Therefore we can factor (5.4.53) in the form:

$$\alpha(c_{aaa}\alpha^2 + 3c_{aab}\alpha\beta + 3c_{abb}\beta^2) = 0. \tag{5.4.55}$$

Assuming a solution with $\alpha_1 \neq 0$ we find from (5.4.55):

$$3c_{abb}\left(\frac{\beta}{\alpha}\right)^2 + 3c_{aab}\left(\frac{\beta}{\alpha}\right) + c_{aaa} = 0, \tag{5.4.56}$$

and we see that the resulting discriminant:

$$\Delta := \frac{9}{4}c_{aab}^2 - 3c_{abb}c_{aaa} \tag{5.4.57}$$

must necessarily be nonnegative for at least one solution with $\alpha_1 \neq 0$. Indeed, one can easily check that a sufficient condition for at least one real nonzero solution in α is provided by requiring that $\Delta > 0$. If $\Delta < 0$, then there are no nonzero solutions in α and hence no other tangents than the one corresponding to the fixed point branch. However, a zero discriminant may yield none or one nonzero solutions in α as $\alpha^2 = 0$ and $\alpha^2 + 2\alpha\beta + \alpha^2 = 0$ show. This case suggests then even higher degeneracies. Finally let us point out that a positive discriminant can still lead to double solutions in $\alpha = 0$ as $\alpha^2 - \alpha\beta = 0$ shows.

We formulate this result for (α, β) in:

Theorem 5.4.5.1 *Let $y_N = (x_N, \lambda_N)$ be a degenerate period-doubling bifurcation point of the map $x = F(x, \lambda)$, satisfying $c_{12} = 0$. Along its fixed point branch let it have a tangential direction corresponding to $(\alpha_0, \beta_0) = (0, 1)$ as above. Suppose that the above discriminant* (5.4.57) *is positive. Then there exists at least one more distinct tangential direction corresponding to the solution (α_1, β_1) of* (5.4.53). *If the above discriminant* (5.4.56) *is negative, then there exists only the tangential direction of the equilibrium branch.*

Note that this theorem gives only necessary conditions for the existence of distinct branches with tangents corresponding to (α_i, β_i). We do not claim that a positive discriminant guarantees at least one distinct bifurcating branch.

Let us apply this result in the one-dimensional case.

Example 5.4.5.1 In example 3.5.0.14:

$$x \mapsto F(x) := x^2 + \lambda x - 1, \tag{5.4.58}$$

we encountered a degenerate period-doubling bifurcation. It is elementary to check that the direction along the fixed points at $(x_0, \lambda_0) = (-1, 1)$ is: $(\dot{x}_0, \dot{\lambda}_0) = \pm(\frac{1}{\sqrt{5}}, \frac{-2}{\sqrt{5}})$ and that $c_{12} = 0$ (and $c_{11} = c_{22} = 0$). Computing the derivatives of $f = F \circ F - x$ we find further that:

$$f^0_{xxx} = -12,\ f^0_{xx\lambda} = -6,\ f^0_{x\lambda\lambda} = -2,\ f^0_{\lambda\lambda\lambda} = 0,\ f^0_{xx} = 0,\ f^0_{x\lambda} = 0.$$

Hence the solutions z_0, z_1, z_2 are irrelevant. Evaluating the above coefficients with $(\dot{x}_0, \dot{\lambda}_0) = (\frac{1}{\sqrt{5}}, \frac{-2}{\sqrt{5}})$ we find that:

$$c_{aaa} = -12,\ c_{aab} = 0,\ c_{abb} = 4/5,\ c_{bbb} = 0$$

and system (5.4.55) reduces to $\alpha(\alpha - \beta/\sqrt{5})(\alpha + \beta/\sqrt{5}) = 0$.

Besides the known solution $(\alpha_0, \beta_0) = (0, 1)$, we find further (normalized) solutions:

$$(\alpha_1, \beta_1) = (1/\sqrt{6}, \sqrt{5}/\sqrt{6}), \qquad (\alpha_2, \beta_2) = (-1/\sqrt{6}, \sqrt{5}/\sqrt{6})$$

. The resulting (normalized) directions follow from (5.4.44): (α_1, β_1) yields $(\dot{x}_1, \dot{\lambda}_1) = \pm(1/\sqrt{2}, -1/\sqrt{2})$ and (α_2, β_2) gives $(\dot{x}_2, \dot{\lambda}_2) = \pm(0, 1)$. Hence we arrive at the picture outlined in example 3.5.0.14. Indeed, it was precisely this calculation that resulted into our description of the system's behaviour.

5.4.6 Applications to Secondary Hopf Bifurcations

The problems appearing when an invariant curve is continued, increase dramatically. First of all, the nature of such an object does no longer admit a fixed point formulation $f(x, \lambda) = 0$ with finite dimensional x (and f). Consequently, one is confined to approximation schemes such as cubic spline interpolation of the curve, see [88], [96]. Secondly, the invariant curve can (and frequently will, see Chapter 7, Section 7.4.1) loose its smoothness and become heavily zig-zagged (see the plots in [49], [18], [109]). These facts lead, in general, quickly to huge systems of nonlinear equations if the invariant curve is to be reasonably approximated. This situation gets even worse, if the curve is "large" in diameter and/or additionally the dimension of the phase space itself is large. Also, if the invariant curve is actually a cross-section of a two-dimensional torus in a continuous flow, the map will not be given analytically — every single point on the cross-section (and we might need many of them) must be found by a combined integration and iteration process. Further problems may occur, if the torus is unstable and only reasonably covered by a "long quasiperiodic" trajectory, or if it approaches a bifurcation and becomes "structurally unstable". The sum of these difficulties is probably the reason why torus continuation is only occasionally reported, as in [96], and seldomly incorporated in packages as in [88].

Coming from the other side however and having located a secondary Hopf bifurcation, we can still compute the critical coefficients "d" and "a", and predict the local behaviour of the system by theorem 3.7.0.6.

In order to find d, we mimic the proof of corollary 5.4.4.1

Corollary 5.4.6.1 *Let $F(x_N, \lambda_N) = x_N$ and $\delta_{1,2} = e^{\pm ic} = \mu \pm i\eta$ be a simple pair of complex conjugate eigenvalues of F_x^N on the unit circle with right eigenvector $v \pm iu$*

and left eigenvector $w \pm i\,z$. *Assume further* F_x^N *has no other eigenvalues of modulus* 1. *Finally, denote* $\mu^N := \mu(\lambda_N)$, $\eta^N := \eta(\lambda_N)$ *and* $\delta := \delta_1$ *corresponding to* $v + i\,u$ *and* $w + i\,z$.

Then the crossing speed d *of* $\|\delta\|$ *with respect to* λ *at* $\lambda = \lambda_N$ *is:*

$$d = \|\delta\|_\lambda^N = \frac{\mu^N \mu_\lambda^N + \eta^N \eta_\lambda^N}{\sqrt{(\mu^N)^2 + (\eta^N)^2}} \tag{5.4.59}$$

where $(\mu_\lambda^N, \eta_\lambda^N)$ *is the solution of the regular linear* 2×2 *system* (5.4.66) *below.*

Proof: By the implicit function theorem 2.1.0.1 we can parametrize the unique fixed point branch across (x_N, λ_N) in terms of λ. Since the eigenvalue δ depends smoothly on λ, we can differentiate $\|\delta(\lambda)\|_2 = \sqrt{\mu(\lambda)^2 + \eta(\lambda)^2}$, yielding equation (5.4.59). It remains to determine the coefficients μ_λ^N and η_λ^N. Consider therefore the complex eigenvalue eigenvector relations:

$$\begin{aligned} F_x(x(\lambda), \lambda)(v(\lambda) + i\,u(\lambda)) &= (\mu(\lambda) + i\,\eta(\lambda))(v(\lambda) + iu(\lambda)) \\ F_x(x(\lambda), \lambda)^*(w(\lambda) + i\,z(\lambda)) &= (\mu(\lambda) + i\,\eta(\lambda))^*(w(\lambda) + iz(\lambda)), \end{aligned}$$

in a neighbourhood of λ_N. Here * denotes complex transpose. Splitting this into its real and imaginary part, we have:

$$F_x(x(\lambda), \lambda)v(\lambda) = \mu(\lambda)v(\lambda) - \eta(\lambda)u(\lambda) \tag{5.4.60}$$

$$F_x(x(\lambda), \lambda)u(\lambda) = \mu(\lambda)u(\lambda) + \eta(\lambda)v(\lambda) \tag{5.4.61}$$

$$w(\lambda)^T F_x(x(\lambda), \lambda) = \mu(\lambda)w(\lambda)^T + \eta(\lambda)z(\lambda)^T \tag{5.4.62}$$

$$z(\lambda)^T F_x(x(\lambda), \lambda) = \mu(\lambda)z(\lambda)^T - \eta(\lambda)w(\lambda)^T. \tag{5.4.63}$$

Now we differentiate (5.4.60), (5.4.61) again and evaluate the derivative at $\lambda = \lambda_N$:

$$\left(F_{xx}^N x_\lambda^N + F_{x\lambda}^N\right) v + F_x^N v_\lambda^N = \mu_\lambda^N v + \mu^N v_\lambda^N - \eta_\lambda^N u - \eta^N u_\lambda^N \tag{5.4.64}$$

$$\left(F_{xx}^N x_\lambda^N + F_{x\lambda}^N\right) u + F_x^N u_\lambda^N = \mu_\lambda^N u + \mu^N u_\lambda^N + \eta_\lambda^N v + \eta^N v_\lambda^N. \tag{5.4.65}$$

Upon multiplying (5.4.64) and (5.4.65) from the left with both w^T and z^T, we have:

$$\begin{aligned} w^T(F_{xx}^N x_\lambda^N + F_{x\lambda}^N)v + w^T F_x^N v_\lambda^N &= \mu_\lambda^N w^T v + \mu^N w^T v_\lambda^N - \eta_\lambda^N w^T u - \eta^N w^T u_\lambda^N \\ z^T(F_{xx}^N x_\lambda^N + F_{x\lambda}^N)v + z^T F_x^N v_\lambda^N &= \mu_\lambda^N z^T v + \mu^N z^T v_\lambda^N - \eta_\lambda^N z^T u - \eta^N z^T u_\lambda^N \\ w^T(F_{xx}^N x_\lambda^N + F_{x\lambda}^N)u + w^T F_x^N u_\lambda^N &= \mu_\lambda^N w^T u + \mu^N w^T u_\lambda^N + \eta_\lambda^N w^T v + \eta^N w^T v_\lambda^N \\ z^T(F_{xx}^N x_\lambda^N + F_{x\lambda}^N)u + z^T F_x^N u_\lambda^N &= \mu_\lambda^N z^T u + \mu^N z^T u_\lambda^N + \eta_\lambda^N z^T v + \eta^N z^T v_\lambda^N. \end{aligned}$$

If we replace $w^T F_x^N$ and $z^T F_x^0$ with the expressions found in (5.4.62), (5.4.63) evaluated at $\lambda = \lambda_N$, then one term drops out in each equation and we are left with:

$$\begin{aligned}
w^T \left(F_{xx}^N x_\lambda^N + F_{x\lambda}^N\right) v + \eta^N z^T v_\lambda^N &= \mu_\lambda^N w^T v - \eta_\lambda^N w^T u - \eta^N w^T u_\lambda^N \\
z^T \left(F_{xx}^N x_\lambda^N + F_{x\lambda}^N\right) v - \eta^N w^T v_\lambda^N &= \mu_\lambda^N z^T v - \eta_\lambda^N z^T u - \eta^N z^T u_\lambda^N \\
w^T \left(F_{xx}^N x_\lambda^N + F_{x\lambda}^N\right) u + \eta^N z^T u_\lambda^N &= \mu_\lambda^N w^T u + \eta_\lambda^N w^T v + \eta^N w^T v_\lambda^N \\
z^T \left(F_{xx}^N x_\lambda^N + F_{x\lambda}^N\right) u - \eta^N w^T u_\lambda^N &= \mu_\lambda^N z^T u + \eta_\lambda^N z^T v + \eta^N z^T v_\lambda^N .
\end{aligned}$$

Diagonally adding the first and fourth of these equations and diagonally subtracting the second and third cancel two more terms. After rearranging terms again, we have the final linear system:

$$A \begin{pmatrix} \mu_\lambda^N \\ \eta_\lambda^N \end{pmatrix} = b, \tag{5.4.66}$$

with:

$$A := \begin{pmatrix} -z^T u - w^T v & -z^T v + w^T u \\ z^T v - w^T u & -z^T u - w^T v \end{pmatrix} \tag{5.4.67}$$

and:

$$b := \begin{pmatrix} -z^T (F_{xx}^N x_\lambda^N + F_{x\lambda}^N) u - w^T (F_{xx}^N x_\lambda^N + F_{x\lambda}^N) v \\ z^T (F_{xx}^N x_\lambda^N + F_{x\lambda}^N) v - w^T (F_{xx}^N x_\lambda^N + F_{x\lambda}^N) u \end{pmatrix}, \tag{5.4.68}$$

where x_λ^N can be found as the unique solution of the regular system (5.4.26).

Finally, we note that the determinant of the matrix (5.4.67) in system (5.4.66) equals $(z^T u + w^T v)^2 + (w^T u - z^T v)^2$ which is nonzero as long as δ is simple. □

We now turn to the computation of the stability coefficient a by using directly formula (3.7.7). Remember that we are dealing here with periodic solutions γ of ordinary differential equations and that the map F is actually the Poincaré map S as defined in definition 2.2.3.5. In this definition the fixed point $\overline{x}_N \in \mathbb{R}^{n-1}$ of S corresponds to the point $x_N \in \gamma \cap \mathbb{R}^n$ via the transformation $x = U\overline{x}_N + x_{\text{orig}}$. Now, if we continue a periodic solution $\overline{x}_{N-1}$ by varying the parameter λ and use the Poincaré map method, then we are led, in general, to the next fixed point $\overline{x}_N$ of S that is only close to the origin, since the new Poincaré map is still defined on the old return plane with $x_{\text{orig}} = x_{N-1}$ and $0 = \overline{x}_{N-1} \in \mathbb{R}^{n-1}$ (see definition 2.2.3.5 and Subsection 5.5.2). Therefore, in order to compute the stability coefficient a for $\overline{x}_N$ as in (3.7.7), we must first shift it to the origin. That can easily be done so that now we may assume that $\overline{x}_N = 0$, that is $S(0) = 0$.

In order not to overload the upcoming calculations with indices, let us confine ourselves to the specific case $n = 5$, as is the case of the laser model. Finally, let us stipulate that the remaining two eigenvalues of the Poincaré map have modulus < 1. From the physical point of view this is certainly the most interesting case, since only then may attractive invariant curves appear.

In order to apply the centre manifold theory, we transform the linear part of $S^0_{\bar{x}}$ into standard form by introducing a new basis in $\mathbb{R}^{n-1}$ containing the (generalized) eigenvectors of $S^0_{\bar{x}}$, that is $x = Vz$ and $z = V^{-1}x$ with $V = V_{ij}$. If we now define the map $F(z) := V^{-1}S(Vz)$, then $F(z)$ describes the Poincaré map in these new coordinates. Its Taylor expansion about the origin up to order three is given by:

$$F(z) \approx F(0) + V^{-1}S^0_{\bar{x}}(Vz) + \frac{1}{2}V^{-1}S^0_{\bar{x}\bar{x}}(Vz)(Vz) + \frac{1}{6}V^{-1}S^0_{\bar{x}\bar{x}\bar{x}}(Vz)(Vz)(Vz), \quad (5.4.69)$$

with $F(0) = 0$ and the linear part in decoupled form:

$$V^{-1}S^0_{\bar{x}}V = \begin{pmatrix} \begin{pmatrix} \cos c & -\sin c \\ \sin c & \cos c \end{pmatrix} & 0 \\ 0 & C \end{pmatrix}, \quad (5.4.70)$$

with $C = C_{ij}$ having its eigenvalues strictly inside the unit circle. Introducing $z = (x, y)$, $x \in \mathbb{R}^2$, $y \in \mathbb{R}^2$) and:

$$B = B_{ij} = \begin{pmatrix} \cos c & -\sin c \\ \sin c & \cos c \end{pmatrix}, \quad (5.4.71)$$

we can reformulate (5.4.69) and use centre manifold terminology as in (2.3.8), (2.3.9). Then the map becomes:

$$x_{n+1} = Bx_n + K(x_n, y_n) \quad (5.4.72)$$

$$y_{n+1} = Cy_n + G(x_n, y_n). \quad (5.4.73)$$

The bulk of the work now lies in applying theorem 2.3.1.4 to approximate the centre manifold $H(x) = (H_1(x_1, x_2), H_2(x_1, x_2))$. We would like to solve:

$$0 = \begin{pmatrix} H_1(Bx + K(x, H(x, y))) \\ H_2(Bx + K(x, H(x, y))) \end{pmatrix} - C\begin{pmatrix} H_1(x_1, x_2) \\ H_2(x_1, x_2) \end{pmatrix} - \begin{pmatrix} G_1(x, H(x_1, x_2)) \\ G_2(x, H(x_1, x_2)) \end{pmatrix}. \quad (5.4.74)$$

Let us assume a Taylor expansion of H_1 and H_2:

$$H_1(x_1, x_2) = \sum_{i=1,j=i}^{2} a_{ij}x_ix_j + \text{ higher order terms} \quad (5.4.75)$$

$$H_2(x_1, x_2) = \sum_{i=1,j=i}^{2} \alpha_{ij}x_ix_j + \text{ higher order terms} \quad (5.4.76)$$

Putting these expressions into the first equation in (5.4.74), we get:

$$\begin{aligned} 0 \;=\; & a_{11}[B_{11}x_1 + B_{12}x_2 + K_1(x_1, x_2, H_1(x_1, x_2), H_2(x_1, x_2))]^2 + \\ & + a_{12}[B_{11}x_1 + B_{12}x_2 + K_1(x_1, x_2, H_1(x_1, x_2), H_2(x_1, x_2))] \\ & \times [B_{21}x_1 + B_{22}x_2 + K_2(x_1, x_2, H_1(x_1, x_2), H_2(x_1, x_2))] \\ & + a_{22}[B_{21}x_1 + B_{22}x_2 + K_2(x_1, x_2, H_1(x_1, x_2), H_2(x_1, x_2))]^2 \\ & - C_{11}[a_{11}x_1^2 + a_{12}x_1x_2 + a_{22}x_2^2] - C_{12}[\alpha_{11}x_1^2 + \alpha_{12}x_1x_2 + \alpha_{22}x_2^2] \\ & - G_1(x_1, x_2, H_1(x_1, x_2), H_2(x_1, x_2)) + \mathcal{O}(3), \end{aligned} \tag{5.4.77}$$

where $\mathcal{O}(3)$ denotes terms of order three and higher. A similar expression holds, of course, for the second equation in (5.4.74). Now we realize that the functions K_1 and K_2 in (5.5.1) do not contribute to the quadratic terms, but only G_1 does! Let us therefore assume:

$$\begin{aligned} G_1(x_1, x_2, y_1, y_2) \;=\; & C_{311}x_1^2 + C_{312}x_1x_2 + C_{313}x_1y_1 + C_{314}x_1y_2 \\ & + C_{322}x_2^2 + C_{323}x_2y_1 + C_{324}x_2y_2 \\ & + C_{333}y_1^2 + C_{334}y_1y_2 + C_{344}y_2^2 + \mathcal{O}(3), \end{aligned} \tag{5.4.78}$$

$$\begin{aligned} G_2(x_1, x_2, y_1, y_2) \;=\; & C_{411}x_1^2 + C_{412}x_1x_2 + C_{413}x_1y_1 + C_{414}x_1y_2 \\ & + C_{422}x_2^2 + C_{423}x_2y_1 + C_{424}x_2y_2 \\ & + C_{433}y_1^2 + C_{434}y_1y_2 + C_{444}y_2^2 + \mathcal{O}(3). \end{aligned} \tag{5.4.79}$$

Then the only part of $G_1(x_1, x_2, H_1(x_1, x_2), H_2(x_1, x_2))$ that contributes to the quadratic terms in (5.5.1) is $C_{311}x_1^2 + C_{312}x_1x_2 + C_{322}x_2^2$. Taking this into account in (5.5.1), we may collect terms of equal powers, and set them to zero. This gives the inhomogeneous linear system for a_{ij} and α_{ij}:

$$\begin{aligned} C_{311} \;=\; & a_{11}B_{11}^2 + a_{12}B_{11}B_{21} + a_{22}B_{21}^2 - C_{11}a_{11} - C_{12}\alpha_{11} \\ C_{312} \;=\; & 2a_{11}B_{11}B_{12} + a_{12}B_{11}B_{22} + a_{12}B_{12}B_{21} + 2a_{22}B_{21}B_{22} - C_{11}a_{12} \\ & - C_{12}\alpha_{12} \\ C_{322} \;=\; & a_{11}B_{12}^2 + a_{12}B_{12}B_{22} + a_{22}B_{22}^2 - C_{11}a_{22} - C_{12}\alpha_{22}. \end{aligned} \tag{5.4.80}$$

The same approach to the second of the equations in (5.4.74) leads to the system:

$$C_{411} \;=\; \alpha_{11}B_{11}^2 + \alpha_{12}B_{11}B_{21} + \alpha_{22}B_{21}^2 - C_{21}a_{11} - C_{22}\alpha_{11}$$

$$
\begin{aligned}
C_{412} &= 2\alpha_{11}B_{11}B_{12} + \alpha_{12}B_{11}B_{22} + \alpha_{12}B_{12}B_{21} + 2\alpha_{22}B_{21}B_{22} - C_{21}a_{12} \\
&\quad - C_{22}\alpha_{12} \\
C_{422} &= \alpha_{11}B_{12}^2 + \alpha_{12}B_{12}B_{22} + \alpha_{22}B_{22}^2 - C_{21}a_{22} - C_{22}\alpha_{22}. \qquad (5.4.81)
\end{aligned}
$$

We now comment on the solvability of the coupled linear system equations (5.4.80) and (5.4.81) for the unknowns a_{ij}, α_{ij}. Introducing the notation

$$
M_1 = \begin{pmatrix} B_{11}^2 & B_{11}B_{21} & B_{21}^2 \\ 2B_{11}B_{12} & B_{11}B_{22} + B_{12}B_{21} & 2B_{21}B_{22} \\ B_{12}^2 & B_{12}B_{22} & B_{22}^2 \end{pmatrix}, \qquad (5.4.82)
$$

we can rewrite the matrix of this coupled linear system as:

$$
\begin{pmatrix} (M_1 - C_{11}\mathrm{id}) & -C_{12}\mathrm{id} \\ -C_{21}\mathrm{id} & (M_1 - C_{22}\mathrm{id}) \end{pmatrix}. \qquad (5.4.83)
$$

If we use (5.4.71) it is an easy exercise to check that the eigenvalues of M_1 are precisely:
$\{1, \cos(2c) \pm i\,\sin(2c)\}$, and since $c \neq k\frac{\pi}{2}$, M_1 has a pair of complex conjugate eigenvalues on the unit circle. Therefore, since $\|C_{11}\|_2 < 1$ and $\|C_{22}\|_2 < 1$, we see that $(M_1 - C_{11}\mathrm{id})$ and $(M_1 - C_{22}\mathrm{id})$ are regular matrices. Hence, if C has two real eigenvalues (of norm less than 1), then $C_{21} = 0$, and equation (5.4.83) gives first a unique solution for α_{ij}, which in (5.4.80) then leads to a unique solution for a_{ij}.

Let us then assume C has a pair of complex conjugate eigenvalues (strictly inside the unit circle). Then $C_{11} = C_{22}$ and $C_{12} = -C_{21}$. We now show that the homogeneous system with matrix (5.4.83) has 0 as its unique solution. This will in turn prove that the coupled linear systems (5.4.80) and (5.4.81) have a unique solution for a_{ij}, α_{ij}. For every fixed $a \in \mathbb{R}^3$, the second equation in (5.4.83) has the unique solution: $\alpha = \alpha(a) = (M_1 - C_{11}\mathrm{id})^{-1}(-C_{12}a)$. Putting this solution into the first equation of (5.4.83), we find after rearranging:

$$
\Big(C_{12}^2(M_1 - C_{11}\mathrm{id})^{-1} + (M_1 - C_{11}\mathrm{id})\Big)a = 0, \qquad (5.4.84)
$$

and upon multiplying this with $(M_1 - C_{11}\mathrm{id})$ we have $0 = \Big(C_{12}^2\mathrm{id} + (M_1 - C_{11}\mathrm{id})^2\Big)a$. If here $a \neq 0$, then we could conclude that $-C_{12}^2$ were an eigenvalue of $(M_1 - C_{11}\mathrm{id})^2$, which in turn would imply that $C_{11} \pm i\,C_{12}$ were an eigenvalue of M_1. But this contradicts the fact that the complex eigenvalue of M_1 is of norm 1, while $|C_{11} \pm iC_{12}| < 1$. Hence we can uniquely solve the linear systems to find the a_{ij} and α_{ij}.

However, we still need the right-hand sides of systems (5.4.80), (5.4.81), that is the as yet unknown C_{ijk}. Since they are the second-order coefficients of G_1 and G_2, a glance at (5.4.69) shows that they are hidden in the last two components of:

$$\begin{aligned}\frac{1}{2}V^{-1}S^0_{\overline{x}\overline{x}}(Vz)(Vz) &= \frac{1}{2}V^{-1}\sum_{j=1,k=1}^{n-1}\frac{\partial^2 S_i}{\partial\overline{x}_j\partial\overline{x}_k}(0)\left(\sum_{p=1}^{n-1}V_{kp}z_p\right)\left(\sum_{m=1}^{n-1}V_{jm}z_m\right)\\ &= \sum_{j=1,k=j}^{n-1}C_{ijk}z_jz_k. \qquad (5.4.85)\end{aligned}$$

and we numerically rearrange (5.4.85) to collect terms of equal powers to find the C_{ijk} for $i=1,\ldots n-1$, $j=i,\ldots n-1$, $k=j,\ldots n-1$. In summary, we now know the second-order terms of the centre manifold:

$$H_1(x_1,x_2) = a_{11}x_1^2+a_{12}x_1x_2+a_{22}x_2^2+\mathcal{O}(3) \qquad (5.4.86)$$

$$H_2(x_1,x_2) = \alpha_{11}x_1^2+\alpha_{12}x_1x_2+\alpha_{22}x_2^2+\mathcal{O}(3). \qquad (5.4.87)$$

But we are not done yet!

In the current notation the reduced system on the centre manifold becomes $x_{n+1} = Bx_n + K(x_n, H(x_n))$. In order to save some indices let us redefine $x=(x,y)\in\mathbb{R}^2$ and $K=(k,g)\in\mathbb{R}^2$. Then, in agreement with the notation used in (2.3.10), the restricted system reads:

$$\begin{pmatrix}x_{n+1}\\y_{n+1}\end{pmatrix} = B\begin{pmatrix}x_n\\y_n\end{pmatrix}+\begin{pmatrix}k(x_n,y_n,H_1(x_n,y_n),H_2(x_n,y_n))\\g(x_n,y_n,H_1(x_n,y_n),H_2(x_n,y_n))\end{pmatrix}, \qquad (5.4.88)$$

and having the stability formula (3.7.7) in mind, we see that we need the third-order terms of k,g. These are of course hidden in: $\frac{1}{6}V^{-1}S^0_{xxx}(Vz)(Vz)(Vz)$. Similar to the quadratic coefficients, we numerically rearrange the terms to express:

$$\frac{1}{6}V^{-1}S^0_{xxx}(Vz)(Vz)(Vz) = \sum_{j=1,k=j,m=k}^{n-1}C_{ijkm}z_jz_kz_m. \qquad (5.4.89)$$

Using the terms C_{ijkm} and the approximations (5.4.86), (5.4.87) in (5.4.88), we collect equal powers of x,y again and finally find the desired derivatives:

$$\begin{aligned}k^0_{xx} &= 2C_{111} \quad\text{and}\quad g^0_{xx}=2C_{222}\\ k^0_{xy} &= C_{112} \quad\text{and}\quad g^0_{xy}=C_{212}\\ k^0_{yy} &= 2C_{122} \quad\text{and}\quad g^0_{yy}=2C_{211}\end{aligned}$$

$$
\begin{aligned}
k^0_{xxx} &= 6(C_{113}a_{11} + C_{114}\alpha_{11} + C_{1111}) \\
k^0_{xxy} &= 2(C_{113}a_{12} + C_{114}\alpha_{12} + C_{123}a_{11} + C_{124}\alpha_{11} + C_{1112}) \\
k^0_{xyy} &= 2(C_{113}a_{22} + C_{114}\alpha_{22} + C_{123}a_{12} + C_{124}\alpha_{12} + C_{1122}) \\
k^0_{yyy} &= 6(C_{124}\alpha_{22} + C_{123}a_{22} + C_{1222}) \\
g^0_{xxx} &= 6(C_{213}a_{11} + C_{214}\alpha_{11} + C_{2111}) \\
g^0_{xxy} &= 2(C_{213}a_{12} + C_{214}\alpha_{12} + C_{223}a_{11} + C_{224}\alpha_{11} + C_{2112}) \\
g^0_{xyy} &= 2(C_{213}a_{22} + C_{214}\alpha_{22} + C_{223}a_{12} + C_{224}\alpha_{12} + C_{2122}) \\
g^0_{yyy} &= 6(C_{224}\alpha_{22} + C_{223}a_{22} + C_{2222}).
\end{aligned}
$$

Together with corollary 5.4.6.1 we can now apply theorem 3.7.0.6 to classify secondary Hopf bifurcations.

5.4.7 Applications to Degenerate Secondary Hopf Bifurcations

If, in addition to the hypothesis of corollary 5.4.4.1, the crossing speed $d = \|\delta\|^N_\lambda = 0$, then one may compute its second derivative $\|\delta\|^N_{\lambda\lambda}$ and check whether the critical Floquet multiplier leaves the unit circle or bounces back into it. A derivation of the formula for $\|\delta\|^N_{\lambda\lambda}$ follows the one for $\|\delta\|^N_\lambda$ and we only outline the calculations. Differentiating $\|\delta(\lambda)\|_2 = \sqrt{\mu(\lambda)^2 + \eta(\lambda)^2}$ twice with respect to the parameter λ and using $\mu^N\mu^N_\lambda + \eta^N\eta^N_\lambda = 0$ yields:

$$
\|\delta\|^N_{\lambda\lambda} = (\mu^N_\lambda)^2 + (\eta^N_\lambda)^2 + \mu^N\mu^N_{\lambda\lambda} + \eta^N\eta^N_{\lambda\lambda}, \tag{5.4.90}
$$

with the only unknowns $\mu^N_{\lambda\lambda}$ and $\eta^N_{\lambda\lambda}$. However, after differentiating the eigenvalue relation

$$
S_{\overline{x}}(\overline{x}(\lambda), \lambda)\,(v(\lambda) + i\,u(\lambda)) - (\mu(\lambda) + i\,\eta(\lambda))\,(v(\lambda) + i\,u(\lambda)) = 0 \tag{5.4.91}
$$

twice and evaluating at (x_N, λ_N), multiplying the outcome from the left with $(w + i\,z)^*$ and splitting the result into its real and imaginary parts, we arrive at a regular, linear, inhomogeneous 2×2 system $Ax = b$ for $x := (\mu^N_{\lambda\lambda}, \eta^N_{\lambda\lambda})$ with:

$$
A := \begin{pmatrix} -w^Tv - z^Tu & w^Tu - v^Tz \\ -w^Tu + v^Tz & -w^Tv - z^Tu \end{pmatrix} \tag{5.4.92}
$$

and:

$$\begin{aligned} b_{11} &:= -w^T X_1 v - z^T X_1 u - 2z^T X_2 u_\lambda^N - 2w^T X_2 v_\lambda^N \\ &\quad + 2w^T \mu_\lambda^N v_\lambda^N - 2w^T \eta_\lambda^N u_\lambda^N + 2z^T \mu_\lambda^N u_\lambda^N + 2z^T \eta_\lambda^N v_\lambda^N \qquad (5.4.93) \\ b_{12} &:= -w^T X_1 u + z^T X_1 v - 2w^T X_2 u_\lambda^N + 2z^T X_2 v_\lambda^N \\ &\quad + 2w^T \mu_\lambda^N u_\lambda^N + 2w^T \eta_\lambda^N v_\lambda^N - 2z^T \mu_\lambda^N v_\lambda^N + 2z^T \eta_\lambda^N u_\lambda^N \qquad (5.4.94) \end{aligned}$$

where

$$X_1 := F_{xxx}^N x_\lambda^N x_\lambda^N + 2F_{xx\lambda}^N x_\lambda^N + F_{xx}^N x_{\lambda\lambda}^N + F_{x\lambda\lambda}^N, \qquad X_2 := F_{xx}^N x_\lambda^N + F_{x\lambda}^N.$$

Here the quantities x_λ^N and $x_{\lambda\lambda}^N$ again solve the regular systems (5.4.26) respectively (5.4.29) while v_λ^N, u_λ^N can be found by differentiating (5.4.91) once and rearranging terms:

$$\left(S_x^N - \delta \mathrm{id}\right)(v_\lambda^N + i\,u_\lambda^N) = (\mu_\lambda^N + i\,\eta_\lambda^N)(v + i\,u) - \left(S_{xx}^N x_\lambda^N + S_{x\lambda}^N\right)(v + i\,u) \quad (5.4.95)$$

with, in addition, $w^T v_\lambda^N + z^T u_\lambda^N = 0$ and $w^T u_\lambda^N - z^T v_\lambda^N = 0$ arising from the differentiation of the normalization of $v(\lambda) + i\,u(\lambda)$ with respect to the left eigenvector $w_N + i z_N$.

5.5 Finding an Initial Solution

In order to start the continuation scheme, we need an initial solution (x_0, λ_0) of $f(x, \lambda) = 0$. If we have a good guess, we can use a corrector, for instance Newton's method, to find (x_0, λ_0). But we could also apply the continuation method itself to solve the homotopy problem:

$$K(x, t) := t f(x, \lambda_0) + (1 - t) g(x) = 0 \qquad (5.5.1)$$

from $t = 0$ to $t = 1$. If a solution x_0 of $K(x, 0) = g(x) = 0$ is readily available, then we can hope that this solution extends to $t = 1$ and yields the desired initial solution.

Global homotopies such as:

$$K(x, t) := f(x, \lambda_0) - e^{-\alpha t} f(x^*, \lambda_0) = 0 \qquad (5.5.2)$$

with $\alpha > 0$ and x^* arbitrary may also be considered. If the initial solution x^* of $K(x, 0) = 0$ exists for all $t > 0$, then, as $t \to \infty$, it must approach a solution x_0 of $f(x, \lambda_0) = 0$.

However, the solution branches of (5.5.1) and (5.5.2) do not necessarily exist for $t = 1$, respectively for $t \to \infty$. For instance, a saddle-node in the parameter t may turn the branches around.

5.5.1 Finding an Initial Periodic Orbit

In our specific case, the solutions to $f(x, \lambda) = 0$ should represent a branch of periodic solutions of (2.2.1). Hence, we need to find an initial periodic orbit γ_0 or, equivalently, any point $x_0 \in \gamma_0$ and its period T_0. The literature provides us with several ideas to achieve this goal. First of all, there is the brute force approach as used for Fig. 3a in [54]. Here one picks an arbitrary initial point x^* and computes the trajectory $\phi(t, x^*, \lambda_0)$. If x^* is choosen sufficiently close to an asymptotically stable periodic orbit γ_0, then, after transients have died out, the trajectory will be indistinguishable from γ_0 and any point $x_0 = \phi(t^*, x^*, \lambda_0)$ with $t^* \gg 0$ will serve as $x_0 \in \gamma_0$. The restrictions of this method are obvious:

- it works only for attractive γ_0,
- the required time t^* may be extremely large resulting in a costly integration,
- the period T_0 remains unknown, and, finally,
- x^* must lie within "the domain of attraction of γ_0" which can be arbitrarily small.

Variations of this idea include computing the "Lyapunov exponents" [52], [131], [187] or the "power spectrum" [26], [30] of the trajectory $\phi(t, x^*, \lambda_0)$.

Some systematic care is needed, if we apply the brute force technique in the neighbourhood of an equilibrium branch, see [148]. We may then hope that a supercritical Hopf bifurcation occurs leading to asymptotically stable, small amplitude periodic solutions of period $T_0 \approx \frac{2\pi}{\omega}$, see theorem 3.6.0.5.

Another method, also aimed at locating only attractive periodic solutions, was proposed by [64]. However, this idea is no longer related to brute force. Starting from a trajectory segment with a relatively low positive Lyapunov exponent "L", it systematically uses Newton's method to iteratively decrease L and find γ_0.

There is also the class of "shooting methods". Any T_0-periodic orbit, stable or unstable, satisfies:

$$\frac{\partial \phi}{\partial t}(t, x, \lambda_0) = f(\phi(t, x, \lambda_0), \lambda_0) \text{ and } \phi(T_0, x_0, \lambda_0) = x_0 \tag{5.5.3}$$

(and $\phi(t, x_0, \lambda_0) \neq x_0$ for $0 < t < T_0$). Assuming good initial guesses x_0^0 and T_0^0 for x_0 and T_0, we expand (5.5.3) into:

$$\begin{aligned} x_0 &= x_0^0 + dx = \phi(T_0, x_0, \lambda_0) = \phi(T_0^0 + dt, x_0^0 + dx, \lambda_0) \\ &\approx \phi(T_0^0, x_0^0, \lambda_0) + f(\phi(T_0^0, x_0^0, \lambda_0), \lambda_0)dt + \frac{\partial \phi}{\partial x}(T_0^0, x_0^0, \lambda_0)dx, \end{aligned} \tag{5.5.4}$$

where the matrix $\frac{\partial \phi}{\partial x}(T_0^0, x_0^0, \lambda_0)$ can be found by solving the first variational equation:

$$\frac{\partial}{\partial t}\left(\frac{\partial \phi}{\partial x}(t, x_0^0, \lambda_0)\right) = \frac{\partial}{\partial x}\left(f(\phi(t, x_0^0, \lambda_0), \lambda_0)\right) = \frac{\partial f}{\partial x}\left(\phi(t, x_0^0, \lambda_0)\right)\frac{\partial \phi}{\partial x}(t, x_0^0, \lambda_0) \tag{5.5.5}$$

from $t = 0$ to $t = T_0^0$ together with the original flow (2.2.1) and initially: $\frac{\partial \phi}{\partial x}(0, x_0^0, \lambda_0) =$ id. Notice that (5.5.4) represents an underdetermined linear system in the unknowns (dx, dt) and we need to impose one further condition. But since any point $x_0 \in \gamma_0$ serves equally well, we may additionally fix its i-th coordinate by requiring that $x_0(i) = \text{const}$. Then we can solve (5.5.4), define $x_0^1 := x_0^0 + dx$ and $T_0^1 := T_0^0 + dt$ and iterate this process. This "simple" shooting method is certainly easiest to implement. Unfortunately though, as pointed in [173], the convergence behaviour is bad if γ_0 crosses the hyperplane $H = \{x |\, x(i) = \text{const}\}$ in a small angle. In fact, the system becomes singular if the trajectory does not transversally cross H.

These difficulties can be avoided by varying the hyperplane H in each iteration step, such that it is always orthogonal to the flow across the last approximation. This leads to the classical orthogonality condition as used in [122], [75], [76].

Should the unknown period T_0 (or the iterations towards it) become "too large", then one can rescale the time by setting:

$$t^* := \frac{t}{T_0}. \tag{5.5.6}$$

Then defining $\varphi(t^*, x) := \phi(t^* T_0, x)$, we see that the nonlinear boundary value problem (5.5.3) becomes:

$$\frac{\partial \varphi}{\partial t^*}(t^*, x, T_0, \lambda_0) = T_0 f(\varphi(t^*, x, T_0, \lambda_0), \lambda_0) \text{ and } \varphi(1, x_0, T_0, \lambda_0) = x_0. \tag{5.5.7}$$

The unknown period has been transformed into an unknown parameter occurring in the vector field for φ and we are now searching for a periodic orbit γ_0 with period equal to 1. Newton's method applied to (5.5.7) leads to:

$$\frac{\partial \varphi}{\partial x}(1, x_0^k, T_0^k, \lambda_0)dx + \frac{\partial \varphi}{\partial T_0}(1, x_0^k, T_0^k, \lambda_0)dt = x_0^k - \varphi(1, x_0^k, T_0^k, \lambda_0), \tag{5.5.8}$$

where the matrix $\frac{\partial \varphi}{\partial x}(1, x_0^k, t_0^k, \lambda_0)$ can be found as in (5.5.5) and the vector $\frac{\partial \varphi}{\partial T_0}(1, x_0^k, T_0^k, \lambda_0)$ by solving additionally:

$$\frac{\partial}{\partial t}\left(\frac{\partial \varphi}{\partial T_0}(t, x_0^k, T_0^k, \lambda_0)\right) = f\left(\varphi(t, x_0^k, T_0^k, \lambda_0), \lambda_0\right) + T_0 \frac{\partial f}{\partial x}\left(\varphi(t, x_0^k, T_0^k, \lambda_0), \lambda_0\right) \tag{5.5.9}$$

with initial conditions $\frac{\partial \varphi}{\partial T_0}(0, x_0^k, T_0^k, \lambda_0) = 0$.

The orthogonality condition, even though it works very well for fixed λ_0, does, however, allows sharp fronts and peaks to move into the branch when continuing γ_0, [42]. An approach designed to prevent these problems from occurring can be found in [85]. Essentially it is the integrated version of the orthogonality condition. This idea has been implemented in the AUTO code, and, in [42], a considerable improvement regarding efficiency is reported. Of course, it is also applicable to finding just one initial periodic orbit. Here the extra condition minimizes the norm between two consecutive approximations with respect to translation in time and can be formulated as:

$$\int_0^1 \varphi(t, x_0^{k+1}, T_0^{k+1}, \lambda_0)^T \varphi(t, x_0^k, T_0^k, \lambda_0)\, dt = 0. \tag{5.5.10}$$

For more detail we refer to [85] or [42]. On the other hand, this idea inherits the slight drawback that imposing condition (5.5.10) leads to an additional differential equation and the resulting linear system becomes $(n+1)$-dimensional. However, the results obtained with it are impressive — in particular when γ approaches a "homoclinic connection" and its period tends to ∞, see [42].

Further literature and methods, more or less related to the above, can be found in [6], [31], [39], [69], [75], [87], [103], [148], [169], [184], [184] where the last two are based upon "moving orthogonal coordinate systems".

Finally, there is the Poincaré map method.

5.5.2 The Poincaré Map Method

Based upon definition 2.2.3.5, this method tries to find a periodic orbit by locating a fixed point of the Poincaré map, i.e. by solving $S(\overline{x}, \lambda_0) = \overline{x}$. Let therefore

x_0 and T_0 be good approximations to a point of γ and the period T, respectively. Shifting the origin to x_0, i.e. $x_{\text{orig}} := x_0$, and introducing a new orthonormal basis in $H \perp f(x_0, \lambda_0)$, we recall first the definition $S(\overline{x}, \lambda_0) := U^T\{\phi(\tau(x, \lambda_0), x, \lambda_0) - x_{\text{orig}}\}$ with $x = U\overline{x} + x_{\text{orig}}$ for $U \in L(\mathbb{R}^{n-1}, \mathbb{R}^n)$. Newton's method gives $\overline{x}^{k+1} = \overline{x}^k - d\overline{x}$ with $d\overline{x}$ the solution of the linear system:

$$\left(S_{\overline{x}}^k - \text{id}\right) d\overline{x} = (S_{\overline{x}}(\overline{x}_k, \lambda_0) - \text{id}) d\overline{x} = S(\overline{x}_k, \lambda_0) - \overline{x}_k. \tag{5.5.11}$$

To compute $S(\overline{x}, \lambda_0)$ for an arbitrary $\overline{x}$ we employ a second iteration scheme: if T_0 is a good approximation for the return time $T = \tau(x, \lambda_0)$ with $x = U\overline{x} + x_{\text{orig}}$, then we have $T = T_0 + dT_0$. Furthermore: $\phi(T_0 + dT_0, x, \lambda_0) - x_{\text{orig}} \perp f(x_{\text{orig}}, \lambda_0)$. Expanding and solving for dT_0 we find:

$$dT_0 = -\frac{< \phi(T_0, x, \lambda_0) - x_{\text{orig}}, f(x_{\text{orig}}, \lambda_0) >}{< f(\phi(T_0, x, \lambda_0), \lambda_0), f(x_{\text{orig}}, \lambda_0) >}. \tag{5.5.12}$$

If T_0 is sufficiently close to T, then the iteration

$$T_{k+1} := T_k + dT_k, \quad k = 0, 1, 2, \ldots, \tag{5.5.13}$$

will converge to T and $S(\overline{x}, \lambda_0) = U^T\{\phi(T, x, \lambda_0) - x_{\text{orig}}\}$ is found.

For the Jacobian matrix in (5.5.11) we have next, see (2.2.23):

$$S_{\overline{x}}^k - \text{id} = U^T\Big(f(\phi(\tau(x_k, \lambda_0), x_k, \lambda_0), \lambda_0)\frac{\partial \tau}{\partial x}(x_k, \lambda_0) + \frac{\partial \phi}{\partial x}(\tau(x_k, \lambda_0), x_k, \lambda_0)\Big)U - \text{id}, \tag{5.5.14}$$

with the matrix $\frac{\partial \phi}{\partial x}(\tau(x_k, \lambda_0), x_k, \lambda_0)$ as in (5.5.5). To find $\frac{\partial \tau}{\partial x}(x, \lambda_0)$ we use theorem 2.2.3.3. Since $< f(x_{\text{orig}}, \lambda_0), \phi(\tau(x, \lambda_0), x, \lambda_0) - x_{\text{orig}} >= 0$ in a neighbourhood of x_{orig}, it follows by differentiation of this identity:

$$\frac{\partial \tau}{\partial x}(x, \lambda_0) = -\frac{f(x_{\text{orig}}, \lambda_0)^T\left(\frac{\partial \phi}{\partial x}(\tau(x, \lambda_0), x, \lambda_0)\right)}{< f(x_{\text{orig}}, \lambda_0), f(\phi(\tau(x, \lambda_0), x, \lambda_0) >}, \tag{5.5.15}$$

and, upon evaluating (5.5.15) at $x = x_k \in \mathbb{R}^n$, $S_{\overline{x}}^k$ in (5.5.14) is found.

We see that the derivative of the return time $\tau(x, \lambda_0)$ with respect to x and hence the derivative of the Poincaré map with respect to x can be expressed in terms of the variational matrix and the return values of x. We also remark that (5.5.11) is indeed $(n-1)$-dimensional, but that we must perform the nested iteration to find the return times $\tau(x_k, \lambda_0)$ and the return values $S(x_k, \lambda_0)$.

Note also that, if the return time $\tau(x, \lambda_0)$ becomes "too large", we can speed up the flow by using the above substitution $\varphi(t^*, x) := \phi(t^*T, x)$ for a fixed $T \approx \tau(x, \lambda_0)$. Then the vector field becomes $\dot{x} = Tf(x, \lambda)$ and, in the scaled time, the return time will be close to 1.

5.6 Continuation of the Poincaré Map

Having set up the equation $S(\overline{x}, \lambda_0) - \overline{x} = 0$ and assuming a solution $(\overline{x}_0, \lambda_0)$ to it, we may now apply pseudo-arclength continuation to compute a branch of periodic solutions. However, we must first prove that the Poincaré map is not only a differentiable function of $\overline{x}$ but also of its parameters. Therefore it is sufficient to show that the return time $\tau = \tau(x, \lambda)$ is a C^1-function of λ, since by theorem 2.2.3.3 we know already that it is a C^1-function of x.

Theorem 5.6.0.1 *Let $y_1 := \phi(T, x_0, \lambda_0)$ and H_0 and H_1 be two hyperplanes in $\mathbb{R}^n$ transversal to the flow across x_0 and y_1, respectively.*

Then there exists an open interval $I(\lambda_0) \subset \mathbb{R}$ and a unique C^1-function $\tau : I \longrightarrow \mathbb{R}$ such that $\phi(\tau(x_0, \lambda), x_0, \lambda) \in H_1$ and $\tau(x_0, \lambda_0) = T$. Furthermore, the derivative of τ with respect to λ is given by:

$$\frac{\partial \tau}{\partial \lambda}(x_0, \lambda) = -\frac{< f(y_1, \lambda_0), \frac{\partial \phi}{\partial \lambda}(\tau(x_0, \lambda), x_0, \lambda)) >}{< f(y_1, \lambda_0), f(\phi(\tau(x_0, \lambda), x_0, \lambda), \lambda) >} \tag{5.6.1}$$

Proof: The proof adopts that of theorem 2.2.3.3. Define $g : \mathbb{R} \times \mathbb{R} \longrightarrow \mathbb{R}$ by:

$$g(x_0, \tau, \lambda) :=< f(y_1, \lambda_0), \phi(\tau, x_0, \lambda) - y_1 >, \tag{5.6.2}$$

with $g(x_0, T, \lambda_0) = 0$ and $\frac{\partial g}{\partial \tau}(x_0, T, \lambda_0) = \|f(y_1, \lambda_0)\|_2^2 \neq 0$. Consequently, the implicit function theorem 2.1.0.1 applies and guarantees the existence of an interval $I(\lambda_0)$ and a unique C^1-function $\tau = \tau(x_0, \lambda) : I \longrightarrow \mathbb{R}$ such that $g(x_0, \tau(x_0, \lambda), \lambda) = 0$ and $\tau(x_0, \lambda_0) = T$. Differentiation of this identity with respect to λ gives now:

$$< f(y_1, \lambda_0), f(\phi(\tau(x_0, \lambda), x_0, \lambda), \lambda) \frac{\partial \tau}{\partial \lambda}(x_0, \lambda) + \frac{\partial \phi}{\partial \lambda}(\tau(x_0, \lambda), x_0, \lambda) >= 0. \tag{5.6.3}$$

If λ is sufficiently close to λ_0, then $< f(y_1, \lambda_0), f(\phi(\tau(x_0, \lambda), x_0, \lambda), \lambda) >\neq 0$, and we may now solve (5.6.3) for $\frac{\partial \tau}{\partial \lambda}(x_0, \lambda)$ to recover (5.6.1). □

Suppose now that we have found $y_N = (\overline{x}_N, \lambda_N)$ with $\overline{x}_N = U^T(x_N - x_{\text{orig}})$ close to $0 \in \mathbb{R}^{n-1}$ as a fixed point of the Poincaré map for $\lambda = \lambda_0$. Hence, x_N is a point of

the periodic orbit γ_N and x_{orig} close to it was the origin in the new coordinates. We can free the parameter λ and add the extra equation (5.1.3) to obtain the augmented system $g(y_{N+1}) = 0$ for the next solution $y_{N+1} = (\overline{x}_{N+1}, \lambda_{N+1})$ along the branch:

$$S(\overline{x}_{N+1}, \lambda_{N+1}) - \overline{x}_{N+1} = 0, \tag{5.6.4}$$

$$< \overline{x}_{N+1} - \overline{x}_N, \dot{\overline{x}}_N > + (\lambda_{N+1} - \lambda_N)\dot{\lambda}_N - \delta s = 0. \tag{5.6.5}$$

For the extra derivative $\frac{\partial S}{\partial \lambda}(\overline{x}, \lambda)$ in Newton's method we now find:

$$\frac{\partial S}{\partial \lambda}(\overline{x}, \lambda) = U^T\Big\{ f(\phi(\tau(x,\lambda), x, \lambda), \lambda)\frac{\partial \tau}{\partial \lambda}(x, \lambda) + \frac{\partial \phi}{\partial \lambda}(\tau(x,\lambda), x, \lambda))\Big\}, \tag{5.6.6}$$

to be evaluated at $(\overline{x}, \lambda) = (\overline{x}^k_{N+1}, \lambda^k_{N+1})$. Here the scalar $\frac{\partial \tau}{\partial \lambda}(x^k_{N+1}, \lambda^k_{N+1})$ is found as in (5.6.1) and the vector $\frac{\partial \phi}{\partial \lambda}(\tau(x^k_{N+1}, \lambda^k_{N+1}), x^k_{N+1}, \lambda^k_{N+1}))$ by solving:

$$\begin{aligned} \frac{\partial}{\partial t}\left(\frac{\partial \phi}{\partial \lambda}(t, x^k_{N+1}, \lambda^k_{N+1})\right) &= \frac{\partial f}{\partial x}(\phi(t, x^k_{N+1}, \lambda^k_{N+1}), \lambda^k_{N+1}) \\ &\quad \cdot \left(\frac{\partial \phi}{\partial \lambda}(t, x^k_{N+1}, \lambda^k_{N+1})\right) \\ &\quad + \frac{\partial f}{\partial \lambda}(\phi(t, x^k_{N+1}, \lambda^k_{N+1}), \lambda^k_{N+1}) \end{aligned} \tag{5.6.7}$$

from $t = 0$ to $t = \tau(x^k_{N+1}, \lambda^k_{N+1})$ with the initial condition $\frac{\partial \phi}{\partial \lambda}(0, x^k_{N+1}, \lambda^k_{N+1}) = 0$. Note that the knowledge of $\frac{\partial \phi}{\partial \lambda}(\tau(x^k_{N+1}, \lambda^k_{N+1}), x^k_{N+1}, \lambda^k_{N+1}))$ gives us immediately $\frac{\partial \tau}{\partial \lambda}(x^k_{N+1}, \lambda^k_{N+1})$ by (5.6.1), so that, in principle, $S^k_\lambda = \frac{\partial S}{\partial \lambda}(\overline{x}^k_{N+1}, \lambda^k_{N+1})$ can be expressed in terms of $\frac{\partial \phi}{\partial \lambda}(\tau(x^k_{N+1}, \lambda^k_{N+1}), x^k_{N+1}, \lambda^k_{N+1}))$.

Now, since periodic solutions can rapidly move and deform themselves in phase space and in particular shrink to an equilibrium, it is advisable to update the return planes H_N. More specifically, to compute the $(N+1)$-st point $y_{N+1} = (x_{N+1}, \lambda_{N+1})$, we shift the previous x_N to the origin, i.e. $x_{\text{orig}} = x_N$, and hence let the new return plane H_{N+1} be the one perpendicular to the flow across x_N. Of course we must then adjust the predictor based upon the tangential direction $\dot{y}_N = (\dot{\overline{x}}_N, \dot{\lambda}_N)$, since it depends on H_N. This is achieved intuitively by the most natural way, namely by projecting it onto H_{N+1}. Strictly speaking, we are then no longer applying the original pseudo-arclength continuation method. In most cases, however, the difference between the projected and unprojected predictor is truly negligible. This drawback can be avoided, with unessentially more effort, if we introduce a new return plane after each step in the iteration towards y_{N+1} by defining H^k_{N+1} to be the one perpendicular

to the flow across x^k_{N+1}, i.e. with normal $f(x^k_{N+1}, \lambda^k_{N+1})$. However, in a strict sense, we are then giving up the original Newton method, since the return plane (the domain of the Poincaré map) slightly varies during the iteration process.

Finally, we remark that, during the k-th iteration in the step from y_N to y_{N+1}, we also need to perform the iteration (5.5.12), (5.5.13) to find the return times $\tau(x^k_{N+1}, \lambda^k_{N+1})$. As an initial guess for this nested iteration, we could choose the trivial predictor, namely the period τ^N of the periodic orbit accepted at the last step. But we can make a much better guess, since from the last step we also have S^N_x and, in particular, the derivatives $\tau^N_x = \frac{\partial \tau}{\partial x}(x_N, \lambda_N)$ and $\tau^N_\lambda = \frac{\partial \tau}{\partial \lambda}(x_N, \lambda_N)$. Hence, without major additional effort, we find:

$$\frac{\partial \tau}{\partial s}(x(s), \lambda(s))|_{s=0} = (\tau^N_x)^T \cdot U \cdot \dot{x}_N + \tau^N_\lambda \dot{\lambda}_N. \tag{5.6.8}$$

This leads to a better Euler estimate for both the period of γ_{N+1} and the return time of the predictor y^0_{N+1} towards it:

$$\tau(y^0_{N+1}) \approx \tau(y_{N+1}) = \tau(y(\delta s)) \approx \tau(y_N) + \left((\tau^N_x)^T U \dot{x}_N + \tau^N_\lambda \dot{\lambda}_N\right)\delta s. \tag{5.6.9}$$

Then, in the iteration with $k > 0$, we may predict the return time as:

$$\begin{aligned} \tau(y^k_{N+1}) \;=\; & \tau(x^k_{N+1}, \lambda^k_{N+1}) = \tau(x^{k-1}_{N+1} - U d\overline{x}, \lambda^{k-1}_{N+1} - d\lambda) \approx \tau(y^{k-1}_{N+1}) \\ & + \frac{\partial \tau}{\partial x}(x^{k-1}_{N+1}, \lambda^{k-1}_{N+1}) U d\overline{x} + \frac{\partial \tau}{\partial \lambda}(x^{k-1}_{N+1}, \lambda^{k-1}_{N+1}) d\lambda, \end{aligned} \tag{5.6.10}$$

with $(d\overline{x}, d\lambda) = (d\overline{x}^{k-1}, d\lambda^{k-1})$ as the last Newton corrections.

5.7 Branch Switching

The vector $\alpha = (\alpha_0, \alpha_1, \ldots, \alpha_k)$ used for determining the direction of an emanating branch depends on second derivatives of the function g. As already mentioned, this can be quite a nuisance, if these derivatives are difficult to obtain or costly to evaluate.

A clever way to surmount this problem was introduced in [42] and incorporated in our codes. In the case $k = 1$, i.e. simple strict bifurcation, then, instead of proceeding along the exact emanating direction, the author proposes to continue in a direction orthogonal to the current one. This direction, $\dot{y}_N = (\dot{x}_N, \dot{\lambda}_N)$, can easily be found by solving:

$$\begin{pmatrix} f^N_x & f^N_\lambda \\ \dot{x}_{N-1} & \dot{\lambda}_{N-1} \end{pmatrix} \begin{pmatrix} \dot{x}_N \\ \dot{\lambda}_N \end{pmatrix} = \begin{pmatrix} 0 \\ 0 \end{pmatrix} \tag{5.7.1}$$

with the additional normalization $\|\dot{y}_N\|_2 = 1$. As pointed out, this method does not necessarily work, but it does in most practical cases — the difficulties occurring when the two branches enclose only a "small" angle.

We conjecture that this idea can be generalized, to the case $k > 1$ if one chooses a direction that is, in some sense, furthest from the ones that one has already obtained.

5.8 Step Length Selection

So far we have only mentioned "δs sufficiently small". And, of course, δs should be kept variable in order to adapt to the development of the continuation process, that is to adjust to possible changes of the behaviour of g in a neighbourhood of its current solution.

On the other hand, δs should also depend on the particular purpose of the continuation run. Perhaps we want to use the continuation scheme as a homotopy tool and are only interested in "continuation as fast as possible", regardless of details along the branch. The only requirement for δs is then that the predictor based upon it leads to a converging corrector. Similarly, we might consider the question whether there exists a solution with one of its components attaining a certain value. Not caring about bifurcations, we would then like to choose δs as large as possible.

However, if one is interested in really approximating the general solution manifold M_{gen} with all its fine details, and in particular bifurcations, then one cannot afford to let δs grow too big. Then we not only want the corrector to converge, but the convergence should also lead to a point on the same branch we are currently continuing. Also, we want to be sure not to have missed some relevant details. Therefore we must keep the step length δs within reasonable upper bounds. On the other hand, to avoid that too many points are computed for what is actually needed, we should also make sure that δs cannot become too large.

In [38] one finds a predictor-corrector strategy for δs that is supposed to adjust itself according to the performance of Newton's method. It is mostly based upon successive ratios of the Newton increments. However, the precise theoretically derived formulae rely upon Lipschitz bounds, second derivatives and certain other constants and hypotheses that are rarely analytically available and must be approximated. Furthermore, these quantities depend on the solution itself and may vary during continuation. After all, the method does not provide us with guaranteed convergence

all along the branch.

A simpler approch uses Newton's second-order convergence. Ideally we expect to gain two digits in each iteration towards the solution, and in particular, the Newton increments δ_y^k in the iteration towards y_N should lead to: $|\delta_y^{k+1}|/|\delta_y^k| < 1$ as well as $\|g(y^{k+1})\|_2/\|g(y^k)\|_2 < 1$. Therefore we should not expect convergence, if these ratios exceed the value 1, and we better restart the step with a smaller step length δs. Another, extremely easy to implement, idea is based upon the number l_N of performed iterations to reach the last solution y_N. Here one tries to modify δs_{N+1} for the step towards y_{N+1}, such that, in the sense of efficiency, a certain optimal number "opt(c,ϵ)" is needed to find it. As indicated, opt(c,ϵ) depends on the corrector and on the error tolerance we have imposed on the acceptance of a solution. In [165] we find for instance opt$(c,\epsilon) = 3$ for $\epsilon = 10^{-4}$ and Newton's method. This approach suggests to adjust the step length to: $\delta s_{N+1} = \text{opt}(c,\epsilon)/\delta s_N$, see also [166].

A further idea can be found in [149]. It uses quadratic Hermite-Birkhoff interpolation on the last two points y_{N-1}, y_N with tangent, $\dot{y}_N$, at y_N to estimate the distance between the predictor and the solution manifold. In order to keep this distance within a certain tolerance ϵ, it is suggested to use as a "tentative step length": $\delta s \approx \sqrt{2\epsilon\|y_N - y_{N-1}\|_2/\|\dot{y}_N - \dot{y}_{N-1}\|_2}$.

In [47] a related scheme is implemented that is based upon estimating the curvature along the solution curve by measuring the angle α_N between two successive tangents $\dot{y}_{N-1}$ and $\dot{y}_N$. If α_N increases past a critical value (e.g. 10 degrees), then δs_{N+1} is decreased, and vice versa for $\alpha_N < 3°$ an increase in δs_{N+1} is recommended.

Lastly, if the corrector does not provide us with any analytical insight, then one can rarely do better than modifying δs_{N+1} according to some interpolating curve across the points $(l_N, \delta s_N)$. If convergence is achieved using a satisfactory number of iterations, then increase δs_{N+1}, else decrease it. For instance, an exponential function was proposed in [90]: $\delta s_{N+1} \approx 2^{(4-l_N)/3}$. Note that this particular choice leads to opt $= 4$ as the optimal number of iterations.

Our case turns out to be a bit more subtle, since a converging step using Newton's method assumes, first of all, success in the nested iteration to find the return times. Suppose we are iterating in the step from y_N to y_{N+1}. Then the scheme (5.5.12), (5.5.13) must converge to find the $\tau(y_{N+1}^k)$ for $k = 1, 2, \ldots$. Hence, if the sequence $(\tau(y_{N+1}^k))_m$, $m = 1, 2, \ldots$, does not converge, then we retry the step towards y_{N+1} with a decreased step length δs_{N+1}. Moreover, in case of convergence, we want the

return times to remain bounded: $0 < \tau(y^k_{N+1}) < M$ and reasonably close to each other: $|\tau(y^k_{N+1})/\tau(y^{k+1}_{N+1})| - 1 < \epsilon$. Since we certainly do not want the return times to double, we may choose for the absolute bound $M := 2\tau(y_N)$. For the relative bound we obtained good results with $\epsilon := 0.1$. Whenever one of these conditions is violated, then, instead of wasting time on a subsequent Newton iteration (which is then highly unlikely to converge), it is advisable to attempt the calculation with a smaller step length δs_{N+1}.

The step length selection in our codes is based upon a mixture of the above outlined ideas. If the number of iterations towards the latest accepted solution y_N exceeds 4, a ratio $\|g(y^{k+1}_{N+1})\|_2/\|g(y^k_{N+1})\|_2$ within the iteration towards y_{N+1} exceeds 1, the angle between the two last tangents $\dot{y}_N$ and $\dot{y}_{N-1}$ exceeds 10 degrees, or the maximal component of $\dot{y}_N$ changed too much, then δs_{N+1} will be decreased, otherwise increased.

5.9 Termination

In order for our codes to terminate, we have to impose a stopping criterion. This point is in no way as trivial as it may appear at first sight, since, in general, we have no idea where the branches of the regular solution manifold will lead nor how complex they are or how "wild" they behave.

First of all, we should stop execution if one of the parameters involved exceeds a pre-specified bound. More generally, we should halt the program if a certain function $k(y)$ of the individual solutions y along the presently continued branch reaches some critical limit. For example, in the case of periodic solutions γ, some invariants of γ, as the period, the maximal Floquet multiplier, the amplitude, the norm of the periodic orbit,... are conceivable measures. Other (noninvariant) functions of γ could be defined at the current point $x \in \gamma$, for example the norm of the vector field evaluated at $x \in \gamma$.

However, these criteria are not sufficient, since the branches could very well stay inside a bounded region but still be infinitely long. It is therefore advisable to impose additional conditions to restrict the calculations with respect to the sum of the (approximate) lengths of the solution branches. This can be achieved by adding the individual step lengths δs_N that successfully lead to the next solution points y_{N+1}. Nevertheless, we may still run into problems as δs_N may become (and then remain)

very small, forcing the code to compute too many points without reaching the pre-specified bound on the length. This can be circumvented by simply bounding the number N of accepted steps along each branch or by terminating the continuation of a branch if $|\delta s_j|$ becomes too small. Difficulties may also occur if the solution contains a closed loop. In order to recognize such a loop and not to trace it twice, we keep the (strongly regular) input data y_0 as a first set of data in a stack file. Then, whenever subsequently a parameter component crosses its input value, the codes use the secant method to find this point precisely. Should then also $|\lambda_N - \lambda_0| < \epsilon_1$, it further checks whether the above function k satisfies additionally: $|k(y_0) - k(y_N)| < \epsilon_2$, for ϵ_i given and "small". Depending on the choice of k, we may then, more or less safely, conclude that a closed loop has been traced. In the case of participating periodic solutions, the function $k(y_N) := \text{period}(\gamma_N)$ proved here to be a suitable choice. Indeed, it is unlikely that, at our initial parameter constellation, a second periodic orbit coexists with the same period.

All of these ideas have been implemented in our codes in the following way: starting from y_0, the codes first keep the initial point y_0 and the negative step length δs_1 in a stack file. Whenever a jump across a bifurcation point y^* has been detected, they put the current tangent and step length in the stack file and then use the secant method to approach y^* more accurately. After convergence to y^* they check whether y^* has been visited before. If not, they try to switch branches by continuing in a direction perpendicular to the current one. After a first successful step towards y_N with step length δs_N along a new emanating branch, we store the predictor $-3\dot{y}_N$ towards a point along the same branch on the other side of y^* in the stack file. If, on the other hand, y^* has been visited before, they erase the data with the same (or negative) directions from the stack file and start following a new branch with the initial value which is the most recent data in the stack file.

Furthermore, along each of the individually continued branches they count the number of accepted points, they estimate the length of the branch and check if $|\delta s_N| > \delta s_{\text{min}}$ and $\lambda_N \in \Omega$, (δs_{min} a prespecified minimal acceptable step length and Ω a pre-specified parameter domain). If the branch becomes too long, δs_N too small, N too large, $\lambda_N \notin \Omega$ anymore or the initial point λ_0 is reached again, they proceed by continuing from the latest data in the stack file.

In this way, our codes are designed to compute, in a single run, a connected component of the general solution manifold M_{gen} in Ω without tracing any part of

M_{gen} twice. In general, this is certainly very difficult to achieve! In particular, higher order degeneracies such as multiple strict bifurcation points or cusps as in example 3.4.0.12, a sufficiently small angle between two crossing branches or nonintersecting branches that very closely approach each other, or terminating branches as in Fig. 7.4 will likely result in trouble, and we may have to analyze the problem and possibly restart the code.

However, using as much information as possible about the system $g(y) = 0$, especially upon exploiting hidden symmetries, we obtained quite good results when administrating the stack file in the above way. For instance, the system with solutions displayed in Figs. 7.1, 7.2 and 7.3 possesses a certain symmetry leading to one component of $\dot{y}$ that remains constant at 0 along the "o-" and "Δ" branches and is of absolute value 1 along the "+" branch at the strict bifurcation points, see Chapter 7. This feature enabled us to refine the underlying code such that these figures were indeed computed in a single run and no part of any branch along them was traced twice.

5.10 Summary

It should be clear at this point, that at the present time, there is no "best" continuation method, in the sense that it solves each and every problem most efficiently. In fact, universal algorithms seem to retain their universality only in low dimensional problems. Let us quote from [97]: "In order to get an effective code in high dimensions, one usually has to consider each bifurcation problem separately". For example, one certainly wants to exploit special matrix structures occurring in the discretization of partial differential equations. Also, different formulations of a problem may differ drastically. Consider, for instance, the following equivalent statements for a $n \times n$ matrix A:

1. $\det(A) = 0$,
2. $\text{rank}(A) < n$,
3. $Ax = 0$ has a nonzero solution,
4. A has a zero eigenvalue.

However, (1) amounts to solving a one-dimensional (nonlinear) equation, (3) contains n (linearly dependent) equations, (2) amounts to find the dimension of the space spanned by the columns of A and (4) is an eigenvalue formulation.

From [153] we quote further "At the present state of the art, it appears to be impossible to compare the (relevant existing continuation) packages, because their aims differ so widely". Indeed, some codes, like LINLBF, concentrate on one specific problem, while others come in packages or libraries, as AUTO and CONEX, that handle several aspects.

In that respect, our algorithms are no exception. They are primarily designed to trace certain nonhyperbolic periodic solutions of smooth, low dimensional systems. Basically they use pseudo-arclength continuation and step length control based upon used iterations or successive ratios of the corrections. Along a given branch they monitor a variety of critical quantities, like the Jacobian matrix (if available), to detect several kinds of bifurcations and optima. If these quantities cross a specific threshold or become zero, the algorithms use a secant scheme to accurately locate the enclosed critical point. After a classification of the degeneracy they may either continue along the original branch or try to proceed in an orthogonal direction.

We are now sufficiently well equipped to begin continuation.

Chapter 6

First Continuations

In this chapter we present some first results obtained by applying the methods outlined in Chapter 5 to the problem of finding and continuing a hyperbolic periodic solution in the laser equations that were introduced in Chapter 4.

6.1 Examples of Periodic Solutions

To find a periodic orbit we apply the Poincaré map method. That is, for a fixed value of the parameter λ, $\lambda = \lambda_0$, we consider the equation $g(\overline{x}) := S(\overline{x}, \lambda_0) - \overline{x} = 0$ with $g : \mathbb{R}^{n-1} \to \mathbb{R}^{n-1}$ and solve:

$$g(\overline{x}_0) = S(\overline{x}_0, \lambda_0) - \overline{x}_0 = U^T\{\phi(\tau(x_0, \lambda_0), x_0, \lambda_0) - x_{\text{orig}}\} - \overline{x}_0 = 0 \qquad (6.1.1)$$

for the unknown $\overline{x}_0 \in \mathbb{R}^{n-1}$. Recall that $x_0 = U\overline{x}_0 + x_{\text{orig}}$ with $x_{\text{orig}} \in \mathbb{R}^n$, close to the periodic orbit, a fixed initial guess that becomes the new origin in the return plane perpendicular to the flow across it and with U as the corresponding orthonormal transformation matrix. Furthermore, $\tau = \tau(x, \lambda_0)$ is the first return time of the point $x \in \mathbb{R}^n$. It is well defined for x sufficiently close to x_{orig}. Let x^k with $x^k = U\overline{x}^k + x_{\text{orig}}$ denote the k-th iterate in Newton's method to find the solution $\overline{x}_0$ of system (6.1.1) — later on, this solution will be continued. Then we need the derivatives of the Poincaré map S with respect to $\overline{x}$. Define $x_\tau := \phi(\tau(x, \lambda_0), x, \lambda_0) \in \mathbb{R}^n$ as the first return point of x and recall the derivative of S with respect to $\overline{x}$:

$$S_{\overline{x}}(\overline{x}, \lambda_0) = U^T\Big\{f[\phi(\tau(x, \lambda_0), x, \lambda_0)]\frac{\partial \tau}{\partial x}(x, \lambda_0) + \frac{\partial \phi}{\partial x}(\tau(x, \lambda_0), x, \lambda_0)\Big\}U. \qquad (6.1.2)$$

Using our short notation with

$$f^k := f(x_\tau^k, \lambda_0),\ \tau^k := \tau(x^k, \lambda_0),\ \tau_x^k := \frac{\partial \tau}{\partial x}(x^k, \lambda_0)\ \phi_x^k := \frac{\partial \phi}{\partial x}(\tau^k, x^k, \lambda_0),$$

evaluation of (6.1.2) at $\overline{x} = \overline{x}^k$ gives:

$$S_{\overline{x}}^k := S_{\overline{x}}(\overline{x}^k, \lambda_0) = U^T\{f^k\tau_x^k + \phi_x^k\}U. \tag{6.1.3}$$

Using the same notation for the derivative $\frac{\partial\tau}{\partial x}(x^k, \lambda_0)$, we recall from (5.5.15):

$$\tau_x^k = \frac{\partial\tau}{\partial x}(x^k, \lambda_0) = \frac{-f(x_{\text{orig}}, \lambda_0)^T\phi_x^k}{f(x_\tau^k, \lambda_0)^T f(x_{\text{orig}}, \lambda_0)} \tag{6.1.4}$$

where the denominator is not zero in a neighbourhood of x_{orig}. Hence, for $S_{\overline{x}}^k$, we "only" need the first variational matrix $\phi_x^k = \frac{\partial\phi}{\partial x}(\tau^k, x^k, \lambda_0)$. Therefore we define $c_{ij} = c_{ij}(t, x^k, \lambda_0) := \frac{\partial\phi_i}{\partial x_j}(t, x^k, \lambda_0)$ for $i, j = 1, 2, \ldots, n$. Then:

$$\dot{c}_{ij} = \frac{\partial}{\partial x_j}\Big(f_i(\phi(t, x, \lambda_0), \lambda_0)\Big)\Big|_{x=x^k} = \sum_{r=1}^{n}\frac{\partial f_i}{\partial x_r}(\phi(t, x^k, \lambda_0), \lambda_0)c_{rj}. \tag{6.1.5}$$

This n^2-dimensional differential equation must be integrated along with the n-dimensional flow from $t = 0$ to $t = \tau^k$. The initial conditions $c_{ij}(0, x^k, \lambda_0)$ equal δ_{ij} since the map $\phi(0, x, \lambda)$ reduces to the identity. Hence, to find a periodic orbit with the Poincaré map method, we must solve an $(n + n^2)$-dimensional, partially coupled, nonlinear ordinary differential equation. For the laser system, $n = 5$, and this reduces to a 30-dimensional equation.

6.1.1 Results

Fixing $Y = 600$, $\Delta = 7.5$, $\Theta = -22$ and, as usual, $k = 0.5$, $c = 500$, $\gamma = 2$, $\sigma = 1$, Table 6.1 shows initial values $x(0)$ and periods T of several coexisting periodic orbits in the laser model. Here, and unless otherwise specified, a "+" in the last column denotes a stable orbit while a "−" in the last column denotes an unstable one. Note that these orbits are certainly distinct since their individual periods are not integer multiples of another one. However, we observe that the period of orbit number 3a is roughly twice the period of orbit number 1a, 2a, 4a and 6a and that the period of orbit number 5a is approximately three times that of orbit number 1a, 2a, 4a and 6a. Indeed, projecting the orbits onto their x_1, x_2 coordinates, we see that orbits 3a and 5a make two, respectively three loops in this particular plane before closing, see Figs. 6.1 and 6.2. For easier reference we may therefore call orbits 1a, 2a, 4a and 6a "simple", orbit 3a "doubled", orbit 5a "tripled" and so on.

Next, taking Y to $Y = 740.00$, Table 6.2 exhibits data of coexisting asymptotically stable periodic orbits. Projections of these periodic orbits into the x_1, x_2 plane reveal

Table 6.1: Coexisting periodic orbits in the laser model at $k = 0.5$, $\Theta = -22$, $\Delta = 7.5$, $c = 500$, $\gamma = 2$ and $\sigma = 1$ and $Y = 600$

No.	Initial value $x(0) = x_1(0), x_2(0), x_3(0), x_4(0), x_5(0)$					Period T	
1a	12.9133842	4.1389482	0.1761365	0.0626055	0.0290909	0.5319068	−
2a	-11.4268611	27.7256959	0.1314038	0.2062820	-0.0857766	0.5250789	−
3a	25.8539308	27.6235569	-0.1005215	-0.1212166	0.1359688	1.0918778	−
4a	-7.6860578	30.2974202	0.1923034	0.0174797	0.2224663	0.4785637	−
5a	-10.3204011	10.6925315	0.0601295	0.1228789	0.2633766	1.5771672	−
6a	-5.7007517	19.4342957	0.3490117	0.1360201	-0.0853813	0.4553995	−

Table 6.2: Coexisting asymptotically stable periodic orbits in the laser model at $k = 0.5$, $\Theta = -22$, $\Delta = 7.5$, $c = 500$, $\gamma = 2$, $Y = 740$ and $\sigma = 1$.

No.	Initial value $x(0) = x_1(0), x_2(0), x_3(0), x_4(0), x_5(0)$					Period	
1b	18.3174006	29.9250948	0.0725962	-0.0973841	0.1473623	1.0190015	+
2b	19.1754073	30.9560298	0.0758161	-0.0651374	0.1582912	1.0336717	+
3b	17.9589886	45.2567983	0.0587626	-0.0305819	-0.0646184	0.5469396	+
4b	-3.4975711	28.1473209	0.2596095	0.0279394	0.1414312	0.4542951	+

Table 6.3: Attractive periodic orbits in the laser model at $k = 0.5$, $\Theta = -22$, $\Delta = 7.5$, $c = 500$, $\gamma = 2$ and $\sigma = 1$ and various values of Y.

No.	Initial value $x(0) = x_1(0), x_2(0), x_3(0), x_4(0), x_5(0)$					Period	Y
1c	-9.8507516	26.8033246	0.2059935	-0.0494500	0.1858028	0.9513571	475.00
2c	-11.4981956	12.2392011	0.0495109	0.1949393	-0.0296149	1.5936218	620.02
3c	19.9158435	31.1352431	0.0669586	-0.0598549	0.1625725	4.1542139	729.34
4c	4.5490243	49.0424416	0.1050371	0.0337089	0.0548807	1.6193308	775.00

further that orbits 1b and 2b are doubled while orbits 3b and 4b correspond to simple periodic orbits. Note also that, for these parameter values, there exists additionally the unique attractive equilibrium.

We close this chapter with Table 6.3 showing four more attractive periodic orbits that do not appear in the diagrams in [54], [55].

6.2 First Continuations

Now we free the parameter $\lambda \in \mathbb{R}$, augment system (6.1.1) by the "arclength equation" (5.1.3) and continue the periodic orbit $\overline{x}_0$ by solving $g(\overline{x}, \lambda) = 0$, $g : \mathbb{R}^{n-1} \times \mathbb{R} \longrightarrow \mathbb{R}^n$, for the successive solutions $y_{N+1} = (\overline{x}_{N+1}, \lambda_{N+1})$:

$$g(\overline{x}_{N+1}, \lambda_{N+1}) := \begin{cases} S(\overline{x}_{N+1}, \lambda_{N+1}) - \overline{x}_{N+1} & = 0 \\ (\overline{x}_{N+1} - \overline{x}_N)^T \dot{\overline{x}}_N + (\lambda_{N+1} - \lambda_N)\dot{\lambda}_N - \delta s & = 0, \end{cases} \tag{6.2.1}$$

with the previous solution $y_N = (\overline{x}_N, \lambda_N)$, the normalized tangent $\dot{y}_N = (\dot{\overline{x}}_N, \dot{\lambda}_N)$ to the branch at y_N and a fixed increment δs along the parametrized solution branch.

Let now (x^k, λ^k) with $x^k = U\overline{x}^k + x_{\text{orig}}$ denote the k-th iterate in Newton's method to find the N-th point $(\overline{x}_N, \lambda_N)$ along the branch. Since the arclength equation is linear in $(\overline{x}_N, \lambda_N)$, its derivatives are easily available. The derivative of S with respect to $\overline{x}$ can be computed as in (6.1.3), (6.1.4), with (6.1.5). In addition, we now need the derivative of S with respect to the parameter λ. Differentiation of the Poincaré map with respect to λ yields:

$$S_\lambda(\overline{x}, \lambda) = U^T \Big\{ f[\phi(\tau(x, \lambda), x, \lambda), \lambda] \frac{\partial \tau}{\partial \lambda}(x, \lambda) + \frac{\partial \phi}{\partial \lambda}(\tau(x, \lambda), x, \lambda) \Big\}. \tag{6.2.2}$$

Subsequent evaluation of (6.2.2) at (x^k, λ^k) gives with $f^k := f(x_\tau^k, \lambda^k)$, $\tau_\lambda^k := \frac{\partial \tau}{\partial \lambda}(x^k, \lambda^k)$,

$\tau^k := \tau(x^k, \lambda^k)$ and $\phi_\lambda^k := \frac{\partial \phi}{\partial \lambda}(\tau^k, x^k, \lambda^k)$:

$$S_\lambda^k := S_\lambda(\overline{x}^k, \lambda^k) = U^T\{f^k \tau_\lambda^k + \phi_\lambda^k\}. \tag{6.2.3}$$

For the derivatives of the return time τ with respect to λ we recall from (5.6.1):

$$\tau_\lambda^k := \frac{\partial \tau}{\partial \lambda}(x^k, \lambda^k) = -\frac{f(x_{\text{orig}}, \lambda^k)^T \phi_\lambda^k}{f(x_{\text{orig}}, \lambda^k)^T f^k} \tag{6.2.4}$$

with denominator $f(x_{\text{orig}}, \lambda^k)^T f^k \neq 0$ in a neighbourhood of $(x_{\text{orig}}, \lambda_{N-1})$. Hence, for S_λ^k we need in addition the quantities $\frac{\partial \phi_i}{\partial \lambda}(\tau^k, x^k, \lambda^k)$ for $i = 1, 2, \ldots n$. Therefore let $w_i = w_i(t, x^k, \lambda^k) := \frac{\partial \phi_i}{\partial \lambda}(t, x^k, \lambda^k)$. Differentiation of w_i with respect to t yields:

$$\begin{aligned} \dot{w}_i &= \frac{\partial}{\partial t}\Big(\frac{\partial \phi_i}{\partial \lambda}(t, x^k, \lambda^k)\Big) = \frac{\partial}{\partial \lambda}\Big(f_i(\phi(t, x^k, \lambda), \lambda)\Big)\Big|_{\lambda=\lambda^k} \\ &= \sum_{r=1}^{n}\Big[\frac{\partial f_i}{\partial x_r}(\phi(t, x^k, \lambda^k), \lambda^k) w_r\Big] + \frac{\partial f_i}{\partial \lambda}(\phi(t, x^k, \lambda^k), \lambda^k), \end{aligned} \tag{6.2.5}$$

giving another n differential equations that must be integrated together with the flow from $t = 0$ to $t = \tau^k$ with initial conditions $w_i(0) = 0$. Hence, to continue a periodic orbit with the Poincaré map method, we need to solve an $(n + n^2 + n)$-dimensional, partially coupled, nonlinear system of ordinary differential equations.

To detect possible bifurcations along the branch, we monitor the determinants of the Jacobian matrix g_y^N as well as of $S_{\overline{x}}^N$, with $y = (\overline{x}, \lambda) \in \mathbb{R}^n$. This enables us to detect strict bifurcations and saddle-nodes with respect to λ. To find period-doubling bifurcations and secondary Hopf bifurcations, we also observe the Floquet multipliers, in particular the one closest to 1 in norm. Since the branch of periodic orbits may terminate in a Hopf bifurcation involving equilibria, we also check the norm $C = C_N := \|f(x_N, \lambda_N)\|_2$. Convergence of C_N to 0 could indicate a Hopf bifurcation involving equilibria. In case $C_N < C^*$, with C^* a pre-specified bound, we also compute the eigenvalues of f_x^N, observe whether there is a pair $\mu = \mu(\lambda_N)$ of complex conjugate ones converging to the imaginary axis and, if so, check the asymptotic expansion:

$$\frac{2\pi}{|\Im(\mu(\lambda_N))|} - \tau(x_N, \lambda_N) \to 0. \tag{6.2.6}$$

Furthermore, in particular when continuing potentially doubled, tripled, quadrupled,... periodic orbits (periodic orbits with K "close" loops in the x_1, x_2 plane), we calculate the distances $D_N^j = D_N^j(\lambda_N) := \|\overline{x}_N - S^{1/j}(\overline{x}_N, \lambda_N)\|_2 = \|S(\overline{x}_N, \lambda_N) - S^{1/j}(\overline{x}_N, \lambda_N)\|_2$ where $j = 2$ for K even and $j = K$ for K odd and $S^{1/j}(\overline{x}, \lambda)$ is

defined as $U^T\left[\phi\left(\frac{\tau(x,\lambda)}{j}, x, \lambda\right) - x_{\text{orig}}\right]$. Whenever D_N^j seems to approch 0 such that C_N remains bounded away from 0, we do not adjust the return plane H_N but keep it constant, since D_N^j depends on it. Then $D_N^j \to 0$ signals a period-halving or division of the period by K.

This quantity, D_N^j, as it turns out, also helps detect "strong resonance", see Subsection 7.4.2 in the next chapter and Figs. 7.23, 7.24 and 7.25.

Only for display purposes we sometimes also compute a genuine norm $\|\cdot\|_{\text{per}}$ of the periodic orbit $\phi(t, x_N, \lambda_N)$ defined as:

$$\|\phi(t, x_N, \lambda_N)\|_{\text{per}} := \left\{\frac{1}{T}\int_0^T < \phi(t, x_N, \lambda_N), \phi(t, x_N, \lambda_N) > dt\right\}^{1/2} \tag{6.2.7}$$

This particular norm is compatible with the Euclidean norm $\|\cdot\|_2$ of an equilibrium undergoing a Hopf bifurcation, in the sense that $\|\phi(t, x_N, \lambda_N)\|_{\text{per}} = \|x_N\|_2$ at the bifurcation value $\lambda = \lambda_N$. This can be advantageous in interpreting graphical results. However, we must solve an additional differential equation to find $\|\phi(t, x_N, \lambda_N)\|_{\text{per}}$. Therefore, we frequently use some other, cheaper to find, invariant to plot versus the continuation parameter, for instance the largest Floquet multiplier (measured in the Euclidean norm), the period, the amplitude, etc. In case of an occurring period-doubling bifurcation, we would then simply plot the norm of the square of the largest Floquet multiplier, respectively twice the period, of the involved single periodic orbit. Finally, let us introduce the following notations and abbreviations used in one-parameter diagrams:

1. "+" for stable periodic orbits.
2. "o" for unstable periodic orbits.
3. "SNB" for a quadratic saddle-node bifurcation.
4. "PBG" for a nondegenerate period-doubling bifurcation.
5. "HF2" for a nondegenerate secondary Hopf bifurcation.
6. "HF1" for a nondegenerate Hopf bifurcation.

Note that the continuation of solutions to our defining equation $g(x, \lambda) = 0$ admits the mere detection of saddle-nodes, period-doublings and (secondary) Hopf bifurcations, but we cannot classify them further, since the necessary second and third derivatives S^k_{xx}, S^k_{xxx} are not available here. However, this will be done in a more general context in the next chapter.

6.2.1 Results

In order to compare our results with the ones in [54], [55], we first vary the parameter Y, i.e. we first choose $\lambda := Y \in \mathbb{R}$.

At first, Figs. 6.3 and 6.4 emphasize an earlier remark, namely that mere graphical results can easily hide important information. Without additional careful inspection of the data produced by our code, we would not be aware of the attractor shown in Fig. 6.4.

Figure 6.5 demonstrates, next, that the brute force approach used in [54], [55] can easily miss attractors. Even though the stable (tripled) periodic orbit in this figure exists for quite a large Y interval, its domain of attraction is probably fairly small. We note here that this periodic orbit bifurcates from a simple one at strong resonance for the above parameter values with Y, Δ changed to $Y = 645.0239764$, $\Delta = 7.2328457$, see Figs. 7.23 and 7.24.

As is seen in Fig. 6.6, the complex critical Floquet multipliers only very slowly leave the unit circle in the secondary Hopf bifurcation HF2 at $Y \approx 653.12349$. In fact, they remain close to 1 and, after they become real, one of them crosses transversally back into the unit circle at the left saddle-node SNB. While this saddle-node involves two unstable periodic orbits, there is a second one involving a stable periodic orbit marking the right bound of the existence interval of this periodic orbit with respect to Y. We also remark that the doubled periodic orbit branch remains close to the simple one and is enclosed by two nondegenerate period-doublings such that their "forks" open towards each other and describe a closed loop. It is therefore reasonable to expect a degenerate period-doubling close by, such that the corresponding Fig. 6.6 does not show any doubled branch at all.

Next, Fig. 6.7 shows a partial bifurcation diagram that was obtained by continuing the stable orbit of Fig. 6.6 at fixed $Y = 810$ with varying parameter c. In order to capture the bifurcating doubled periodic orbits from $c \approx 565$ in a consistent diagram, we plotted here twice the periodic time of the simple periodic orbit. The crossing of the stable and unstable branch for $c \approx 500$ and for the two unstable branches at $c \approx 620$ does not constitute a bifurcation but merely reflects the fact of two coexisting periodic orbits of the same (doubled) period. We expect that, for "slightly" different parameter choices, the quadratic saddle-node will coalesce with the crossing point $(c, \text{period}) \approx (500, 1.062)$ such that the loop shrinks to a degenerate point and the corresponding Fig. 6.7 will exhibit a cusp similar as in example 3.4.0.12.

Finally, we include Fig. 6.8. It was obtained by continuing the lower branch of Fig. 6.7 up to $c = 1472$, and then freeing Y again. It gives the same information as in Fig. 6.6 except for a different value of c — all other parameters remained unchanged. While Fig. 6.6 does not contain any Hopf bifurcations but constitutes a closed loop of a simple periodic orbit, the equivalent branch in Fig. 6.8 terminates at both end points in Hopf bifurcations involving equilibria. Hence, when deforming Fig. 6.6 into Fig. 6.8 by varying c, we must encounter some kind of bifurcation. We also emphasize the fact that for $y \approx 1300$, this branch of periodic orbits alone gives rise to five coexisting stable periodic orbits, a phenomenon that has not been previously reported in this model.

We could easily spend (waste?) hundreds of hours of more CPU-time and produce plots as the above enough to wallpaper our university. But, having our introductory goal in mind, it makes much more sense to "continuously transform such a figure" and see where it qualitatively changes. In other words, to systematically continue some of the essential elements of the above one-parameter diagrams. That is, to continue saddle-nodes, period-doublings and (secondary) Hopf bifurcations.

Chapter 7

Second Continuations

The bifurcations mentioned in the previous chapter have one thing in common, namely a Floquet multiplier δ of norm 1. Hence there is a $\beta = \beta \bmod 2\pi \in [0, 2\pi)$ such that $\delta = e^{i\beta}$. We can therefore treat the continuation of this occurrence by freeing a second parameter and augment system (6.2.1) by imposing this special condition as a further equation to be satisfied. Since δ comes along with a corresponding eigenvector $v + i\,u$, we can express this requirement in a system that has been incorporated in the AUTO package, [42]. That is, we consider here the system $g(y) = 0$ with $y := (\overline{x}, v, u, \beta, \lambda)$ and the function $g : \mathbb{R}^{n-1} \times \mathbb{R}^{n-1} \times \mathbb{R}^{n-1} \times \mathbb{R} \times \mathbb{R}^2 \to \mathbb{R}^{3n}$, and solve $g(y_{N+1}) :=$

$$\begin{cases} S(\overline{x}_{N+1}, \lambda_{N+1}) - \overline{x}_{N+1} & = 0 \\ S_{\overline{x}}(\overline{x}_{N+1}, \lambda_{N+1})(v_{N+1} + i\,u_{N+1}) - e^{i\beta_{N+1}}(v_{N+1} + i\,u_{N+1}) & = 0 \\ (v_{N+1} + i\,u_{N+1})^*(v_N + i\,u_N) - 1 & = 0 \\ (\overline{x}_{N+1} - \overline{x}_N)^T \dot{\overline{x}}_N + (\lambda_{N+1} - \lambda_N)^T \dot{\lambda}_N + (v_{N+1} - v_N)^T \dot{v}_N & \\ \quad + (u_{N+1} - u_N)^T \dot{u}_N + (\beta_{N+1} - \beta_N)\dot{\beta}_N - \delta s & = 0 \end{cases} \tag{7.0.1}$$

for the the next solution point $y_{N+1} = (\overline{x}_{N+1}, v_{N+1}, u_{N+1}, \beta_{N+1}, \lambda_{N+1})$ with $\lambda = (\nu, \xi) \in \mathbb{R}^2$. Here "$*$" denotes complex transposed, $(\overline{x}_N, v_N, u_N, \beta_N, \lambda_N) = y_N$ denotes the previous solution and $\dot{y}_N = (\dot{\overline{x}}_N, \dot{v}_N, \dot{u}_N, \dot{\beta}_N, \dot{\lambda}_N)$ corresponds to the normalized oriented tangent at y_N. Note that we normalize the new right eigenvector $v_{N+1} + i\,u_{N+1}$ with respect to the previous one $v_N + i\,u_N$. Related systems and more details can be found in [156], [158], [144].

In case of a saddle-node- or period-doubling bifurcation, β becomes a trivial variable with constant value $\beta = 0 \bmod 2\pi$, respectively $\beta = \pi \bmod 2\pi$. Consequently, the vector u_N will be a multiple of the vector v_N. Therefore, if we were interested

only in bifurcations with $\delta = e^{i\beta} = \pm 1$, we could decrease the dimension of the system (7.0.1) by considering its real version with β fixed at 0 or π and u_N fixed at 0. However, the above complex formulation is necessary in case of secondary Hopf bifurcations. Moreover, as it will turn out soon, the simultaneous treatment of the three bifurcations in a single system admits the discovery of interesting strict bifurcation phenomena with the choice of immediate branch switching.

For Newton's method, as well as for the further characterization of the bifurcations, we now need the additional second derivatives $S_{\overline{x}\overline{x}}$, $S_{\overline{x}\nu}$, $S_{\overline{x}\xi}$. All other entries of the Jacobian matrix g_y^k, occurring in the iteration towards y_N, are either trivially obtainable or can be found as the ones occurring in system (6.2.1). For an arbitrary but fixed iterate $y^k = (\overline{x}^k, v^k, u^k, \beta^k, \lambda^k)$ in Newton's method to find the N-th point $y_N = (\overline{x}_N, v_N, u_N, \beta_N, \lambda_N)$ along the branch, let again $\tau = \tau(x^k, \lambda^k) = \tau(U\overline{x}^k + x_{\text{orig}}, \lambda^k)$ be the first return time of x^k and $x_\tau^k = \phi(\tau(x^k, \lambda^k), x^k, \lambda^k)$ the first return point of x^k in the original coordinates. For fixed $\lambda = \lambda^k$ we multiply (6.1.2) with an arbitrary vector $z \in \mathbb{R}^{n-1}$. Subsequent differentiation with respect to $\overline{x}$ yields:

$$\begin{aligned} S_{\overline{x}\overline{x}}(\overline{x}, \lambda)z \;=\; & U^T\Big\{\frac{\partial f}{\partial x}[\phi(\tau(x,\lambda),x,\lambda),\lambda]\Big(f[\phi(\tau(x,\lambda),x,\lambda),\lambda] \\ & \cdot \frac{\partial \tau}{\partial x}(x,\lambda) + \frac{\partial \phi}{\partial x}(\tau(x,\lambda),x,\lambda)\Big)\frac{\partial \tau}{\partial x}(x,\lambda)Uz \\ & + f[\phi(\tau(x,\lambda),x,\lambda),\lambda](Uz)^T\frac{\partial}{\partial x}\Big(\frac{\partial \tau}{\partial x}(x,\lambda)^T\Big) \\ & + \frac{\partial f}{\partial x}[\phi(\tau(x,\lambda),x,\lambda),\lambda]\frac{\partial \phi}{\partial x}(\tau(x,\lambda),x,\lambda)Uz \\ & \cdot \frac{\partial \tau}{\partial x}(x,\lambda) + \frac{\partial^2 \phi}{\partial x^2}[\tau(x,\lambda),x,\lambda]Uz\Big\}U \end{aligned} \tag{7.0.2}$$

Evaluation of (7.0.2) at $(\overline{x}^k, \lambda^k)$ gives in our abbreviated notation:

$$\begin{aligned} S_{\overline{x}\overline{x}}^k z \;=\; & U^T\Big\{f_x^k\Big(f^k\tau_x^k + \phi_x^k\Big)\tau_x^k Uz + f^k(Uz)^T\frac{\partial}{\partial x}\Big(\frac{\partial \tau}{\partial x}(x,\lambda)^T\Big)\Big|_{x=x^k,\lambda=\lambda^k} \\ & + f_x^k\phi_x^k Uz\tau_x^k + \phi_{xx}^k Uz\Big\}U. \end{aligned} \tag{7.0.3}$$

Here the matrix $\tau_{xx}^k := \frac{\partial}{\partial x}\Big(\frac{\partial \tau}{\partial x}(x,\lambda)^T\Big)\Big|_{x=x^k,\lambda=\lambda^k}$ can be found by differentiating the identity (5.5.15) once more with respect to x. Then it follows:

$$0 \;=\; \frac{\partial}{\partial x}\Big(\frac{\partial \tau}{\partial x}(x,\lambda)^T\Big)f(x_{\text{orig}},\lambda)^T\Big(f[\phi(\tau(x,\lambda),x,\lambda),\lambda]\Big)$$

$$
\begin{aligned}
&+ \frac{\partial}{\partial x}\Big(\frac{\partial \phi}{\partial x}(\tau(x,\lambda),x,\lambda)^T f(x_{\text{orig}},\lambda)\Big) \\
&+ \frac{\partial \tau}{\partial x}(x,\lambda)^T f(x_{\text{orig}},\lambda)^T \cdot \frac{\partial f}{\partial x}[\phi(\tau(x,\lambda),x,\lambda),\lambda] \\
&\cdot \Big(f[\phi(\tau(x,\lambda),x,\lambda),\lambda]\frac{\partial \tau}{\partial x}(x,\lambda) + \frac{\partial \phi}{\partial x}[\tau(x,\lambda),x,\lambda)\Big), \qquad (7.0.4)
\end{aligned}
$$

and upon evaluating (7.0.4) at $x = x^k$, $\lambda = \lambda^k$ we find:

$$
\begin{aligned}
0 \;=\; & \tau^k_{xx} f(x_{\text{orig}},\lambda^k)^T f^k + \left(\tau^k_x\right)^T f(x_{\text{orig}},\lambda^k)^T f^k_x (f^k \tau^k_x + \phi^k_x) \\
& + \left(\phi^T_x\right)^k_x f(x_{\text{orig}},\lambda^k) + (f^k_x \phi^k_x)^T f(x_{\text{orig}},\lambda^k)\tau^k_x. \qquad (7.0.5)
\end{aligned}
$$

Note that we can solve equation (7.0.5) for the matrix τ^k_{xx} in a neighbourhood of $(x_{\text{orig}},\lambda^k)$ as here the scalar $f(x_{\text{orig}},\lambda^k)^T f^k \neq 0$ in a neighbourhood of $(x_{\text{orig}},\lambda_{N-1})$. Since for the Jacobian matrix we need the submatrices $S^k_{\overline{x}x}v^k$ and $S^k_{\overline{x}x}u^k$, in our application the vector z will be either v^k or u^k.

An inspection of equation (7.0.5) shows that we must solve the second variational equation to find the quantities $\frac{\partial^2 \phi_i}{\partial x_j x_k}(\tau(x^k,\lambda^k),x^k,\lambda^k)$ for $i,\, j,\, k = 1,2,\ldots n$, occurring in ϕ^k_{xx}. For fixed parameter $\lambda = \lambda^k$ we therefore define $c_{ik} = c_{ik}(t,x^k) := \frac{\partial \phi_i}{\partial x_k}(t,x^k)$ and $z_{ikj} = z_{ikj}(t,x^k) := \frac{\partial}{\partial x_j}(c_{ik}(t,x^k)) = \frac{\partial^2 \phi_i}{\partial x_j \partial x_k}(t,x^k)$. Differentiation of z_{ikj} with respect to t yields:

$$
\begin{aligned}
\dot{z}_{ikj} \;=\; & \frac{\partial}{\partial t}\Big(\frac{\partial}{\partial x_j}\Big(\frac{\partial \phi_i}{\partial x_k}(t,x)\Big)\Big)\Big|_{x=x^k} = \frac{\partial}{\partial x_k}\Big(\frac{\partial}{\partial x_j}\Big(f_i(\phi(t,x))\Big)\Big)\Big|_{x=x^k} \\
=\; & \sum_{r=1}^{n}\Big\{\Big[\sum_{m=1}^{n}\frac{\partial^2 f_i}{\partial x_m \partial x_r}(\phi(t,x^k))\frac{\partial \phi_m}{\partial x_k}(t,x^k)\Big]\frac{\partial \phi_r}{\partial x_j}(t,x^k) \\
& + \frac{\partial f_i}{\partial x_r}(\phi(t,x^k))\frac{\partial^2 \phi_r}{\partial x_j \partial x_k}(t,x^k)\Big\} \\
=\; & \sum_{r=1}^{n}\Big(\sum_{m=1}^{n}\frac{\partial^2 f_i}{\partial x_m \partial x_r}(\phi(t,x^k))c_{mk}\Big)c_{rj} + \frac{\partial f_i}{\partial x_r}(\phi(t,x^k))z_{rjk}. \qquad (7.0.6)
\end{aligned}
$$

This n^3-dimensional differential equation must be integrated along with the n-dimensional flow and the n^2-dimensional first variational equation (for the $c_{ik}(t,x^k)$) from $t = 0$ to $t = \tau(x^k,\lambda^k)$ with initial conditions $z_{ikj}(0,x^k) = 0$. However, because of the symmetry $z_{ikj} = z_{ijk}$, it is sufficient to solve "only" an additional $[n^2(n+1)/2]$-dimensional system.

But we also need the mixed derivatives $S^k_{\overline{x}\nu} = S_{\overline{x}\nu}(\overline{x}^k,\lambda^k)$ and $S^k_{\overline{x}\xi} = S_{\overline{x}\xi}(\overline{x}^k,\lambda^k)$. Differentiating (6.2.2) with respect to $\overline{x}$ yields:

$$
S_{\overline{x}\nu}(\overline{x},\lambda) \;=\; U^T\Big\{\Big[\frac{\partial f}{\partial x}[\phi(\tau(x,\lambda),x,\lambda),\lambda]\Big(f[\phi(\tau(x,\lambda),x,\lambda),\lambda]
$$

$$\cdot \frac{\partial \tau}{\partial \nu}(x,\lambda) + \frac{\partial \phi}{\partial \nu}[\tau(x,\lambda),x,\lambda]\Big) + \frac{\partial f}{\partial \nu}[\phi(\tau(x,\lambda),x,\lambda),\lambda]\Big]$$
$$\cdot \frac{\partial \tau}{\partial x}(x,\lambda) + f[\phi(\tau(x,\lambda),x,\lambda),\lambda]\frac{\partial^2 \tau}{\partial x \partial \nu}(x,\lambda)$$
$$+ \frac{\partial f}{\partial x}[\phi(\tau(x,\lambda),x,\lambda),\lambda]\frac{\partial \phi}{\partial x}[\tau(x,\lambda),x,\lambda]\frac{\partial \tau}{\partial \nu}(x,\lambda)$$
$$+ \frac{\partial^2 \phi}{\partial \nu \partial x}[\tau(x,\lambda),x,\lambda]\Big\}, \tag{7.0.7}$$

and upon evaluating (7.0.7) at $x = x^k$, $\lambda = \lambda^k$ we get:

$$S^k_{x\nu} = U^T\Big\{\Big[f^k_x\Big(f^k\tau^k_\nu + \phi^k_\nu\Big) + f^k_\nu\Big]\tau^k_x + f^k\tau^k_{x\nu} + f^k_x\phi^k_x\tau^k_\nu + \phi^k_{x\nu}\Big\}. \tag{7.0.8}$$

Here the row vector $\tau^k_{x\nu} = \frac{\partial^2 \tau}{\partial x \partial \nu}(x^k,\lambda^k)$ can be found by differentiating the identity (5.5.15) with respect to ν. Then it follows:

$$\begin{aligned} 0 \;=\; & \frac{\partial^2 \tau}{\partial x \partial \nu}(x,\lambda) f(x_{\text{orig}},\lambda)^T f[\phi(\tau(x,\lambda),x,\lambda),\lambda] + f(x_{\text{orig}},\lambda)^T \\ & \cdot \Big[\frac{\partial f}{\partial x}[\phi(\tau(x,\lambda),x,\lambda),\lambda]\frac{\partial \phi}{\partial x}(\tau(x,\lambda),x,\lambda)\frac{\partial \tau}{\partial \nu}(x,\lambda) \\ & + \frac{\partial^2 \phi}{\partial \nu \partial x}(\tau(x,\lambda),x,\lambda)\Big] + \frac{\partial \tau}{\partial x}(x,\lambda)\Big\{f(x_{\text{orig}},\lambda)^T \\ & \cdot \Big[\frac{\partial f}{\partial x}[\phi(\tau(x,\lambda),x,\lambda),\lambda]\Big(f[\phi(\tau(x,\lambda),x,\lambda),\lambda]\frac{\partial \tau}{\partial \nu}(x,\lambda) \\ & + \frac{\partial \phi}{\partial \nu}[\tau(x,\lambda),x,\lambda]\Big) + \frac{\partial f}{\partial \nu}[\phi(\tau(x,\lambda),x,\lambda),\lambda]\Big]\Big\}. \end{aligned} \tag{7.0.9}$$

Evaluated at $x = x^k$, $\lambda = \lambda^k$, equation (7.0.9) becomes:

$$0 = \tau^k_{x\nu} f(x_{\text{orig}},\lambda^k)^T\Big\{f^k + \Big[f^k_x\phi^k_x\tau^k_\nu + \phi^k_{x\nu}\Big] + \Big[f^k_x\Big(f^k\tau^k_\nu + \phi^k_\nu\Big) + f^k_\nu\Big]\tau^k_x\Big\}. \tag{7.0.10}$$

Again we see that we can solve equation (7.0.10) for the desired quantity $\tau^k_{x\nu}$, since $f(x_{\text{orig}},\lambda^k)f^k \neq 0$ in a neighbourhood of $(x_{\text{orig}},\lambda_{N-1})$. However, we still need the matrix $\phi^k_{x\nu} = \frac{\partial^2 \phi}{\partial x \partial \nu}(\tau(x^k,\lambda^k),x^k,\lambda^k)$. Similar to the above procedure for finding the $\frac{\partial^2 \phi_i}{\partial x_j \partial x_k}(\tau^k,x^k)$, we define here, with $\lambda = (\nu,\eta)$, the quantities $c_{ij} = c_{ij}(t,x^k,\lambda^k) := \frac{\partial \phi_i}{\partial x_j}(t,x^k,\lambda^k)$, $a_i = a_i(t,x^k,\lambda^k) := \frac{\partial \phi_i}{\partial \nu}(t,x^k,\lambda^k)$. Moreover, to compute the mixed derivatives, we define $b_{ij} = b_{ij}(t,x^k,\lambda^k) := \frac{\partial}{\partial \nu}\Big(\frac{\partial \phi_i}{\partial x_j}(t,x^k,\lambda)\Big)\Big|_{\lambda=\lambda^k}$. Differentiation of b_{ij} with respect to t yields:

$$\dot{b}_{ij} \;=\; \frac{\partial}{\partial t}\Big(\frac{\partial c_{ij}}{\partial \nu}(t,x^k,\lambda^k)\Big) = \frac{\partial}{\partial \nu}\Big(\frac{\partial}{\partial x_j}\Big(f_i(\phi(t,x,\lambda))\Big)\Big)\Big|_{x=x^k,\,\lambda=\lambda^k}$$

$$
\begin{aligned}
&= \frac{\partial}{\partial \nu}\Big(\sum_{r=1}^{n}\frac{\partial f_i}{\partial x_r}(\phi(t,x^k,\lambda),\lambda)\frac{\partial \phi_r}{\partial x_j}(t,x^k,\lambda)\Big)\Big|_{\lambda=\lambda^k}\\
&= \sum_{r=1}^{n}\Big\{\Big[\sum_{m=1}^{n}\Big(\frac{\partial^2 f_i}{\partial x_r \partial x_m}(\phi(t,x^k,\lambda^k),\lambda^k)\frac{\partial \phi_m}{\partial \nu}(t,x^k,\lambda^k)\Big)\\
&\quad + \frac{\partial^2 f_i}{\partial \nu \partial x_r}(\phi(t,x^k,\lambda^k),\lambda^k)\Big]\frac{\partial \phi_r}{\partial x_j}(t,x^k,\lambda^k)\\
&\quad + \frac{\partial f_i}{\partial x_r}(\phi(t,x^k,\lambda^k),\lambda^k)\frac{\partial^2 \phi_r}{\partial \nu \partial x_j}(t,x^k,\lambda^k)\Big\} \qquad (7.0.11)
\end{aligned}
$$

In short:

$$
\begin{aligned}
\dot{b}_{ij} &= \sum_{r=1}^{n}\Big\{c_{rj}\Big[\sum_{m=1}^{n}\Big(\frac{\partial^2 f_i}{\partial x_r \partial x_m}(\phi(t,x^k,\lambda^k),\lambda^k)a_m\Big)\\
&\quad + \frac{\partial^2 f_i}{\partial \nu \partial x_r}(\phi(t,x^k,\lambda^k),\lambda^k)\Big]\\
&\quad + \frac{\partial f_i}{\partial x_r}(\phi(t,x^k,\lambda^k),\lambda^k)b_{rj}\Big\} \qquad (7.0.12)
\end{aligned}
$$

These n^2 equations must be integrated together with with the n-dimensional flow, the n^2-dimensional first variational equation and the n-dimensional system for the a_i from $t=0$ to $t=\tau^k$. The initial conditions read again $b_{ij}(0,x^k,\lambda^k)=0$.

Since a similar system arises for the second parameter ξ, the overall system to solve for the continuation of saddle-nodes, period-doublings and secondary Hopf bifurcations, i.e. system (7.0.1), consists of $3n+3n^2+n^2(n+1)/2$ partially coupled, nonlinear ordinary differential equations. In the laser model $n=5$ which results in a 165-dimensional system.

7.1 Degenerate Saddle-Node Bifurcations

If now one of these bifurcations has been computed, then the Jacobian matrix g_y^N with $y=(\overline{x}_N,v_N,u_N,\beta_N,\lambda_N)$ delivers in particular the entries $S^N_{\overline{xx}}v_N$, S^N_ν and S^N_ξ. In case of a saddle-node, after the additional computation of the (normalized) left eigenvector w_N, $w_N^T S_x^N = w_N^T$, we can therefore easily calculate the important quantities:

$$
w_N^T S^N_{\overline{xx}} v_N v_N,\ \ w_N^T S^N_\nu,\ \ w_N^T S^N_\xi,\ \ w_N^T v_N.
$$

Generically they will be nonzero and without any major additional effort we find:

$$
\dot{\kappa}_N = \frac{w_N^T S^N_{\overline{xx}} v_N v_N}{w_N^T v_N} \qquad (7.1.1)
$$

for the crossing speed of the critical +1 Floquet multiplier with respect to arclength,

$$\dot{\nu}_N = -\frac{w_N^T S_{xx}^N v_N v_N}{w_N^T S_\nu^N} \tag{7.1.2}$$

for the direction of the saddle-node occurring in the corresponding one-parameter family $S(\overline{x}, \nu, \xi_N) - \overline{x} = 0$ with respect to ν, and

$$\dot{\xi}_N = -\frac{w_N^T S_{xx}^N v_N v_N}{w_N^T S_\xi^N} \tag{7.1.3}$$

for the direction of the saddle-node occurring in the corresponding one-parameter family $S(\overline{x}, \nu_N, \xi) - \overline{x} = 0$ with respect to ξ. The quantities $\dot{\nu}_N$ in (7.1.2) and $\dot{\xi}_N$ in (7.1.3) refer here to one-parameter problems. They should not be confused with the components $\dot{\nu}_N$, $\dot{\xi}_N$ of the tangent $\dot{y}_N$ at the solution y_N of system (7.0.1). Also, after having computed the numbers N_{in} and N_{out} of the Floquet multipliers strictly inside and strictly outside the unit circle, we can further check whether the corresponding quadratic saddle-node contains two unstable periodic orbits or a stable and an unstable one.

Even though $\dot{\kappa}_N$, $\dot{\nu}_N$ and $\dot{\xi}_N$ are typically well defined and nonzero, the two-parameter continuation of the saddle-nodes may lead to a solution with accompanying numerator or denominator in (7.1.1), (7.1.2), (7.1.3) being zero.

7.1.1 Detecting a Hysteresis Point

Let us consider the case $y_N = (\overline{x}_N, v_N, u_N, \beta_N, \nu_N, \xi_N)$ with $\dot{\kappa}_N = 0$. Then $S_{xx}^N v_N v_N \in \text{Range}\left[S_x^N - \text{id}\right]$. Also, $S_{xx}^N u_N v_N = c S_{xx}^N v_N v_N$ for some constant c, so that $S_{xx}^N u_N v_N \in \text{Range}\left[S_x^N - \text{id}\right]$ as well, and we can verify that the direction $(\dot{\overline{x}}_N, \dot{v}_N, \dot{u}_N, \dot{\beta}_N, \dot{\nu}_N, \dot{\xi}_N) = \dot{y}_N$ at the solution y_N of system (7.0.1) equals $(\dot{\overline{x}}_N, \dot{v}_N, \dot{u}_N, 0, 0, 0)$. Hence, generically, the two parameters will simultaneously change directions, and the projection of the locally regular solution manifold M_{reg} into the ν, ξ plane will show a cusp. Also, for ξ fixed at ξ_N, respectively ν fixed at ν_N, and $\ddot{\nu}_N \neq 0$, respectively $\ddot{\xi}_N \neq 0$, the one-parameter families $S(\overline{x}, \nu, \xi_N) - \overline{x} = 0$ and $S(\overline{x}, \nu_N, \xi) - \overline{x} = 0$ will show the cubic saddle-node or hysteresis point in a one-parameter diagram of some invariant of the periodic orbits versus ν.

7.1.2 Detecting Isola Formation/Transcritical Bifurcation Points

We continue by assuming the component $\dot{\nu}_N$ of $\dot{y}_N$ satisfies $\dot{\nu}_N = 0$ at y_N, i.e. y_N makes a saddle-node point with respect to ν of system (7.0.1). Then the components $\dot{\bar{x}}_N$ and $\dot{\xi}_N$ of $\dot{y}_N$ satisfy then in particular: $(S^N_{\bar{x}} - \mathrm{id})\dot{\bar{x}}_N + S^N_\xi \dot{\xi}_N = 0$, so that $S^N_\xi \in$ Range $\left[S^N_{\bar{x}} - \mathrm{id}\right]$ and $\psi_N^T S^N_\xi = 0$. Hence $(\bar{x}_N, \xi_N)$ is, for fixed $\nu = \nu_N$, a potential strict bifurcation point for the one-parameter problem $S(\bar{x}, \nu_N, \xi) - \bar{x} = 0$. However, at this point we do not have the existence of a (trivial) branch across it. Now $+1$ will typically be a simple eigenvalue of $S^N_{\bar{x}}$, so that we can choose a basis $\phi_0 = (v_N^T, 0)^T$ and $\phi_1 = (\rho^T, 1)^T$ of null $\left[S^N_{\bar{x}} - \mathrm{id} \;\; S^N_\xi\right]$. Then we can consider the corresponding algebraic bifurcation equation (5.3.6):

$$c_{11}\alpha^2 + 2c_{12}\alpha\beta + c_{22}\beta^2 = 0 \tag{7.1.4}$$

with coefficients:

$$c_{11} := w_N^T S^N_{\bar{x}\bar{x}} v_N v_N,\; c_{12} := w_N^T (S^N_{\bar{x}\bar{x}}\rho + S^N_{\bar{x}\xi}) v_N,\; c_{22} := w_N^T (S^N_{\bar{x}\bar{x}}\rho\rho + 2S^N_{\bar{x}\xi}\rho + S^N_{\xi\xi}).$$

We see that for a negative discriminant:

$$\Delta := c_{12}^2 - c_{11}c_{22} \tag{7.1.5}$$

there is no solution branch at all across $(\bar{x}_N, \xi_N)$ and $(\bar{x}_N, \xi_N)$ is recognized as an isola formation point. However, for a positive discriminant there will be, in general (depending on the isolated root condition), two distinct solution branches across $(\bar{x}_N, \xi_N)$.

7.1.3 Detecting Takens-Bogdanov Bifurcation Points

Let us now investigate the case $w_N^T v_N = 0$. Then $+1$ will no longer be algebraically simple. In general though, it will remain geometrically simple, such that $S^N_{\bar{x}}$ has a corresponding Jordan block: $\begin{pmatrix} 0 & 1 \\ 0 & 0 \end{pmatrix}$. Its codimension two tells us that, in general, we will not encounter this phenomenon in one-parameter problems. In the case of equilibria the resulting bifurcation has been sudied extensively, see, for instance, [66]. It is commonly called a"Takens-Bogdanov bifurcation point" or "B-point" or "origin of a Hopf branch". In particular, we mention that branches of global bifurcations,

branches of Hopf bifurcations and branches of so-called "inverse Hopf bifurcations" (a pair of real eigenvalues of f_x with sum being zero) may bifurcate off. To emphasize the fact that we are concerned here with periodic solutions, we prefer the terminology "periodic Takens–Bogdanov point" or "periodic B-point" or "origin of a secondary Hopf branch".

While the name "Takens–Bogdanov" honours the two mathematicians who, independently from each other, worked out a lot of the fine details characterizing this bifurcation, the name "origin of a (secondary) Hopf branch" describes already the behaviour of the system in a neighbourhood of $\lambda_N = (\nu_N, \xi_N)$. Indeed, under fairly general conditions, it can be shown that the double Floquet multiplier $+1$ splits into a pair of complex conjugate ones remaining on the unit circle such that a curve of (secondary) Hopf bifurcations originates at $y_N = (\overline{x}_N, v_N, u_N, \beta_N, \lambda_N)$ from the saddle-node branch. In fact, $\det\left(g_y^N\right) = 0$ and a strict bifurcation of the system (7.0.1) occurs at y_N. We note that the number of Floquet multipliers outside the unit circle and along the saddle-node branch typically changes when y_N is crossed. In particular, when N_{out} changes from 0 to 1, then the corresponding saddle-nodes will involve two unstable periodic orbits on one side of y_N while a stable periodic orbit will participate on the other side.

Furthermore, it has been shown in [174] that, if we consider ν (or ξ) as a variable and ξ (or ν) as a distinguished bifurcation parameter, then y_N constitutes a pitchfork bifurcation point with respect to the bifurcation parameter. From a geometrical point of view this is not too much of a surprise since, regardless of the arclength equation and the "dummy" variables v and u, the function $g(y)$ in (7.0.1) is symmetric in β with respect to the hyperplanes $\beta := 2m\pi$: whenever $(\overline{x}_N, v_N, u_N, \beta_N, \lambda_N)$ with $\beta_N := 2m\pi + \beta_*$ solves $g(y) = 0$, then so will $(\overline{x}_N, u_N, v_N, 2m\pi - \beta_*, \lambda_N)$. If now $y_i = (\overline{x}_i, v_i, u_i, \beta_i, \lambda_i)$ approaches y_N, then β_* approaches 0 such that the two different solutions along the same symmetric branch move together and annihilate each other in a pitchfork bifurcation at y_N. It is essentially this hidden symmetry in g that allows the pitchfork bifurcation to occur.

Both branches (the symmetric secondary Hopf bifurcation one and the saddle-node bifurcation one) are one-dimensional manifolds in the locally two-dimensional regular solution manifold M_{reg} of $S(\overline{x}, \nu, \xi) = \overline{x}$.

A geometrical argument reveals now that a projection of these branches into the ν, ξ plane generically encloses a 0 angle, see Fig. 7a.

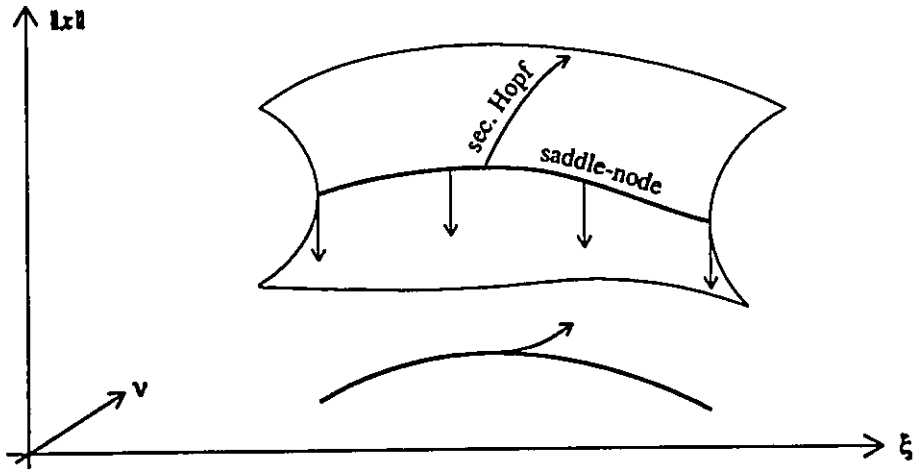

Figure 7a: The projection of M_{reg} into the two-dimensional parameter plane reveals a 0 angle between the saddle-node branch and the secondary Hopf branch.

A closer inspection of g shows next that it is also symmetric in β with respect to the hyperplanes $\beta := (2m+1)\pi$. For $\beta_N = (2m+1)\pi$ we have a double -1 Floquet multiplier — a phenomenon without a counterpart in equilibrium theory. But, just as in the double $+1$ case, this situation admits the splitting of the double -1 into a pair of complex conjugate ones remaining on the unit circle. In fact, our algorithm signals a strict bifurcation at y_N and it can be made to switch onto a branch of secondary Hopf bifurcations emerging from a period-doubling branch. Comparable to the double $+1$ case, the period-doublings change across y_N since, generically, N_{out} will be different on both sides of y_N. In particular, if N_{out} changes from 0 to 1, then, on one side of y_N, the period-doublings will only involve unstable periodic orbits while a stable simple periodic orbit participates on the other side of y_N. Let us now consider the second iterate of the Poincaré map $S^2 := S \circ S$ or, equivalently, the given periodic orbit with twice its period. It is easy to see then that the system $g(y) = 0$ becomes singular along the period-doubling branch. However, it remains regular along the emanating secondary Hopf branch. The Floquet multipliers simply get squared such that the double -1 turns into a double $+1$ at y_N. Of course, the system (7.0.1), with S replaced by S^2, is also singular at y_N, but our algorithm was able to detect and switch towards an emanating branch of truly doubled periodic orbits undergoing a secondary Hopf bifurcation. Therefore y_N is found to be a multiple strict bifurcation point for system (7.0.1) with S being

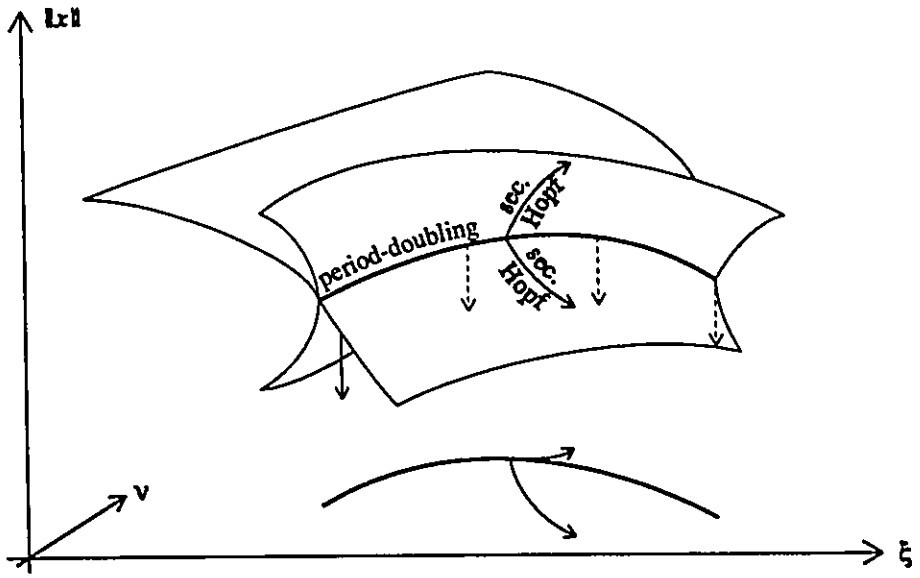

Figure 7b: The projection of M_{reg} into the two-dimensional parameter plane reveals a 0 angle between the period-doubling branch and the secondary Hopf branch of truly doubled periodic orbits. In addition, there originates a second secondary Hopf branch of simple periodic orbits from χ_N .

replaced by S^2. It admits three crossing solution branches: the period doubling branch and two pitchforks corresponding to secondary Hopf bifurcations of simple and doubled periodic orbits. Moreover, our above geometric reasoning concerning the 0 angle between the projected saddle-node- and secondary Hopf branch remains valid [154], see Fig. 7b.

7.2 Degenerate Period-Doublings and Secondary Hopf Bifurcations

Unfortunately, the further classification of period-doublings and secondary Hopf bifurcations requires substantially more effort, since it relies on the third derivative of the Poincaré map evaluated at the solution: S^N_{xxx}. This differentiation has been carried out and implemented in our code. Even though the necessary arithmetic is straightforward, it is quite tedious and lengthy and would extend over several pages. The details will therefore be omitted. We only mention here that, besides the first and second variational equations, we now need the additional n^4 third derivatives $\frac{\partial^3 \phi_l}{\partial x_i \partial x_j \partial x_m}(\tau^N, x_N, \lambda_N)$ for $l, i, j, m = 1, 2, \ldots n$. Fortunately though, upon exploiting

the symmetry:

$$\frac{\partial^3 \phi_l}{\partial x_i \partial x_j \partial x_m}(\tau^N, x_N, \lambda_N) = \frac{\partial^3 \phi_l}{\partial x_{i_1} \partial x_{j_1} \partial x_{m_1}}(\tau^N, x_N, \lambda_N) \tag{7.2.1}$$

for all permutations (i_1, j_1, m_1) of (i, j, m), we find after careful calculations that it is sufficient to solve an additional $\frac{n}{2}\left(\frac{n(n+1)(2n+1)}{6} + \frac{n(n+1)}{2}\right)$-dimensional system for the minimum number of necessary third order derivatives. To obtain this system, we let again $c_{li} = c_{li}(t, x_N, \lambda_N) := \frac{\partial \phi_l}{\partial x_i}(t, x_N, \lambda_N)$, $z_{lij} = z_{lij}(t, x_N, \lambda_N) := \frac{\partial^2 \phi_l}{\partial x_j \partial x_i}(t, x_N, \lambda_N)$ and additionally $p_{lijm} = p_{lijm}(t, x_N, \lambda_N) := \frac{\partial^3 \phi_l}{\partial x_m \partial x_j \partial x_i}(t, x_N, \lambda_N)$. Differentiation of p with respect to t yields:

$$\begin{aligned}
\dot{p}_{lijm} \;=\; & \sum_{r=1}^{n} \Big\{ c_{ri} \Big[\sum_{s=1}^{n} c_{sj} \Big(\sum_{q=1}^{n} \frac{\partial^3 f_l}{\partial x_q \partial x_s \partial x_r}(\phi(t, x_N, \lambda_N), \lambda_N) c_{qm} \Big) \\
& + \frac{\partial^2 f_l}{\partial x_s \partial x_r}(\phi(t, x_N, \lambda_N), \lambda_N) z_{sjm} \Big] \\
& + z_{rim} \Big(\sum_{s=1}^{n} \frac{\partial^2 f_l}{\partial x_s \partial x_r}(\phi(t, x_N, \lambda_N), \lambda_N) c_{sj} \Big) \\
& + z_{rij} \Big(\sum_{s=1}^{n} \frac{\partial^2 f_l}{\partial x_s \partial x_r}(\phi(t, x_N, \lambda_N), \lambda_N) c_{sm} \Big) + \\
& + \frac{\partial f_l}{\partial x_r}(\phi(t, x_N, \lambda_N), \lambda_N) p_{rijm} \Big\}.
\end{aligned} \tag{7.2.2}$$

For $l, i = 1, 2, \ldots n$, $j = i, i+1, \ldots n$, and $m = j, j+1, \ldots n$, the system (7.2.2) constitutes a $\frac{n}{2}\left(\frac{n(n+1)(2n+1)}{6} + \frac{n(n+1)}{2}\right)$-dimensional system that must be integrated along with the n-dimensional flow, the n^2-dimensional first variational equation for the c_{li} and the $n(n+1)n/2$-dimensional minimal system for the necessary second order terms z_{lij}. The integration time stretches here over the full period of the periodic orbit with initial conditions $p_{lijm}(0, x_N, \lambda_N) = 0$. In case of the laser model $n = 5$, and we are dealing here with a 280-dimensional, partially coupled ordinary differential equation.

At this point one might ask why not numerical differentiation? The answer is twofold. Firstly, when experimenting with numerical differentiation, we did not recognize a faster computation of the (approximate) derivatives. And secondly, we need the third order derivatives anyway as accurately as possible for our further analysis.

7.2.1 Detecting Degenerate Period-Doubling Bifurcations

After the computation of $S^N_{\bar{x}\bar{x}\bar{x}}$ we are ready to classify the period-doublings. Since the case of a double -1 Floquet multiplier has been treated above, we may now assume -1 is simple, i.e. $w_N^T v_N \neq 0$ for the left eigenvector w_N to the eigenvalue -1 of $S^N_{\bar{x}}$. For fixed $\nu = \nu_N$, respectively $\xi = \xi_N$, we recall first the definitions:

$$c^* := w_N^T(S^N_{\bar{x}\bar{x}\bar{x}}v_N v_N + 3S^N_{\bar{x}\bar{x}}p_0)v_N,\ c^\xi_{12} := w_N^T(S^N_{\bar{x}\bar{x}}\dot{\bar{x}}_N + S^N_{\bar{x}\xi}\dot{\xi}_N)v_N,\ c^\nu_{12} := w_N^T(S^N_{\bar{x}\bar{x}}\dot{\bar{x}}_N + S^N_{\bar{x}\nu}\dot{\nu}_N)v_N.$$

Here $(\dot{\bar{x}}_N, \dot{\xi}_N)$, respectively $(\dot{\bar{x}}_N, \dot{\nu}_N)$ are the normalized tangents at the solutions $(\bar{x}_N, \xi_N)$, respectively $(\bar{x}_N, \nu_N)$, of the one-parameter problems $S(\bar{x}, \nu_N, \xi) - \bar{x} = 0$, respectively $S(\bar{x}, \nu, \xi_N) - \bar{x} = 0$. They should not be confused with the components $\dot{\bar{x}}_N$, $\dot{\nu}_N$ and $\dot{\xi}_N$ of the tangent $\dot{y}_N$ at the solution y_N of system (7.0.1). Generically these quantities and $\dot{\xi}_N$, $\dot{\nu}_N$ are nonzero and we may calculate:

$$k^N_\xi = \frac{c^\xi_{12}}{w_N^T v_N \dot{\xi}_N} \tag{7.2.3}$$

$$k^N_\nu = \frac{c^\nu_{12}}{w_N^T v_N \dot{\nu}_N} \tag{7.2.4}$$

for the crossing speeds of the critical Floquet multiplier -1 with respect to ξ and ν in the one-parameter families $S(\bar{x}, \nu_N, \xi) - \bar{x} = 0$ and $S(\bar{x}, \nu, \xi_N) - \bar{x} = 0$,

$$\ddot{\xi}_N = -\frac{c^*}{3c^\xi_{12}} \tag{7.2.5}$$

$$\ddot{\nu}_N = -\frac{c^*}{3c^\nu_{12}} \tag{7.2.6}$$

for the directions of the emanating doubled periodic orbits in the one-parameter families, and

$$\ddot{\kappa}_N = \frac{2c^*}{3w_N^T v_N} \tag{7.2.7}$$

for the stability of the doubled periodic orbits.

Similarly to the saddle-nodes, we consider now the case of y_N along a period-doubling branch with component $\dot{\nu}_N$ of $\dot{y}_N$ satisfying $\dot{\nu}_N = 0$. Then the linear system for $\dot{y}_N$ gives in particular:

$$\left(S^N_{\bar{x}} - \mathrm{id}\right)\dot{\bar{x}}_N + S^N_\xi \dot{\xi}_N = 0 \tag{7.2.8}$$

$$S^N_{\bar{x}\bar{x}}v_N\dot{\bar{x}}_N + \left(S^N_{\bar{x}} + \mathrm{id}\right)\dot{\nu}_N + S^N_{\bar{x}\xi}v_N\dot{\xi}_N = 0. \tag{7.2.9}$$

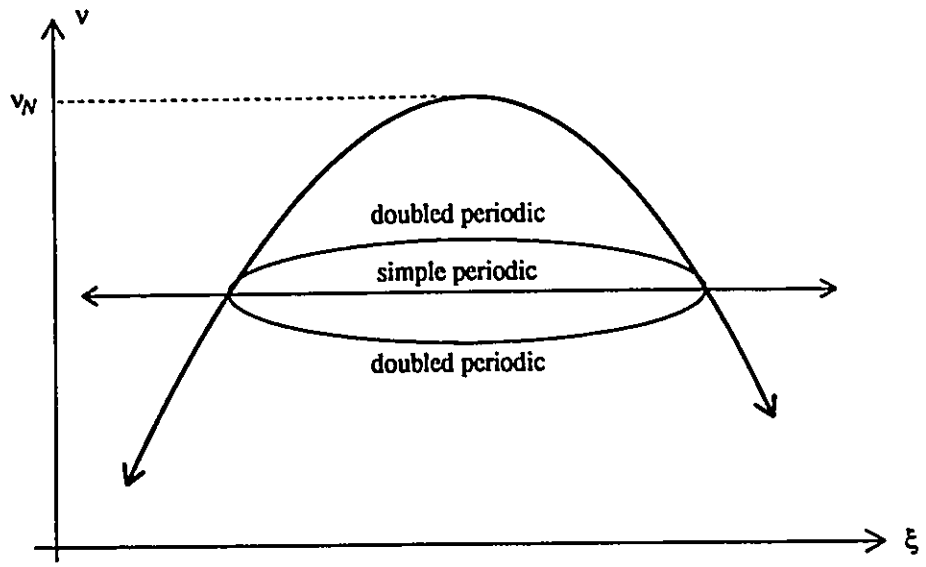

Figure 7c: Decreasing ν across ν_N creates an isolated loop of doubled periodic orbits. The "forks" open towards each other.

Since $\left(S_x^N - \mathrm{id}\right)$ is regular, equation (7.2.8) determines the unique tangent vector (up to orientation and normalization) of the one-parameter problem $S(\overline{x}, \nu^N, \xi) - \overline{x} = 0$. Multiplying (7.2.9) with w_N^T from the left gives further:

$$0 = w_N^T \left(S_{xx}^N \dot{x}_N + S_{x\xi}^N \dot{\xi}_N\right) v_N = c_{12}^{\xi} \tag{7.2.10}$$

and $k_\xi^N = 0$. Hence the period-doubling is degenerate in the sense that the crossing speed of the critical Floquet multiplier -1 is not transversal. In order to decide which case occurs, we can calculate the discriminant Δ introduced in Subsection 5.4.5. For $\Delta < 0$ the point $(\overline{x}_N, \nu_N, \xi_N)$ will, generically, be an isola formation point for doubled periodic orbits: the one-parameter family $S(\overline{x}, \nu_N, \xi) - \overline{x} = 0$ admits only the fixed point branch across $(\overline{x}_N, \xi_N)$, see Fig. 7c. For $\Delta > 0$ the point $(\overline{x}_N, \nu_N, \xi_N)$ will, generically, be a transcritical bifurcation point of doubled periodic orbits: the one-parameter family $S(\overline{x}, \nu^N, \xi) - \overline{x} = 0$ admits two distinct branches of doubled periodic orbits crossing each other at $(\overline{x}_N, \xi_N)$, see Fig. 7d. Of course we may interchange ξ and ν and get the corresponding results for the one-parameter problem $S(\overline{x}, \nu, \xi_N) - \overline{x} = 0$.

7.2.2 Detecting Degenerate Secondary Hopf Bifurcations

Finally, let us analyse the case of a secondary Hopf branch. Suppose $\delta = e^{i\beta_N}$ with $\delta^n \neq 1$ for $n = 1, 2, 3, 4$. For fixed $\nu = \nu_N$ we compute, according to Subsection 5.4.6,

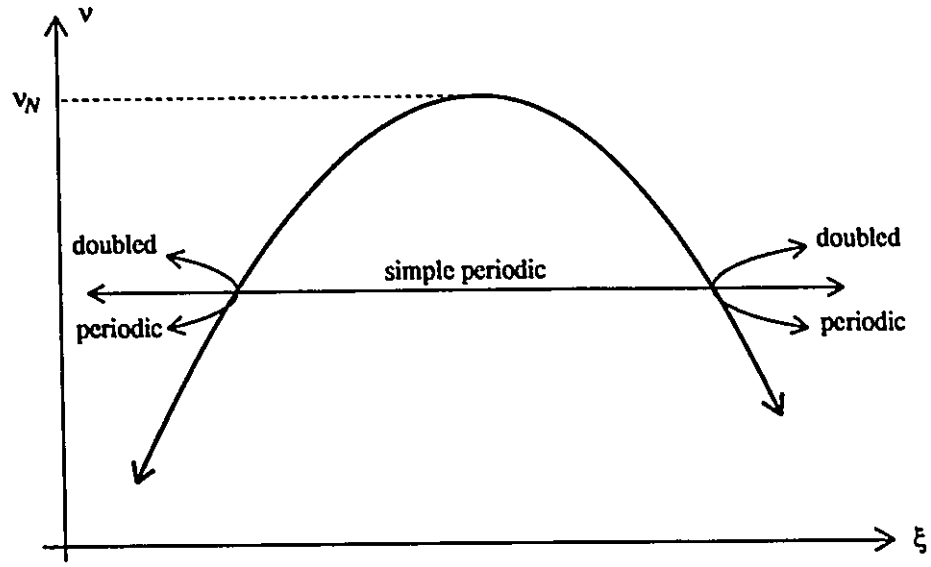

Figure 7d: Decreasing ν across ν_N creates two period-doubling bifurcations. The "forks" open away from each other.

the crossing speed $d = \|\delta\|_\xi^N$ with respect to ξ and, upon using $S^N_{\bar{x}\bar{x}\bar{x}}$, the stability coefficient $a = a(\xi_N)$. Also, analogously to the period-doubling case, it is not difficult to show that $\dot{\nu}_N = 0$ generically implies that $\|\delta\|_\xi^N = 0$. Let us briefly outline the calculations. The equation for $\dot{y}_N$ leads in particular to:

$$\begin{aligned} 0 &= S^N_{\bar{x}\bar{x}} v_N \dot{\bar{x}}_N + S^N_{\bar{x}} \dot{v}_N + \cos\beta_N (u_N \dot{\beta}_N - \dot{v}_N) \\ &\quad + \sin\beta_N (\dot{u}_N + v_N \dot{\beta}_N) + S^N_{\bar{x}\xi} v_N \dot{\xi}_N \qquad (7.2.11) \\ 0 &= S^N_{\bar{x}\bar{x}} u_N \dot{\bar{x}}_N + S^N_{\bar{x}} \dot{u}_N - \cos\beta_N (v_N \dot{\beta}_N + \dot{u}_N) \\ &\quad - \sin\beta_N (\dot{v}_N - u_N \dot{\beta}_N) + S^N_{\bar{x}\xi} u_N \dot{\xi}_N \qquad (7.2.12) \\ 0 &= (S_{\bar{x}} - \mathrm{id})\, \dot{\bar{x}}_N + S^N_\xi \dot{\xi}_N. \qquad (7.2.13) \end{aligned}$$

We now multiply (7.2.11) from the left with w_N^T and (7.2.12) from the left with z_N^T ($w_N + i\, z_N$ being the left eigenvector of $S^N_{\bar{x}}$ to the eigenvalue $\delta = e^{i\beta_N}$) and add both equations. Similarly, we multiply the first from the left with $-z_N^T$ and the second from the left with w_N^T and again add the equations. Upon using $(w_N - i\, z_N)^T S^N_{\bar{x}} = (w_N - i\, z_N)^T (\cos(\beta_N) + i\, \sin(\beta_N))$, the resulting equations simplify to:

$$\begin{aligned} 0 &= -w_N^T \left(S^N_{\bar{x}\bar{x}} \dot{\bar{x}}_N + S^N_{\bar{x}\xi} \dot{\xi}_N \right) v_N - z_N^T \left(S^N_{\bar{x}\bar{x}} \dot{\bar{x}}_N + S^N_{\bar{x}\xi} \dot{\xi}_N \right) u_N \\ &\quad + \sin\beta_N \dot{\beta}_N (w_N^T v_N + z_N^T u_N) - \cos\beta_N \dot{\beta}_N (z_N^T v_N - w_N^T u_N) \qquad (7.2.14) \end{aligned}$$

$$
\begin{aligned}
0 &= z_N^T \left(S_{\overline{x}\overline{x}}^N \dot{\overline{x}}_N + S_{\overline{x}\xi}^N \dot{\xi}_N \right) v_N - w_N^T \left(S_{\overline{x}\overline{x}}^N \dot{\overline{x}}_N + S_{\overline{x}\xi}^N \dot{\xi}_N \right) u_N \\
&\quad - \sin\beta_N \dot{\beta}_N (z_N^T v_N - w_N^T u_N) - \cos\beta_N \dot{\beta}_N (z_N^T u_N + w_N^T v_N). \qquad (7.2.15)
\end{aligned}
$$

In (7.2.14) and (7.2.15) we now replace $\dot{\overline{x}}_N$ and $\dot{\beta}_N$ with $\overline{x}_\xi^N \dot{\xi}_N$ and $\beta_\xi^N \dot{\xi}_N$. Generically $\dot{\xi}_N \neq 0$ and dividing (7.2.14), (7.2.15) by $\dot{\xi}_N$ yields the linear system:

$$
\begin{aligned}
0 &= -w_N^T \left(S_{\overline{x}\overline{x}}^N \overline{x}_\xi^N + S_{\overline{x}\xi}^N \right) v_N - z_N^T \left(S_{\overline{x}\overline{x}}^N \overline{x}_\xi^N + S_{\overline{x}\xi}^N \right) u_N \\
&\quad + \sin\beta_N \beta_\xi^N (w_N^T v_N + z_N^T u_N) - \cos\beta_N \beta_\xi^N (z_N^T v_N - w_N^T u_N) \qquad (7.2.16) \\
0 &= z_N^T \left(S_{\overline{x}\overline{x}}^N \overline{x}_\xi^N + S_{\overline{x}\xi}^N \right) v_N - w_N^T \left(S_{\overline{x}\overline{x}}^N \overline{x}_\xi^N + S_{\overline{x}\xi}^N \right) u_N \\
&\quad - \sin\beta_N \beta_\xi^N (z_N^T v_N - w_N^T u_N) - \cos\beta_N \beta_\xi^N (z_N^T u_N + w_N^T v_N). \qquad (7.2.17)
\end{aligned}
$$

A comparison with system (5.4.66) shows that $\sin\beta_N\beta_\xi^N$ and $-\cos\beta_N\beta_\xi^N$ are precisely the derivatives of the real and imaginary part of the critical Floquet multiplier $\delta = \delta(\xi) = r(\xi)e^{i\beta(\xi)}$ with respect to ξ, evaluated at $\xi = \xi_N$. That is:

$$
\sin\beta_N\beta_\xi^N = (r\cos\beta)_\xi^N \quad \text{and} \quad -\cos\beta_N\beta_\xi^N = (r\sin\beta)_\xi^N \qquad (7.2.18)
$$

Hence, by corollary 5.4.6.1, we find: $\|\delta\|_\xi^N =$

$$
\frac{\Re\delta^N (r\cos\beta)_\xi^N + \Im\delta^N (r\sin\beta)_\xi^N}{\sqrt{(\Re\delta^N)^2 + (\Im\delta^N)^2}} = \frac{\cos\beta_N \sin\beta_N \beta_\xi^N - \sin\beta_N \cos\beta_N \beta_\xi^N}{\sqrt{(\Re\delta^N)^2 + (\Im\delta^N)^2}} = 0. \qquad (7.2.19)
$$

Therefore, in a completely analogous way to the period doubling case, $\dot{\nu}_N = 0$ corresponds to a degenerate secondary Hopf bifurcation in the sense of a nontransversal crossing of the critical complex Floquet multiplier. In view of this similarity we find it reasonable to conjecture about the behaviour of the flow in a neighbourhood of this bifurcation in the following way: Generically, the solution $y_N = (\overline{x}_N, v_N, u_N, \beta_N, \nu_N, \xi_N)$ of system (7.0.1) with $\dot{\nu}_N = 0$ will be either a "transcritical bifurcation point for branches of invariant curves" or an "isola formation point for branches of invariant curves". That is, the one-parameter family $S(\overline{x}, \nu_N, \xi) - \overline{x} = 0$ will either admit two distinct branches of invariant curves (including the trivial one made of the single intersection point of the periodic orbit with the return plane) that cross each other at $(\overline{x}_N, \xi_N)$, see Fig. 7e, or no such branch at all, see Fig. 7f. Unfortunately though, we do not have more analytical insight to distinguish between the two cases. But suppose y_N corresponds to a local maximum (minimum) in the parameter ν. Then, when continuing the secondary Hopf branch with $\dot{\nu}$ approaching 0, we simply observe whether the direction of the emanating branches of invariant curve is in the direction

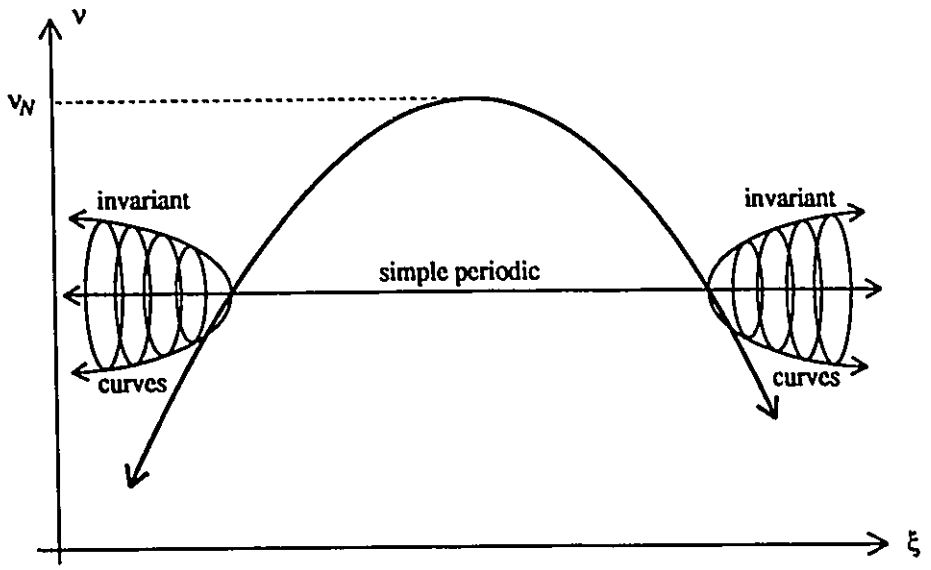

Figure 7e: Decreasing ν across ν_N creates two secondary Hopf bifurcations, such that the invariant curves create two hyperboloids opening away from each other.

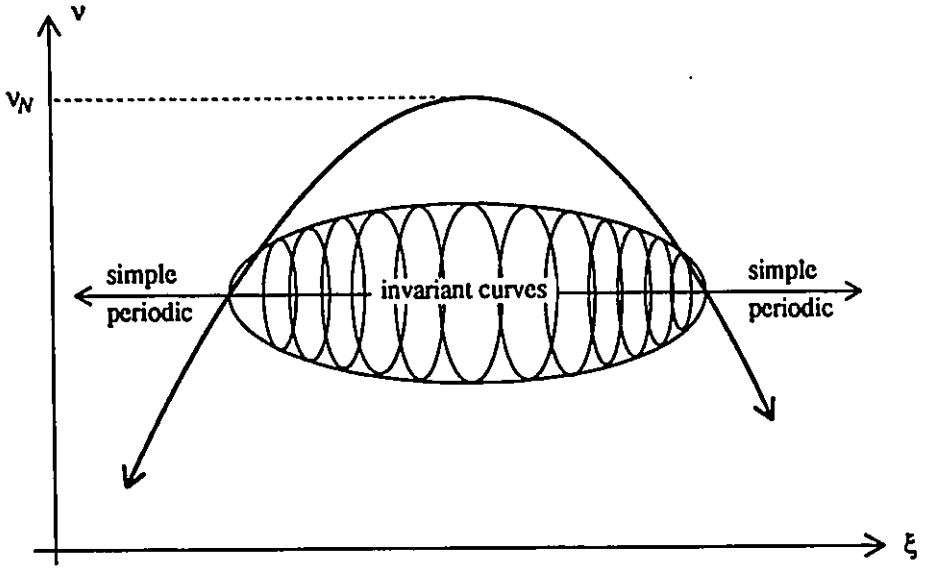

Figure 7f: Decreasing ν across ν_N creates two secondary Hopf bifurcations, such that the invariant curves create two hyperboloids opening towards each other and form an ellipsoid.

of decreasing (increasing) ν, as in Fig. 7e, or in the direction of increasing (decreasing) ν, as in Fig. 7f. Again we note that interchanging ν and ξ leads to similar results for the one-parameter family $S(\overline{x}, \nu, \xi_N) - \overline{x} = 0$.

7.3 Summary

In summary, when continuing a branch $y_1, y_2, y_3, \ldots, y_N, \ldots$ of an initial solution $y_0 = (\overline{x}_0, v_0, u_0, \beta_0, \nu_0, \xi_0)$ of system (7.0.1), we keep track of a variety of important quantities. First of all, we monitor the determinant of the Jacobian matrix g_y^N and the determinants of the two $3n-1 \times 3n-1$-submatrices $\left(g_y^N\right)_i$, $i = 1, 2$, obtained from g_y^N by deleting the last row and the column corresponding to the derivatives with respect to one of the two parameters ν or ξ. These quantities serve to detect strict bifurcation points and saddle-nodes of system (7.0.1) with respect to one of the two occurring parameters.

Since a saddle-node branch may terminate in a Hopf branch of equilibria, we also observe the norm $C_N = C(x_N, \nu_N, \xi_N) := \|f(x_N, \nu_N, \xi_N)\|_2$. In case $C_N < C^*$, with C^* a pre-specified bound, then we also compute the spectrum of f_x^N and watch for eigenvalues converging to the imaginary axis. To be able to detect possible cusps and to distinguish between isola formation points and transcritical bifurcation points, we compute the left eigenvector w_N and subsequently the characteristic quantities: $w_N^T S_{xx}^N v_N$, $w_N^T S_\nu^N$, $w_N^T S_\xi^N$ and $w_N^T v_N$.

Along a period-doubling- and secondary Hopf branch we compute the crossing speeds of the critical Floquet multiplier with respect to the two parameters and, in case we opted to compute S_{xxx}^N, we also calculate the stability and directions of the emanating branches of double periodic orbits and invariant curves. The degenerate case $0 = k_\nu^N$ $(0 = k_\xi^N)$ could further be analyzed by computing the discriminant of the underlying quadratic, respectively by comparing the directions of the emanating invariant curves with $\dot{\nu}_N$ $(\dot{\xi}_N)$. While continuing secondary Hopf bifurcations, our algorithm also searches for strong resonance points, i.e. $\beta = \pi/2$ or $\beta = 2\pi/3$. If such a value has been crossed, then the secant method is used to accurately compute the corresponding bifurcation point.

For all branches we additionally observe the period and count the Floquet multipliers in, on and outside the unit circle. Thereby we pay particular attention to the one with largest absolute value.

And finally, whenever the generic case assumes rank$[A] = m$ for any occurring $i \times j$ matrix A, then, in order to detect a possible rank deficiency, our algorithm computes and monitors the smallest pivot element in the reduction of A to an $m \times j$ matrix in row echelon form.

At last, in order to avoid tracing parts of any branch twice, we create and administer a stack file by strongly exploiting the symmetry hidden in system (7.0.1): all along a saddle-node- and period-doubling branch we have $\dot{\beta} = 0$ for the critical angle $e^{i\beta}$. In contrary, along a secondary Hopf branch at a periodic Takens-Bogdanov bifurcation point y^*, we have $\dot{\lambda} = 0$, and the dominant coordinate of $\dot{y}$ will be $\dot{\beta}$. These observations are very useful to ensure convergence towards y^* along one and the same branch, since in a neighbourhood of y^* a check on the critical Floquet multiplier is not very reliable because of its multiplicity > 1. Moreover, since the secondary Hopf branch bifurcates off symmetrically at a periodic Takens-Bogdanov point, we need to continue only one "fork" of it — either the "upper" one with $\beta > 0$ or the "lower" one with $\beta < 2\pi$ (at a periodic Takens-Bogdanov point with a double -1 multiplier either the "upper" one with $\beta > \pi$ or the "lower" one with $\beta < \pi$). This special property of the function $g(y)$ considerably facilitates the efficient continuation of multiple branch diagrams. Again we remark that Figs. 7.1, 7.2 and 7.3 were produced without tracing any part of any occurring branch more than once.

For the upcoming two-parameter diagrams we still introduce the following notations and abbreviations:

1. "Δ" for a saddle-node branch.
2. "o" for a period-doubling branch.
3. "+" for a secondary Hopf branch.
4. "HF1" for a nondegenerate Hopf bifurcation.
5. "CSP" for a cusp (or hysteresis).
6. "IFP" for an isola formation point.
7. "TBP" for a transcritical bifurcation point.
8. "PTB1" for a periodic Takens-Bogdanov point (double $+1$ Floquet multiplier with one-dimensional nullspace).

9. "PTB2" for a periodic Takens–Bogdanov point (double -1 Floquet multiplier with one-dimensional nullspace).

10. "DHF2a" for a degenerate secondary Hopf bifurcation with stability coefficient $a = 0$ (change from sub- to supercritical if all Floquet multipliers have norm ≤ 1).

11. "DHF2b" for a degenerate secondary Hopf bifurcation with nontransversal crossing speed of the critical Floquet multiplier.

12. "DHF1a" for a degenerate Hopf bifurcation with stability coefficient $a = 0$ (change from sub- to supercritical if all eigenvalues of f_x^0 have negative real parts).

13. "DHF1b" for a degenerate Hopf bifurcation with additional eigenvalues on the imaginary axis.

7.4 Results

The stable periodic orbit 3b, which is represented along the upper smooth branch in Fig. 3a in [54], undergoes a secondary Hopf bifurcation at $Y = 653.1234188$, see Fig. 6.6. In addition to Y we now free the parameter Δ, keep $k = 0.5$, $\Theta = -22$, $c = 500$, $\gamma = 2$ and $\sigma = 1$, and continue this particular bifurcation in Δ and Y. The projection of the resulting solution curve into the parameter plane is shown in Fig. 7.1. In the same way we fixed $\Delta = 7.5$ and varied Y and Θ in Fig. 7.2 respectively for fixed $Y = 653.1234188$ and variable Θ and Δ in Fig. 7.3.

Let us comment on Fig. 7.1. We remark first that it is complete in the sense that it does not contain any uncontinued branch. But, of course, there may very well coexist other, disconnected branches elsewhere in Y, Δ parameter space, see Fig. 7.4. In Fig. 7.1 the inner secondary Hopf branch — the one surrounded by the ellipse shaped loop of period-doublings and stretched between the two periodic Takens–Bogdanov points $\mathrm{PTB2}_1 = (688.58549, 8.76145)$ and $\mathrm{PTB2}_2 = (764.47384, 13.23661)$ — corresponds to doubled periodic orbits undergoing a secondary Hopf bifurcation. All other branches represent bifurcations of simple periodic orbits. We also observe the 0 angles between the saddle-node branches and the emanating secondary Hopf

branches at the periodic Takens–Bogdanov points $\mathrm{PTB1}_1 = (592.32887, 5.07091)$ and $\mathrm{PTB1}_2 = (893.90245, 9.28063)$.

Next to the periodic Takens–Bogdanov points, the points with extremal values in Y or Δ are most important. Let us first give their parameter coordinates for the saddle-node loop: At IFP_1 with $(Y_0, \Delta_0) = (626.83666, 2.91555)$ we computed an isola formation point for the one parameter family $S(\overline{x}, \Delta_0, Y) = \overline{x}$, which constitutes the minimal saddle-node (with respect to Y) for $S(\overline{x}, \Delta, Y_0) = \overline{x}$. Similarly, at IFP_2 with $(Y_0, \Delta_0) = (896.48502, 18.0845)$, we found a second isola formation point for the one-parameter problem $S(\overline{x}, \Delta_0, Y) = \overline{x}$. This time it represents the maximal saddle-node (with respect to Y) for $S(\overline{x}, \Delta, Y_0) = \overline{x}$. Conversely, at IFP_3 with $(Y_0, \Delta_0) = (589.66467, 4.17431)$, we confirmed an isola formation point for $S(\overline{x}, \Delta, Y_0) = \overline{x}$, constituting the minimal saddle-node (with respect to Δ) for $S(\overline{x}, \Delta_0, Y) = \overline{x}$. Finally, at IFP_4 with $(Y_0, \Delta_0) = (967.77, 15.298)$, we verified another isola formation point for $S(\overline{x}, \Delta, Y_0) = \overline{x}$. It represents the farthest reachable saddle-node (with respect to Δ) for $S(\overline{x}, \Delta_0, Y) = \overline{x}$.

For the period-doubling loop we arrive at the following picture: At DPDB_1 with $(Y_0, \Delta_0) = (710.02655, 7.20138)$ we computed a degenerate period-doubling with corresponding negative discriminant. It represents an isola formation point for doubled periodic orbits for $S(\overline{x}, \Delta_0, Y) = \overline{x}$, respectively the minimal period-doubling (with respect to Y) for $S(\overline{x}, \Delta, Y_0) = \overline{x}$. In the same way, DPDB_2 with $(Y_0, \Delta_0) = (817.91851, 14.06712)$ represents a second degenerate period-doubling with underlying negative discriminant. This time, the corresponding isola formation point for doubled periodic orbits for $S(\overline{x}, \Delta_0, Y) = \overline{x}$ establishes the maximal reachable period-doubling (with respect to Y) for $S(\overline{x}, \Delta, Y_0) = \overline{x}$. Conversely, at DPDB_3 with $(Y_0, \Delta_0) = (687.7501, 8.3238)$, we find the minimal period-doubling (with respect to Δ) of $S(\overline{x}, \Delta_0, Y) = \overline{x}$. It makes an isola formation point of doubled periodic orbits for $S(\overline{x}, \Delta, Y_0) = \overline{x}$. Finally, at DPDB_4 with $(Y_0, \Delta_0) = (847.27043, 12.88717)$, the same degeneracy leads to the maximal reachable period-doubling (with respect to Δ) for $S(\overline{x}, \Delta_0, Y) = \overline{x}$, respectively to a second isola formation point of doubled periodic orbits for the one-parameter problem $S(\overline{x}, \Delta, Y_0) = \overline{x}$.

In summary, the saddle-nodes along the right half of the saddle-node branch connecting IFP_3 and IFP_4 open to the left, while they open to the right on the remaining left part. Similarly, the period-doublings along the right half of the period-doubling branch connecting DPDB_1 and DPDB_2 open to the left, while they open to

the right on the left counter part.

Concerning stability, we remark that the saddle-nodes along the lower part of the saddle-node branch between $PTB1_1$ and $PTB1_2$ contain a stable periodic orbit, while they involve two unstable ones on the remaining upper branch connecting $PTB1_1$ and $PTB1_2$. For the period-doublings our calculations show that they are supercritical on the longer part of the period-doubling branch connecting $PTB2_1$ and $PTB2_2$. In contrary, along the remaining shorter part, just to the left of the secondary Hopf branch of doubled periodic orbits, they only involve unstable periodic orbits. This leads us to the characterization of the secondary Hopf bifurcations.

According to our calculations, all the secondary Hopf bifurcations are supercritical with the exception of several intervals bounded by the occurrence of a 0 stability coefficient a and the two points $DHF2b_i$ below. Along the branch connecting $PTB2_2$ and $PTB1_2$, we computed $a > 0$ for $DHF2a_1 < Y <DHF2a_2$, along the branch connecting $PTB1_1$ and $PTB2_1$, we found $a > 0$ for $DHF2a_3 < Y <DHF2a_4$. For the secondary Hopf branch between $PTB2_1$ and $PTB2_2$ we computed $a > 0$ for $DHF2a_5 < Y <DHF2a_6$ and $DHF2a_7 < Y <DHF2a_8$. We found $DHF2a_1 \approx 794.5$, $DHF2a_2 \approx 811.6$, $DHF2a_3 \approx 593.2$ and $DHF2a_4 \approx 624.5$. Finally, there are two more codimension-two bifurcations hidden in this figure, namely degenerate secondary Hopf bifurcations with 0 crossing speed d of the critical Floquet multiplier. We found $d = \|\delta\|_Y^0 = 0$ at $DHF2b_1 = (Y_0, \Delta_0) \approx (896.63421, 18.08244)$ and $d = \|\delta\|_\Delta^0 = 0$ at $DHF2b_2 = (Y_0, \Delta_0) \approx (966.86895, 15.31435)$. An analysis of the directions of the emanating invariant curves shows that $DHF2b_1$ is a transcritical bifurcation point for branches of invariant curves. It represents the maximal reachable secondary Hopf bifurcation (with respect to Y) for $S(\overline{x}, \Delta, Y_0) = \overline{x}$. Vice versa, $DHF2b_2$ represents the maximal reachable secondary Hopf bifurcation (with respect to Δ) for $S(\overline{x}, \Delta_0, Y) = \overline{x}$.

We also mention two secondary Hopf bifurcations at strong resonance between $PTB1_1$ and $PTB2_1$: at $STR_1 \approx (645.02397641, 7.23284570)$ we computed $\beta = \frac{2\pi}{3}$ while $\beta = \frac{\pi}{2}$ at $STR_2 \approx (617.9616485, 6.34547483)$.

We continue with Figs. 7.4 to 7.9 obtained for the same parameters as in Fig. 7.1 and Fig. 6.6. Fig. 7.7 shows in another one-parameter diagram the (doubled) period of a periodic orbit versus Y and Fig. 7.8 exhibits in an enlargement the behaviour of Fig. 7.7 in a neighbourhood of $(Y, \text{period}) = (460, 0.947)$. In the same way, Fig. 7.9 shows the norm of a third periodic orbit, disconnected from Fig. 7.7, versus Y. Fig. 7.4

finally shows the continuation of the saddle-node SNB_1 in Fig. 7.7. This picture used several hours of CPU-time — it was produced at an earlier stage of the development of the algorithm and we had to restart itseveral times. First of all, it impressively demonstrates the complexity in the bifurcation behaviour of this periodic orbit. It contains a much larger variety of codimension-two bifurcations than Fig. 7.1. In addition, we now encounter cusps and degenerate Hopf bifurcations. However, because of the huge scale, a lot of the fine details becomes only visible in enlargements. For example, in Fig. 7.5 we see a secondary Hopf branch of doubled periodic orbits between $PTB2_1$ and $PTB2_2$ and a period-doubling branch of doubled periodic orbits (a quadrupling of the original periodic orbit) across $PTB2_2$. We find it remarkable, that, apparently, both secondary Hopf branches continue smoothly into another. We were also surprised that, in contrary to the above Fig. 7b, the angle between the secondary Hopf branch of doubled periodic orbits and the period-doublings across $PTB2_1$ is, apparently, nonzero. The enlargement in Fig. 7.6, on the other hand, shows the behaviour we had expected. Namely, an apparently 0 angle between the branch of doubled periodic orbits undergoing a secondary Hopf bifurcation and the period-doubling branch across $PTB2_1$. Indeed, these results are still puzzling us — are we misled by the figures? Does there exist some hidden dependence or unnoticed symmetries among the parameters leading to the nongeneric case? Unfortunately, it seems to us that one needs the second derivatives $\ddot{y}$ along the secondary Hopf branches evaluated at the bifurcation points to clarify the situation. However, these quantities are extremely costly to find and we did not pursue the analysis further. In addition there are several degenerate period-doublings and secondary Hopf bifurcations, altogether four cusps, plenty of isola formation/transcritical bifurcation points and four degenerate Hopf bifurcations hidden in Fig. 7.4.

For the interested reader we include the final data we computed along a saddle-node branch apparently terminating in a degenerate Hopf bifurcation $DHF1a_1$, see Fig. 7.4: Parameters: $Y = 443.127454493$, $\Delta = -2.341334922$, $k = 0.5$, $\Theta = -22$, $c = 500$, $\gamma = 2$, $\sigma = 1$, initial value of periodic orbit:

$$x = \begin{pmatrix} 3.545167405 \\ 24.068756790 \\ -0.088451988 \\ 0.054112904 \\ 0.010735340 \end{pmatrix},$$

period, $\|f(x,\lambda)\|_2$ and critical Floquet multiplier:

$$0.637920092,\ 0.8362885,\ +1.$$

Computing the eigenvalues of $\frac{\partial f}{\partial x}(x,\lambda)$, we find indeed $\mu_{1,2} = 0.0003062\ldots \pm i\,\omega$ with $\omega = 9.8635973\ldots$ close to the imaginary axis. Moreover, the ratio $2\pi/\omega = 0.63723407$ seems to approach the period.

Proceeding, we give the final data along a secondary Hopf branch terminating apparently in a degenerate Hopf bifurcation DHF1b, see Fig. 7.4: Parameters: $Y = 115.079712886$, $\Delta = -1.736097141$, $k = 0.5$, $\Theta = -22$, $c = 500$, $\gamma = 2$, $\sigma = 1$, initial value of periodic orbit:

$$x = \begin{pmatrix} 9.052599395 \\ 2.086395262 \\ 0.060130229 \\ 0.197073498 \\ 0.044438892 \end{pmatrix},$$

period, $\|f(x,\lambda)\|_2$ and critical Floquet multiplier(s):

$$2.066075184,\ 0.0023401,\ 0.99999431 \pm i\,0.00337146.$$

Computing the eigenvalues of $\frac{\partial f}{\partial x}(x,\lambda)$, we find $\mu_{1,2} = 0.00144629\ldots \pm i\,\omega$ with $\omega = 3.0436689\ldots$ close to the imaginary axis. The ratio $2\pi/\omega = 2.0643519$ is again quite close to the period. Also, there seems to be another, third eigenvalue converging to the imaginary axis: we found additionally $\mu_3 = -0.0027018612$.

Close to these bifurcation points we decreased the error tolerance for the integration routine to 10^{-10} and kept the return plane constant and observed that $\dot{\lambda} \to 0$. We emphasize that these codimension-two bifurcations were not found by solving equations involving equilibria but as terminating points of branches of nonhyperbolic periodic orbits.

Even though Fig. 7.4 was obtained by continuing the saddle-node SNB_1 of Fig. 7.7, it also contains all of the information for the simple periodic orbit in Fig. 7.9 along its cross-section at $\Delta = 7.5$. This is possible, since a careful inspection of Fig. 7.4 shows that the disconnected branches of Figs. 7.7 and 7.9 move together for decreasing Δ, touch each other in the transcritical bifurcation point $TBP_1 = (Y, \Delta) \approx (635.77, 5.07)$ and subsequently form a single branch, see Figs. 7.10 and 7.11. However, Fig. 7.10 tells us immediately that Fig. 7.7 must have qualitatively changed before, that is for $5.07 < \Delta < 7.5$. The solution lies in the transcritical bifurcation point TBP_2. Here

Fig. 7.7 touches a fourth branch of periodic orbits terminating at both ends in Hopf bifurcations involving equilibria. We have not included a one-parameter figure of this branch — for $\Delta = 7.5$ it looks relatively simple containing only one saddle-node at $Y \approx 426.64$ and terminating in a subcritical Hopf bifurcation at $Y \approx 520$, respectively in a supercritical Hopf bifurcation at $Y \approx 732.17$. The stable part of it can be seen in Fig. 3a in [54]. In Fig. 7.4 this saddle-node is marked SNB_3.

This result, and the complexity of Fig. 7.4, suggests that we need additional information about Hopf bifurcation branches in Y and Δ in order to properly decode Fig. 7.4 further. This information is undoubtably much easier to obtain than its equivalent for periodic orbits, i.e. Figs. 7.1 and 7.4, but our codes do not handle the corresponding continuation of nonhyperbolic equilibria — many other existing codes do. Once this information is at hand, a complete and consistent interpretation of Fig. 7.4, in the same way as we just outlined, is straigthforward (but remains lengthy).

7.4.1 Attractive Invariant Curves in the Laser Model

In order to graphically demonstrate a supercritical secondary Hopf bifurcation, we first include Fig. 7.12. It shows 3000 successive intersections (again in local coordinates) of $\phi_1(t, x, \lambda)$,

$$\begin{pmatrix} 17.42447482 \\ 7.47416023 \\ 0.14187432 \\ 0.07729066 \\ -0.0367528 \end{pmatrix},$$

with the return plane H chosen to be the one perpendicular to the flow across x. The parameters are given by $Y = Y_T = 686.3$, $\Delta = 8.67591019$ and the other ones as above. We believe that transients in the long term run of $\phi_1(t, x, \lambda)$ have died out, since x itself was obtained after 20000 previous intersections, and that this trajectory is indeed attracted by a small diameter invariant curve. The successive return times of $\phi_1(t, x, \lambda)$ are close to the period of the now unstable periodic orbit, namely ≈ 0.551. The relevant secondary Hopf bifurcation occurred at $Y = Y_0 = 686.354612244$ with crossing speed $d = \|\delta\|_Y^0 = -0.001900855$, stability coefficient $a = -7.11888$, critical angle $\beta = 2.944148652$. We emphasize that the details of Fig. 7.12 depend on the integration routine, the error tolerance for this routine and the method and error tolerance for computing and accepting the successive intersections. Furthermore,

slight perturbations in the initial condition x may quickly lead the trajectory to different coexisting attractors. In fact,

$$x = \begin{pmatrix} 17.466127647 \\ 7.676300815 \\ 0.135450344 \\ 0.069233268 \\ 0.041177391 \end{pmatrix}$$

and the same parameters as in Fig. 7.12 lead to Fig. 7.13. The shown 3000 intersections of the resulting trajectory $\phi_2(t, x, \lambda)$ suggest a coexisting attractive torus at resonance. Again, the return plane H is chosen to be the one perpendicular to the flow across $\phi_2(T^*, x, \lambda_0)$ with $T^* >> 1$. We remark that the two trajectories ϕ_1 and ϕ_2 approach each other much closer than the two different initial conditions suggest. To visualize the dependence on the initial condition once more, we also include Fig. 7.14 showing 3000 intersections of another trajectory $\phi_3(t, x, \lambda)$. Here $x = (17.4, 7.5, 0.13, 0.07, -0.04)$ and the parameters were kept as in Figs. 7.12 and 7.13. The resulting trajectory $\phi_3(t, x, \lambda_0)$ drifts quickly away and settles down on a seemingly strange attractor.

Even though we did not define bifurcations of invariant curves, Fig. 7.15 may demonstrate such a phenomenon. The 3000 successive intersections of $\phi(t, x, \lambda)$ with

$$x = \begin{pmatrix} 7.42233296 \\ 7.33779153 \\ 0.26539256 \\ -0.02472344 \\ -0.07974316 \end{pmatrix},$$

$Y = Y_T = 397.6716$, $\Delta = -16.719282$, $\Theta = 3.02454605$ and the other parameters unchanged clearly show the attraction of x to an invariant curve. We are very much tempted to believe that the attractor is in fact a doubled torus. However, here, and in the other figures as well, one should not forget that the shown cross-sections represent only projections of a four-dimensional return plane into a two-dimensional one. In this example the corresponding supercritical secondary Hopf bifurcation occurred at a slightly larger $Y_H = 397.67170653$ and all other parameters as above. It is not contained in Fig. 7.1 but takes place along a different, disconnected branch included in Fig. 7.4.

The next two figures emphasize again the impact of small changes in the initial value on the fate of the trajectories. We first verified a supercritical secondary Hopf

bifurcation at $Y = Y_0 = 534.42029866$, $\Delta = 4.495233938$, $\Theta = -22.0$, $c = 501.0$, $k = 0.5$, $\gamma = 2.0$ and $\sigma = 1$ with $d = \|\delta\|_Y^0 \approx -1.69$ and $a \approx -73$. At $Y = Y_T = 534.4$ the periodic orbit is unstable with maximal norm of Floquet multiplier ≈ 1.4, and Fig. 7.16 shows 1000 successive returns (in local coordinates) of

$$x = \begin{pmatrix} -4.826114475 \\ 13.239627752 \\ 0.246016665 \\ 0.095396322 \\ 0.007319056 \end{pmatrix}$$

in the lower right corner of this figure. This point x is, up to 8(!) digits, a point of the unstable periodic orbit — in fact it is the outcome of Newton's method to find it. After initial transients have died out it is seen that $\phi(t, x, \lambda)$ approaches an attractive torus. It turns out that for Y a little larger than Y_0 the unstable periodic orbit becomes stable in a saddle-node bifurcation and then remains stable for Y decreasing to Y_T. At this value of Y, Fig. 7.17 shows the attraction of the initial point

$$x = \begin{pmatrix} -4.826110 \\ 13.239627 \\ 0.246010 \\ 0.095390 \\ 0.007310 \end{pmatrix}$$

to the fixed point representing the stable periodic orbit.

We continue by exploring another supercritical secondary Hopf bifurcation. This one happens at $Y = Y_0 = 413.13109351$. Fig. 7.18 shows the familiar picture of 3000 successive intersections of $\phi(t, x, \lambda)$ with

$$x = \begin{pmatrix} -2.8287133098 \\ 13.4362252669 \\ 0.2347273812 \\ 0.1216002742 \\ -0.0060302862 \end{pmatrix},$$

$Y = Y_T = 413.1$, $\Delta = 3.2572312$, $\Theta = -16.719282$, $c = 500.0$, $k = 0.5$, $\gamma = 2.0$ and $\sigma = 1$. The intersections "uniformly" fill an attractive closed loop. This situation changes if Y is decreased a bit further to $Y = 413.05$. Then, as Fig. 7.19 shows, the

3000 intersections of the initial value

$$x = \begin{pmatrix} -3.0651853734 \\ 11.9261210864 \\ 0.2367724574 \\ 0.1101350529 \\ 0.0061482553 \end{pmatrix}$$

accumulate in the neighbourhood of 48 distinguished points. They do not "densely" fill this cross-section — the winding number has changed. This dependence of the winding number on Y is also observed when Y decreases further to $Y = 413.03$. Fig. 7.20 shows the fate of

$$x = \begin{pmatrix} -1.7019245586 \\ 16.7509036239 \\ 0.2278382479 \\ 0.1473120558 \\ 0.0249917962 \end{pmatrix}$$

indicating another change in the winding number.

Decreasing Y further makes the invariant loop apparently undergo a "torus-doubling". Indeed, at $Y = 413.01$ the 3000 intersections in Fig. 7.21 exhibit that the invariant curve has doubled and now loops around twice before it closes. The initial condition was chosen as

$$x = \begin{pmatrix} 4.8087908935 \\ 20.0859087031 \\ 0.1940350933 \\ -0.0783101356 \\ 0.1839537725 \end{pmatrix}.$$

A further decrease in Y makes the inner loop more and more zig-zagged, see Fig. 7.22 for $Y = 413.00$. In fact, the successive intersections seem to densely fill a section of the return plane with nonzero volume and suggest a bifurcation to a three-torus — a phenomena that very well can happen in a five-dimensional phase space.

These results involving attractive tori may raise more questions than they actually answer. But they reveal for the first time the existence of such objects in the laser model. It is not surprising that they have not been discovered using the brute force approach, since their basin of attraction as well as their interval of existence in Y-space and additionally the diameter of their chosen cross-sections appear to be

quite small. This situation however might very well change in different parameter directions. The continuation of these tori along with a characterization of possibly occurring torus-bifurcations could therefore prove to be an important tool with regards to further analysis.

7.4.2 Strong Resonance

At the points $\mathrm{STR}_1 = (Y_R, \Delta_R) = (645.02397641, 7.23284570)$ and $\mathrm{STR}_2 = (Y_R, \Delta_R) = (617.9616485, 6.34547483)$ in Fig. 7.1, the periodic orbit is at strong resonance. Here the critical angle β equals $\frac{2\pi}{3}$, respectively $\frac{\pi}{2}$, and, generically, tripled, respectively quadrupled, periodic orbits will bifurcate off. It is interesting to note that, when we continued this tripled (quadrupled) periodic orbit with fixed $\Delta = \Delta_R$ and variable Y across y_R, the determinant of the underlying Jacobian did not change sign but merely touched 0. Without additionally monitoring the Floquet multipliers or the distances D_N^j we would not have discovered this bifurcation. The case $\beta = \frac{2\pi}{3}$ is illustrated in Figs. 7.23, 7.24 showing the norm $\|\cdot\|_{\mathrm{per}}$, respectively the distance $\|x - \phi(\frac{T}{3}, x, Y)\|_2$, versus Y. We see that for the tripled periodic orbit $D_N^j > 0$ except at the bifurcation value where $D_N^j = 0$. In contrary, for the simple periodic orbit $D_N^j = 0$ over the Y range shown. It turns out that the lower branch of the tripled periodic orbit gains stability in a period-doubling bifurcation at $Y \approx 772$ and looses it again for $Y \approx 780$ where it bends around in a saddle-node to close a loop with its upper partner in Fig. 6.5. The data of the stable periodic orbit at $Y = 775.0$ can be found in Table 6.1.1.

We close this chapter with Fig. 7.25 showing the behaviour of the maximal Floquet multiplier about the strong resonance case with $\beta = \frac{\pi}{2}$. In contrary to the two-sided bifurcation for $\beta = \frac{2\pi}{3}$, this time the figure reveals two distinct branches of unstable quadrupled periodic orbits existing only on one side of Y_R.

Chapter 8

Third Continuations

The idea used in the last chapter will apply again here. We free a third parameter to continue the essential points of Figs. 7.1 and 7.4. In particular, we shall continue periodic Takens–Bogdanov points with a double $+1$ and a double -1 Floquet multiplier, cusps, isola formation/transcritical bifurcation points, degenerate period-doublings and secondary Hopf bifurcations with nontransversal crossing of the critical Floquet multiplier, and, to start with, secondary Hopf bifurcations at strong resonance.

8.1 Continuation of Strong Resonance

As an introductory example of a three-parameter continuation, we mention the continuation of bifurcation points at strong resonance. Instead of treating the critical angle β along a secondary Hopf branch as a variable, we can compute a secondary Hopf branch of constant critical angle $\beta = \beta_0 \in [0, 2\pi)$ by freezing β at β_0 and, instead, freeing a third parameter ζ. That is, we consider the system $g(y) = 0$ with $y := (\overline{x}, v, u, \lambda)$ and $g : \mathbb{R}^{n-1} \times \mathbb{R}^{n-1} \times \mathbb{R}^{n-1} \times \mathbb{R}^3 \to \mathbb{R}^{3n}$, and solve:

$$g(y_{N+1}) := \begin{cases} S(\overline{x}_{N+1}, \lambda_{N+1}) - \overline{x}_{N+1} & = 0 \\ S_{\overline{x}}(\overline{x}_{N+1}, \lambda_{N+1})(v_{N+1} + i\,u_{N+1}) - e^{i\beta_0}(v_{N+1} + i\,u_{N+1}) & = 0 \\ (v_{N+1} + i\,u_{N+1})^*(v_N + i\,u_N) - 1 & = 0 \\ (\overline{x}_{N+1} - \overline{x}_N)^T \dot{\overline{x}}_N + (\lambda_{N+1} - \lambda_N)^T \dot{\lambda}_N & \\ \quad + (v_{N+1} - v_N)^T \dot{v}_N + (u_{N+1} - u_N)^T \dot{u}_N - \delta s & = 0 \end{cases} \tag{8.1.1}$$

for the next solution $y_{N+1} = (\overline{x}_{N+1}, v_{N+1}, u_{N+1}, \lambda_{N+1})$ with $\lambda = (\nu, \xi, \zeta) \in \mathbb{R}^3$. Again "$*$" denotes complex transpose, $y_N = (\overline{x}_N, v_N, u_N, \lambda_N)$ is the previous solution and $\dot{y}_N = (\dot{\overline{x}}_N, \dot{v}_N, \dot{u}_N, \dot{\lambda}_N)$ corresponds to the normalized oriented tangent at y_N. For

$\beta_0 = 2\pi/3$ or $\beta_0 = \pi/2$, we would then continue a secondary Hopf bifurcation at strong resonance.

A comparison with system (7.0.1) shows that the Jacobian matrix g_y^k, occurring in the iteration towards the N-th solution point y_N of system (8.1.1), requires the additional new quantities S_ζ^k and $S_{\bar{x}\zeta}^k$, which can be found in the same way as S_ξ^k and $S_{\bar{x}\xi}^k$ above.

Of course, when continuing an initial solution y_0 of (8.1.1), we observe the determinant of g_y^N and check for saddle-nodes (of secondary Hopf bifurcations at strong resonance) with respect to one of the three parameters. We also compute and monitor the stability coefficient, the crossing speeds (with respect to the various parameters), the Floquet multipliers, the period and the norm $\|f(x^N, \lambda^N)\|_2$.

Applied to the laser model, we now additionally free the parameter Θ and continue the strong resonance point STR_1 with $\beta_0 = 2\pi/3$ of Fig. 7.1. The projection of the resulting solution curve into the Y, Δ parameter plane is shown in Fig. 8.1. Notice that the third parameter Θ disappears in this projection. However, besides the point STR_1 with $(Y, \Delta, \Theta) = (645.023976, 7.2328457, -22)$, the intersections of this curve with the hyperplane $\Theta = -22$ reveal a second of these strong resonance points, STR^1, with parameter coordinates $(Y, \Delta, \Theta) = (776.4862716, 14.75357844, -22)$. In Fig. 7.1 this point lies along the secondary Hopf branch between $\mathrm{PTB2}_2$ and $\mathrm{DHF2b}_2$. We see that increasing (or decreasing) Θ towards its extremal values moves STR_1 and STR^1 together and makes them finally disappear in a saddle-node of secondary Hopf bifurcations at strong resonance with respect to Θ. This implies, in particular, that, before this can happen, the two secondary Hopf branches in Fig. 7.1 must somehow join together. At least intuitively, this can be accomplished if the periodic Takens-Bogdanov points $\mathrm{PTB2}_1$ and $\mathrm{PTB2}_2$ move together, touch and annihilate each other in a saddle-node of periodic Takens-Bogadanov points with respect to Θ such that a single secondary Hopf branch, detached from the inner period doubling loop, is created.

Let us therefore proceed with the continuation of periodic Takens-Bogdanov points.

8.2 Continuation of Periodic Takens–Bogdanov Points

A periodic Takens-Bogdanov point $y_0 = (\overline{x}_0, v_0, u_0, \beta_0, \nu_0, \xi_0)$ of system (7.0.1) is characterized by a double $+1$ or a double -1 Floquet multiplier with corresponding one-dimensional eigenspace. Hence, we augment system (7.0.1) by fixing β at $\beta_0 = 0$ or at $\beta_0 = \pi$ and further imposing $S_{\overline{x}}(\overline{x}, \lambda)u\, e^{i\beta_0}u = v$, $u^T v = 0$, for the generalized right eigenvector u. That is, we consider the system $g(y) = 0$ with $y := (\overline{x}, v, u, \lambda)$ and $g : \mathbb{R}^{n-1} \times \mathbb{R}^{n-1} \times \mathbb{R}^{n-1} \times \mathbb{R}^3 \to \mathbb{R}^{3n}$, and solve:

$$g(y_{N+1}) := \begin{cases} S(\overline{x}_{N+1}, \lambda_{N+1}) - \overline{x}_{N+1} & = 0 \\ S_{\overline{x}}(\overline{x}_{N+1}, \lambda_{N+1})v_{N+1} - e^{i\beta_0}v_{N+1} & = 0 \\ S_{\overline{x}}(\overline{x}_{N+1}, \lambda_{N+1})u_{N+1} - e^{i\beta_0}u_{N+1} - v_{N+1} & = 0 \\ v_{N+1}^T v_N - 1 & = 0 \\ u_{N+1}^T v_{N+1} & = 0 \\ (\overline{x}_{N+1} - \overline{x}_N)^T \dot{\overline{x}}_N + (\lambda_{N+1} - \lambda_N)^T \dot{\lambda}_N & \\ + (v_{N+1} - v_N)^T \dot{v}_N + (u_{N+1} - u_N)^T \dot{u}_N - \delta s & = 0 \end{cases} \tag{8.2.1}$$

for the next solution $y_{N+1} = (\overline{x}_{N+1}, v_{N+1}, u_{N+1}, \lambda_{N+1})$ with $\lambda = (\nu, \xi, \zeta) \in \mathbb{R}^3$. For more information (and different defining systems) we mention [44], [155], and [174]. Similarly to the continuation of secondary Hopf bifurcations at strong resonance, the new elements in the Jacobian matrix g_y^k occurring in iterating Newton's method towards Y_N are here S_ζ^k and $S_{\overline{x}\zeta}^k$.

During continuation, we again monitor the determinant of g_y^N and watch for saddle-nodes (of periodic Takens-Bogdanov points) with respect to one of the three parameters. We also check the remaining nondegeneracy conditions for the crossing saddle-node branch (if a double $+1$ is continued) respectively for the crossing period-doubling branch (if a double -1 is continued) in the corresponding two-parameter diagrams. In addition, we observe the dimension of the eigenspace of $S_{\overline{x}}(\overline{x}_N, \lambda_N) - e^{i\beta_0}\mathrm{id}$, the Floquet multipliers, the period and the norm $\|f(x_N, \lambda_N)\|_2$.

Applied to the laser model, we now again free the parameter Θ and continue the point $\mathrm{PTB2}_1$ in Fig. 7.1. The projection of the resulting curve into Y, Θ space is shown in Fig. 8.2. Note that a cross-section along $\Theta = -22$ also exibits the

second periodic Takens–Bogdanov point, $PTB2_2$, from Fig. 7.1. The extremal values in Θ (or saddle-nodes with respect to Θ) are found to be $\Theta_{max} = -9.60253$ and $\Theta_{min} = -22.96589$. And indeed, as the two-parameter Fig. 8.3 for variable Y, Δ at fixed $\Theta = -22.96589073$ shows, $PTB2_1$ and $PTB2_2$ move together and annihilate each other in a saddle-node. The period-doubling loop becomes detached for Θ slightly less than Θ_{min} and continues to exist "to the right" of the secondary Hopf branch. We remark that a similar numerical experiment for Θ slightly less than Θ_{max} gives qualitatively the same picture — the period-doubling loop detaches again on the same side of the secondary Hopf branch. Hence, we may say that varying Θ pushes in and pulls out the loop of period-doublings into the neighbouring branch of secondary Hopf bifurcations.

The situation seems to be much more complex if we continue a periodic Takens–Bogdanov points with a double +1 Floquet multiplier of Fig. 7.1. Indeed, Fig. 8.4, showing the projection of the continuation of the point $PTB1_1$ in Fig. 7.1 into the Y, Δ parameter space, exhibits only a small section of the resulting complete three-parameter curve in Fig. 8.5. We found that, even though it does not contain any strict bifurcation points (as, for instance, indicated by a "triple point" with a third nontrivial +1 Floquet multiplier), the curve occasionally attains a third Floquet multiplier of magnitude +0.9. On the other hand, the full curve contains plenty of saddle-nodes in all of its parameters, see Fig. 8.6, it wildly winds around and ultimately terminates at both endpoints in degenerate Hopf bifurcations with an additional zero eigenvalue of the corresponding Jacobian matrix on the imaginary axis. For the endpoints we found: $(Y, \Delta, \Theta) \approx (558.544, 4.850, -11.147)$ and $(Y, \Delta, \Theta) \approx (104.652, 0.105, -3.939)$. Also, as only a detailed inspection of the data reveals, the points Q_1 , Q_2 and Q_3 in Fig. 8.6 do not constitute cusps (in this projection). Rather, they are extremely sharp, but still smooth, saddle-nodes.

Let us investigate the fate of the points $PTB1_1$ and $PTB1_2$ in Fig. 7.1 by interpreting Fig. 8.4. It turns out that the following happens: As Θ decreases from -22 to $\Theta_1 = -22.37966071$ with $(Y, \Delta) = (913.015405901, 18.39123579)$ the secondary Hopf branch between $PTB2_2$ and $PTB1_2$ moves towards the surrounding saddle-node loop, touches it for $\Theta = \Theta_1$ with $(Y, \Delta) \approx (913, 18.4)$, and for $\Theta < \Theta_1$ it splits into two disconnected parts. As is seen from Fig. 8.4, $PTB1_1$ is not affected by this bifurcation. The corresponding two parameter Fig. 7.1 would now contain three secondary Hopf branches and six periodic Takens–Bogdanov points. The two

newly created ones, $PTB1_3$ and $PTB1_4$, can be seen in the enlargement Fig. 8.7 for Θ just below Θ_1, $PTB1_3 = (910.11338, 18.3925)$ and $PTB1_4 = (916.424, 18.3943)$. A consistent decoding of Fig. 8.4 is now obvious. $PTB1_4$ and $PTB1_2$ move together along the surrounding saddle-node loop, and for $\Theta = \Theta_2 = -26.3593047$ with $(Y, \Delta) = (1200.29526557, 15.92377165)$ the secondary Hopf branch spanned between them disappears.

We see that the coalescence of periodic Takens–Bogdanov points can lead to different codimension-three bifurcation points P_i: the connection of two secondary Hopf branches to a single one and the annihilation of one. Of course, this reflects nothing else than two different ways in which two pitchforks can approach and annihilate each other. If the "forks" (i.e. the symmetric secondary Hopf branches) open towards each other such that they describe a closed loop, then P_i is an isola formation point for loops of secondary Hopf branches in system (7.0.1). On the other hand, if the "forks" open away from each other, then P_i will be a multiple strict bifurcation point for system (7.0.1) with a saddle-node branch and two symmetric secondary Hopf branches across it, such that the Hopf branches undergo a transcritical bifurcation — we recall that the secondary Hopf branches coincide if projected into any two-dimensional parameter space. For instance

$$P_1 = (Y, \Delta, \Theta) = (913.015405901, 18.39123579, -22.37966071)$$

makes a multiple strict bifurcation point and

$$P_2 = (Y, \Delta, \Theta) = (1200.29526557, 15.92377165, -26.3593047)$$

is an isola formation point.

A further decrease of Θ makes the remaining points $PTB1_1$ and $PTB1_3$ first to occur at the same Y value. This happens when the curve crosses itself (only in the projection) for $\Theta = \Theta_3 \approx -29.8$, see Fig. 8.4. Then they move together, touch and disappear at $\Theta = \Theta_4 = -33.86918$ in another multiple strict bifurcation. Since the period-doubling loop detached already at $\Theta = \Theta_3 \approx -22.96589$, we find that, at $\Theta = \Theta_4$, the secondary Hopf bifurcation loop detaches from the saddle-nodes. This can be seen in Fig. 8.8 for $\Theta = -33.86917974$.

Notice that, at this point, we do not know what happened to the period-doubling loop — it might still exist inside the secondary Hopf loop at Θ_4.

Now, in order for this picture to be true, some of the periodic Takens–Bogdanov points must become degenerate along their continuation, namely when they occur as

extremal points (or saddle-nodes) with respect to Y or Δ in the corresponding two-parameter diagrams, i.e. Fig. 7.1. At these Θ values we encounter this additional degeneracy in the form $w^T S_Y = 0$ or $w^T S_\Delta = 0$. For instance, varying Θ from -22 in Fig. 7.1 to Θ_4 in Fig. 8.8 makes $\mathrm{PTB1}_1$ attain a minimal value in Δ for a value of Θ in between. Here $w^T S_Y = 0$ and $\mathrm{PTB1}_1$ coalesces with an isola formation point. A similar situation occurs for the points $\mathrm{PTB1}_3$ and $\mathrm{PTB1}_4$. A glance at Fig. 8.7 shows us that their first appearance is already quite close to the isola formation point IFP_2. Indeed, we find that for Θ slightly less than Θ_1, precisely at $\Theta_5 = -22.37987141$, $\mathrm{PTB1}_4$ coalesces with IFP_2 at $(Y, \Delta) = (913.7285040, 18.391492383)$. In the same way $\mathrm{PTB1}_3$ becomes degenerate for Θ slightly larger than Θ_4, namely at $\Theta_6 = -33.83017293$ with corresponding $(Y, \Delta) = (1582.942535872, 21.032318816)$. Hence, at

$$P_3 = (Y, \Delta, \Theta) = (913.7285040, 18.391492383, -22.37987141)$$

and

$$P_4 = (Y, \Delta, \Theta) = (1582.942535872, 21.032318816, -33.83017293)$$

we encounter degenerate isola formation points for the one-parameter family $S(\overline{x}, Y) - \overline{x} = 0$.

Also, from another point of view, the development of Fig. 7.1 becomes much more complicated for increasing Θ since a section at $\Theta = -22$ across the complete curve reveals several, but not all, periodic Takens–Bogdanov points that are also present in Fig. 7.4. To be specific, starting from $\mathrm{PTB1}_1$ or $\mathrm{PTB1}_2$ in Fig. 7.1 the curve eventually crosses precisely the periodic Takens–Bogdanov points PTB_i, $i = 1, 2, \ldots 8$, in Fig. 7.4 as well. Therefore, Figs. 7.1 and 7.4 must somehow join if Θ increases — a possible mechanism for such a connection will be presented in Section 8.4. In fact, besides the periodic Takens–Bogdanov curve above (with degenerate Hopf bifurcations at its ends), we computed two more, different, disconnected ones, describing closed loops in (Y, Δ, Θ) space. The first one of these precisely interconnects PTB_9 and PTB_{10} while the second one crosses $\Theta = -22$ in PTB_{11} and PTB_{12}, see Fig. 7.4.

However, recalling that the curve in Fig. 8.4 terminates at both ends in degenerate Hopf bifurcations, we must also take the equilibria behaviour into consideration in order to completely determine the fate of Fig. 7.1, and hence of Fig. 7.4. This is not so much of a surprise, since Fig. 7.4 already inherits several codimension-two bifurcations involving equilibria. In view of this complexity, we deem the complete

determination of the fate of Fig. 7.1, and hence of Fig. 7.4, a challenging but not hopeless task.

On the other hand, concerning again the development of Fig. 7.1 for decreasing Θ, we can systematically and more easily improve our prediction by continuing its isola formation points IFP_i, its degenerate period-doublings and secondary Hopf bifurcations DPDB_i, respectively $\mathrm{DHF2b}_i$. This will be our remaining task in the next sections.

8.3 Continuation of Isola Formation/Transcritical Bifurcation Points

Suppose now the point $y_0 = (\overline{x}_0, v_0, u_0, 0, \nu_0, \xi_0)$ is a quadratic saddle-node with respect to ν (or ξ) of system (7.0.1), i.e. y_0 constitutes a saddle-node with respect to ν (or ξ) along a branch of saddle-nodes. Then $(\overline{x}_0, \nu_0, \xi_0)$ is a transcritical bifurcation or isola formation point for the one-parameter family $S(\overline{x}, \nu_0, \xi) - \overline{x} = 0$, respectively for $S(\overline{x}, \nu, \xi_0) - \overline{x} = 0$. Therefore $w^T S^0_\xi = 0$, respectively $w^T S^0_\nu = 0$, for the left eigenvector w of $S^0_{\overline{x}} - \mathrm{id}$ with the eigenvalue 0. Hence, for the continuation of this occurrence, we may consider the system $g(y) = 0$ with $y := (\overline{x}, w, \lambda)$ and $g : \mathbb{R}^{n-1} \times \mathbb{R}^{n-1} \times \mathbb{R}^3 \to \mathbb{R}^{2n+1}$, and solve:

$$g(y_{N+1}) := \begin{cases} S(\overline{x}_{N+1}, \nu_{N+1}, \xi_{N+1}, \zeta_{N+1}) - \overline{x}_{N+1} &= 0 \\ w^T_{N+1} S_{\overline{x}}(\overline{x}_{N+1}, \nu_{N+1}, \xi_{N+1}, \zeta_{N+1}) - w^T_{N+1} &= 0 \\ w^T_{N+1} S_{\xi}(\overline{x}_{N+1}, \nu_{N+1}, \xi_{N+1}, \zeta_{N+1}) &= 0 \\ w^T_{N+1} w_N - 1 &= 0 \\ (\overline{x}_{N+1} - \overline{x}_N)^T \dot{\overline{x}}_N + +(\nu_{N+1} - \nu_N)^T \dot{\nu}_N & \\ + (\xi_{N+1} - \xi_N)^T \dot{\xi}_N + (\zeta_{N+1} - \zeta_N)^T \dot{\zeta}_N & \\ + (w_{N+1} - w_N)^T \dot{w}_N - \delta s &= 0 \end{cases} \tag{8.3.1}$$

(respectively $w^T_{N+1} S_\nu(\overline{x}_{N+1}, \nu_{N+1}, \xi_{N+1}, \zeta_{N+1}) = 0$) for the next solution $y_{N+1} = (\overline{x}_{N+1}, w_{N+1}, \nu_{N+1}, \xi_{N+1}, \zeta_{N+1})$. More about the continuation of these bifurcations can be found in [86], [175], [129], [124], [123]. Besides $S^k_{\overline{x}\zeta}$, we now need additionally the mixed parameter derivatives $S^k_{\xi\nu}$, $S^k_{\xi\xi}$ and $S^k_{\xi\zeta}$. A second differentiation of (6.2.2) with respect to another parameter $\mu \in \{\nu, \xi, \zeta\}$ gives ($\lambda \in \mathbb{R}$):

$$0 \;=\; -S_{\lambda\mu}(\overline{x}, \lambda, \mu) + U^T \Big\{ \Big[\frac{\partial f}{\partial x} [\phi(\tau(x, \lambda, \mu), x, \lambda, \mu), \lambda, \mu]$$

$$
\begin{aligned}
&\cdot \Big(f[\phi(\tau(x,\lambda,\mu),x,\lambda,\mu),\lambda,\mu]\frac{\partial\tau}{\partial\mu}(x,\lambda,\mu) + \frac{\partial\phi}{\partial\mu}(\tau(x,\lambda,\mu),\lambda,\mu)\Big) \\
&+ \frac{\partial f}{\partial\mu}[\phi(\tau(x,\lambda,\mu),x,\lambda,\mu),\lambda,\mu]\Big]\frac{\partial\tau}{\partial\lambda}(x,\lambda,\mu) \\
&+ f[\phi(\tau(x,\lambda,\mu),x,\lambda,\mu),\lambda,\mu]\frac{\partial\tau^2}{\partial\mu\partial\lambda}(x,\lambda,\mu) \\
&+ \Big(\frac{\partial f}{\partial x}[\phi(\tau(x,\lambda,\mu),x,\lambda,\mu),\lambda,\mu]\frac{\partial\phi}{\partial\lambda}(\tau(x,\lambda,\mu),\lambda,\mu) \\
&+ \frac{\partial f}{\partial\lambda}[\phi(\tau(x,\lambda,\mu),\lambda,\mu),\lambda,\mu]\Big)\frac{\partial\tau}{\partial\mu}(x,\lambda,\mu) \\
&+ \frac{\partial\phi^2}{\partial\mu\partial\lambda}(\tau(x,\lambda,\mu),\lambda,\mu)\Big\} \qquad (8.3.2)
\end{aligned}
$$

Evaluation of (8.3.2) at (x^k,λ^k,μ^k) gives for $S^k_{\lambda\mu} := S_{\lambda\mu}(\overline{x}^k,\lambda^k,\mu^k)$ in short:

$$
S^k_{\lambda\mu} = U^T\{[f^k_x(f^k\tau^k_\mu+\phi^k_\mu)+f^k_\mu]\tau^k_\lambda + f^k\tau^k_{\mu\lambda} + (f^k_x\phi^k_\lambda + f^k_\lambda)\tau^k_\mu + \phi^k_{\lambda\mu}\}. \qquad (8.3.3)
$$

Differentiation of (6.2.4) with respect to μ and evaluation at (x^k,λ^k,μ^k) lead to:

$$
\begin{aligned}
0 \;=\; & \tau^k_{\mu\lambda} f(x_{\text{orig}},\mu^k,\lambda^k)^T f^k + \tau^k_\mu f(x_{\text{orig}},\mu^k,\lambda^k)^T[f^k_x(f^k\tau^k_\lambda+\phi^k_\lambda)+f^k_\lambda] \\
& + f(x_{\text{orig}},\mu^k,\lambda^k)^T[(f^k_x\phi^k_\mu + f^k_\mu)\tau^k_\lambda + \phi^k_{\mu\lambda}], \qquad (8.3.4)
\end{aligned}
$$

which can be solved for $\tau^k_{\mu\lambda} := \frac{\partial\tau^2}{\partial\mu\partial\lambda}(x^k,\lambda^k,\mu^k)$ since $f(x_{\text{orig}},\mu^k,\lambda^k)^T f^k \neq 0$ in a neighbourhood of $(x_{\text{orig}},\lambda_{N-1},\mu_{N-1})$. It remains to determine the quantities $\phi^k_{\mu\lambda} := \frac{\partial^2\phi_i}{\partial\mu\partial\lambda}(\tau^k,x^k,\lambda^k\mu^k)$ for $i = 1,2,\ldots n$. Let $w_i = w_i(t,x^k,\lambda^k,\mu^k) := \frac{\partial\phi_i}{\partial\lambda}(t,x^k,\lambda^k,\mu^k)$, $u_i = u_i(t,x^k,\lambda^k,\mu^k) := \frac{\partial\phi_i}{\partial\mu}(t,x^k,\lambda^k,\mu^k)$, $v_i = v_i(t,x^k,\lambda^k,\mu^k) := \frac{\partial w_i}{\partial\mu}(t,x^k,\lambda^k,\mu^k)$. Differentiation of v_i with respect to t yields:

$$
\begin{aligned}
\dot{v} \;=\; & \frac{\partial^2 f}{\partial x^2}(\phi(t,x^k,\lambda^k,\mu^k),\lambda^k,\mu^k)w(t,x^k,\lambda^k,\mu^k)u(t,x^k,\lambda^k,\mu^k) \\
& + \frac{\partial^2 f}{\partial x\partial\mu}(\phi(t,x^k,\lambda^k,\mu^k),\lambda^k,\mu^k)w(t,x^k,\lambda^k,\mu^k) \\
& + \frac{\partial^2 f}{\partial x\partial\lambda}(\phi(t,x^k,\lambda^k,\mu^k),\lambda^k,\mu^k)u(t,x^k,\lambda^k,\mu^k) \\
& + \frac{\partial f}{\partial x}(\phi(t,x^k,\lambda^k,\mu^k),\lambda^k,\mu^k)v(t,x^k,\lambda^k,\mu^k) \\
& + \frac{\partial^2 f}{\partial\mu\partial\lambda}(\phi(t,x^k,\lambda^k,\mu^k),\lambda^k,\mu^k). \qquad (8.3.5)
\end{aligned}
$$

This n-dimensional system must be integrated along with the n-dimensional flow and the two n-dimensional systems (if $\mu \neq \lambda$) for $w(t,x^k,\lambda^k,\mu^k)$ and $u(t,x^k,\lambda^k,\mu^k)$ from $t = 0$ to $t = \tau^k$ with initial condition $v(0,x^k,\lambda^k,\mu^k) = 0$.

During continuation we monitor the determinant of the Jacobian matrix g_y^N of (8.3.1) and watch for saddle-nodes (of saddle-nodes of saddle-nodes) with respect to one of the parameters involved. We also check the remaining nondegeneracy conditions and observe the Floquet multipliers, the period and the norm $\|f(x^N, \lambda^N)\|_2$. Furthermore, for each point y_N we compute the discriminant (7.1.5) of the underlying quadratic equation and watch for a change in its sign.

Applied to the laser model, we again free the parameter Θ. As a first example we continue the isola formation point IFP_2 of Fig. 7.1 — which turns out to be the same as in Fig. 8.7. Along the path with decreasing Θ we first recover the above degenerate periodic Takens–Bogdanov points at Θ_5 and Θ_6 which, in this context, may also be called degenerate isola formation points. Then, for Θ just a little below Θ_4, precisely at $\Theta_7 = -33.878828571$, the curve undergoes a (quadratic) saddle-node with respect to Θ. Here IFP_2 with $(Y, \Delta) = (1586.00505528, 20.30099111)$ coalesces with the lower isola formation point IFP_1 from Fig. 7.1: at Θ_7 the two-parameter diagram Fig. 7.1 degenerates to a single point which we may call an isola formation point for a branch of codimension-one bifurcations (the saddle-node loop). Consequently, the (Y, Δ, Θ) parameter domain of existence of the periodic orbit of Fig. 6.1 attains a local minimum in Θ at this point

$$P_5 = (Y, \Delta, \Theta) = (1586, 00505528, 20.30099111, -33.878828571).$$

Moreover, by observing the variation in Δ and after additional continuation of IFP_4, see Fig. 7.1, we can state that, at least in a neighbourhood of P_5, this domain looks like the interior of an ellipsoid, thin in a Δ, Θ cross-section and relatively long in the Y direction. Now, if we were to continue IFP_3 (or IFP_4), we would of course recover P_5. This tells us that the degeneracy at P_5 can be characterized by $w^T S_Y = w^T S_\Delta = 0$. Hence, we could continue it by freeing a fourth parameter, α, and augmenting system (8.3.1) by:

$$w_1^T S_\Delta(\overline{x}_1, \lambda_1) = 0 \tag{8.3.6}$$

with $\lambda = (Y, \Delta, \Theta, \alpha) \in \mathbb{R}^4$. At a saddle-node P with respect to α we could then find isola formation points for loops of isola formation points each of which creating a loop of saddle-nodes. By augmenting the augmented system again with $w^T S_\zeta = 0$, freeing a fifth parameter, ι, we could then continue and continue and ....

Another interesting bifurcation can be found by continuing the transcritical bifurcation point TBP_3 with $(Y, \Delta) = (263.97030548, -1.46657657)$ in Fig. 7.4 close to the cusp CSP_1 and sightly above the isola formation point IFP_1 with $(Y, \Delta) = (267.55810869, -1.471563423)$. First of all, an enlargement of this region shows that the cusp is still "bended upwards", see Fig. 8.9. However, following TBP_3 with decreasing Θ bends the cusp down and moves the three points TBP_3, IFP_1 and CSP_1 together until they coalesce at

$$P_6 = (Y, \Delta, \Theta) = (273.254431525, -1.581301937, -22.2855225),$$

see Fig. 8.10. During continuation we observe this degeneracy by bending across a saddle-node in Θ at $\Theta_8 = -22.2855225$ with $(Y, \Delta) = (273.254431525, -1.581301937)$ accompanied by a simultaneous change in sign of the discriminant (7.1.5) from positive (for TBP_1) to negative (for IFP_1). That this particular example indeed deserves its name "winged cusp", can best be understood by interpreting Fig. 8.11 showing a projection of the three-parameter continuation into Δ, Θ space: we see that varying Θ makes the curve in Fig. 8.9 flap up and(!) down like a wing. For a collection of stable two-parameter diagrams in a neighbourhood of this organizing centre we refer to [61], [62].

We proceed to continue the transcritical bifurcation point TBP_2 close to the degenerate Hopf bifurcation $DHF1a_1$ of Fig. 7.4. We find that decreasing Θ leads to a saddle-node at $\Theta_9 = -37.6465747$ with $(Y, \Delta) = (1048.921888383, 2.684821205)$. At $\Theta = -37.64468227$, just above this saddle-node, Fig. 8.12 shows that TBP_2 has already separated from Fig. 7.4 and is in the process of shrinking to the single degenerate transcritical bifurcation point

$$P_7 = (Y, \Delta, \Theta) = (1048.921888383, 2.684821205, -37.6465747).$$

Again, we may call P_7 an isola formation point for a branch of codimension-one bifurcations. This time, in a neighbourhood of P_7 the domain of existence of the periodic orbits involved resembles the exterior of a relatively long (with respect to Y) ellipsoid. By continuing TBP_5, see Fig. 7.4, we find that this domain has a local maximum in Y at $Y = 1072.68379$. However, our description is incomplete. For instance, we do not know where the continuation of TBP_2 leads after it has bent around the saddle-node at Θ_9, nor do we anticipate the fate of the degenerate Hopf bifurcation $DHF1a_1$, see Fig. 7.4. And having seen that already a small change in

Θ can be sufficient for many distinct, drastic changes to occur, we do not speculate further. It simply gets too complex!

We conclude this chapter with the continuation of TBP_4, see Fig. 7.4. It turns out that the curve undergoes a saddle-node with respect to Θ at $\Theta_{10} = -31.627587851$ with $(Y, \Delta) = (580.422645129, -0.499760969)$ and with a simultaneous change of the discriminant from positive to negative. An enlargement of the corresponding two-parameter Fig. 8.13 reveals the cubic saddle-node

$$P_8 = (Y, \Delta, \Theta) = (580.422645129, -0.499760969, -31.627587851)$$

along a branch of saddle-nodes. For $\Theta > \Theta_{10}$ it disappears and for $\Theta < \Theta_{10}$ it is perturbed into two quadratic saddle-nodes. The one with the smaller Y corresponds to a transcritical bifurcation and the other to an isola formation point (both with respect to Δ). With this information a complete analysis of the behaviour in a neighbourhood of P_8 is now fairly obvious.

Similarly to the continuation of these degenerate saddle-nodes, we could now proceed and continue degenerate period-doublings and secondary Hopf bifurcation. Following the $DPDB_i$ and the $DHF2b_i$ of Figs. 7.1 and 8.8, we may answer the question for which value of $\Theta > -33.878828571$ the loops of secondary Hopf bifurcations and period-doublings occur. However, once again, this requires substantially more effort than the continuation of transcritical bifurcation points or isola formation points, since the characterization of the 0 crossing speed of the critical Floquet multiplier at $DPDB_i$ and $DHF2b_i$ needs second derivatives of the Poincaré map: $S_{\overline{x}\overline{x}}(\overline{x}, \lambda)$. Consequently, with $\lambda = (\xi, \mu, \zeta) \in \mathbb{R}^3$, Newton's method would need the additional third derivatives: $S_{\overline{x}\overline{x}\overline{x}}(\overline{x}, \lambda)$, $S_{\overline{x}\overline{x}\xi}(\overline{x}, \lambda)$, $S_{\overline{x}\overline{x}\mu}(\overline{x}, \lambda)$ and $S_{\overline{x}\overline{x}\zeta}(\overline{x}, \lambda)$.

At this point we must admit that our approach to this problem reaches its limit: the sum of the dimensions of the necessary variational systems simply grows too large to justify their integration, and the formulation of the third derivatives in terms of their solutions, even though it remains straightforward, becomes too tedious.

One way to surmount these difficulties is to give up Newtons' method and use a different corrector. This will be carried out in a more general framework in Section 8.5. For now let us introduce this idea when we continue a somewhat simpler codimension-two bifurcation, namely the cusp, the formulation of the degeneracy of which also requires $S_{\overline{x}\overline{x}}(\overline{x}, \lambda)$.

8.4 Continuation of Cusps

We assume that the point $y_0 = (\bar{x}_0, v_0, u_0, 0, \nu_0, \xi_0)$ is a cusp of system (7.0.1). Then $w_0^T S^0_{\bar{x}\bar{x}} v_0 v_0 = 0$ so that $S^0_{\bar{x}\bar{x}} v_0 v_0 \in \text{Range}[S^0_{\bar{x}} - \text{id}]$. For the continuation of a cusp we may therefore consider the system $g(y) = 0$ with $y := (\bar{x}, v, u, \lambda)$ and $g : \mathbb{R}^{n-1} \times \mathbb{R}^{n-1} \times \mathbb{R}^{n-1} \times \mathbb{R}^3 \to \mathbb{R}^{3n}$, and solve:

$$g(y_{N+1}) := \begin{cases} S(\bar{x}_{N+1}, \lambda_{N+1}) - \bar{x}_{N+1} & = 0 \\ S_{\bar{x}}(\bar{x}_{N+1}, \lambda_{N+1}) v_{N+1} - v_{N+1} & = 0 \\ \big(S_{\bar{x}}(\bar{x}_{N+1}, \lambda_{N+1}) - \text{id}\big) u_{N+1} - S_{\bar{x}\bar{x}}(\bar{x}_{N+1}, \lambda_{N+1})(v_{N+1})^2 & = 0 \\ v_{N+1}^T v_N - 1 & = 0 \\ v_{N+1}^T u_{N+1} & = 0 \\ (\bar{x}_{N+1} - \bar{x}_N)^T \dot{\bar{x}}_N + (\lambda_{N+1} - \lambda_N)^T \dot{\lambda}_N & \\ \quad + (v_{N+1} - v_N)^T \dot{v}_N + (u_{N+1} - u_N)^T \dot{u}_N - \delta s & = 0 \end{cases} \tag{8.4.1}$$

for the next solution $y_{N+1} = (\bar{x}_{N+1}, v_{N+1}, u_{N+1}, \lambda_{N+1})$ with $\lambda =: (\nu, \xi, \zeta) \in \mathbb{R}^3$. For more detail we refer here to [130], [157], [159], [175] and [176].

Besides $S^k_{\bar{x}\zeta}$ we now need the additional third derivatives $S^k_{\bar{x}\bar{x}\bar{x}}$, $S^k_{\bar{x}\bar{x}\xi}$, $S^k_{\bar{x}\bar{x}\nu}$ and $S^k_{\bar{x}\bar{x}\zeta}$. We have already mentioned above a formula that expresses $S^k_{\bar{x}\bar{x}\bar{x}}$ in terms of $\frac{\partial^3 \phi}{\partial x^3}(x^k, \lambda^k)$. The result is accurate in that it only contains errors introduced by the numerical integration of system (7.2.2). In very much the same way we could develop analytical expressions for the other third derivatives. Instead, we implemented here a combination of numerical differentiation and Broyden's update: only for the first iteration in the very first step from y_0 to y_1 we use numerical differentiation to approximate the terms $S^k_{\bar{x}\bar{x}\xi}$, $S^k_{\bar{x}\bar{x}\nu}$ and $S^k_{\bar{x}\bar{x}\zeta}$ and use the above formulae for all other elements of the Jacobian g^k_y. Then, while iterating towards y_1, we update g^k_y using Broyden's scheme. Suppose now y_N has been found in this way. To obtain y_{N+1} we proceed by using the secant predictor and by taking as initial approximation for g^k_y the latest update from the step towards y_N.

We emphasize that this simple strategy resulted into a surprisingly good performance along regular branches. In fact, except for saddle-nodes, we did not encounter any other bifurcations. One drawback remains though: the lack of the Jacobian matrix makes an immediate and proper analysis of degenerate cusps impossible. And we will soon see that a saddle-node along a cusp curve, i.e. a solution branch of system

(8.4.1), may lead to quite distinct phenomena.

During continuation we check for saddle-nodes (of cusps) and monitor the Floquet multipliers, the period and the norm $\|f(y_N)\|_2$. We also watch for a change in sign in the nondegeneracy condition (3.1.5).

Applied to the laser model, we again free the parameter Θ and continue the cusp CSP_2 of Fig. 7.4. Decreasing Θ to $\Theta_{11} = -22.2755248$ leads to a saddle-node with respect to Y at

$$P_9 = (Y, \Delta, \Theta) = (603.580093, 2.16107413, -22.2755248).$$

Fig. 8.14 shows the two-parameter continuation in Δ and Θ for $Y = 603.57908$, just before the two cusps coincide. We anticipate that for $Y > 603.580093$ an isolated loop of saddle-nodes will separate off such that two disconnected, smooth saddle-node branches are created. This gives us an idea how the disconnected Figs. 7.1 and 7.4 could join for increasing Θ.

We can encounter a different codimension-three bifurcation involving the coalescence of two cusps if we continue the above cusp curve beyond the saddle-node in Y. It turns out that at $\Theta_{12} = -11.139881684$ with $(Y, \Delta) = (321.598030306, 2.05900883)$ we meet a cusp in the full three-dimensional parameter space where $\dot{Y}$, $\dot{\Delta}$ and $\dot{\Theta}$ simultaneously change direction. For fixed $Y = 321.608092271$, just before the two cusps, CSP_1 and CSP_2, coalesce and annihilate themselves, the corresponding Δ, Θ parameter diagram in Fig. 8.15 justifies another name for this bifurcation, namely a "swallow tail". Note that in this figure the coordinates have been nonlinearly transformed to spread the angles at the two cusps and the "+" denotes a saddle-node. The dynamics in a neighbourhood of

$$P_{10} = (Y, \Delta, \Theta) = (321.598030306, 2.05900883, -11.139881684)$$

are straightforward to describe. We only mention the quartic saddle-node for the one-parameter problems $S(\overline{x}, \lambda) = \overline{x}$ across it. In fact, we disproved the inequation (3.1.5) in definition 3.1.0.3 for a cubic saddle-node at P_{10}, that is, we verified that:

$$w^T(S_{\overline{x}\overline{x}\overline{x}}vv + 3S_{\overline{x}\overline{x}}z)v = 0.$$

This in turn proves "beyond doubt" that our subroutine for the third derivative of the Poincaré map with respect to phase space coordinates is indeed correct. We

also remark that the two-parameter continuation in Fig. 8.15 detected even more cusps quite close to the two shown. We are therefore tempted to believe that the continuation of the swallow tail by freeing a fourth parameter will detect a quintic saddle-node, or "butterfly", where (3.1.6) is violated as well. Who knows — maybe there are even "mixed up octopusses" or a "bunch of tangled spiders" around?

Continuing the cusp curve further will provide an example of a third kind of degeneracies in cusps. At $\Theta_{13} = -12.195457673$ with the other parameters given by $(Y, \Delta) = (400.116906324, 3.405353438)$ we arrive at the coalescence of a periodic Takens–Bogdanov point with the continued cusp, see Fig. 8.16, where we plotted the nonlinearly transformed coordinates, Y and Δ, of their two-parameter continuation at fixed $\Theta = \Theta_{13}$. Note that there is a second nondegenerate periodic Takens–Bogdanov point (PTB_1) close by. However, it does not affect the local phenomenon in a neighbourhood of the degenerate cusp "DegCSP". Computing the Floquet multipliers, we see that Θ crossing $\Theta_{13} = -12.195457673$ changes the cusp in that the corresponding hysteresis point in a one-parameter continuation changes from asymptotically stable to unstable. The complete characterization of the periodic dynamics near

$$P_{11} = (Y, \Delta, \Theta) = (400.116906324, 3.405353438, -12.195457673)$$

remains an easy exercise.

We now turn to our final problem — the continuation of degenerate secondary Hopf bifurcations with nontransversal crossing of the critical pair of Floquet multipliers. In fact, the formulation of the problem makes the code simultaneously suitable for the continuation of degenerate period-doublings.

8.5 Continuation of Degenerate Period-Doublings and Degenerate Secondary Hopf Bifurcations

We suppose the point $y_0 = (\overline{x}_0, \nu_0, u_0, \beta_0, \nu_0, \xi_0)$ is a degenerate secondary Hopf bifurcation in the sense that we have a nontransversal crossing of the critical pair of Floquet multipliers $\delta_0 = e^{i\beta_0} = \mu_0 + i\,\eta_0$ on the unit circle. Then:

$$d = \|\delta\|_\xi^0 = \mu^0 \mu_\xi^0 + \eta^0 \eta_\xi^0 = 0 \tag{8.5.1}$$

for the one-parameter problem $S(\overline{x}, \nu_0, \xi) - \overline{x} = 0$. We now extend system (7.0.1) to include equation (8.5.1), where μ_ξ^0 and η_ξ^0, the solutions of the regular, linear system

(5.4.66), (5.4.67), (5.4.68) are expressed in terms of $\overline{x}_0$ and λ_0 by means of Cramer's rule. For the continuation of this degeneracy we free a third parameter ζ and consider the system $g(y) = 0$ with $y := (\overline{x}, v, u, w, z, \alpha, \omega, \beta, \lambda)$, $g : \mathbb{R}^{n-1} \times \mathbb{R}^{n-1} \times \mathbb{R}^{n-1} \times \mathbb{R}^{n-1} \times \mathbb{R}^{n-1} \times \mathbb{R} \times \mathbb{R} \times \mathbb{R} \times \mathbb{R}^3 \to \mathbb{R}^{5n+1}$, and solve successively: $g(y_{N+1}) :=$

$$
\left\{
\begin{array}{ll}
S(\overline{x}_{N+1}, \lambda_{N+1}) - \overline{x}_{N+1} & = 0 \\
S_{\overline{x}}(\overline{x}_{N+1}, \lambda_{N+1})(v_{N+1} + i\,u_{N+1}) - e^{i\beta_{N+1}}(v_{N+1} + i\,u_{N+1}) & \\
-\,(\alpha_{N+1} + i\,\omega_{N+1})(w_N + i\,z_N) & = 0 \\
(w_{N+1} + i\,z_{N+1})^* S_{\overline{x}}(\overline{x}_{N+1}, \lambda_{N+1}) - (w_{N+1} + i\,z_{N+1})^* e^{i\beta_{N+1}} & = 0 \\
(v_{N+1} + i\,u_{N+1})^*(v_N + i\,u_N) - 1 & = 0 \\
(w_{N+1} + i\,z_{N+1})^*(w_N + i\,z_N) - 1 & = 0 \\
\cos(\beta_{N+1}) \det \begin{pmatrix} -z^T X u - w^T X v & -z^T v + w^T u \\ z^T X v - w^T X u & -z^T u - w^T v \end{pmatrix}_{N+1} & \\
+\sin(\beta_{N+1}) \det \begin{pmatrix} -z^T u - w^T v & -z^T X u - w^T X v \\ z^T v - w^T u & z^T X v - w^T X u \end{pmatrix}_{N+1} & = 0 \\
(\overline{x}_{N+1} - \overline{x}_N)^T \dot{\overline{x}}_N + +(v_{N+1} - v_N)^T \dot{v}_N + (u_{N+1} - u_N)^T \dot{u}_N & \\
+\,(w_{N+1} - w_N)^T \dot{w}_N + (z_{N+1} - z_N)^T \dot{z}_N + (\alpha_{N+1} - \alpha_N)^T \dot{\alpha}_N & \\
+\,(\omega_{N+1} - \omega_N)^T \dot{\omega}_N + (\beta_{N+1} - \beta_N)^T \dot{\beta}_N + (\lambda_{N+1} - \lambda_N)^T \dot{\lambda}_N - \delta s & = 0
\end{array}
\right. \tag{8.5.2}
$$

for $y_{N+1} = (\overline{x}_{N+1}, v_{N+1}, u_{N+1}, w_{N+1}, z_{N+1}, \alpha_{N+1}, \omega_{N+1}, \beta_{N+1}, \lambda_{N+1})$, $N = 1, 2, \ldots$. Here the matrix X is given by $X := -S^{N+1}_{\overline{x}\overline{x}}(S^{N+1}_{\overline{x}} - \mathrm{id})^{-1} S^{N+1}_{\xi} + S^{N+1}_{\overline{x}\xi}$, $\lambda = (\nu, \xi, \zeta) \in \mathbb{R}^3$, and the subscripts $N+1$ in the sixth equation mean evaluation of v, u, w, z at v_{N+1}, u_{N+1}, w_{N+1}, z_{N+1}. Note also that we introduced the "dummy" variables $(\alpha, \omega) \in \mathbb{R}^2$. It is straightforward to show that any solution of (8.5.2) satisfies necessarily $(\alpha, \omega) = (0, 0)$.

A closer inspection of this system reveals further that it is also solved by degenerate period-doublings with a nontransversal crossing of the critical -1 Floquet multiplier. This holds since $\beta_{N+1} = \pi$ in the additional equation gives: $\sin(\beta_{N+1}) = 0$ and $u_N = v_N$, $w_N = z_N$ leads to:

$$
\det \begin{pmatrix} -z^T_{N+1} X u_{N+1} - w^T_{N+1} X v_{N+1} & -z^T_{N+1} v_{N+1} + w^T_{N+1} u_{N+1} \\ z^T_{N+1} X v_{N+1} - w^T_{N+1} X u_{N+1} & -z^T_{N+1} u_{N+1} - w^T_{N+1} v_{N+1} \end{pmatrix} = 0 \tag{8.5.3}
$$

by 5.3.3.1. The scheme cannot work though if the starting point y_0 is a transcritical bifurcation point or isola formation point since the Floquet multiplier $+1$ makes $(S^1_{\overline{x}} - \mathrm{id})$ singular.

Similarly to the continuation of cusps, we now need the additional third derivatives $S^k_{\bar{x}\bar{x}\bar{x}}$, $S^k_{\bar{x}\bar{x}\xi}$, $S^k_{\bar{x}\bar{x}\nu}$, $S^k_{\bar{x}\bar{x}\zeta}$, $S^k_{\bar{x}\xi\xi}$, $S^k_{\bar{x}\xi\nu}$ and $S^k_{\bar{x}\xi\zeta}$. These quantities are approximated by using the idea that is implemented in the continuation of cusps. That is, only in the first iteration in the very first step from y_0 to y_1 do we compute $S^k_{\bar{x}\bar{x}\bar{x}}$ accurately and use numerical differentiation to approximate the other third derivatives. Then, while iterating towards y_1, we update the Jacobian g^k_y using Broyden's scheme, and from y_N we proceed towards y_{N+1} by taking as initial approximation for g^k_y the latest updated one from the step towards y_N. Again we would like to report unexpectedly good results along regular branches. Unfortunately though, automatic branch switching turns out to be quite difficult — not surprisingly, as we do not have the Jacobian matrix at possible bifurcation points y^* (and we do expect strict bifurcations if β_N crosses 0 mod 2π and π mod 2π). This fact is certainly a major drawback of our formulation of the problem in system (8.5.2) and should provide a good starting point for further improvements of the code.

During continuation we watch for saddle-nodes (of degenerate secondary Hopf bifurcations) and monitor the Floquet multipliers, the period and the norm $\|f(y_N)\|_2$. Also, if $k_\xi = 0$, then we compute the crossing speed with respect to ν, k_ν, and vice versa, if $k_\nu = 0$, we compute k_ξ, see (7.2.3) and (7.2.4). Generically, the second of these quantities will be nonzero and we may then opt to compute the direction and stability of the emanating branches of doubled orbits, respectively invariant curves, along this parameter. Although not as much as the evaluation of the discrimant (5.4.57), this calculation immensely increases the computational effort. However, we may further characterize the degeneracy according to Figs. 7c to 7f in Chapter 7.

Applied to the laser model, we again free the parameter Θ and first follow the period-doubling loop of Fig. 7.1 with Θ decreasing from -22 by continuing DPDB_2. We know already that it somehow disappears at a value $\Theta_{14} > \Theta_7 = -33.878828571$ since at Θ_7 the surrounding saddle-node loop bifurcates out of Θ space. Indeed, we do not have to wait too long: at $\Theta_{14} \approx -23.5232$ with $(Y, \Delta) \approx (848.2746, 12.0096)$ the curve bends around in a saddle-node at a (local) minimum in Θ (see its projection into the Y, Θ parameter space in Fig. 8.17). Moreover, a further continuation, now with increasing Θ, bends almost immediately around in a saddle-node with respect

to Y and eventually recovers DPDB_1 in Fig. 7.1. Hence,

$$P_{12} = (Y, \Delta, \Theta) \approx (848.2746, 12.0096, -23.5232)$$

can be regarded as an isola formation point for closed loops of period-doublings as the one in Fig. 7.1. A slice across the three-dimensional Y, Δ, Θ parameter domain of existence of the period-doublings at $\Theta = -23.51179719$, shortly before the loop degenerates to a single point, is presented in Fig. 8.18.

We close this last section of the thesis with our last example concerning the existence of a loop of secondary Hopf bifurcations by continuing DHF2b, see Fig. 8.8. For $\Theta = \Theta_4 = -33.86918$, the loop splits and moves inside the surrounding saddle-node loop. Hence, a lower bound for its existence is provided by the lower bound for the existence of the saddle-node loop, namely $\Theta_7 = -33.878828571$. Our continuation of this point reveals a saddle-node with respect to Θ at $\Theta_{15} \approx -33.87543762$ in between Θ_4 and Θ_7 with $(Y, \Delta) \approx (1588.2728965, 20.337674809)$ almost immediately followed by a saddle-node in Y. Fig. 8.19 shows the projection of this continuation into Y, Θ parameter space. In fact, that these values are quite accurat, can be seen in Fig. 8.20 which shows the Y, Δ parameter continuation (7.0.1) for fixed $\Theta = \Theta_{15}$. A tiny loop of secondary Hopf bifurcations, shortly before degenerating to a point, still exists (inside the surrounding saddle-nodes). These secondary Hopf bifurcations were found to be supercritical. Since the periodic orbits with (Y, Δ) chosen from the inside of that loop are asymptotically stable, the invariant curves bifurcate to the outside of it. Of course, tracing this Hopf loop using system (7.0.1) was quite challenging, as every point on it is almost singular. In this respect it resembles example 3.1.0.5.

At last we mention, that the continuation of a degenerate period-doubling point with $k_\Delta = 0$ along the wiggled part in the lower left corner of Fig. 7.4 could lead to a higher degeneracy with $k_{\Delta\Delta} = 0$, i.e. annihilation of two saddle-nodes along a period-doubling branch. We conjecture then, that the one-parameter problem $S(\overline{x}, \Delta) - \overline{x} = 0$ undergoes a period-doubling such that the doubled orbits enclose a cusp. However, we did not pursue this problem any further.

Figures

For easy reference, this chapter contains Figs. 6.1 to 6.8 of Chapter 6, Figs. 7.1 to 7.25 of Chapter 7, and Figs. 8.1 to 8.20 of Chapter 8.

We recall that Fig. 5a will be found in Chapter 5 and Figs. 7a to 7f will be found in Chapter 7.

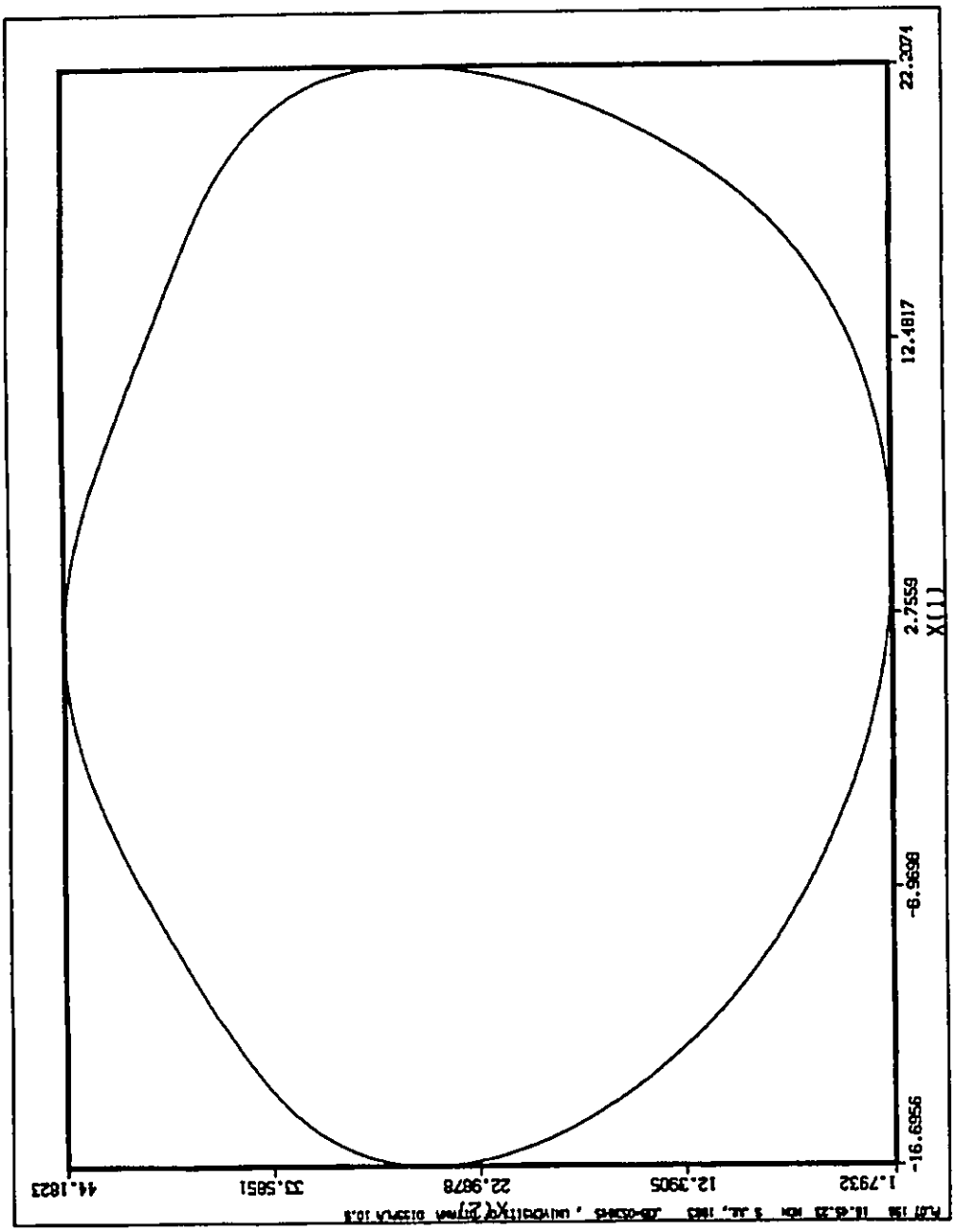

Figure 6.1: The projection of the periodic orbit number 1a in Table 6.1 into the x_1, x_2 plane shows a single loop. We may call it a simple periodic orbit.

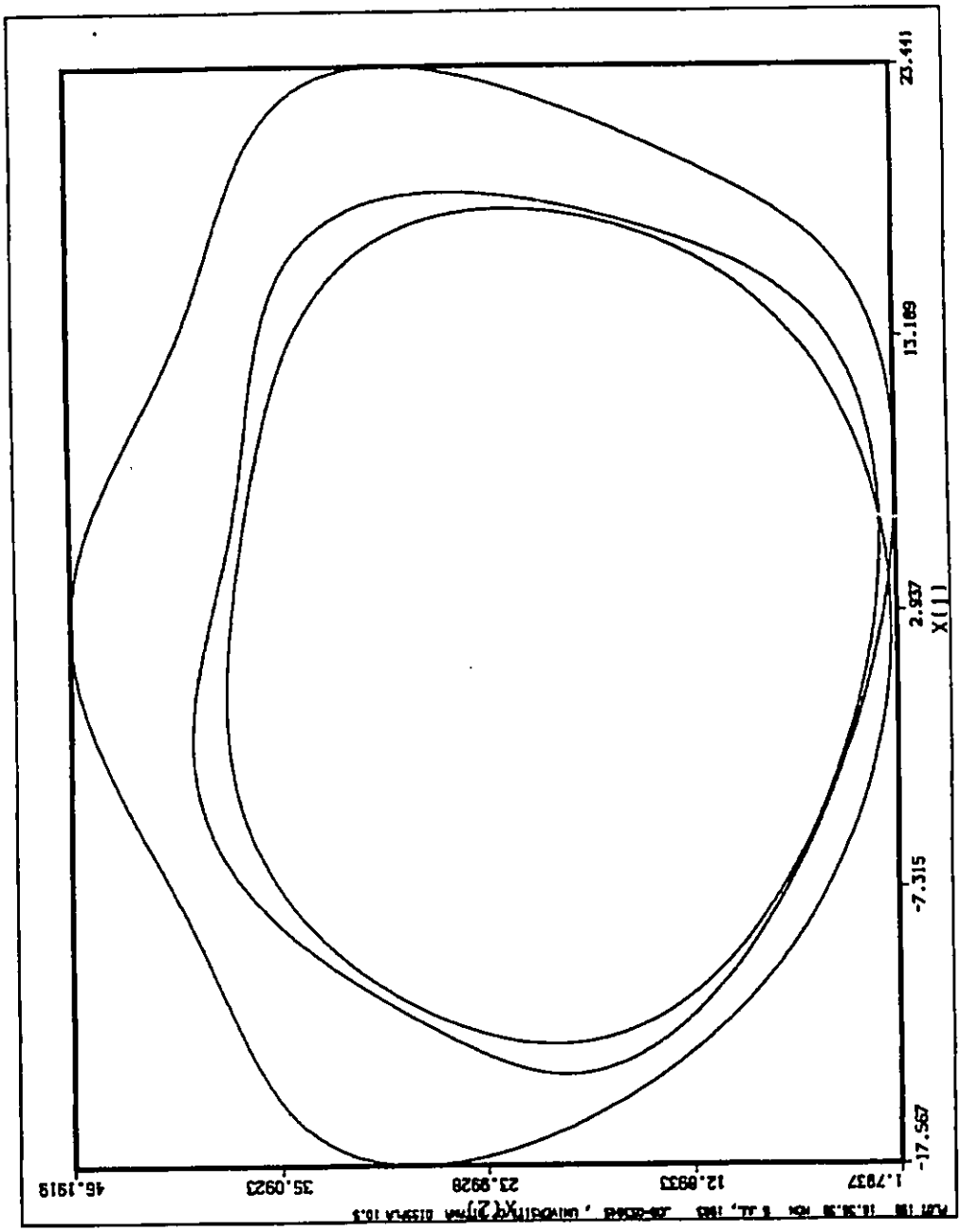

Figure 6.2: The projection of the periodic orbit number 5a in Table 6.1 into the x_1, x_2 plane shows three loops. We may call it a tripled periodic orbit.

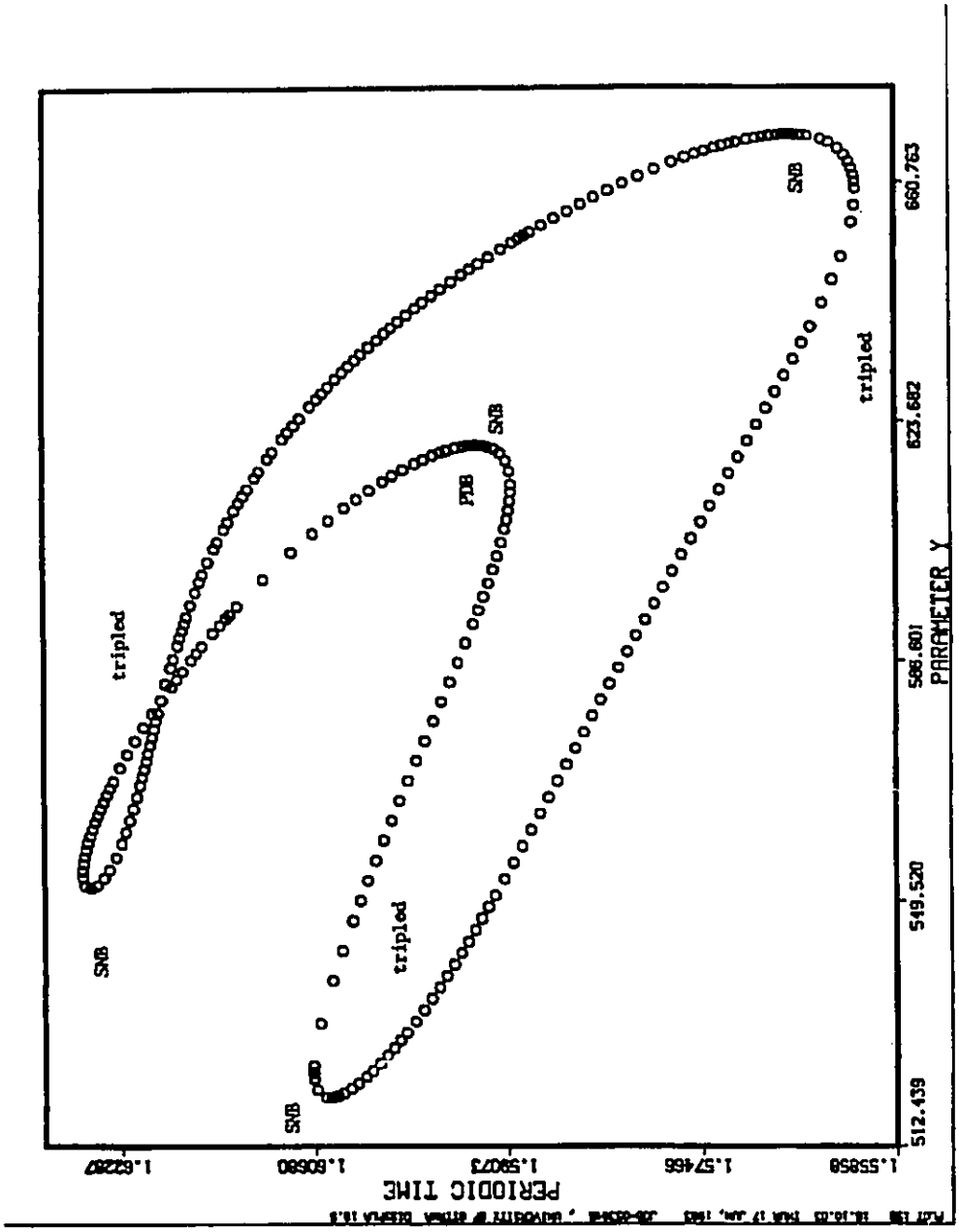

Figure 6.3: The projection of the period versus Y for the tripled orbit 2c in Table 6.3. The orbit remains throughout unstable except for a tiny interval about $Y = 620.02$.

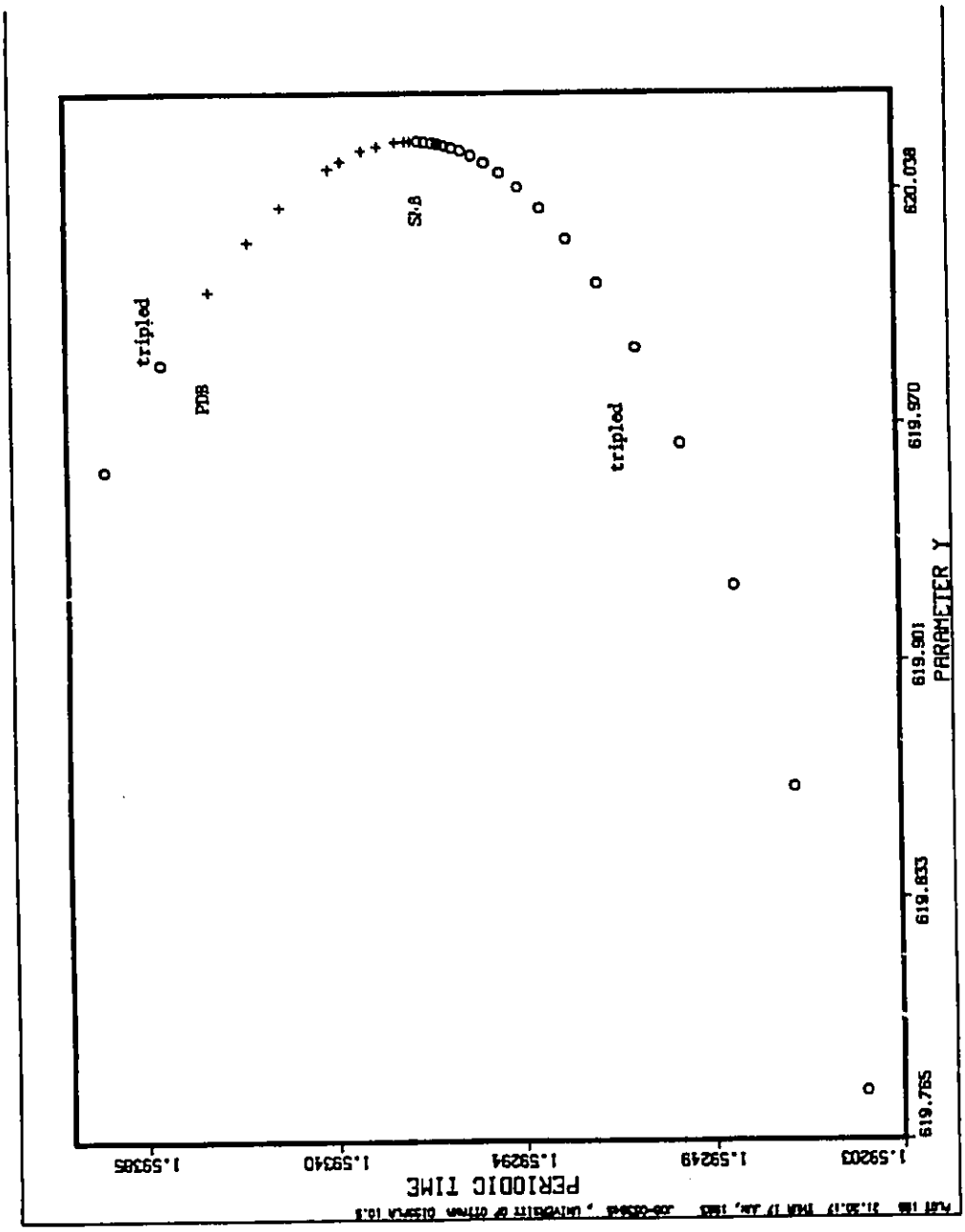

Figure 6.4: Enlargement of figure 6.3 about $(Y, \text{period}) = (620.02, 1.5936218)$. A small Y interval of stable tripled periodic orbits becomes visible.

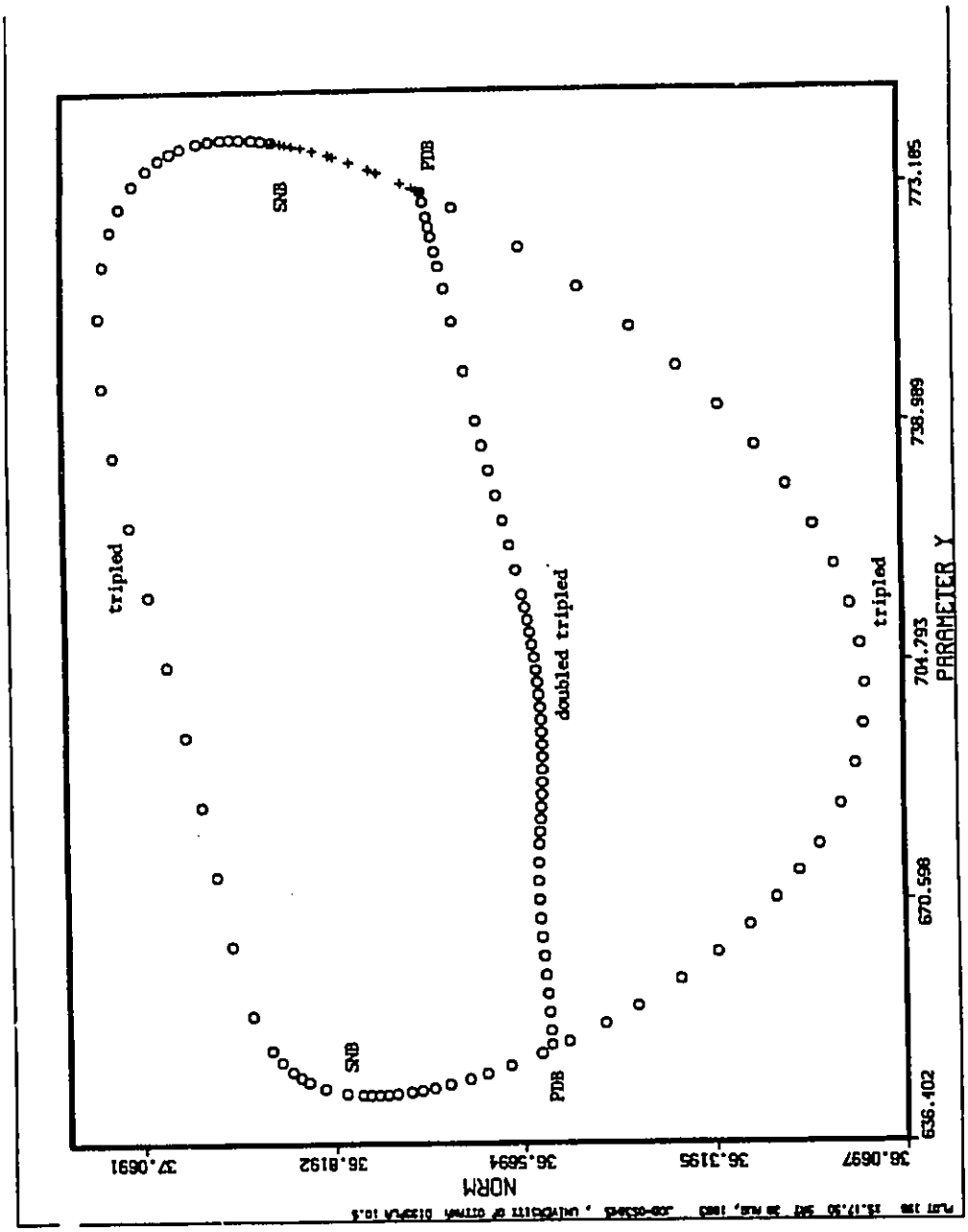

Figure 6.5: The projection of the norm versus Y for the tripled periodic orbit 4c in Table 6.3. An "observable" interval of stable tripled periodic orbits exists around $Y = 775$.

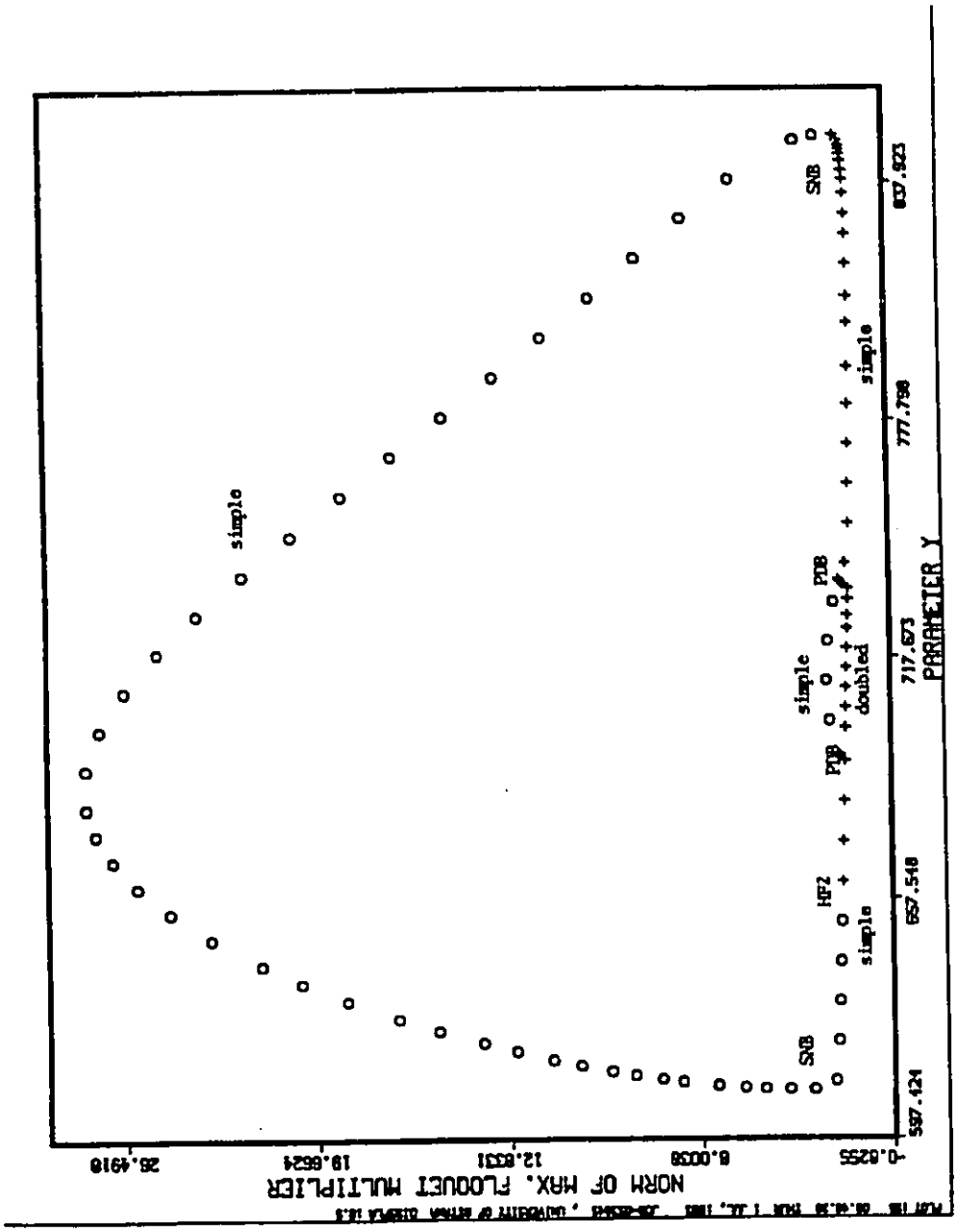

Figure 6.6: The projection of the norm of the maximal (squared) Floquet multiplier versus Y of the periodic orbit number 3b in Table 6.2 (and in Fig. 3 of reference [55]). There are two supercritical period-doubling bifurcations such that the two "forks" open towards each other and a stable, doubled periodic orbit is enclosed.

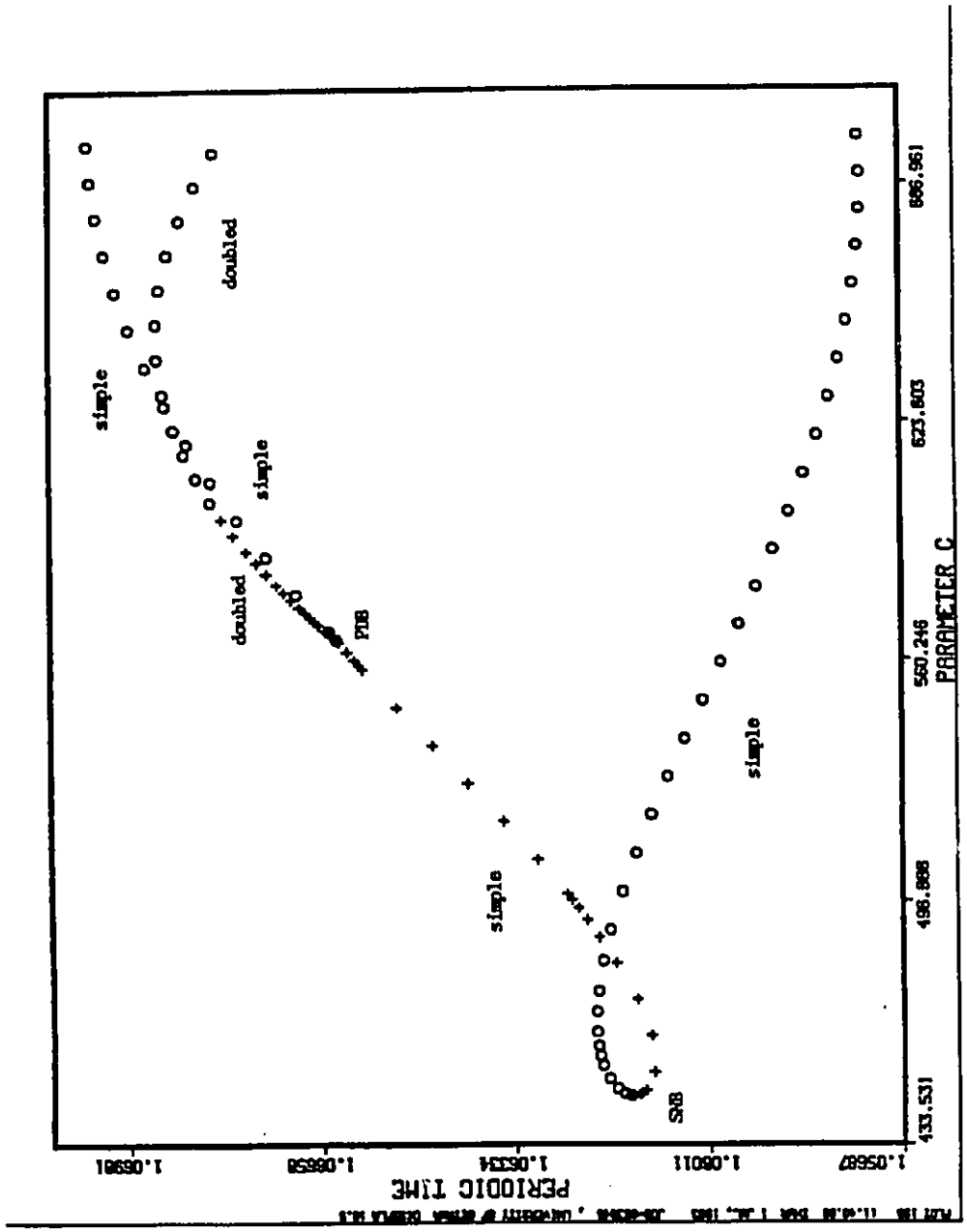

Figure 6.7: The projection of the (doubled) period versus c for the stable orbit 3b in Table 6.2 after is has been continued to $Y = 810$ in Fig. 6.6. The other parameters remained at $\Delta = 7.5$ and $\Theta = -22$. The two crossings of the simple, respectively doubled and simple, periodic orbits reflect coexistence of these solutions.

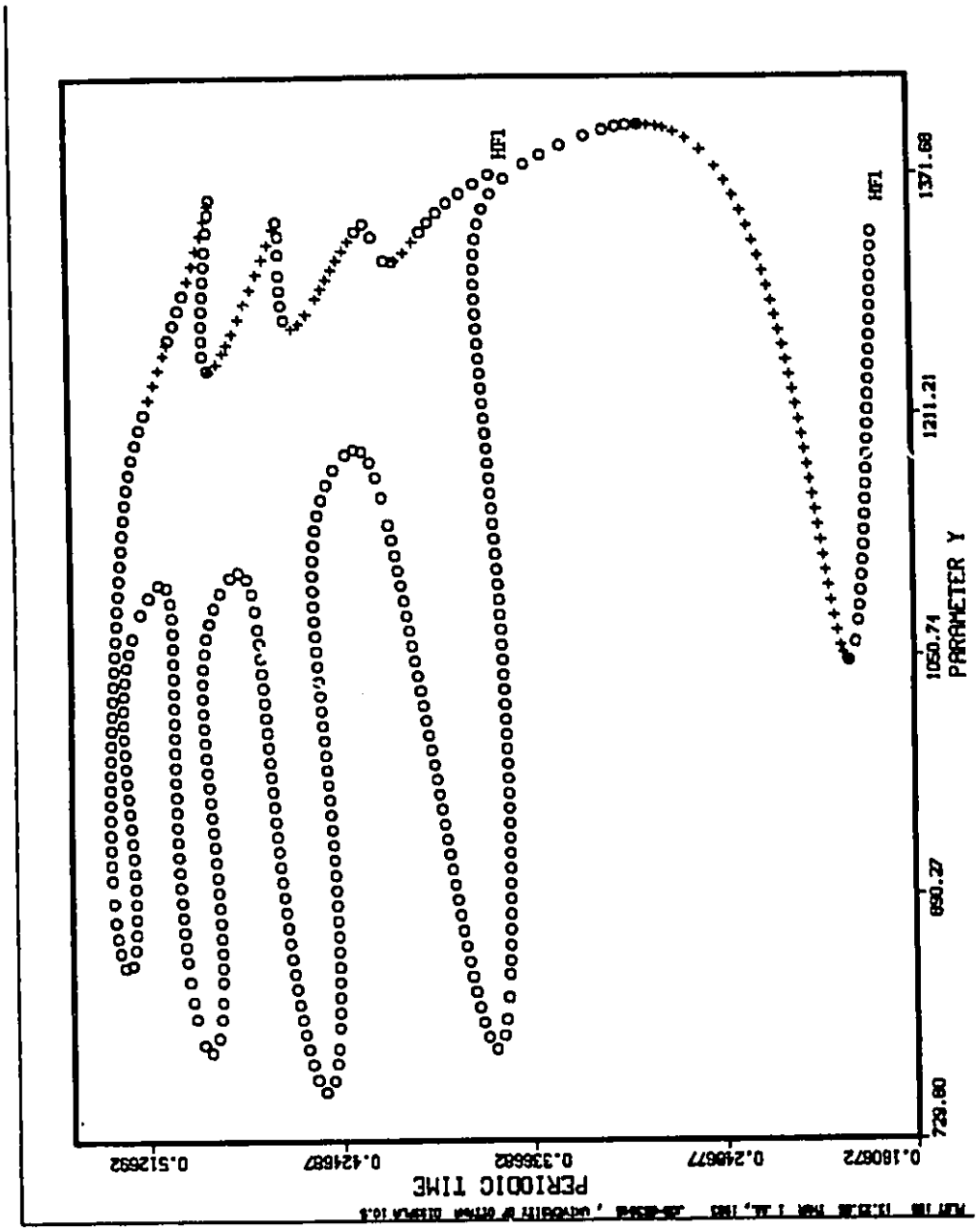

Figure 6.8: Period versus Y for the periodic orbit 3b in Table 6.2 after it has first been continued to $Y = 810$ in Fig. 6.6 and subsequently to $c = 1472$ in Fig. 6.7. The other parameters remained at $\Delta = 7.5$ and $\Theta = -22$. Several period-doublings and secondary Hopf bifurcations along this branch have not been indicated. In contrary to the closed loop in Fig. 6.6, where $c = 500$, the corresponding branch in Fig. 6.8, where $c = 1472$, terminates at both end points in Hopf bifurcations.

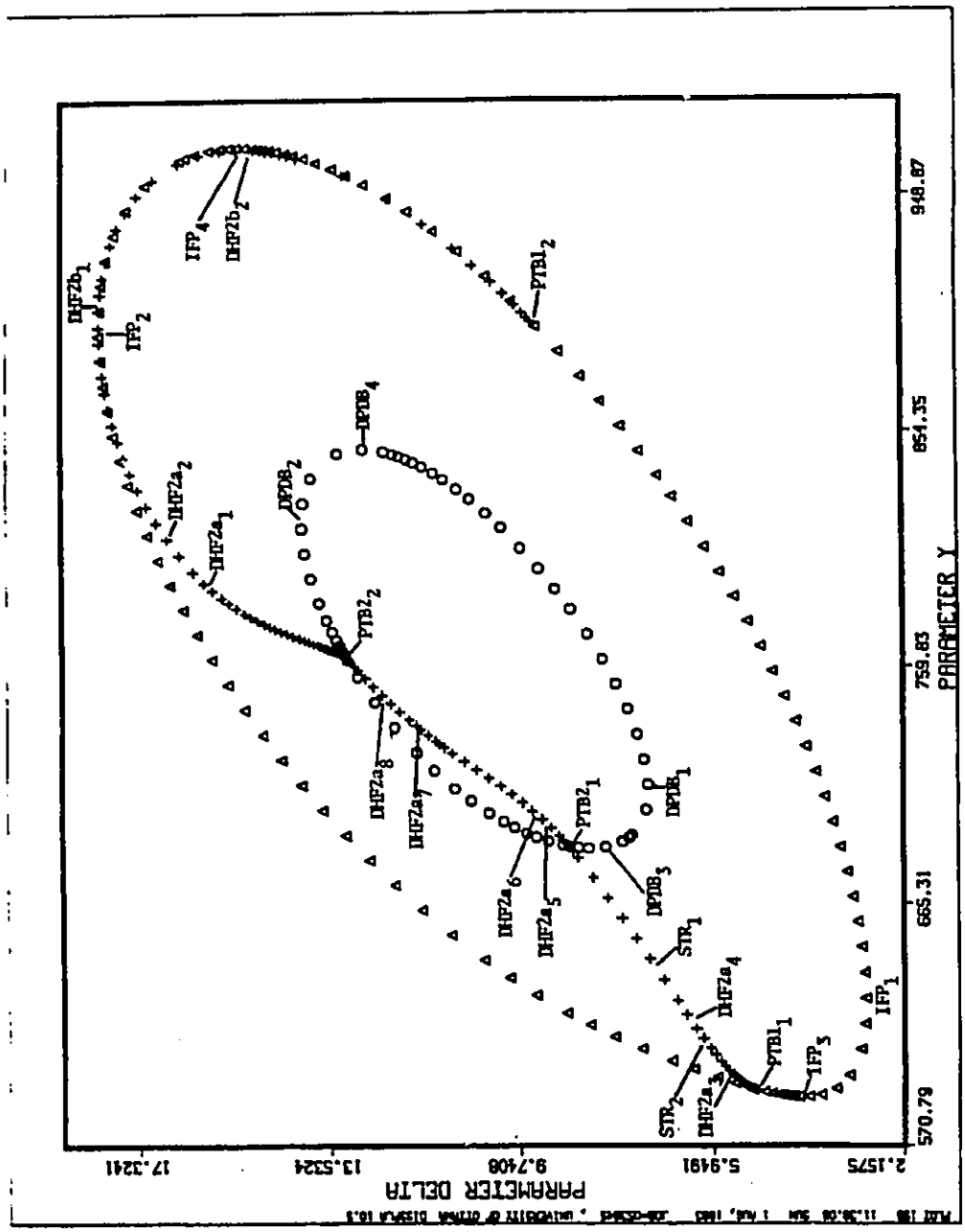

Figure 7.1: The projection of the continuation of the Hopf bifurcation in Fig. 6.6 into the Y, Δ parameter plane, $\Theta = -22$. A closed loop of period-doubling bifurcations is surrounded by a closed loop of saddle-nodes. They are connected by three secondary Hopf branches where the one inside the period-doublings corresponds to doubled periodic orbits.

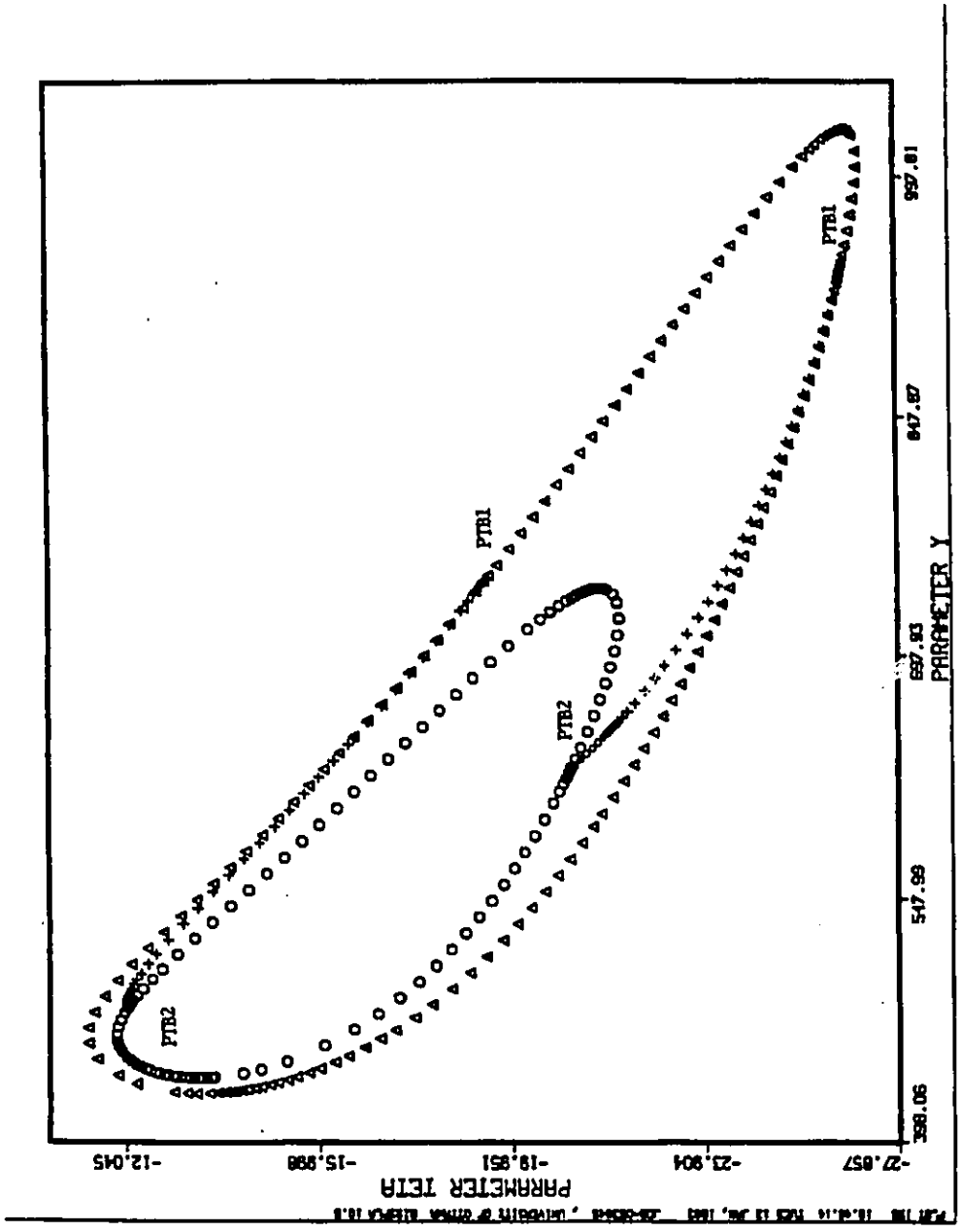

Figure 7.2: Same as in Fig. 7.1 with Θ variable and instead Δ fixed at $= 7.5$.

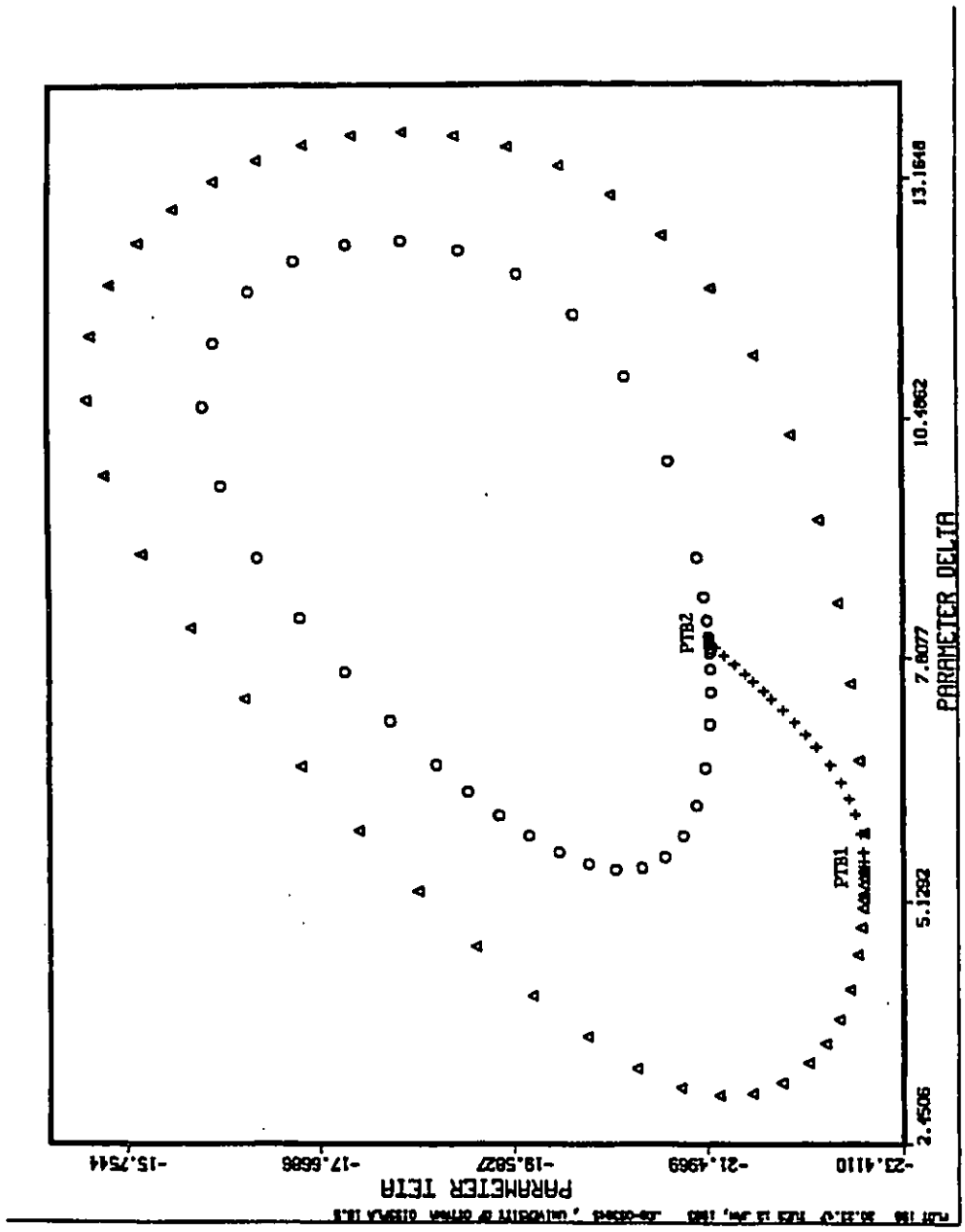

Figure 7.3: Same as in Figs. 7.1 and 7.2 with Θ and Δ variable and instead Y fixed at 653.1234188.

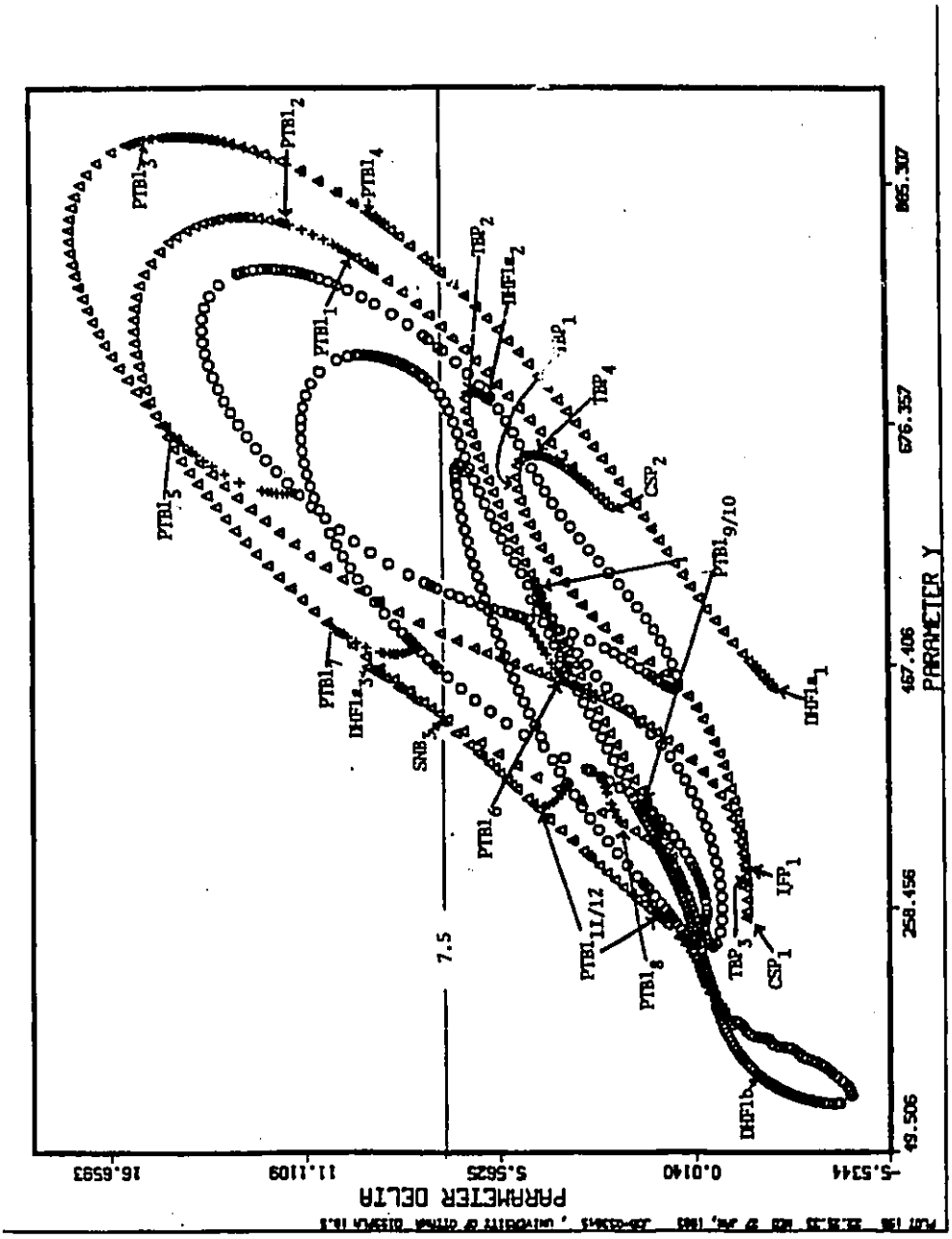

Figure 7.4: The projection of the continuation of the saddle-node SNB_1 in Fig. 7.7. In contrary to Figs. 7.1, 7.2 and 7.3, we now discover additionally the cusps CSP_i and branches terminating in the degenerate Hopf bifurcations DHF1b and $DHF1a_i$.

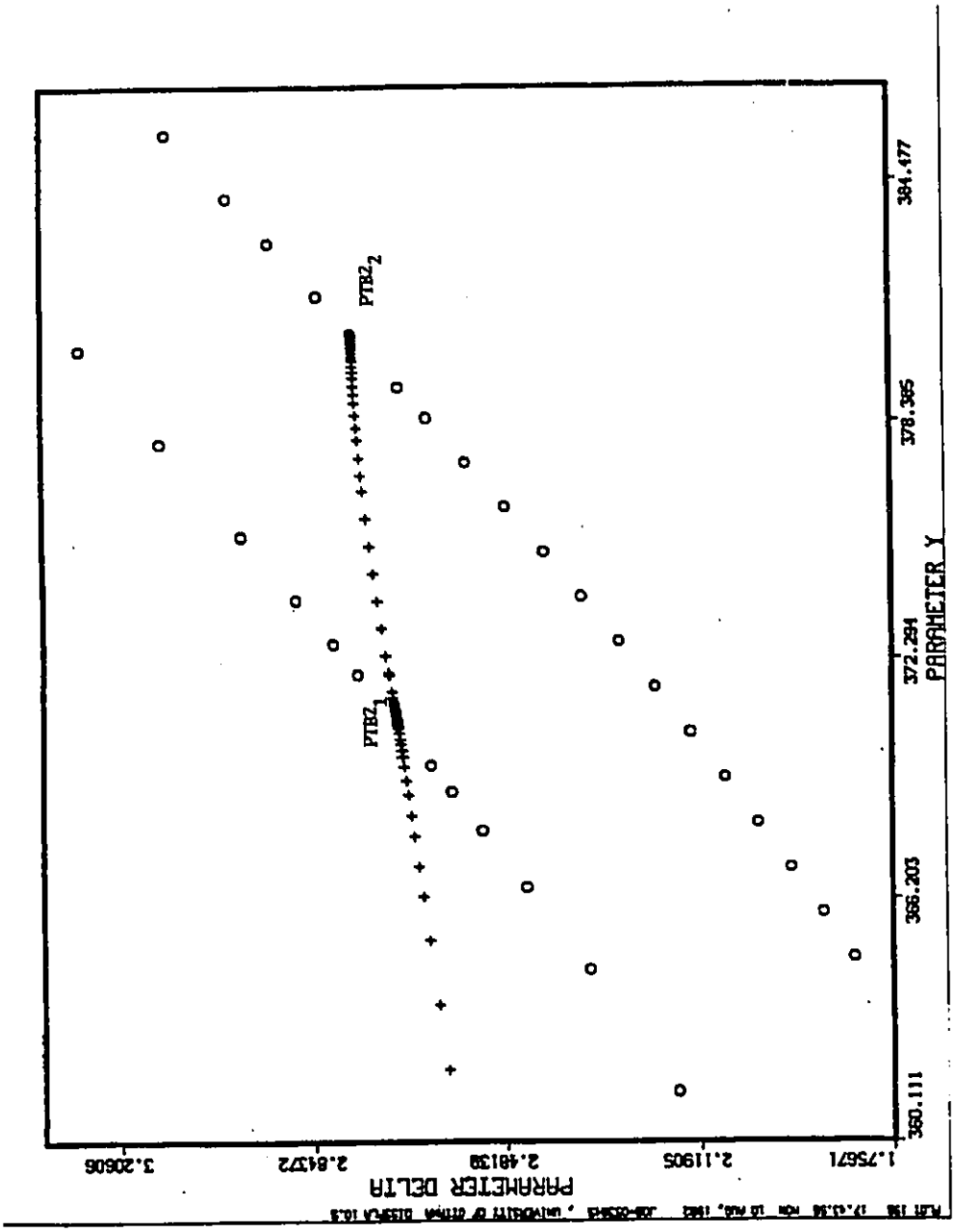

Figure 7.5: Enlargement of Fig. 7.4. The period-doubling branch across $PTB2_1$ correspond to simple periodic orbits and the one across $PTB2_2$ to doubled periodic orbits. To the right of the latter branch we find quadrupled periodic orbits (and, in fact, a period-doubling scenario). The secondary Hopf branch of doubled periodic orbits apparently does not enclose a 0 angle with the period-doubling branch across $PTB2_1$. Moreover, it apparently continues smoothly into the secondary Hopf branch of simple periodic orbits.

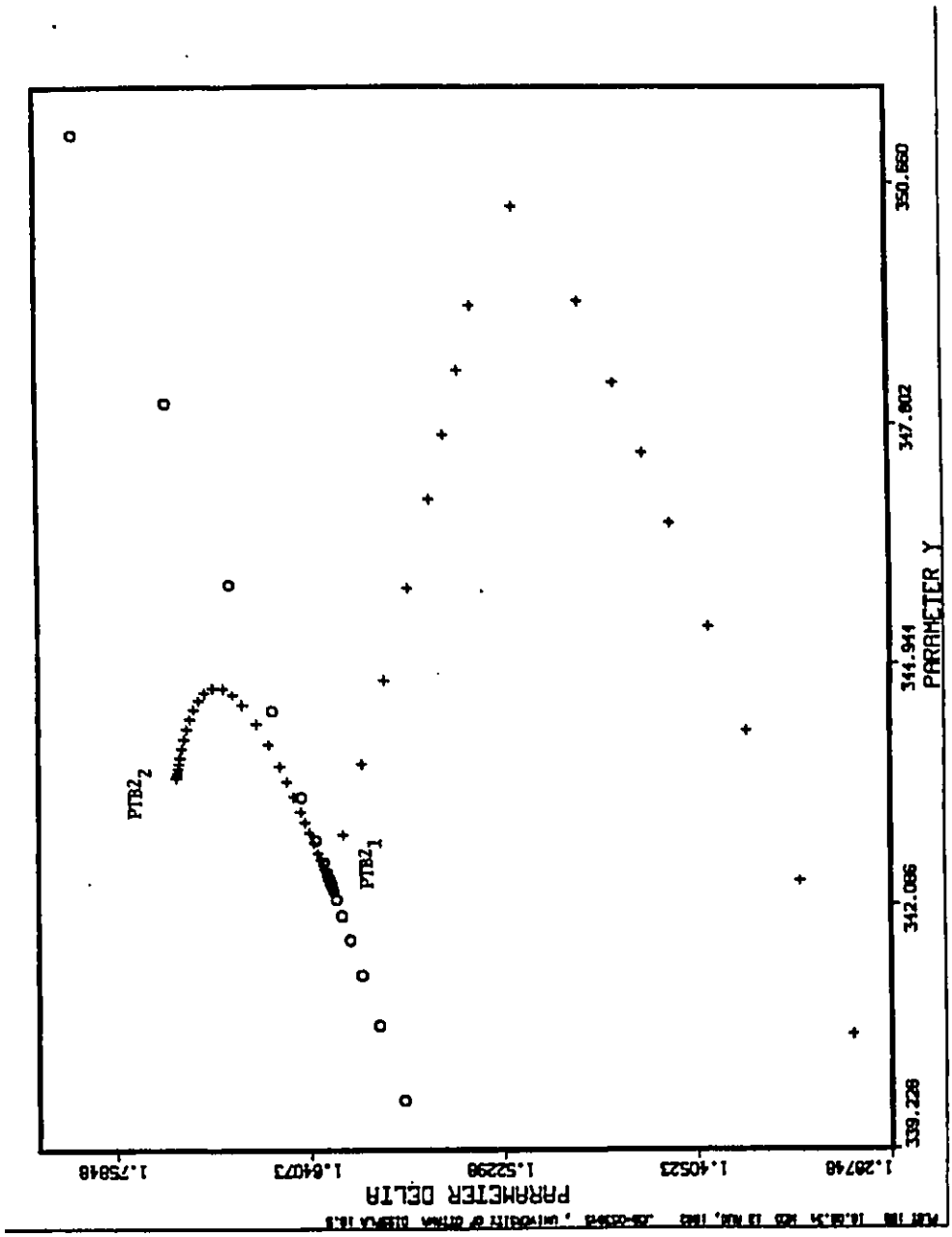

Figure 7.6: Enlargement of Fig. 7.4. The secondary Hopf branch of doubled periodic orbits, stretched between $PTB2_1$ and $PTB2_2$, apparently does enclose a 0 angle with the period-doubling branch. Moreover, it apparently does not continue smoothly into the secondary Hopf branch of simple periodic orbits.

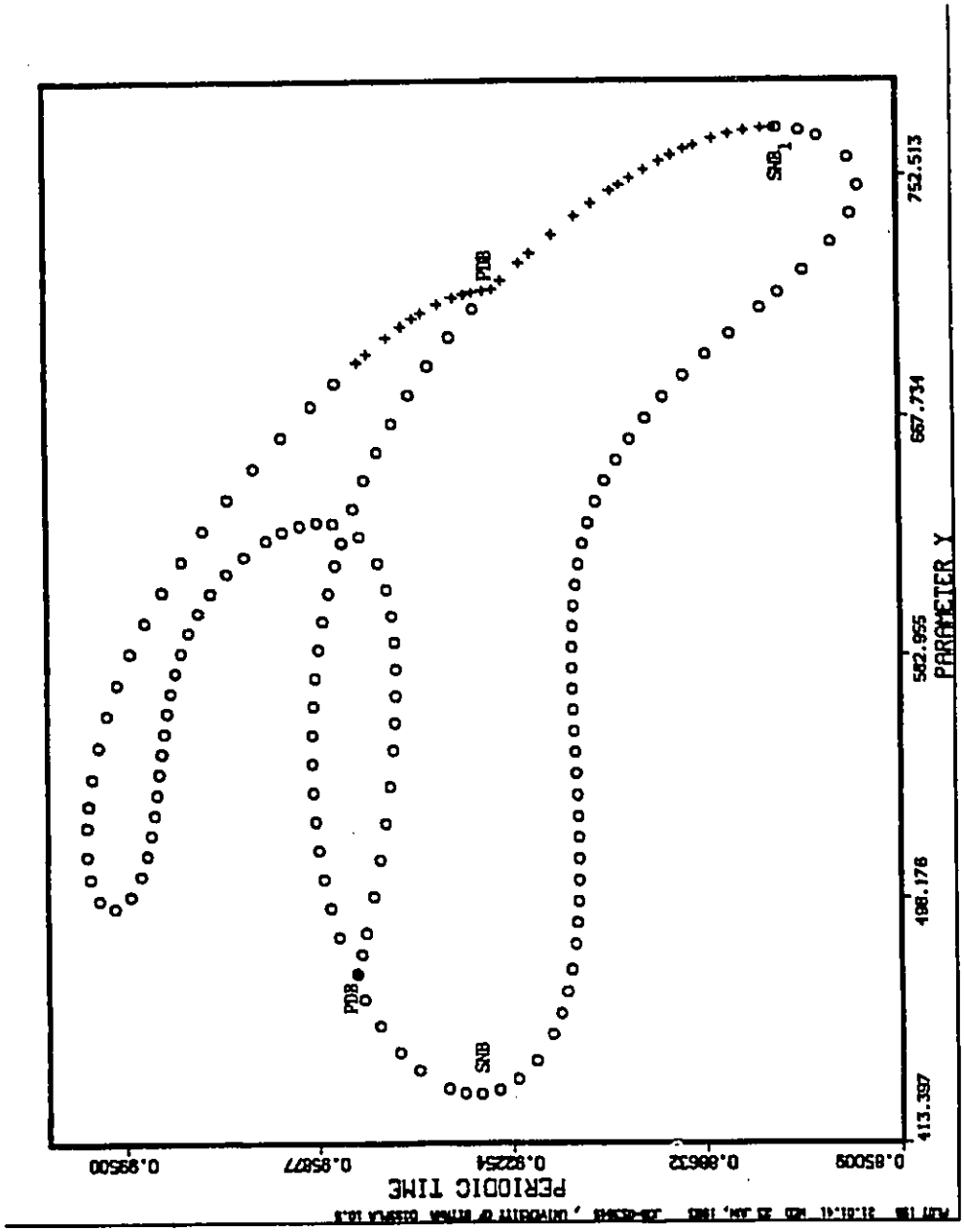

Figure 7.7: The projection of the (doubled) period versus Y for another periodic orbit, coexisting with Fig. 6.6. Starting from the right period-doublings at $Y_1 = 712.1664308$ we computed successive further doublings at $Y_2 = 685.678709$, $Y_3 = 682.70934$, $Y_4 = 682.229624$ and $Y_5 = 682.133321$. The resulting ratios seem to approach Feigenbaum's number and suggest a period-doubling cascade.

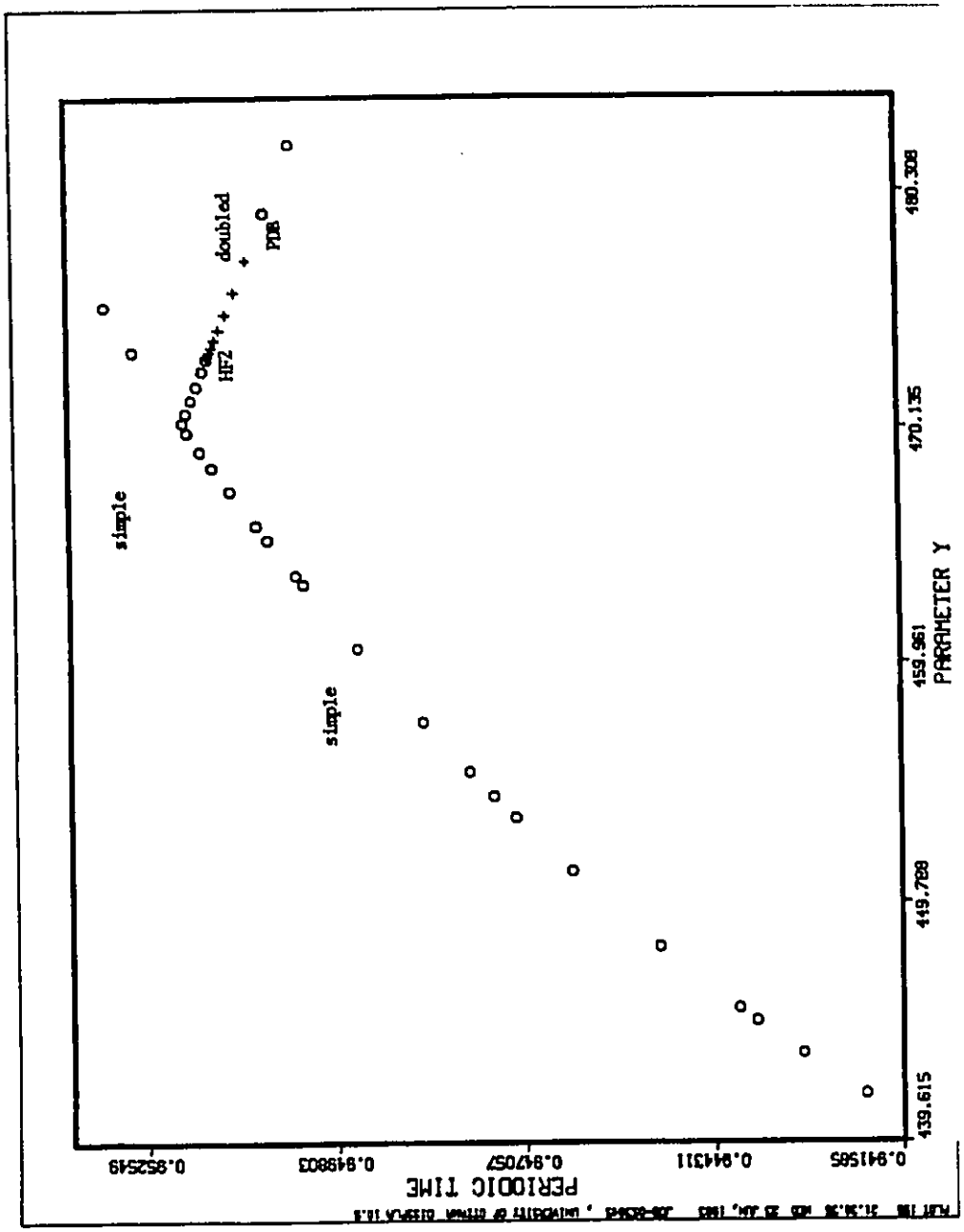

Figure 7.8: Enlargement of Fig. 7.7. At the period-doubling we confirmed some further doublings of another period-doubling scenario. In contrary to the one in Fig. 7.7 though, this time it develops with increasing Y.

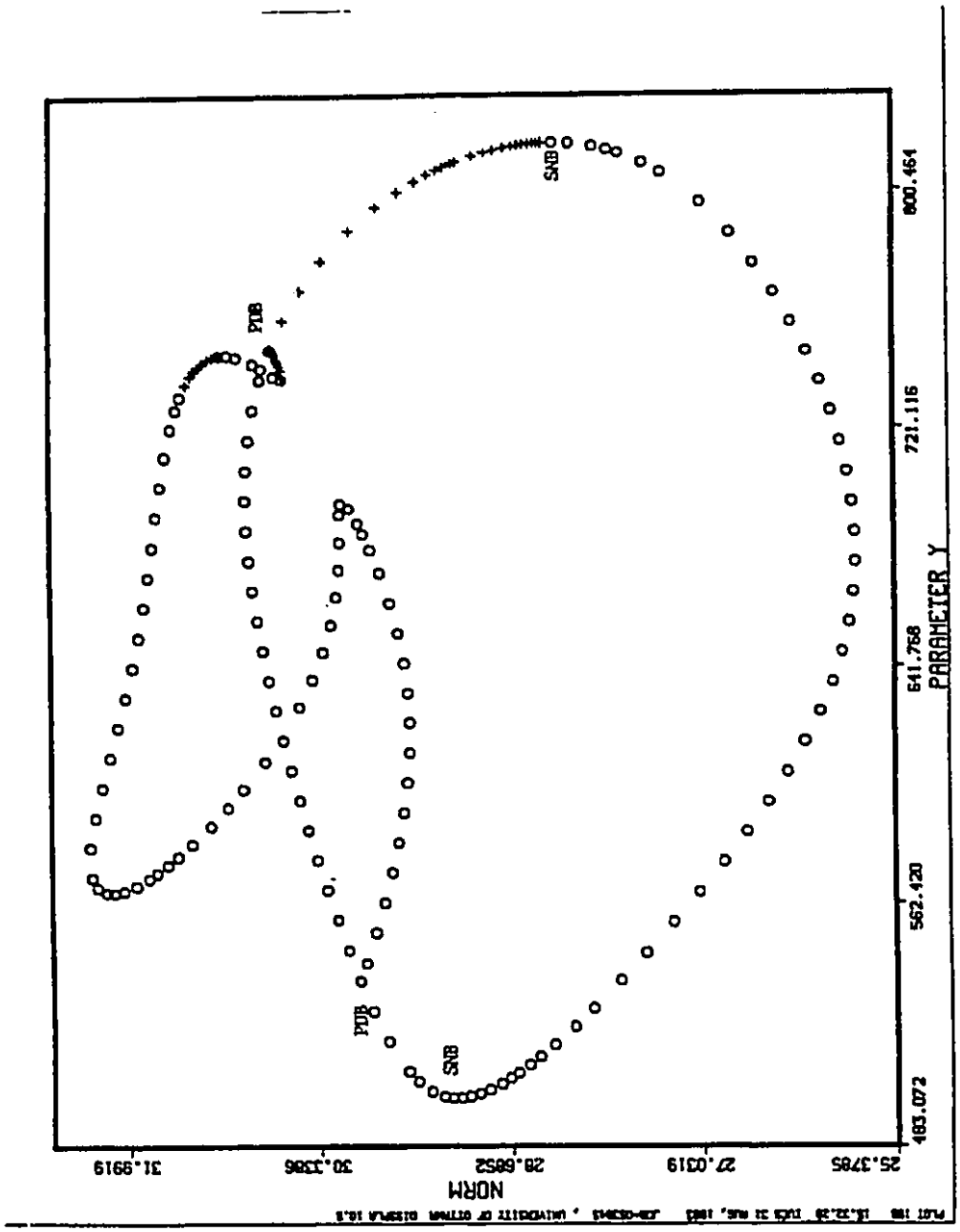

Figure 7.9: The projection of the norm versus Y for another periodic orbit, coexisting with Figs. 6.6 and 7.7. For $Y \in (737.47, 747)$, this figure reveals two coexisting stable doubled periodic orbits. Moreover, another period-doubling cascade seems to bifurcate off from the "upper" branch. Using the Feigenbaum ratios we extrapolated and found $Y_\infty \approx 729.1$. In fact, the periodic orbit 3c in Table 6.3 represents its stable doubled quadrupled element.

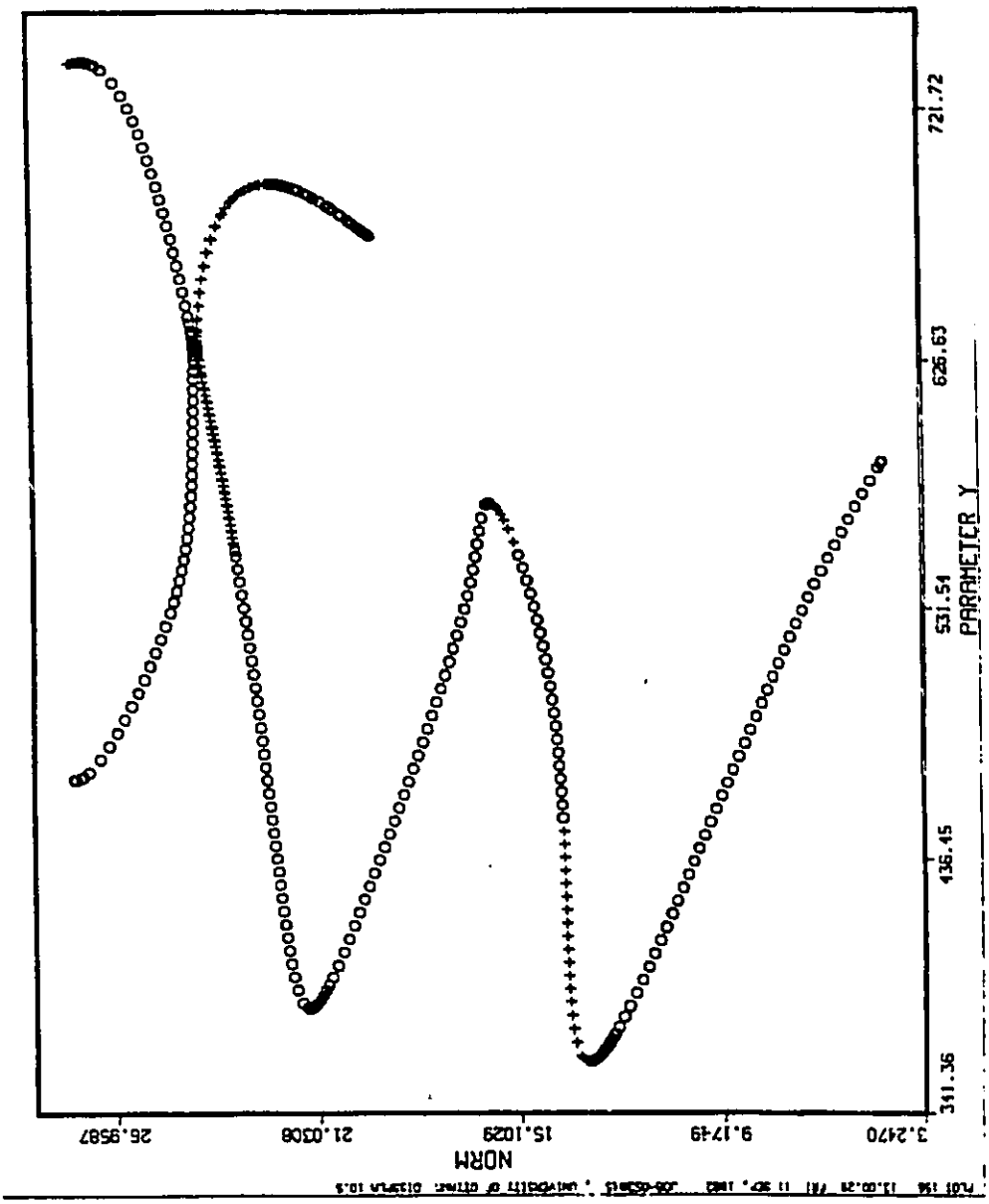

Figure 7.10: The branches in Figs. 7.7 and 7.9 touch in a transcritical bifurcation at $(Y, \Delta) \approx (635.77, 5.07)$ and subsequently, i.e. for smaller Δ, form a single branch, see the enlargement in Fig. 7.11. However, the branch in Fig. 7.7 has already before, i.e. $5.07 < \Delta < 7.5$, attached to a fourth branch of periodic orbits which introduced Hopf bifurcations at its end points. A careful interpretation of a cross-section of Fig. 7.4 in a neighbourhood of $\Delta = 5.07$ explains the details.

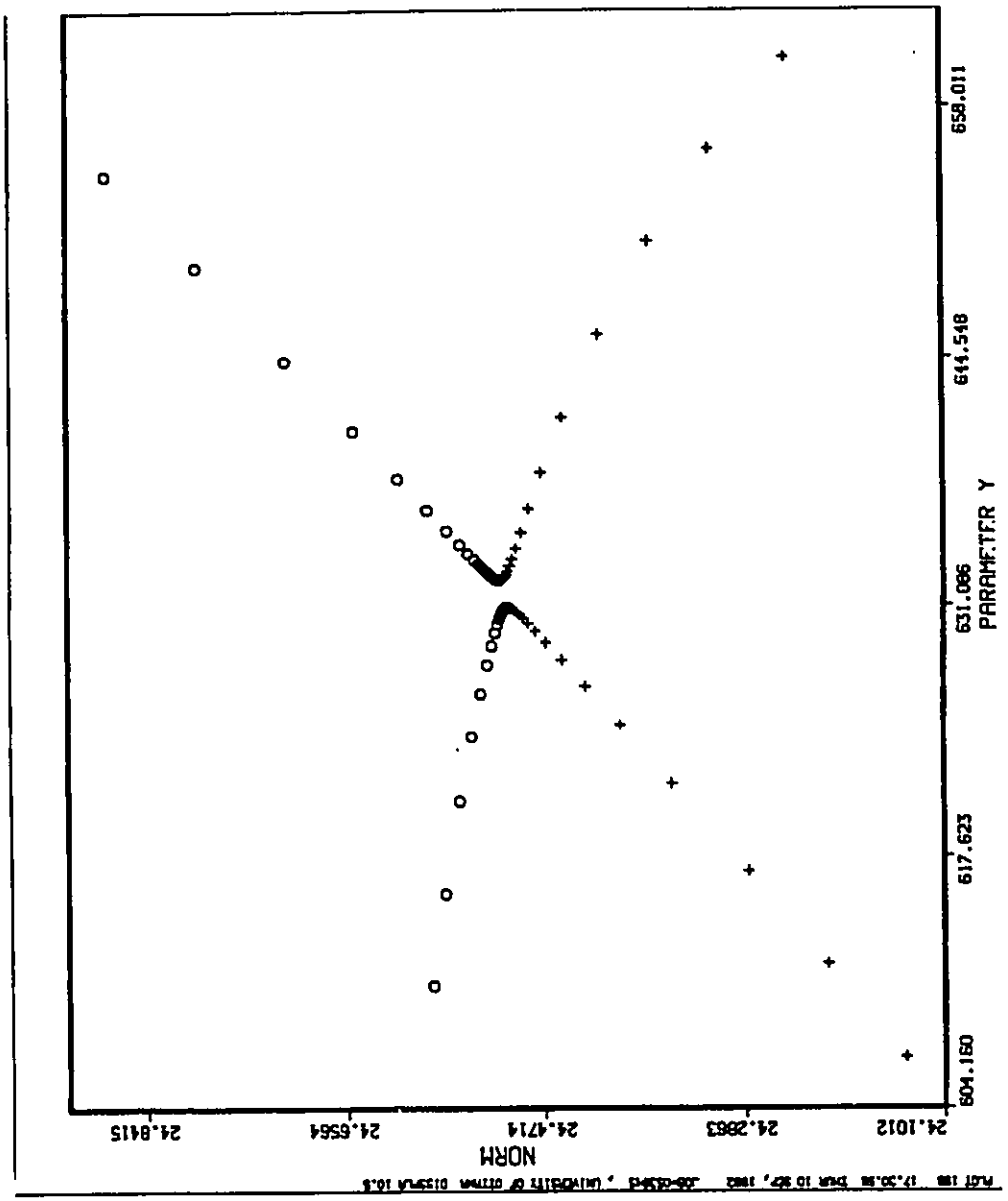

Figure 7.11: $\Delta = 5.05$. After the branches in Figs. 7.7 and 7.9 touched in a transcritical bifurcation with $\Delta \approx 5.07$, they now form a single branch by introducing two more saddle-nodes into Fig. 7.4.

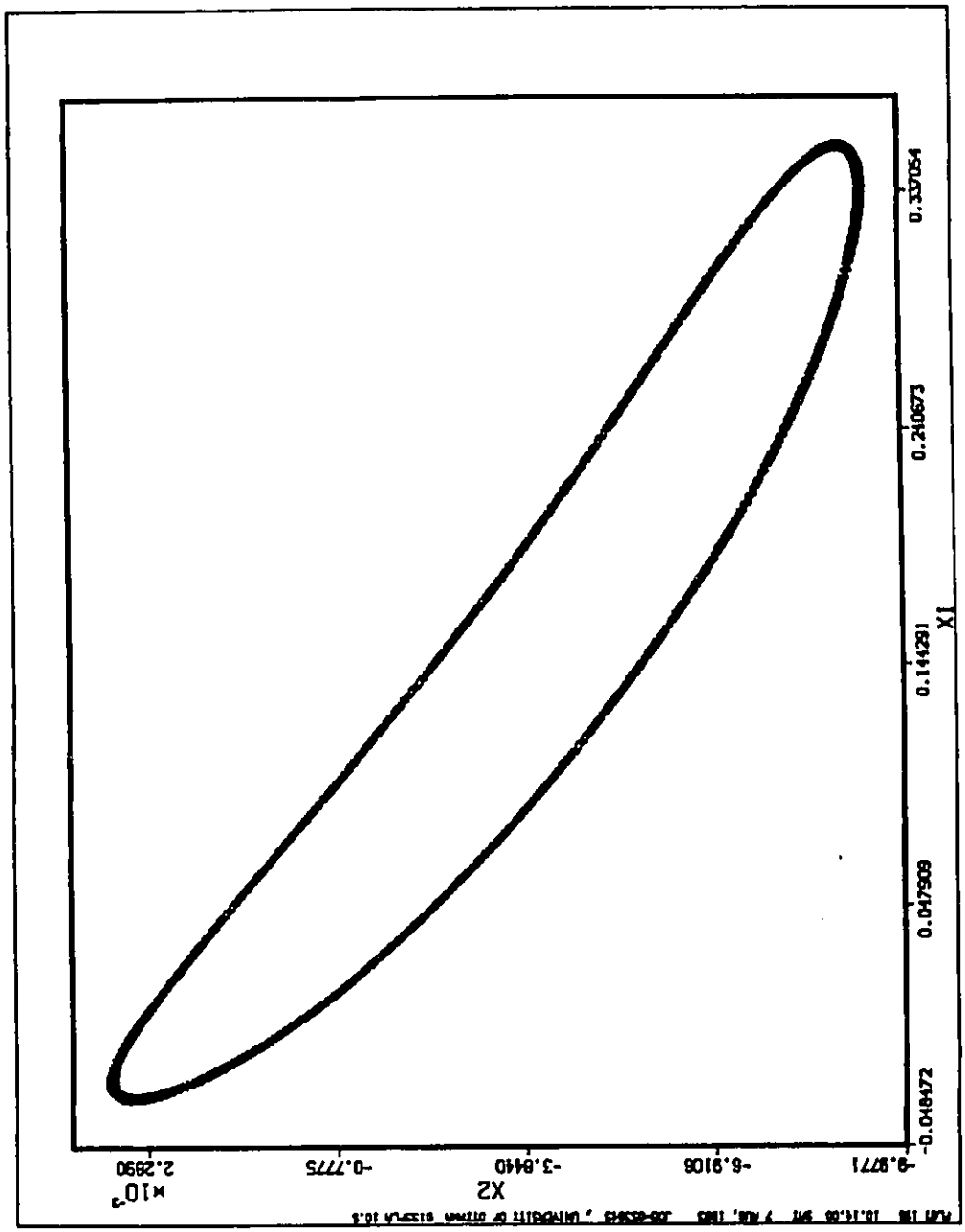

Figure 7.12: $Y = 686.3$, $\Delta = 8.67591019$. After 20000 previous intersections, the 3000 successive images of the Poincaré map shown suggest an attractive torus. It is born in a supercritical secondary Hopf bifurcation at $Y = 686.354612244$.

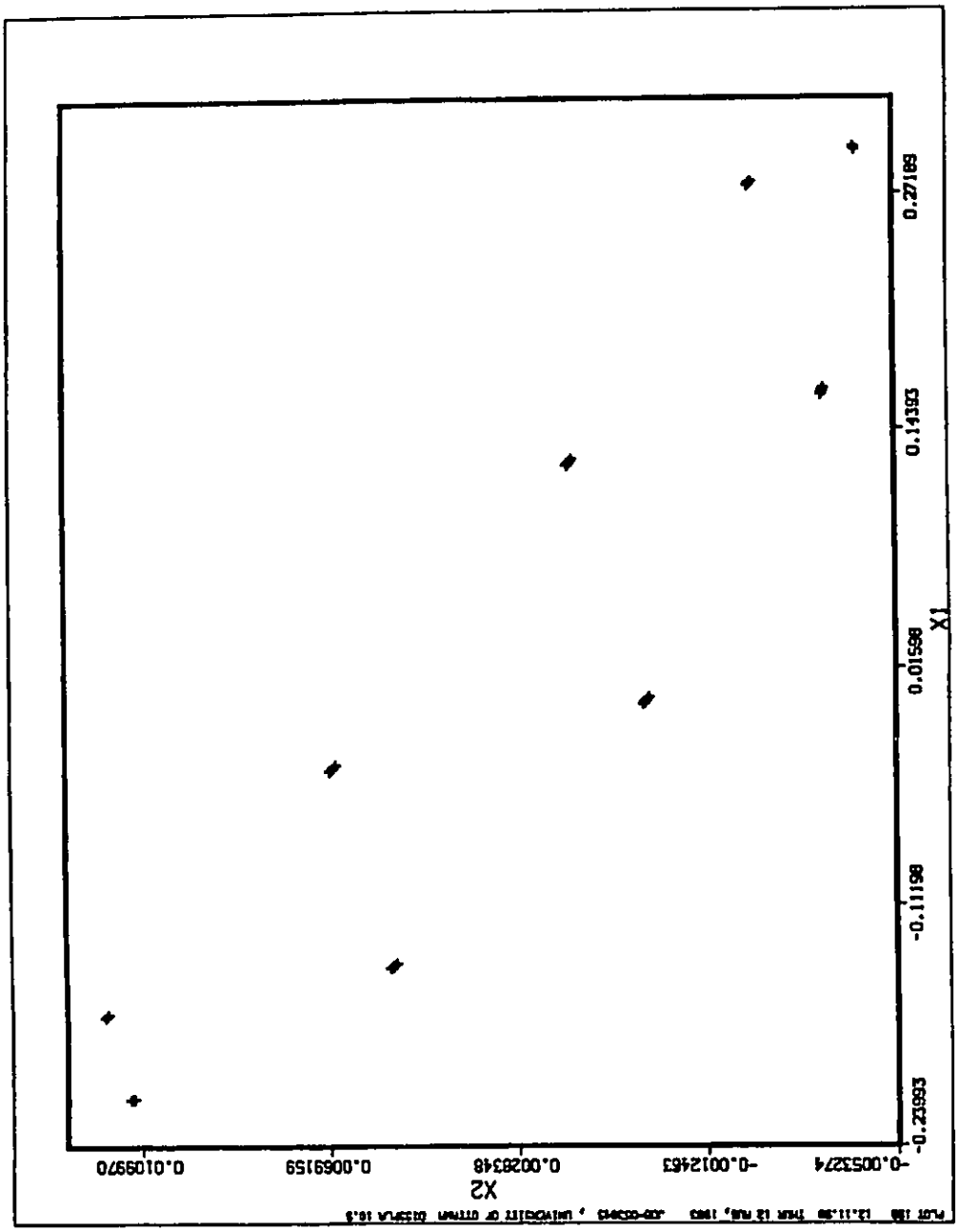

Figure 7.13: The same parameters as in Fig. 7.12 but with slightly different initial conditions. After the initial transiencies have died out, the 3000 successive images of the Poincaré map shown give evidence of a coexisting attractive torus at resonance.

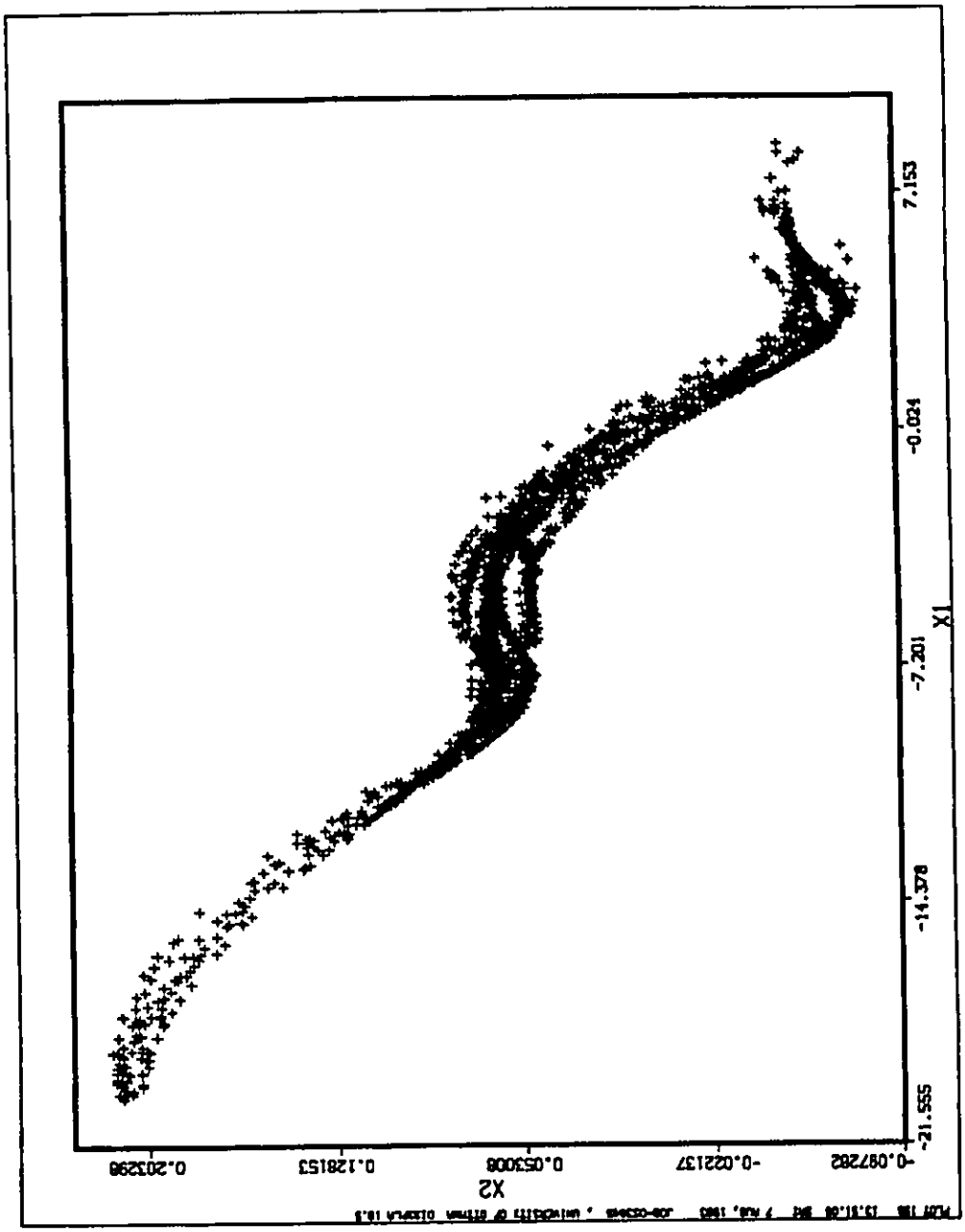

Figure 7.14: The same parameters as in Figs. 7.12 and 7.13 but with slightly perturbed initial conditions. The resulting trajectory quickly drifts away and settles down on an apparently strange attractor.

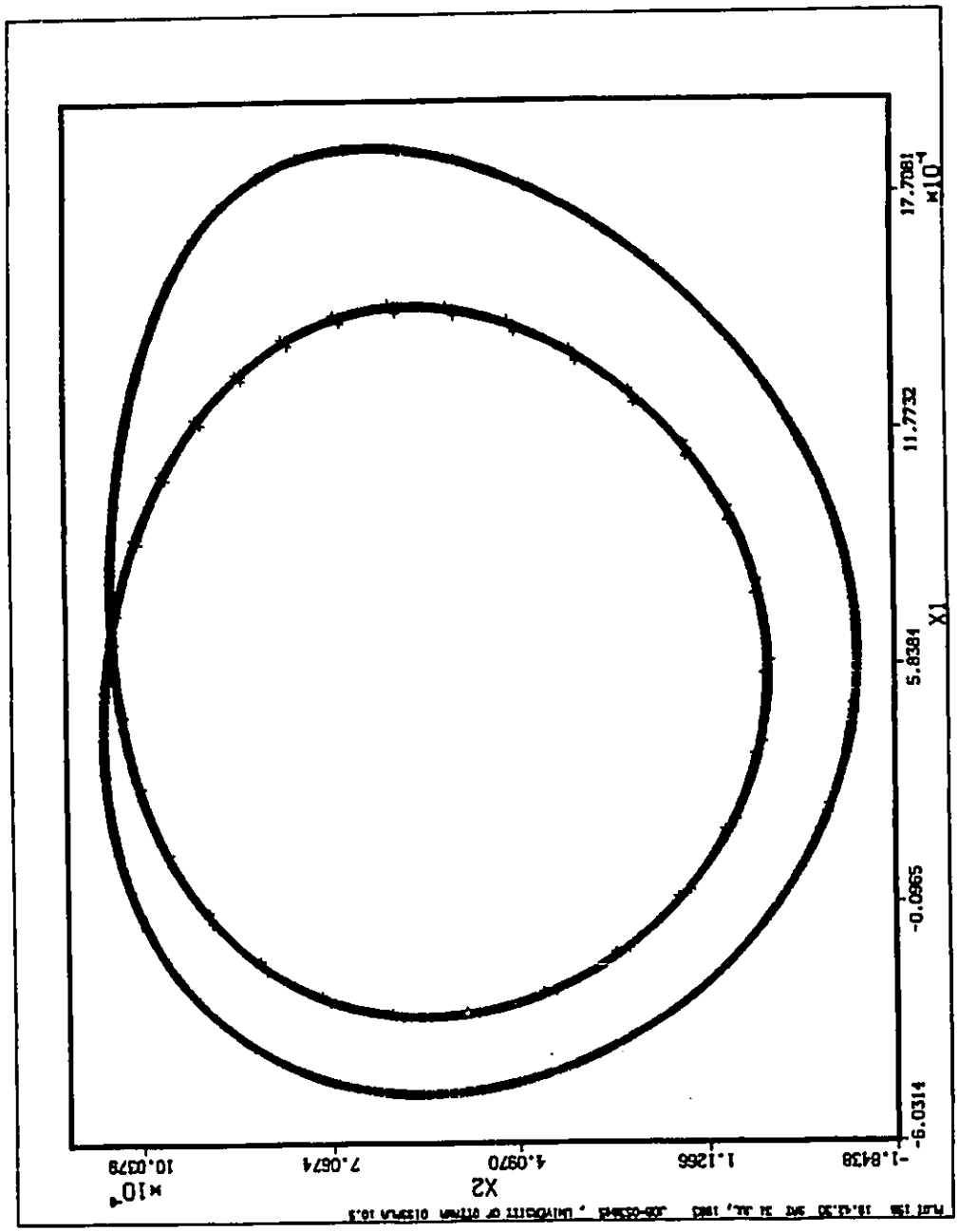

Figure 7.15: $Y = 397.6716$, $\Delta = -16.719282$ and $\Theta = 3.02454605$. It is seen that our initial condition is attracted to an invariant curve that strongly resembles (and suggests!) an attractive doubled torus.

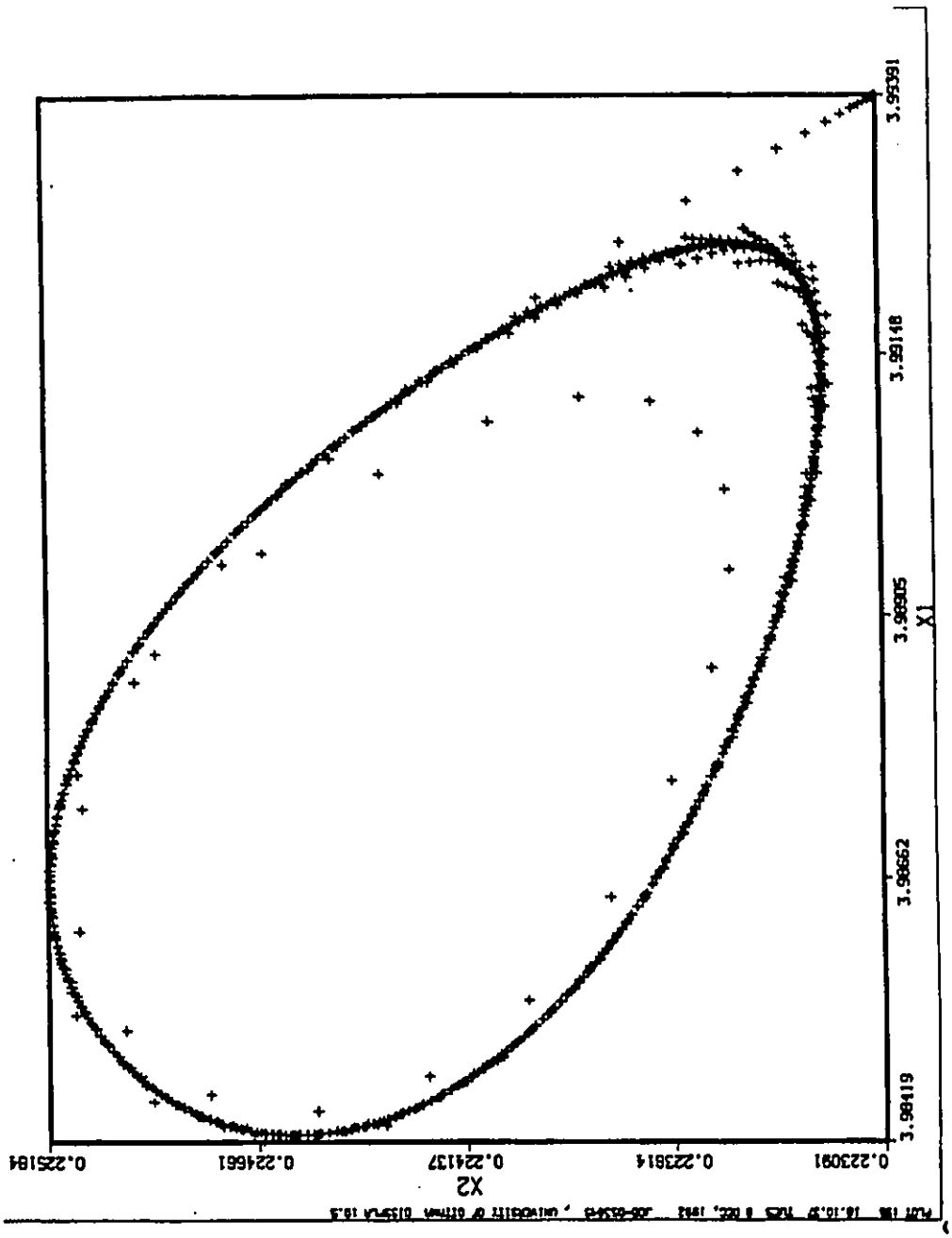

Figure 7.16: $Y = 534.4$, $\Delta = 4.495233938$. An attractive two-torus captures a neighbourhood of the unstable periodic orbit in the lower right corner.

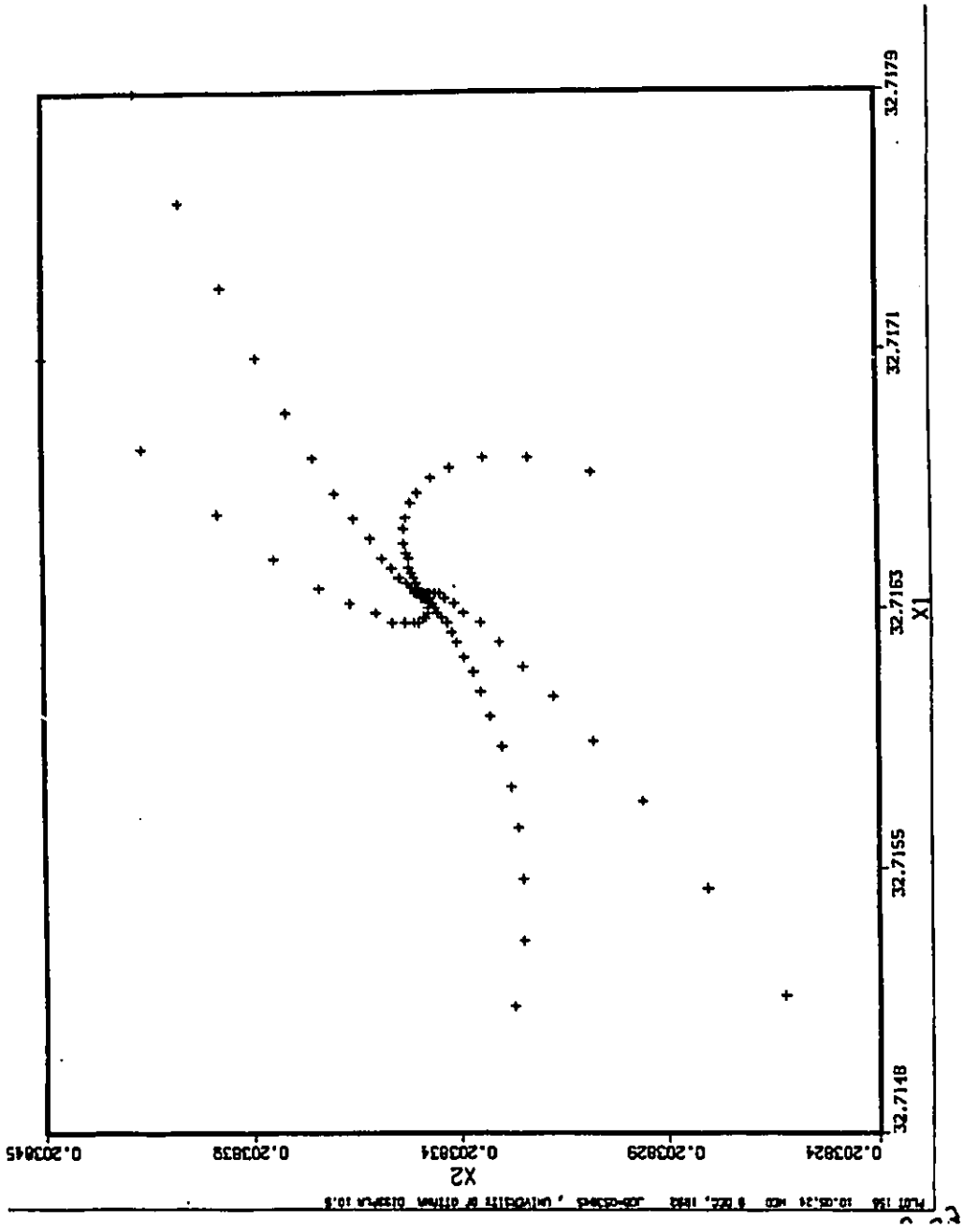

Figure 7.17: The same parameters as in Fig. 7.16, but an attractive periodic orbit captures slightly different initial conditions than the one in Fig. 7.16.

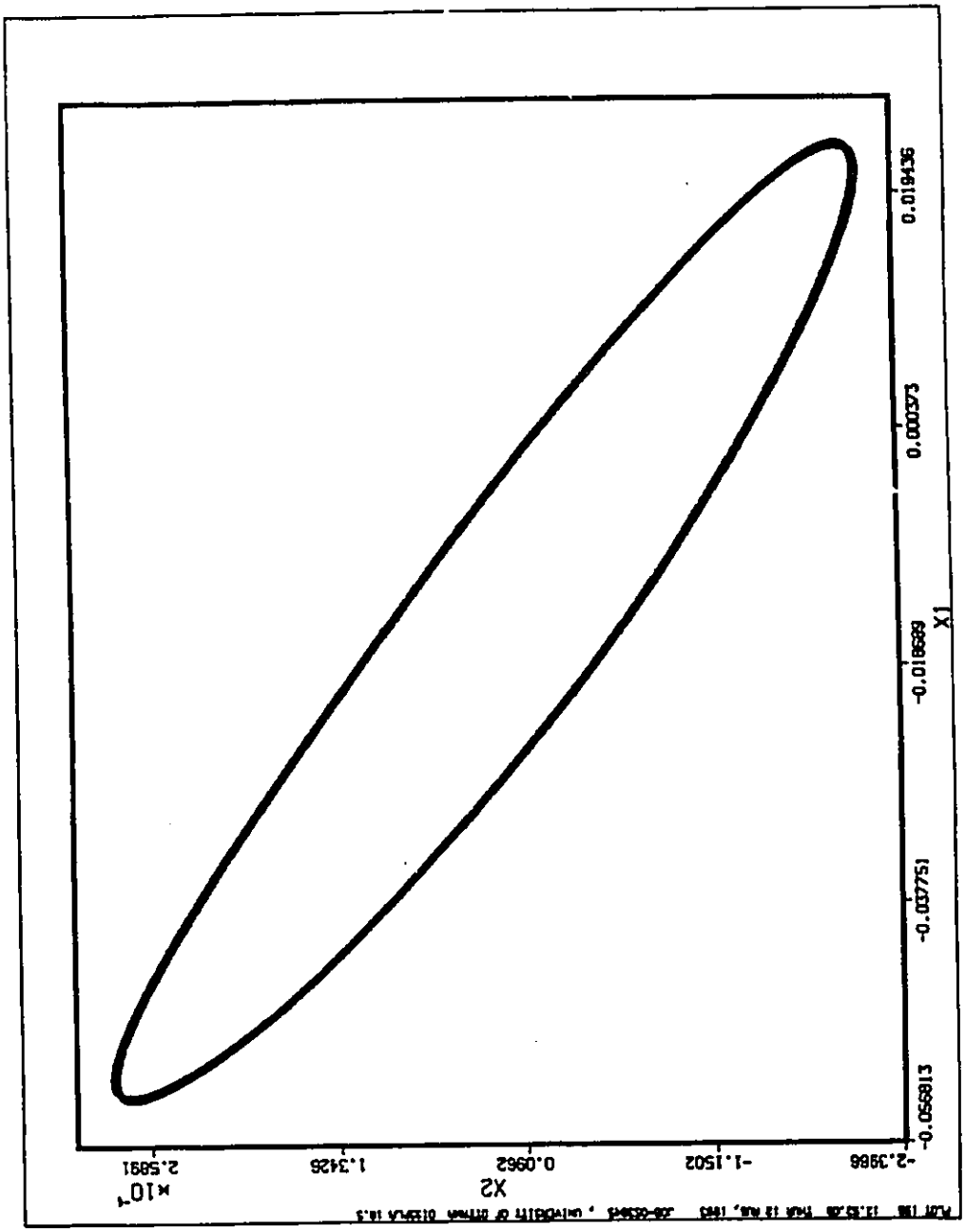

Figure 7.18: $Y = Y_T = 413.1$, $\Delta = 3.2572312$ and $\Theta = -16.719282$. Attractive two-torus close to its birth in a supercritical secondary Hopf bifurcation at $Y = 413.13109351$. The successive images uniformly fill an apparently smooth invariant curve.

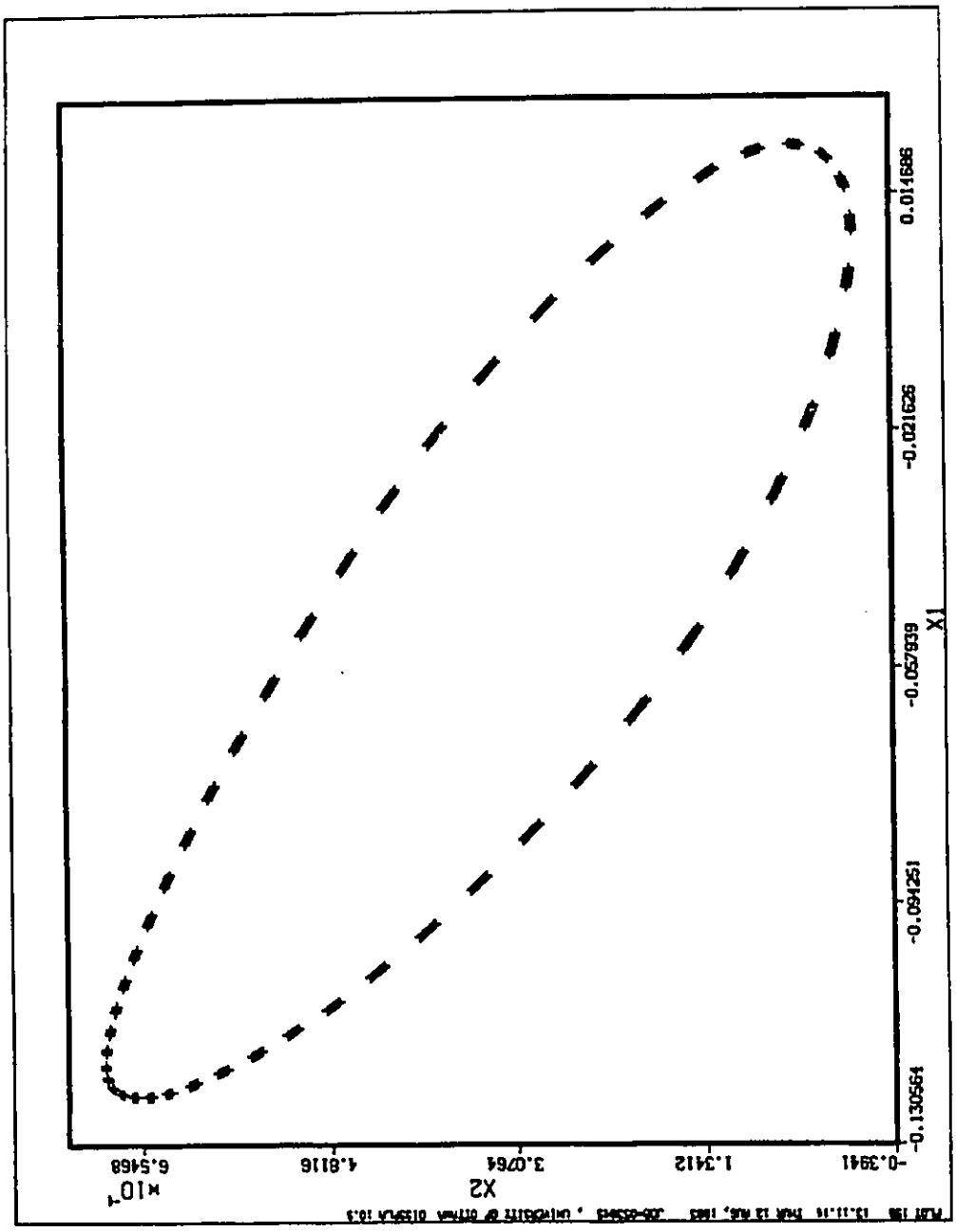

Figure 7.19: The same parameters as in Fig. 7.18, but with Y decreased to $Y = 413.05$. Apparently the winding number has changed and the attractive torus is at resonance. The intersections acccumulate in a neighbourhood of 48 distinguishable points.

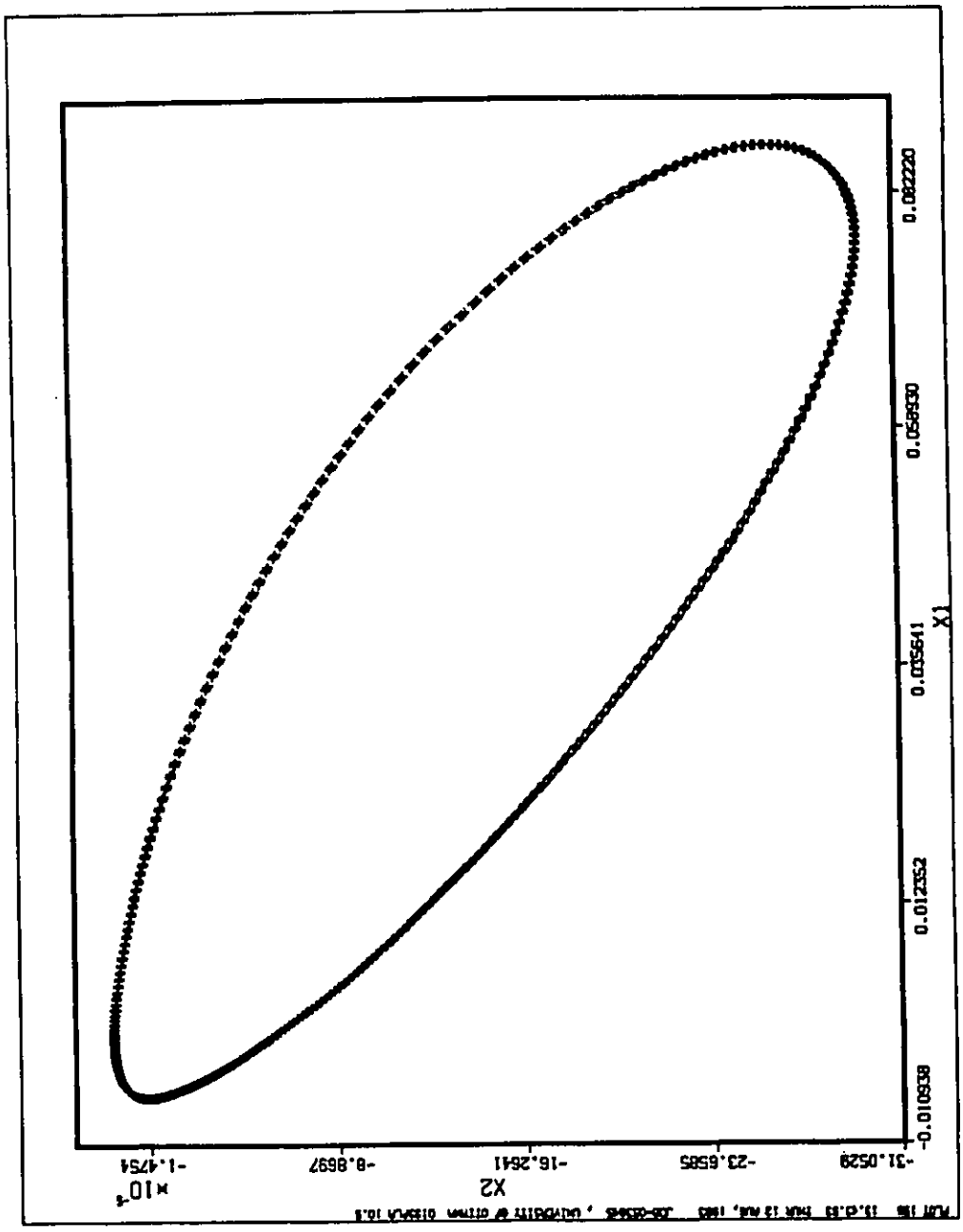

Figure 7.20: The same parameters as in Fig. 7.18, but with Y further decreased to $Y = 413.03$. The winding number apparently has changed again.

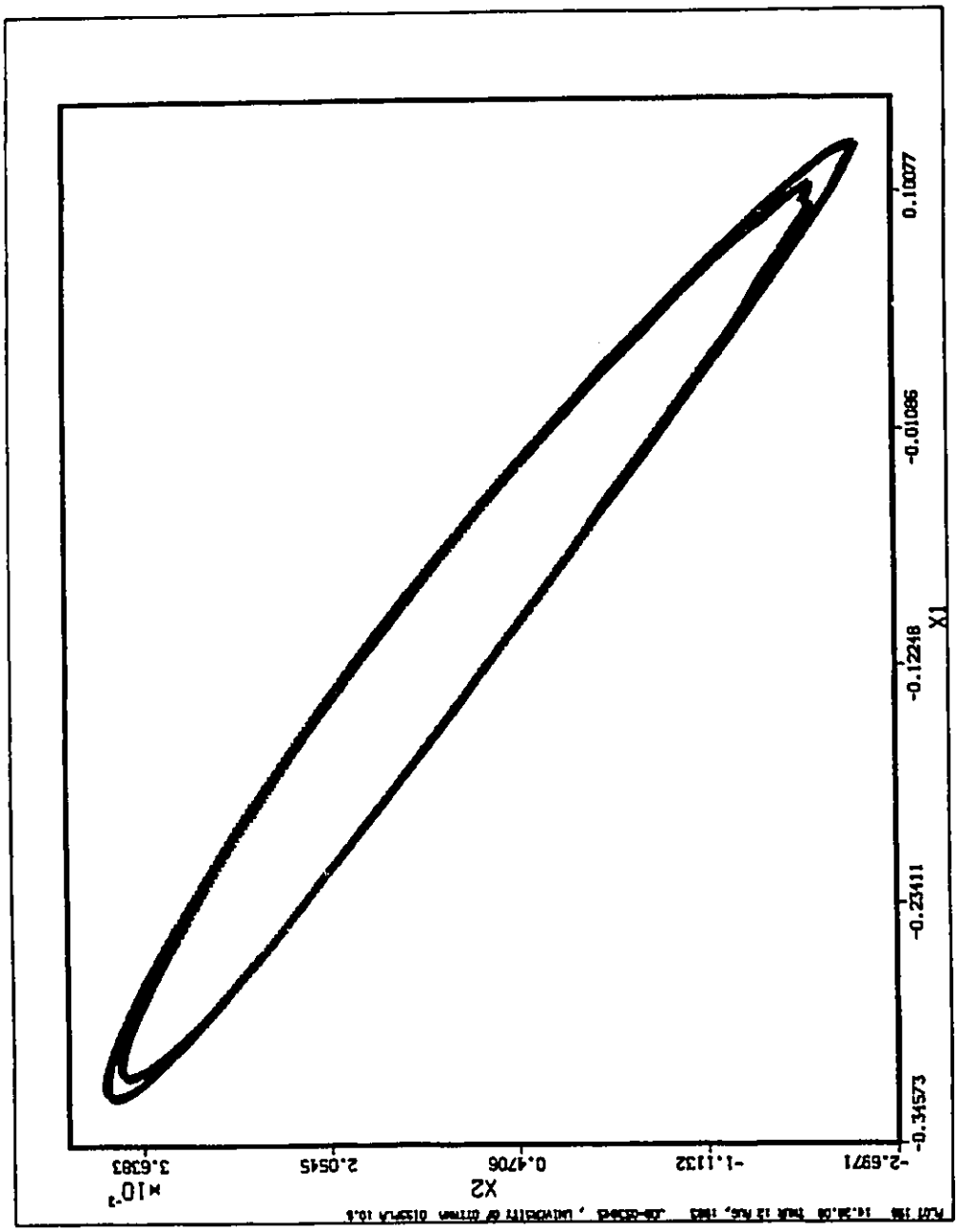

Figure 7.21: The same parameters as in Fig. 7.18, but with Y further decreased to $Y = 413.01$. The intersections shown suggest that the two-torus has doubled. Notice also the loss of smoothness when compared to Figs. 7.18, 7.19 and 7.20.

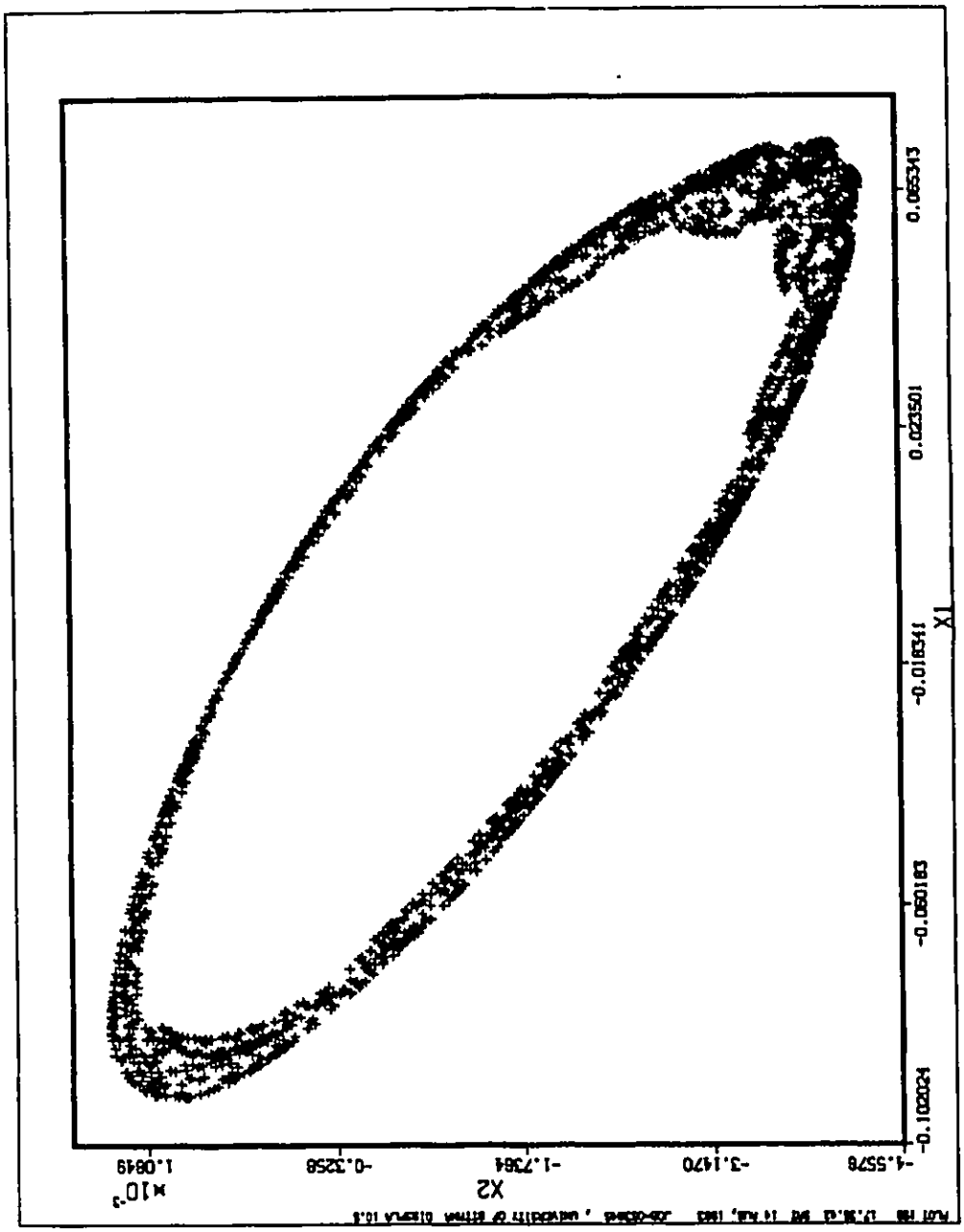

Figure 7.22: The same parameters as in Fig. 7.18, but with Y further decreased to $Y = 413.00$. The 3000 intersections now seem to densely fill a band of nonzero width and suggest that the initial value is attracted to a three-torus.

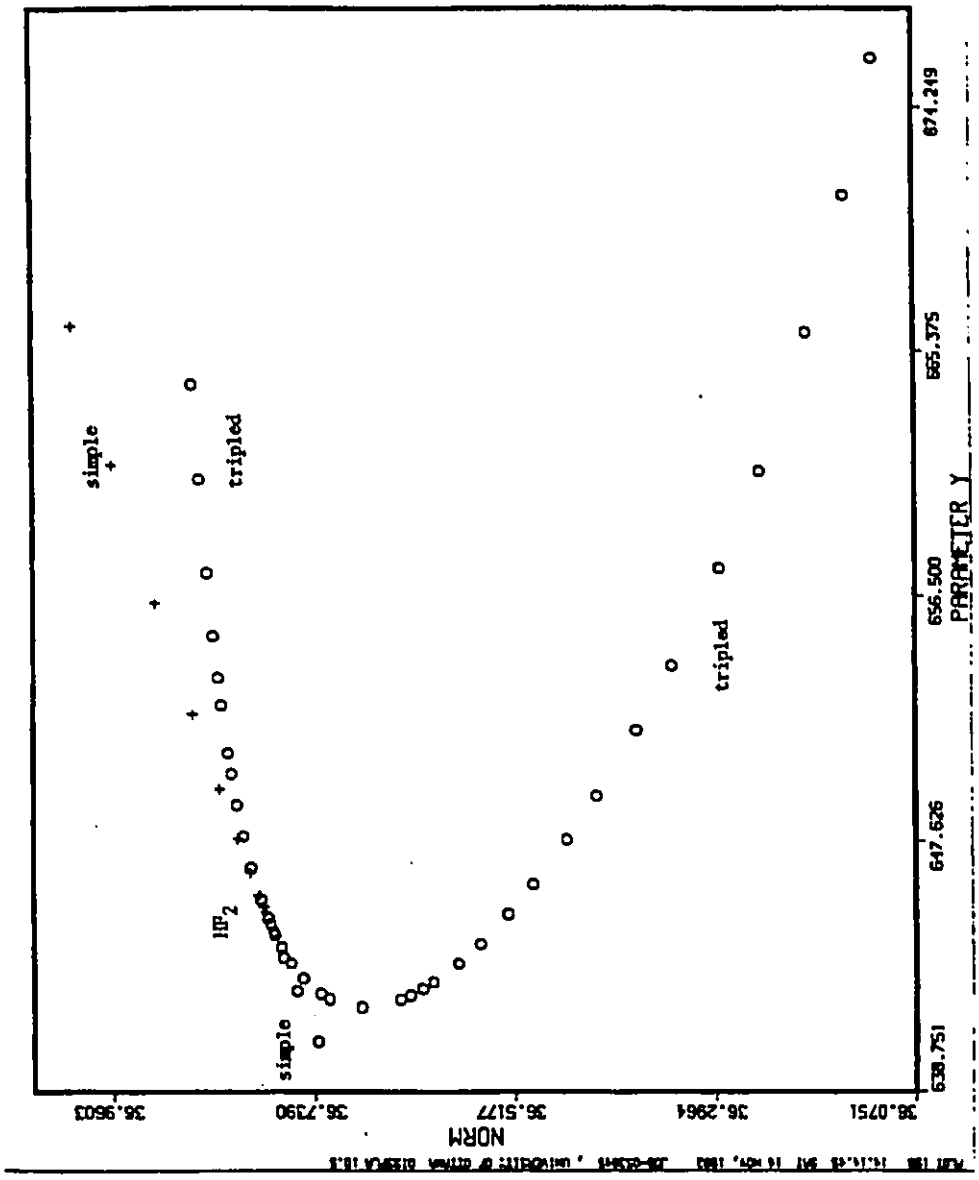

Figure 7.23: The norm versus Y in a one-parameter cross section of Fig. 7.1 at $\Delta = 7.2328457$. Here the simple periodic orbit looses stability in a secondary Hopf bifurcation at strong resonance with $\beta = \frac{2\pi}{3}$. A tripled unstable periodic orbit, existing on both sides of the bifurcation value $Y^* = 645.023976413$, bifurcates off. The data of it for $\Delta = 7.5$, $Y = 775$ can be found under number 4c in Table 6.3.

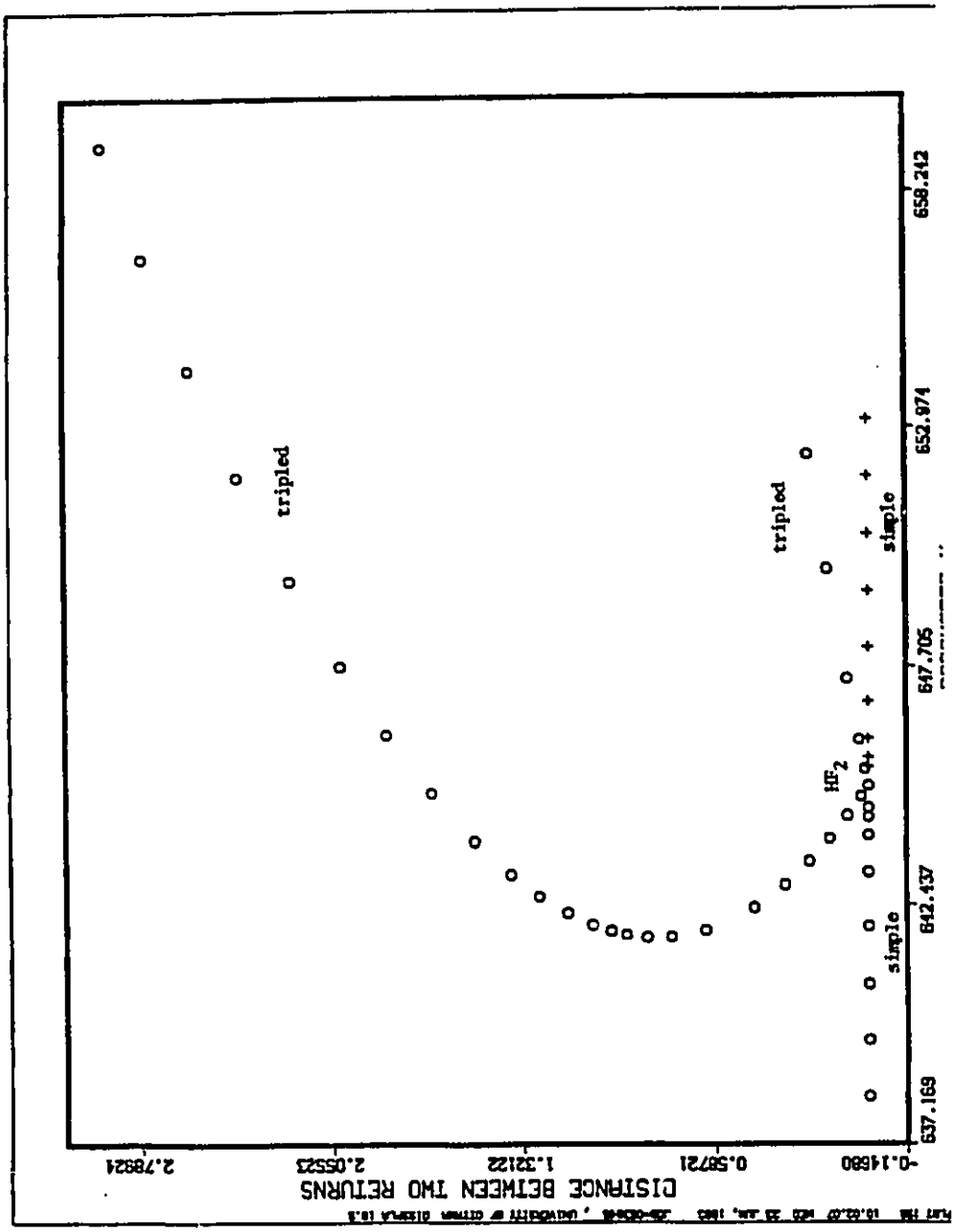

Figure 7.24: The same data as in Fig. 7.23, except that the distances $D^3(Y) = \|\bar{x} - S^{1/3}(\bar{x}, Y)\|_2$ are plotted versus Y. While $D^3(Y) = 0$ for the simple periodic orbit, it is nonzero for the tripled one, except at the bifurcation value $y^* = 645.023976413$.

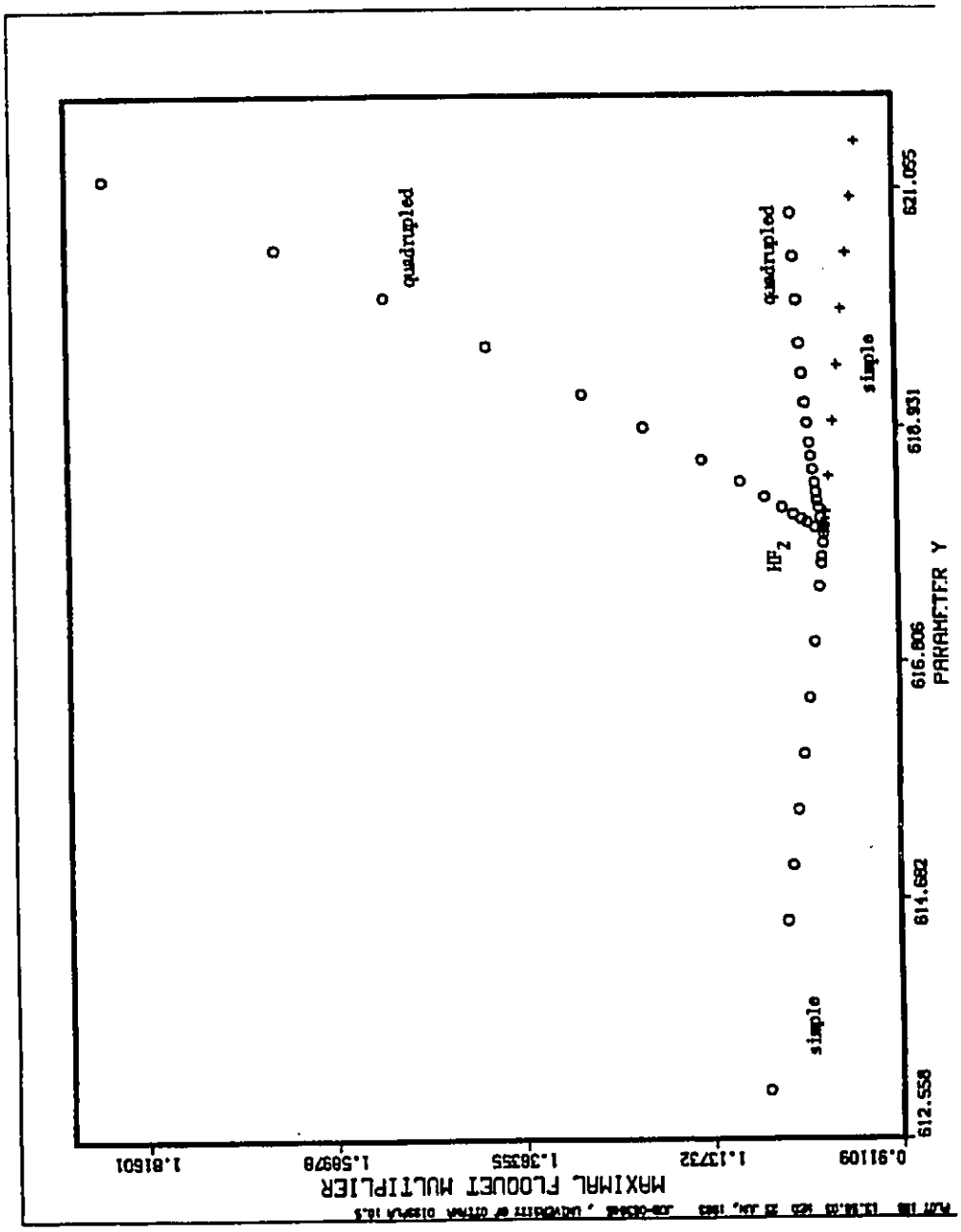

Figure 7.25: The maximal Floquet multiplier versus Y in a one-parameter cross-section of Fig. 7.1 at $\Delta = 6.34547483$. Here the simple periodic orbit looses stability in a secondary Hopf bifurcation at strong resonance with $\beta = \frac{\pi}{2}$. Two unstable quadrupled periodic orbits, existing on one side of the bifurcation value $Y^* = 617.9616485$, bifurcate off.

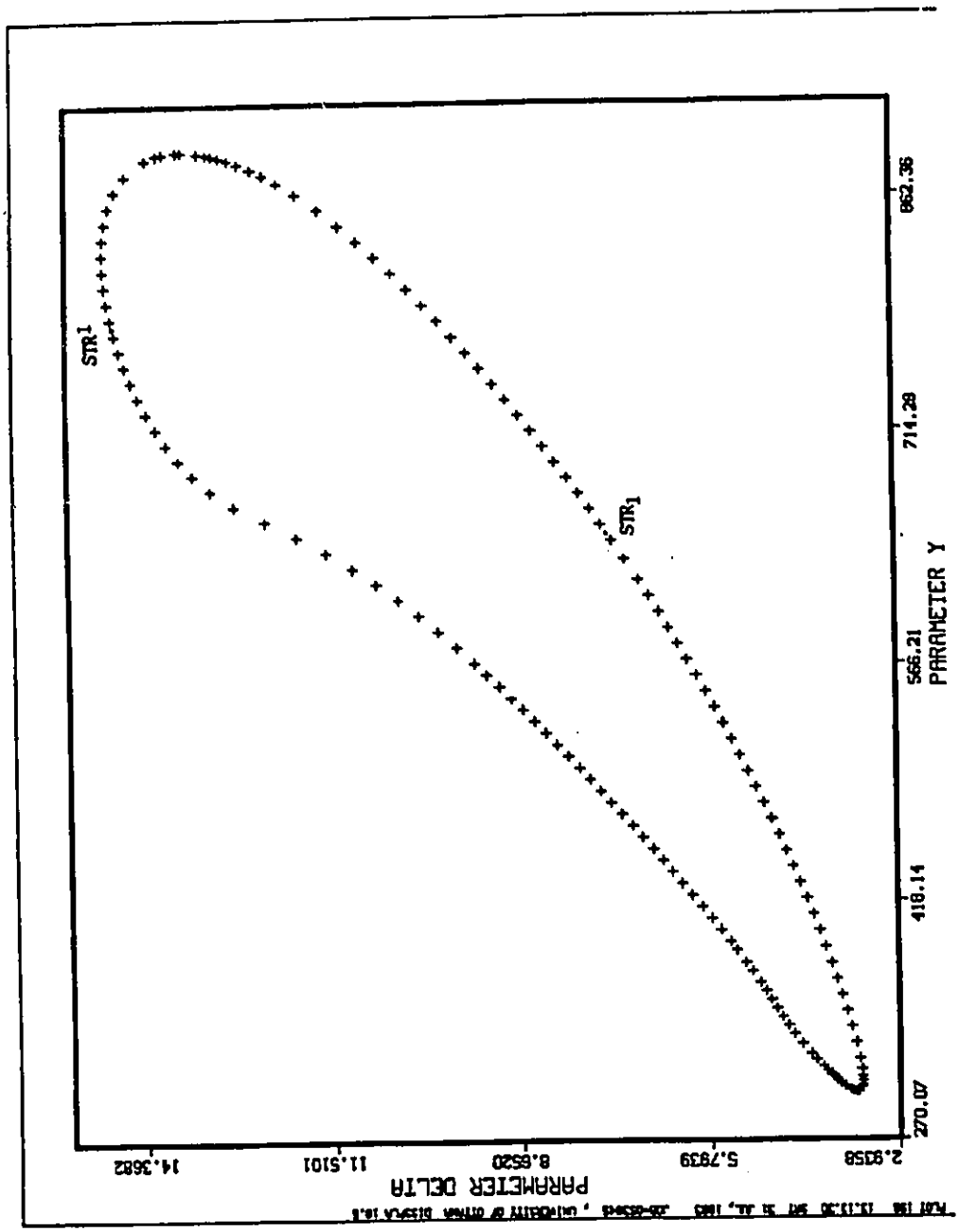

Figure 8.1: The projection of the three-parameter continuation of the secondary Hopf bifurcation at strong resonance with $\beta = \frac{2\pi}{3}$, STR_1, in Fig. 7.1 into Y, Δ parameter space shows a closed loop. The point STR^1 lies along the secondary Hopf branch between $\mathrm{PTB2}_3$ and $\mathrm{PTB1}_2$, see Fig. 7.1.

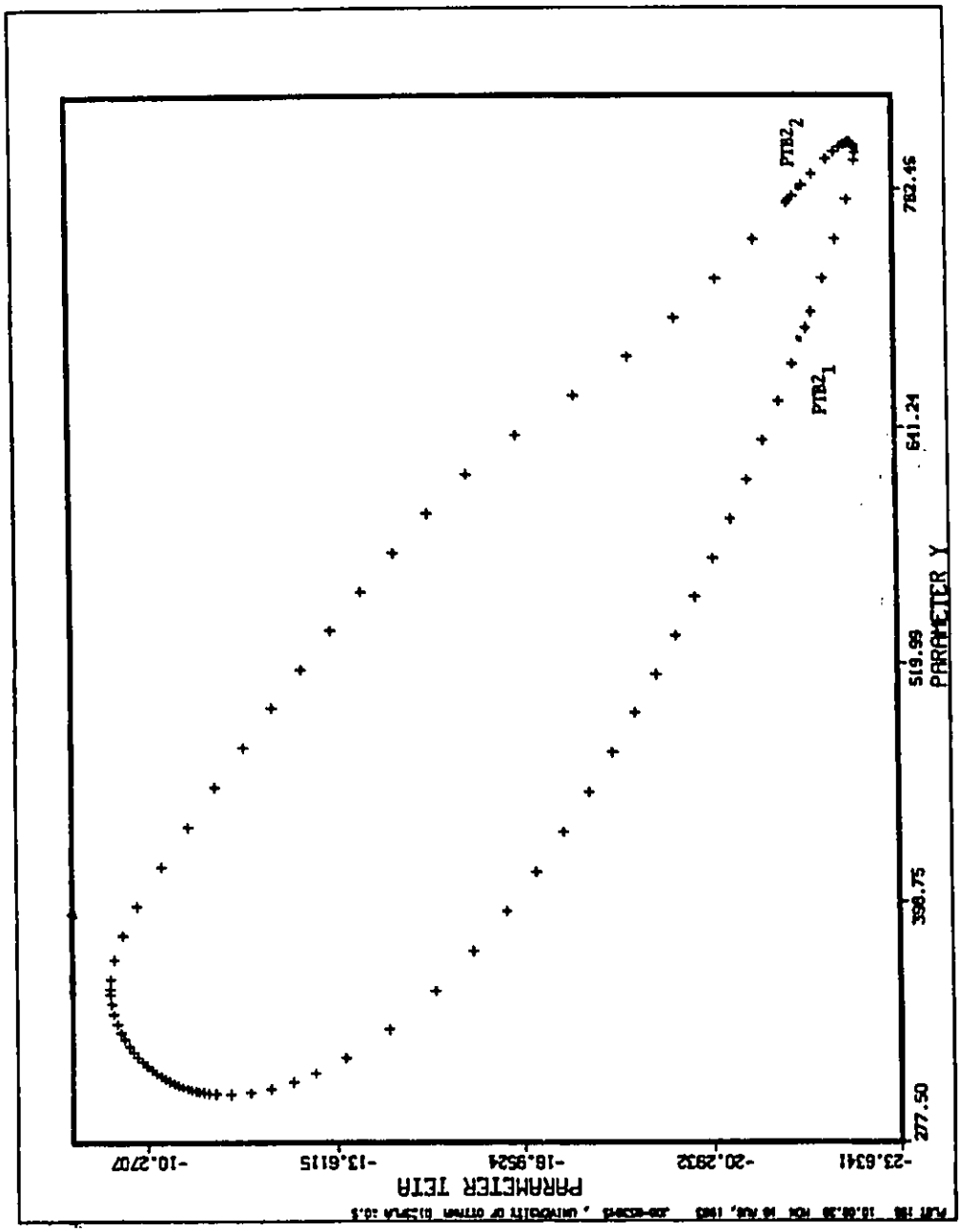

Figure 8.2: The projection of the three-parameter continuation of $PTB2_1$ in Fig. 7.1 into Y, Θ parameter space exhibits a closed loop with two saddle-nodes (extremal points) in Θ. The point $PTB2_2$ refers to the second periodic Takens-Bogdanov point with a double -1 Floquet multiplier in Fig. 7.1.

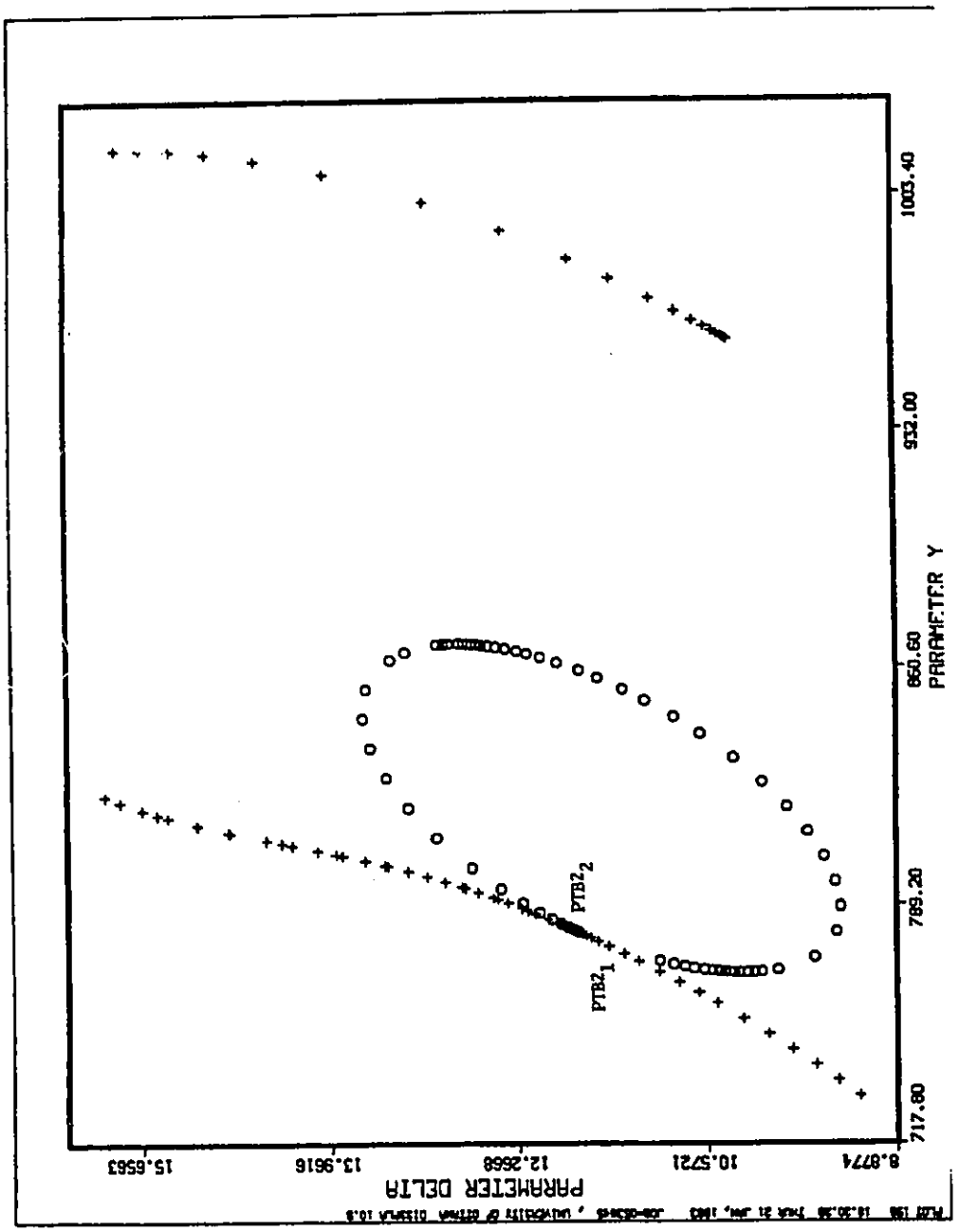

Figure 8.3: The continuation in the two parameter Y and Δ with Θ fixed at $= -22.96589073$, just above the lower saddle node in Fig. 8.2, reveals that the two secondary Hopf branches join to form a single one and the period-doubling loop detaches.

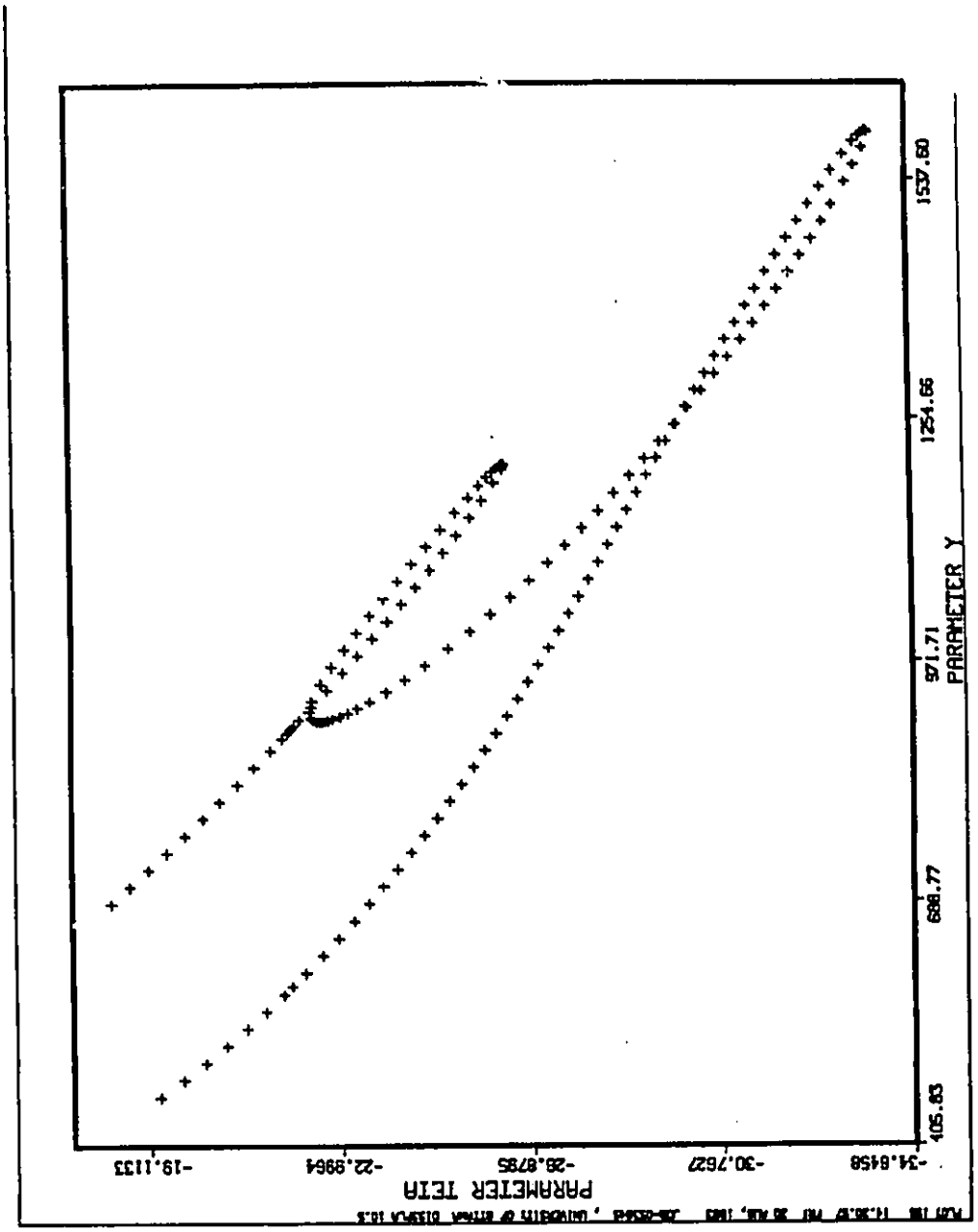

Figure 8.4: A small section of the Y, Θ projection of the three-parameter continuation of the periodic Takens–Bogdanov point $PTB1_1$ in Fig. 7.1. For a projection of the complete curve see Fig. 8.5 and compare also with Fig. 8.6.

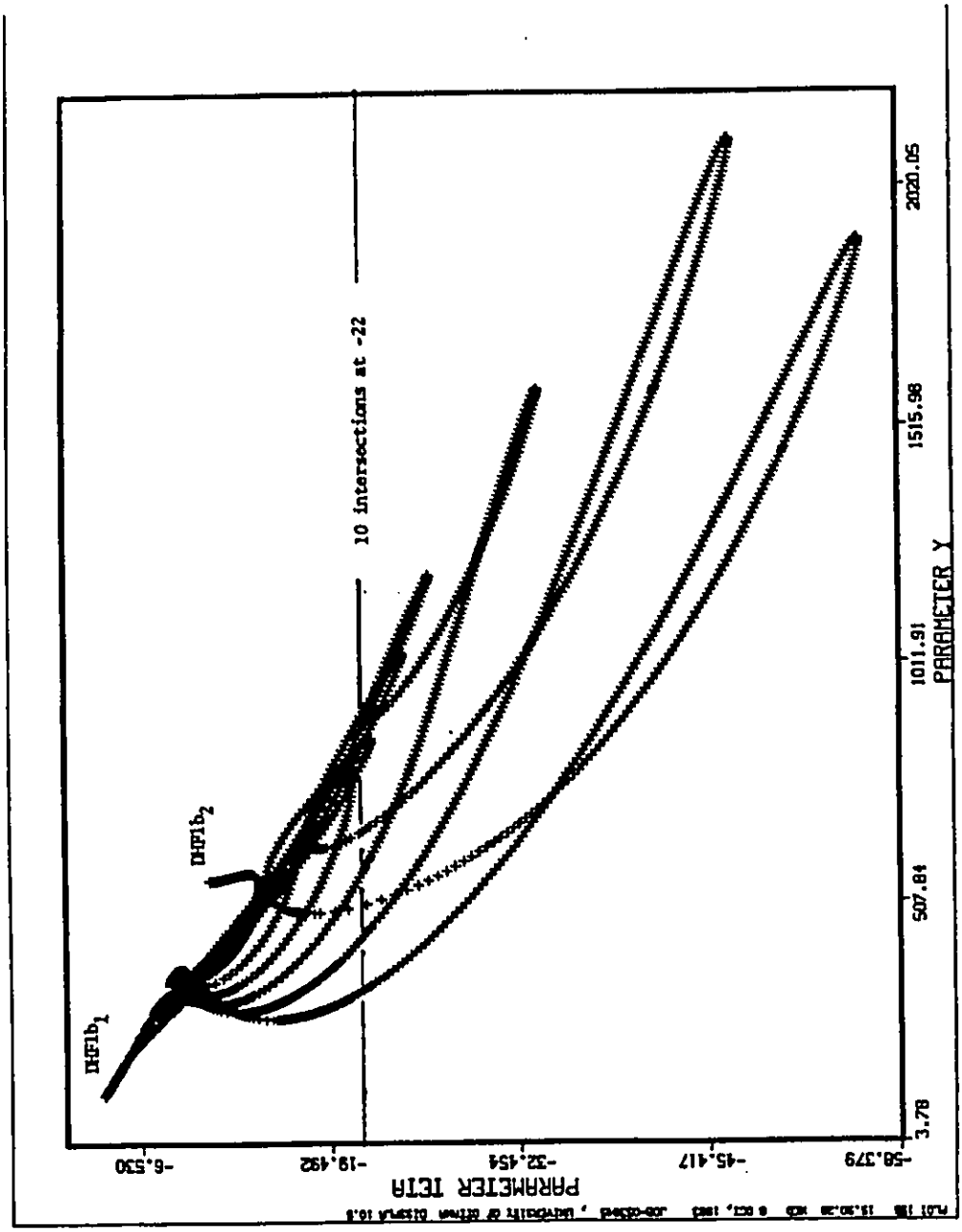

Figure 8.5: The projection of the three-parameter continuation of the periodic Takens-Bogdanov point $\mathrm{PTB1}_1$ in Fig. 7.1 into Y, Θ parameter space. The curve is quite long, it shows plenty of saddle-nodes with respect to each parameter and it terminates at both ends in the degenerate Hopf bifurcations $\mathrm{DHF1b}_i$, see also Fig. 8.6. A section across it at $\Theta = -22$ reveals precisely the points $\mathrm{PTB1}_1$, $\mathrm{PTB1}_2$ in Fig. 7.1 and the eight points $\mathrm{PTB1}_i$, $i = 1, 2, \ldots, 8$, in Fig. 7.4. Hence, varying Θ will eventually attach Figs. 7.1 and 7.4.

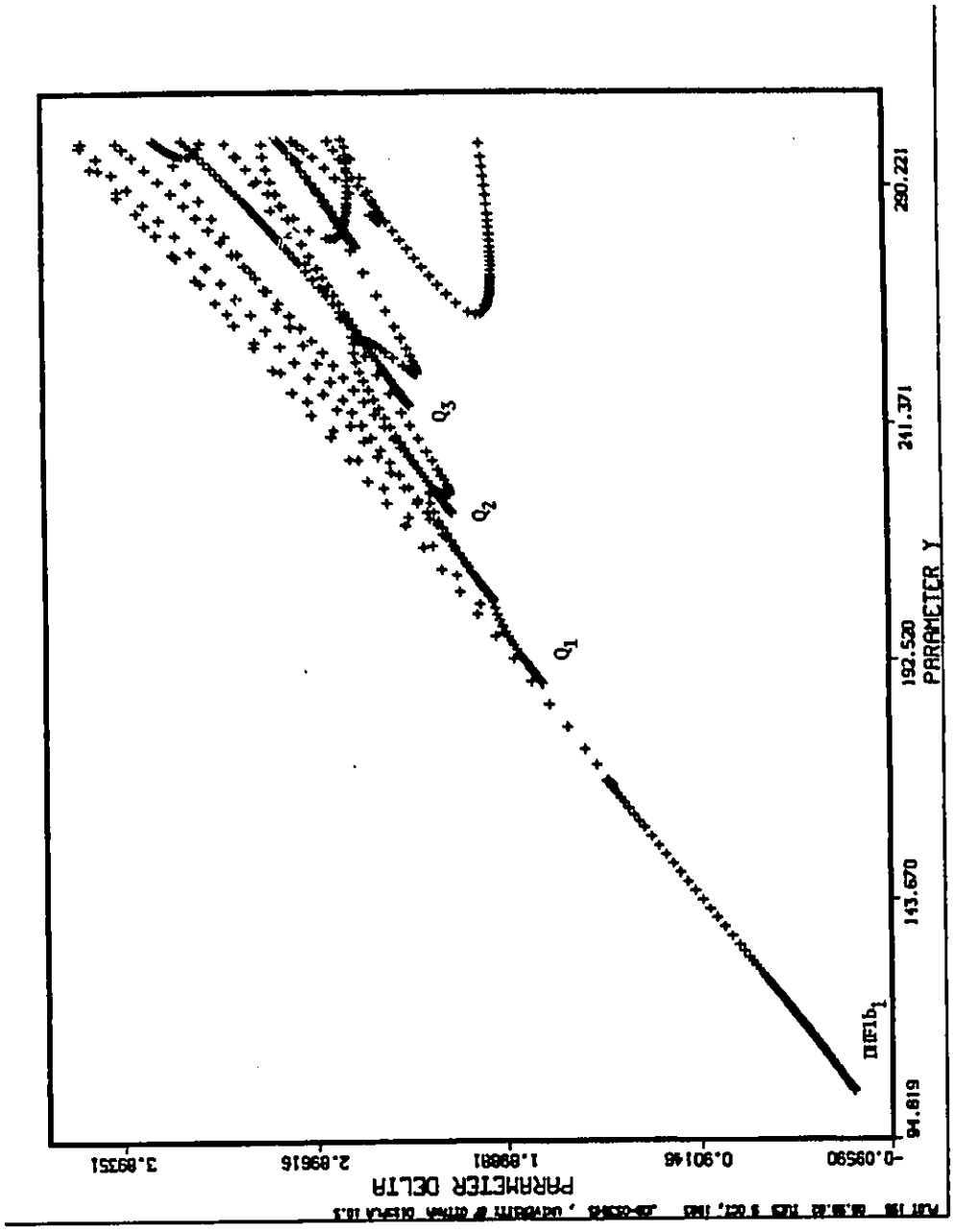

Figure 8.6: This enlargement of Fig. 8.5, projected into Y, Δ space, shows the termination point $\mathrm{DIF1b_1}$ and plenty of, occasionally very sharp, saddle-nodes.

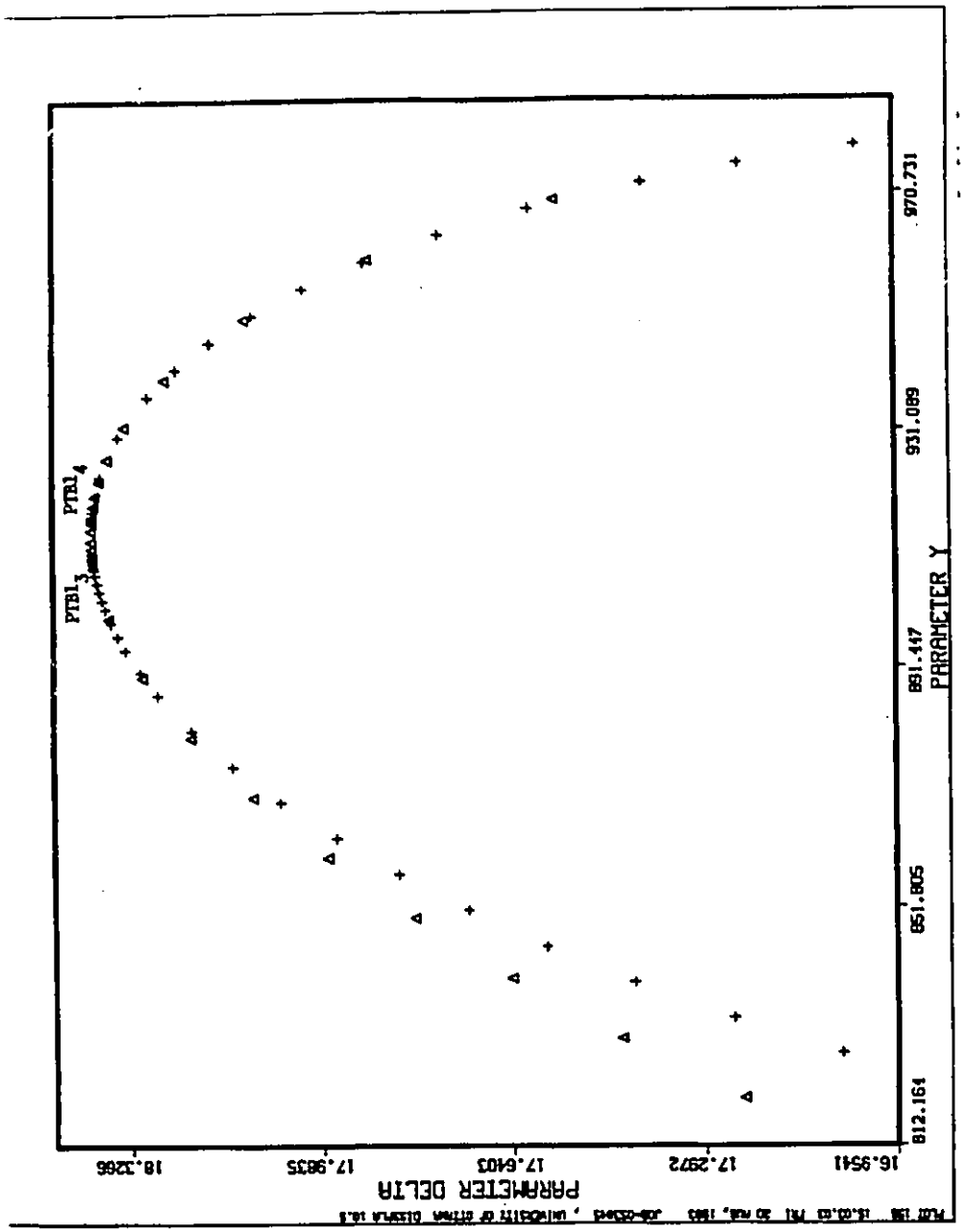

Figure 8.7: At $\Theta = -22.37966071 - \epsilon$, the secondary Hopf branch in the corresponding Fig. 7.1 between $PTB2_2$ and $PTB1_2$ has just touched the surrounding saddle-node loop and split into two disconnected ones, thereby creating the additional two periodic Takens–Bogdanov points $PTB1_3$ and $PTB1_4$.

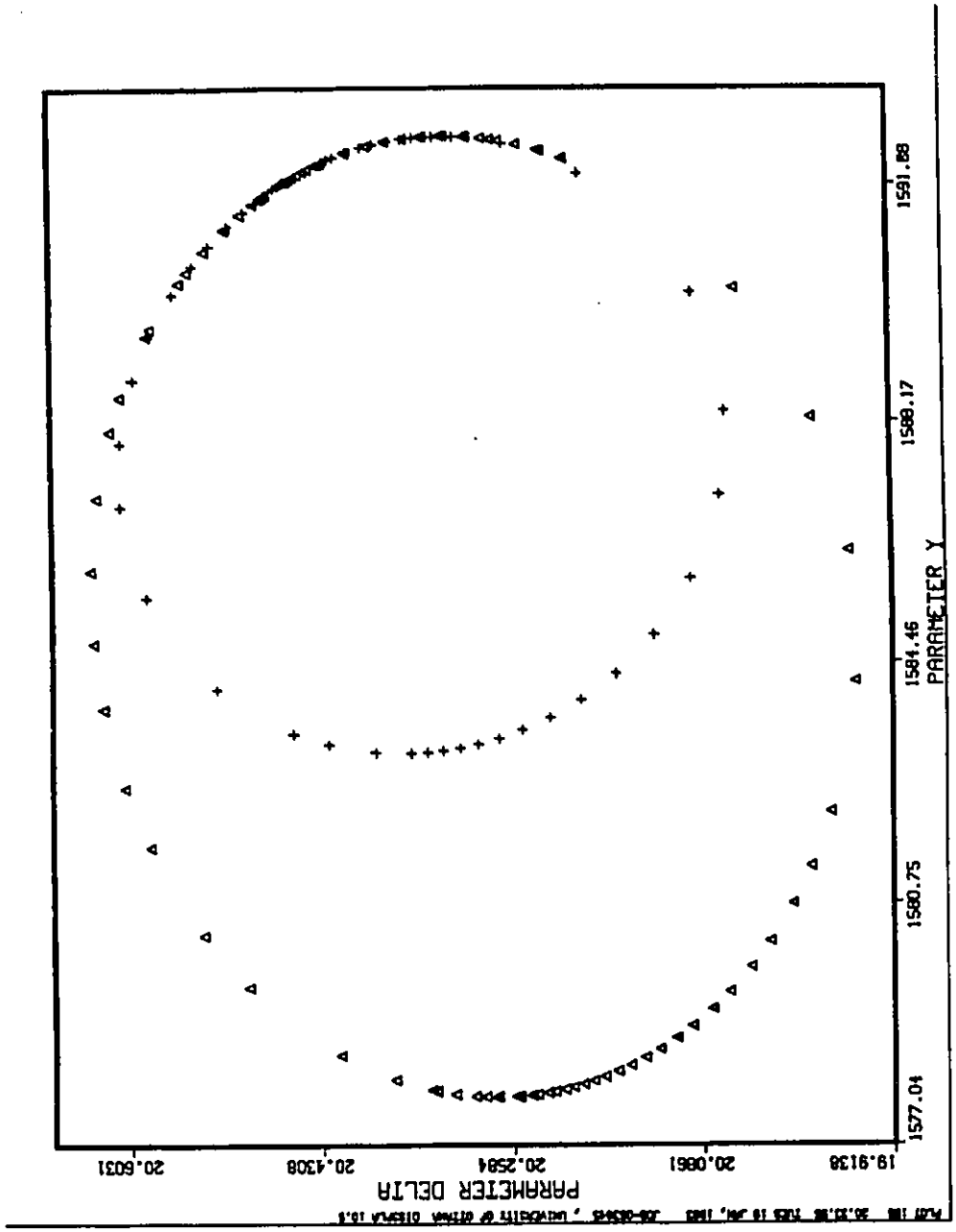

Figure 8.8: At $\Theta = -33.86917974$, the periodic Takens-Bogdanov points $PTB1_1$ from Fig. 7.1 and $PTB1_3$ from Fig. 8.7 move together, touch and disappear. Thereby the attached secondary Hopf branches join and form a single one — in fact a closed loop.

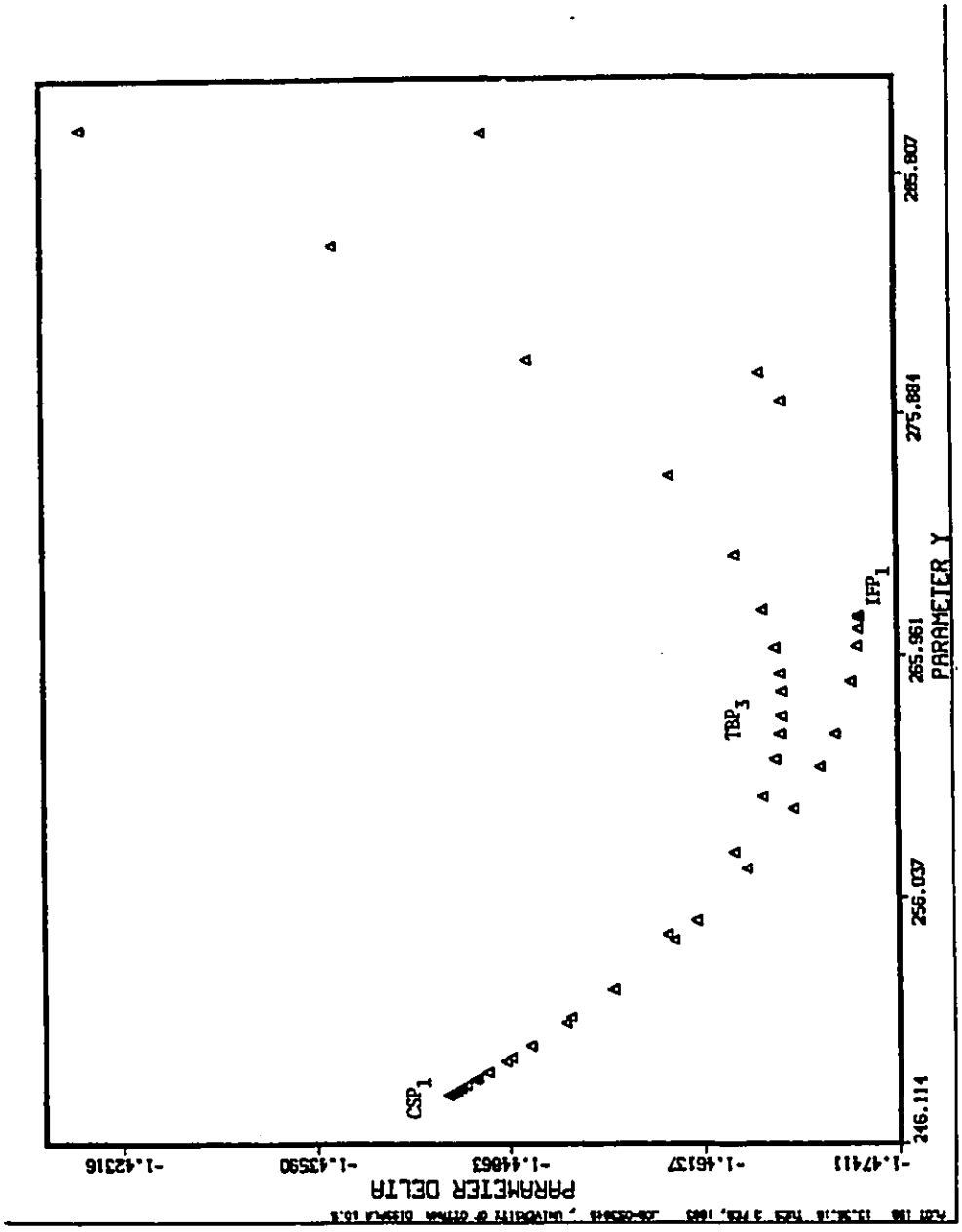

Figure 8.9: This enlargement of Fig. 7.4 shows that the cusp CSP_1 is curved upwards giving rise to two (local) extremal points in the parameter Δ. These are, respectively, the transcritical bifurcation point TBP_3 and the isola formation point IFP_1, see Fig. 7.4.

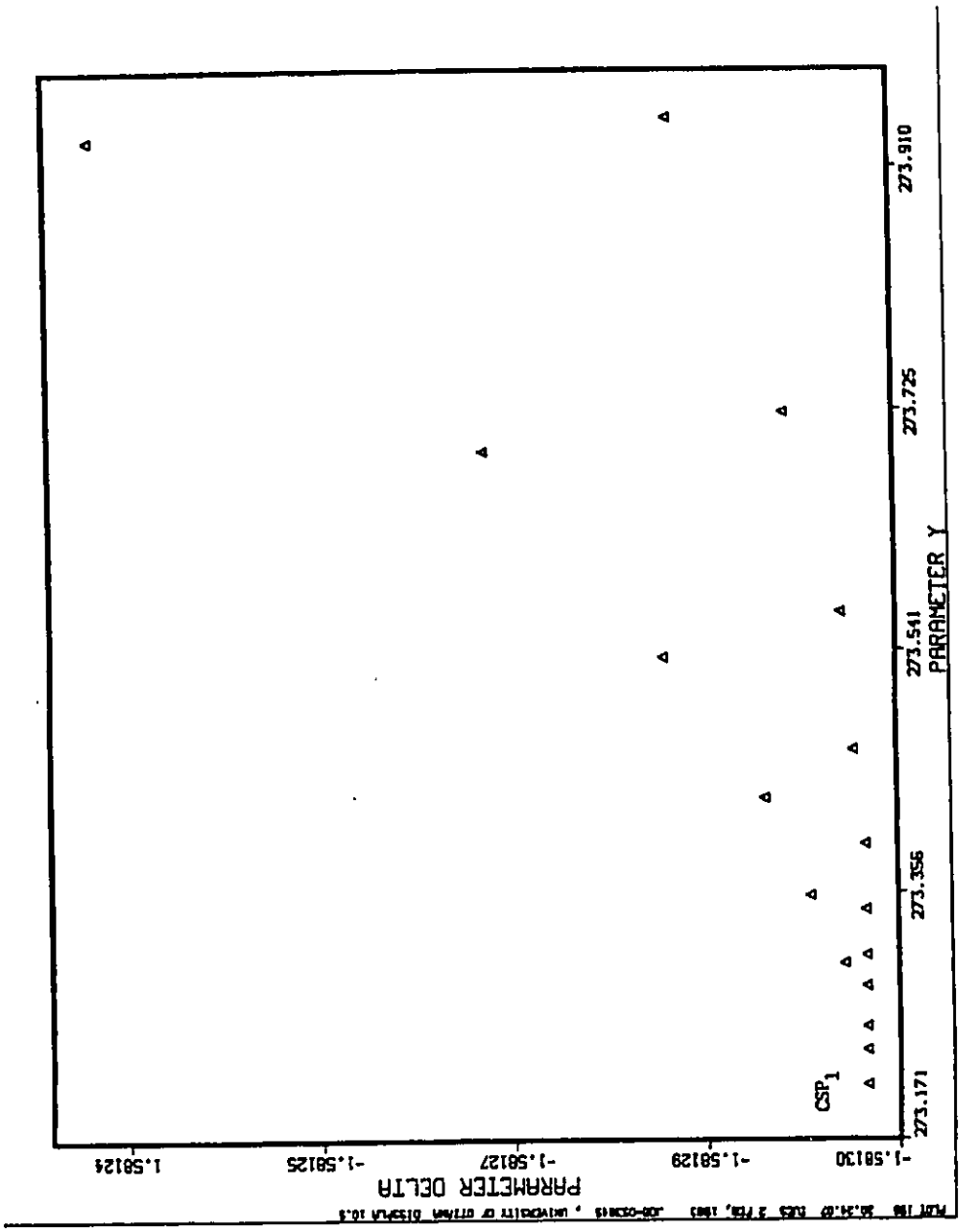

Figure 8.10: At $\Theta = -22.2855225$ the transcritical bifurcation point TBP_3 and the isola formation point IFP_1 touch and flatten the cusp CSP_1, compare with Fig. 8.9. A further decrease of Θ bends CSP_1 downwards and makes TBP_3 and IFP_1 disappear, compare with Fig. 8.11.

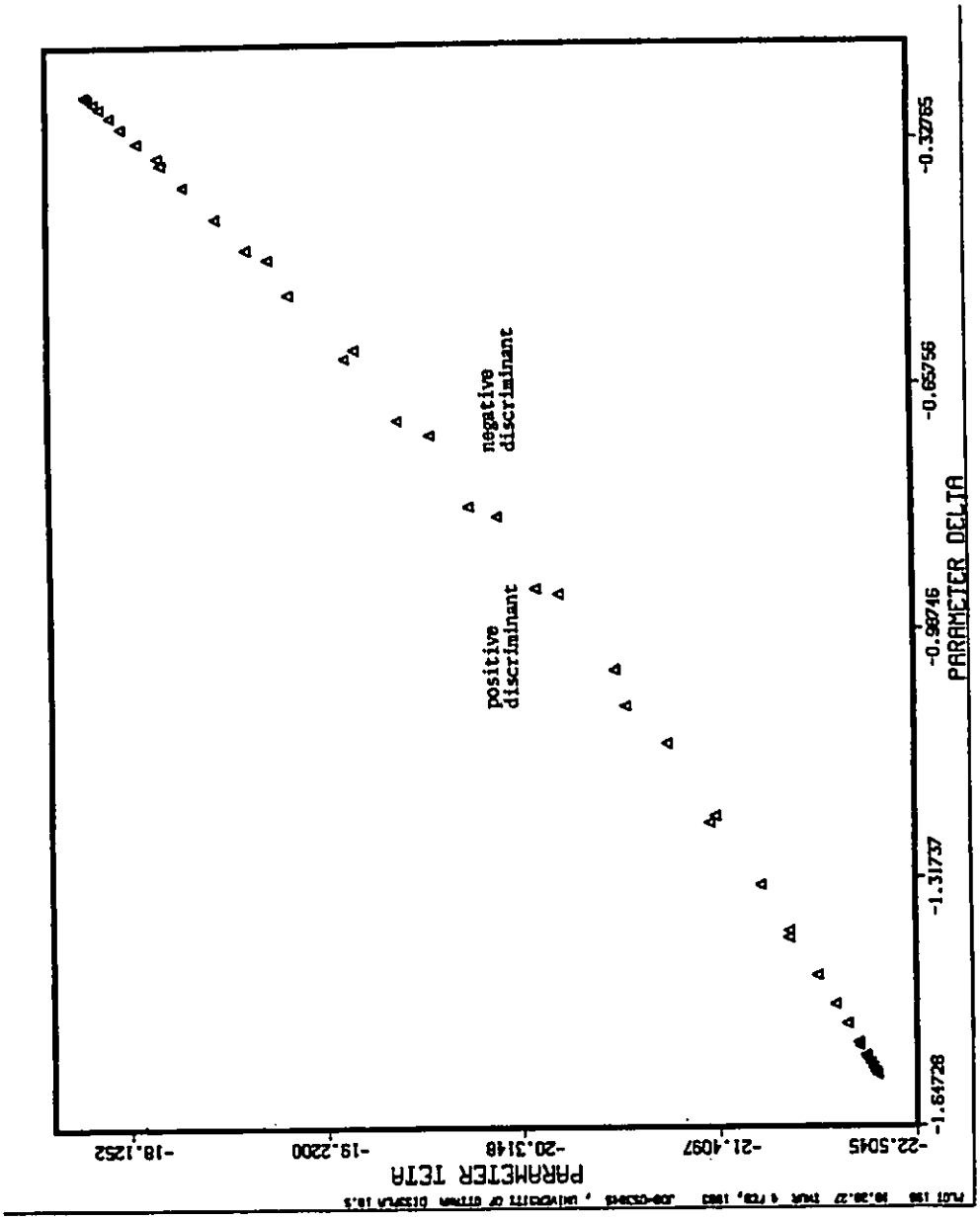

Figure 8.11: The Δ, Θ projection of the three-parameter continuation of the transcritical bifurcation TBP_3 in Fig. 7.4. Varying Θ between its extremal values (and beyond) makes the "wing" in Fig. 8.9 flap up and down (and beyond its horizontal position).

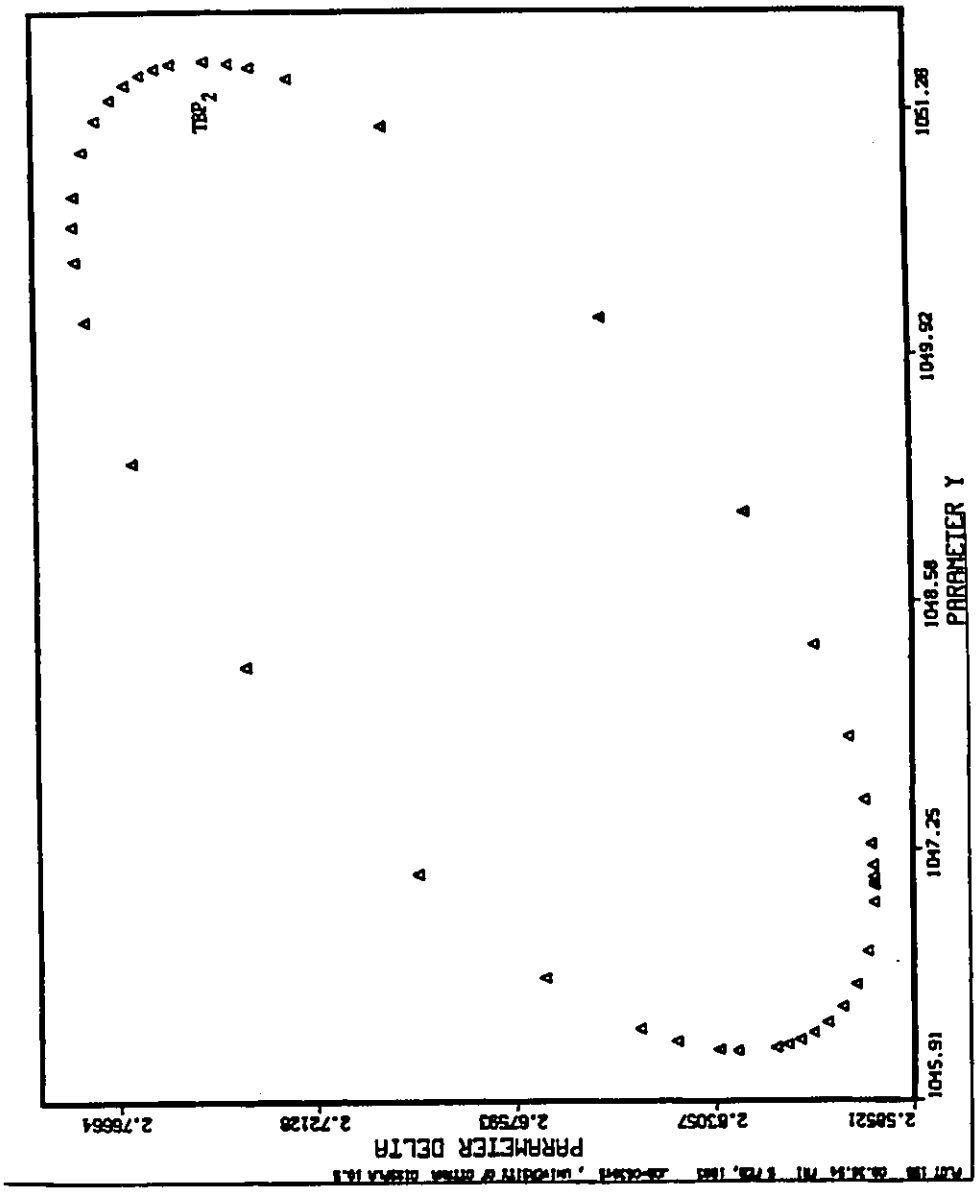

Figure 8.12: The transcritical bifurcation point TBP_2 in Fig. 7.4 was continued to reach $\Theta = -37.64468227$. This two-parameter figure shows that TBP_2 had already detached from the remaining of Fig. 7.4 and now lies on a closed loop shortly before degenerating to a single point.

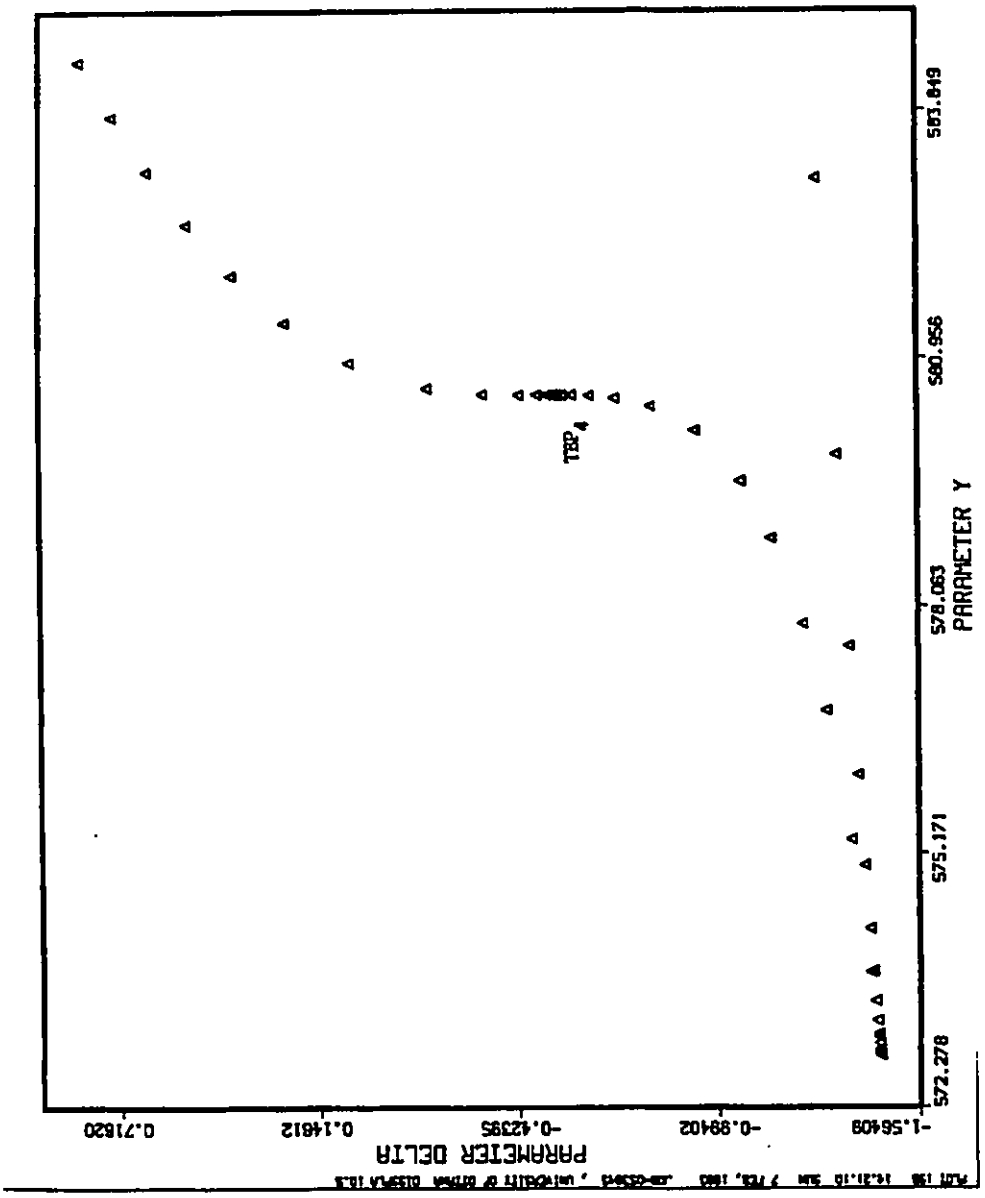

Figure 8.13: At $\Theta = -31.627587851$ the transcritical bifurcation point TBP_4 in Fig. 7.4 degenerates in that it coincides with an isola formation point to form a cubic saddle-node of quadratic saddle-nodes.

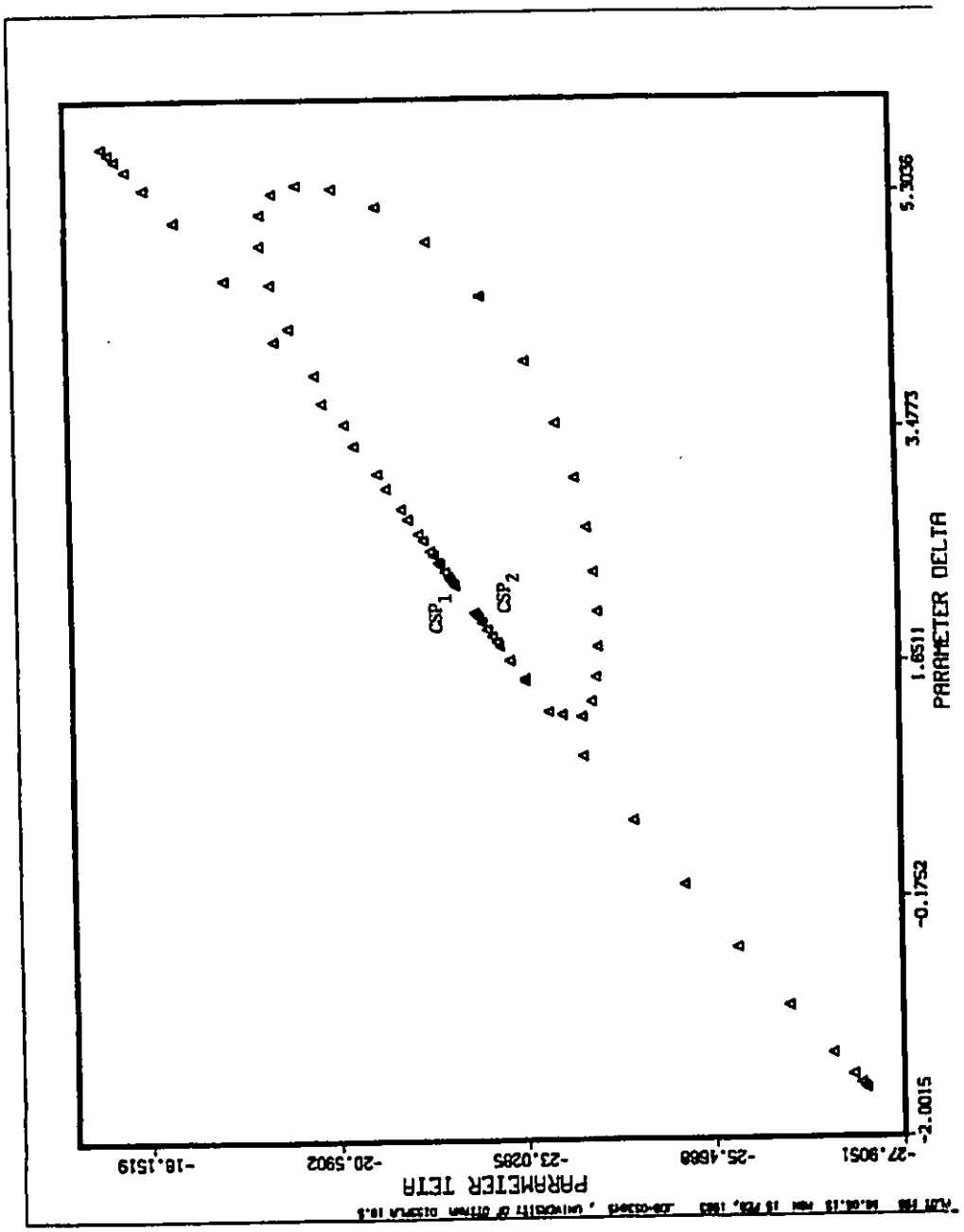

Figure 8.14: For $Y = 603.57908$ the Δ, Θ projection of the corresponding Fig. 7.4 shows that the cusp CSP_2 approaches a second one. At the precise bifurcation value the two cusps will join, annihilate each other and an isolated loop of saddle-nodes will detach.

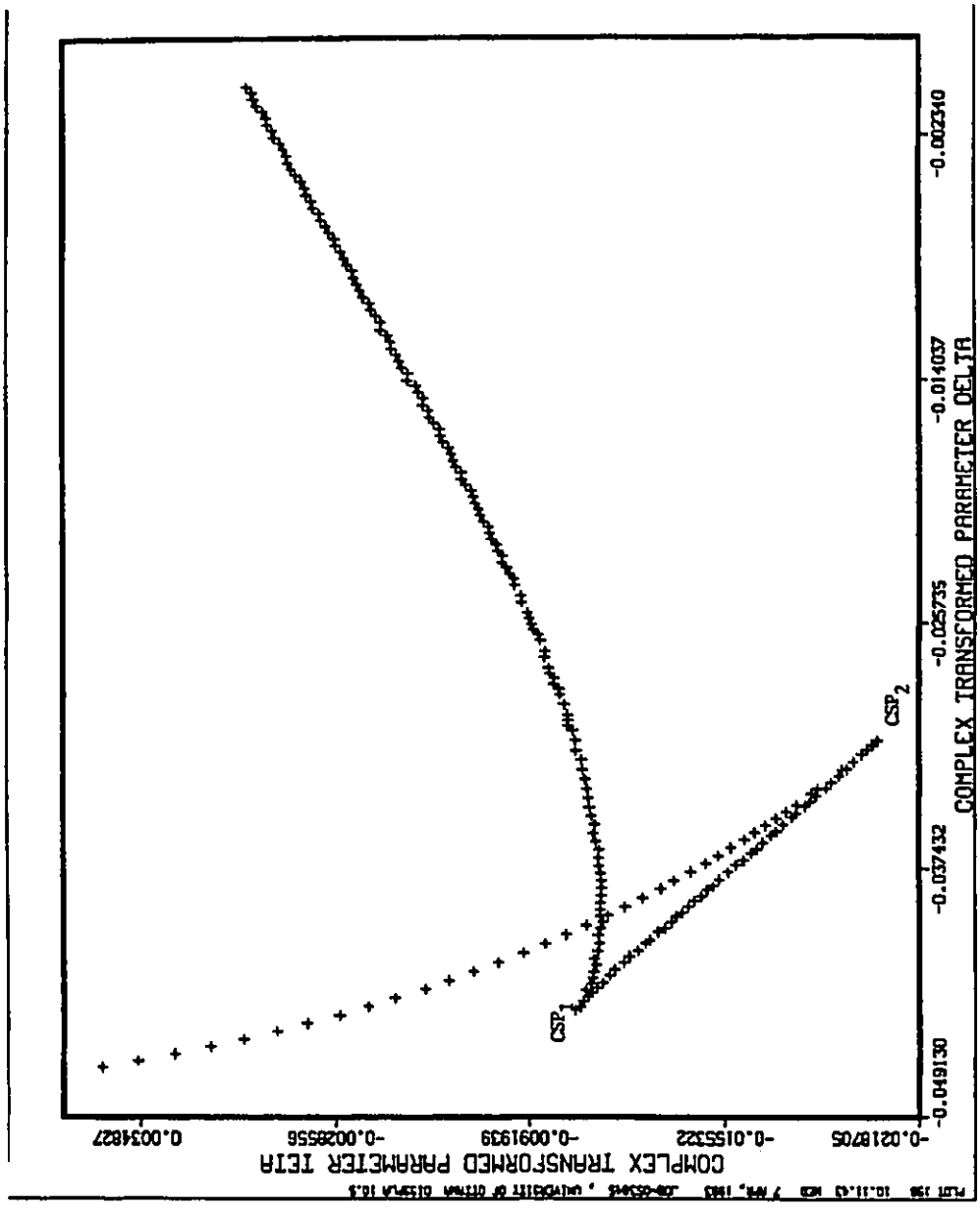

Figure 8.15: At $Y = 321.608092271$ the Δ, Θ projection of the corresponding Fig. 7.4 exhibits a swallow tail. Note that the Δ, Θ coordinates have been nonlinearly transformed to separate the cusps further and to spread the angles between the saddle-node branches.

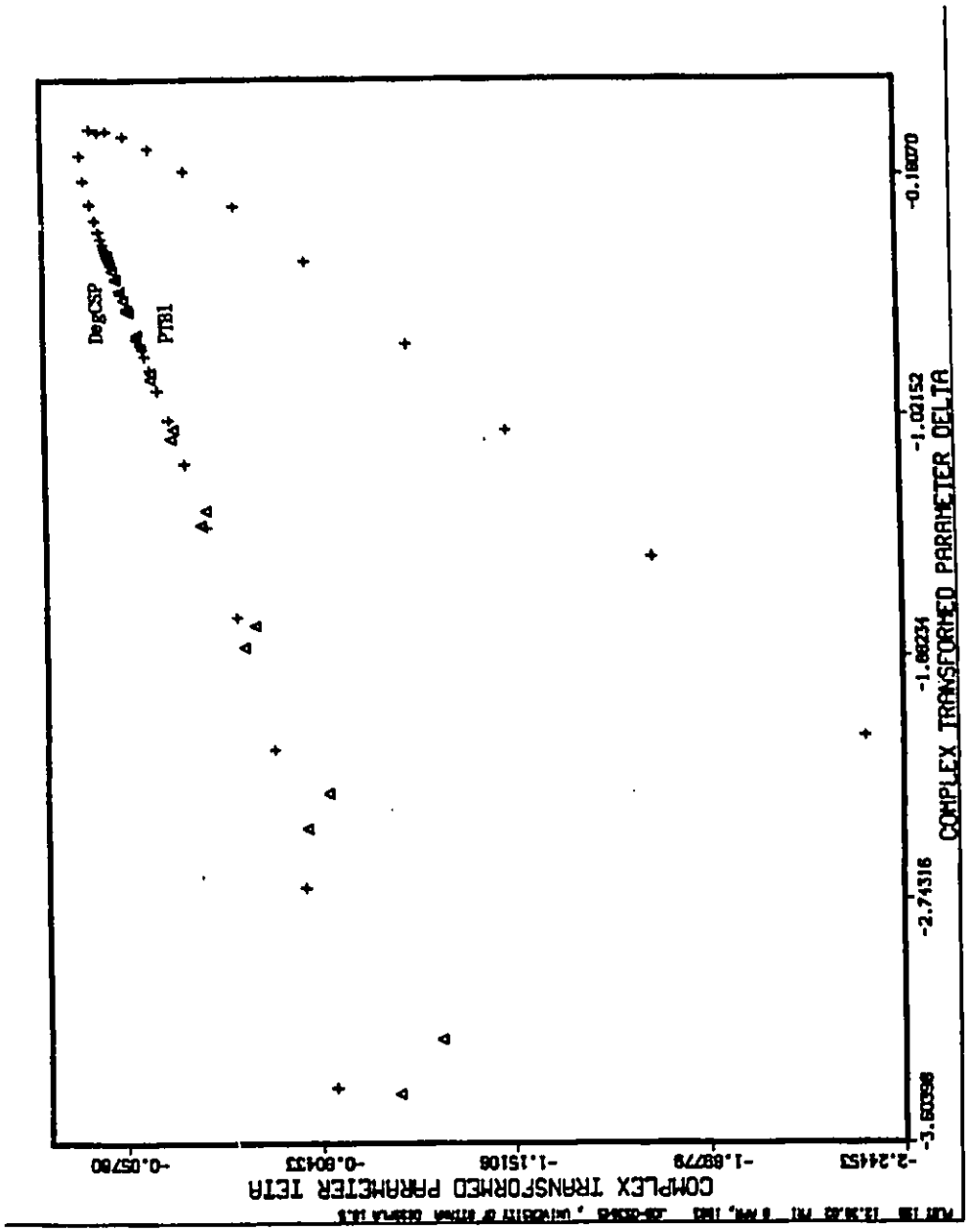

Figure 8.16: At $\Theta = -12.195457673$ the cusp concides with a periodic Takens–Bogdanov point. As in Fig. 8.15 the Y, Δ coordinates have been nonlinearly transformed.

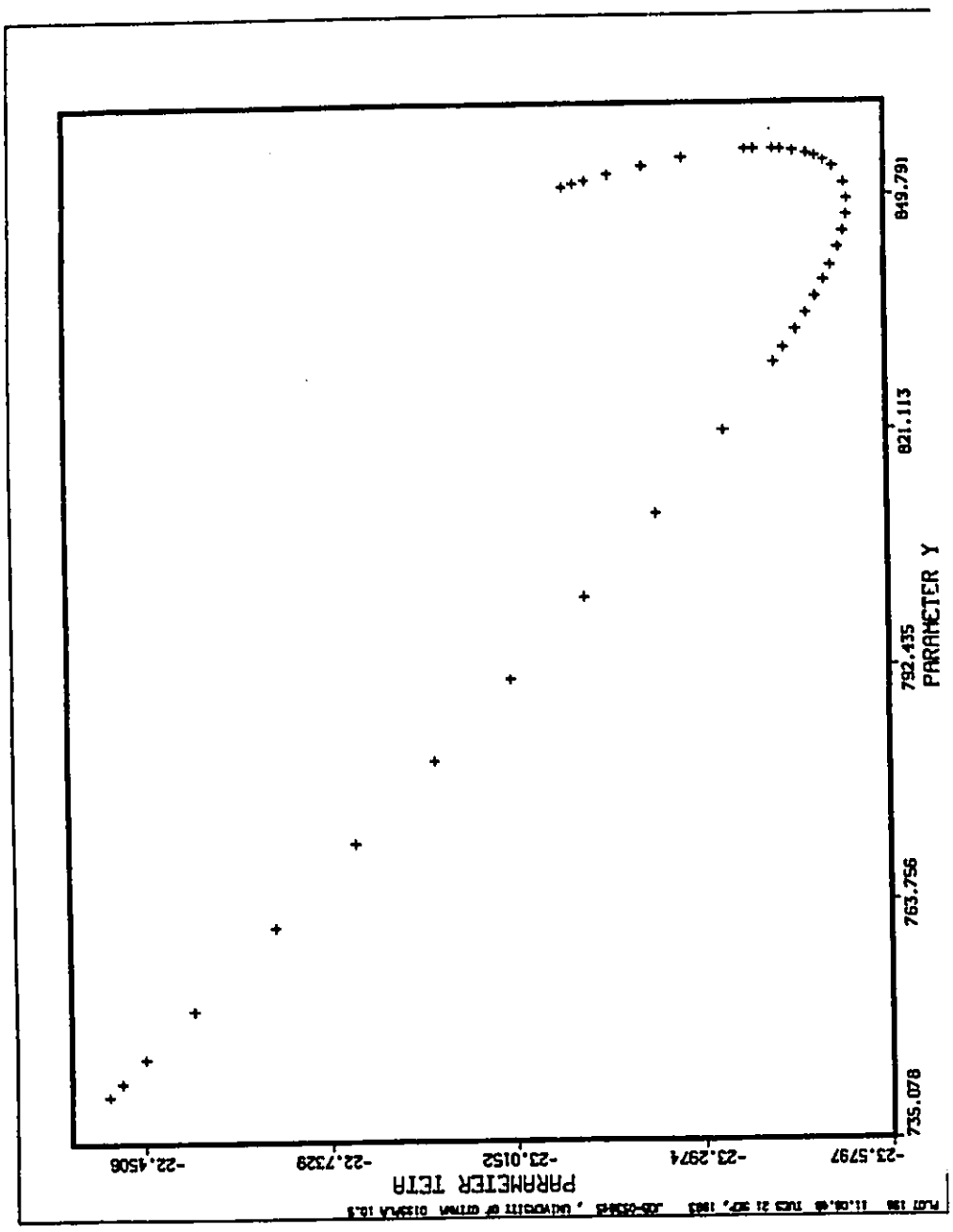

Figure 8.17: This enlargement of the projection of the three-parameter continuation of the degenerate period-doubling point $DPDB_2$ in Fig. 7.1 into Y, Θ parameter space shows saddle-nodes in Θ and Y.

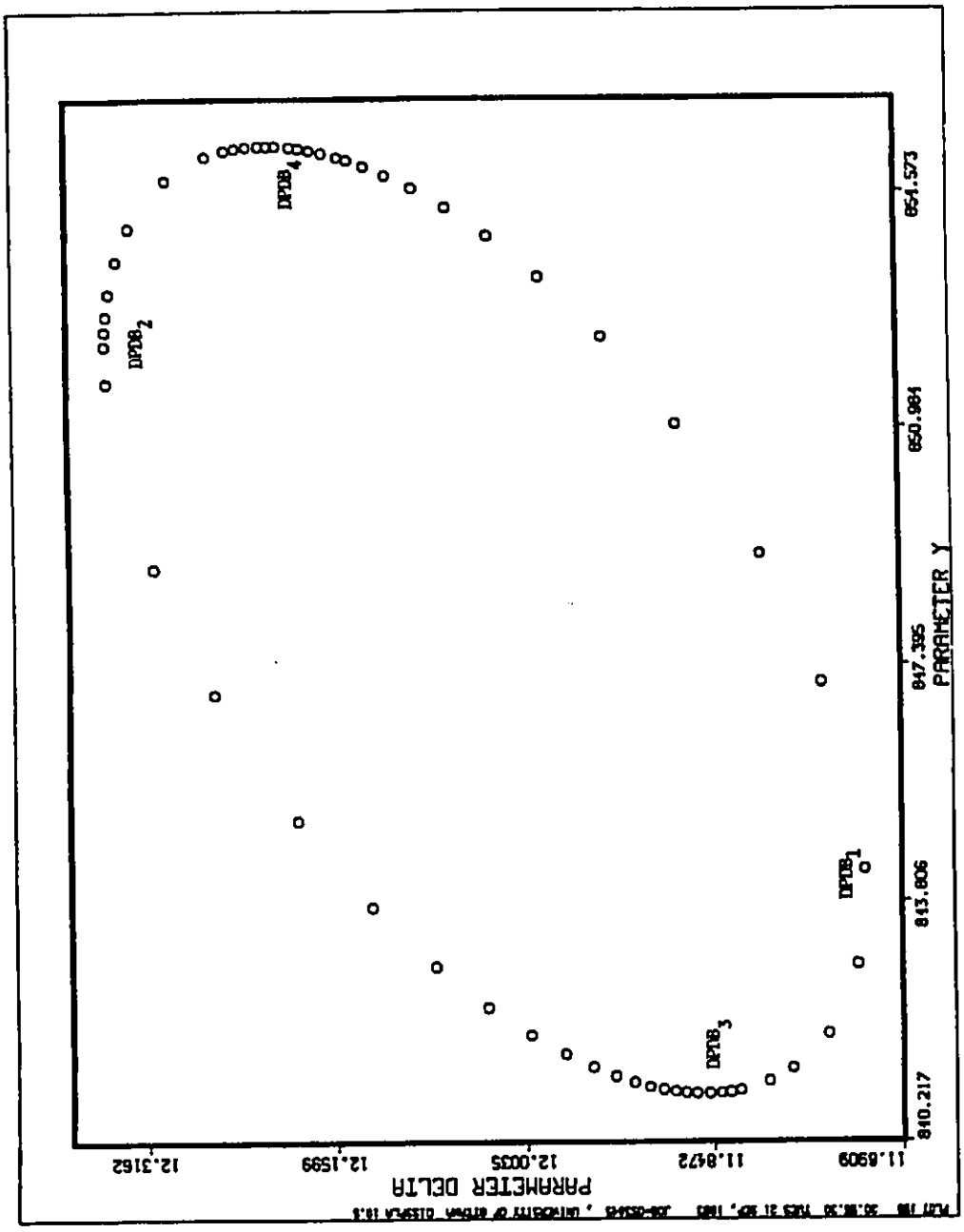

Figure 8.18: The period-doubling loop of Fig. 7.1 at $\Theta = -23.51179719$, shortly before it collapses to a single point at $\Theta \approx -23.5232$.

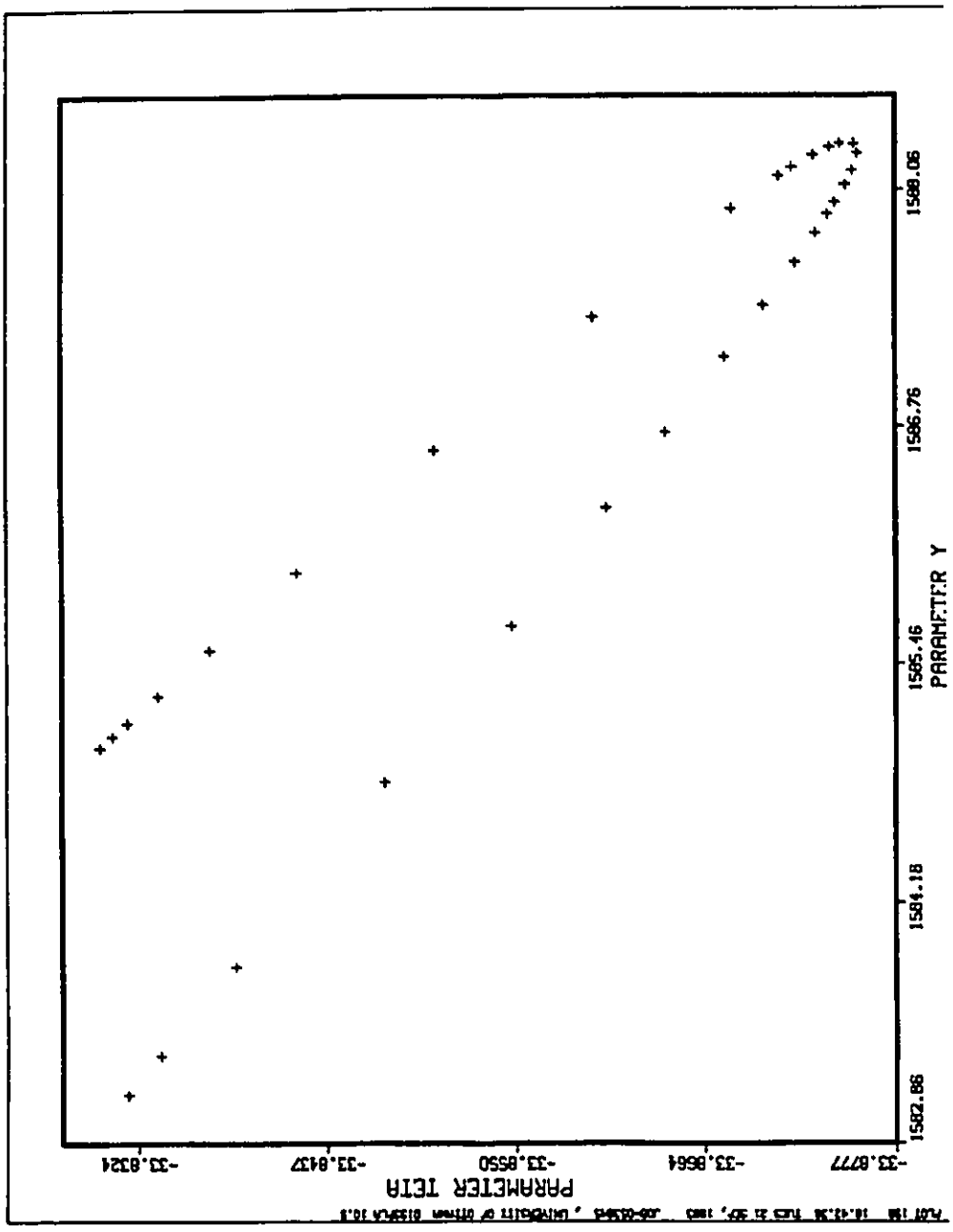

Figure 8.19: The enlargement of the projection of the three-parameter continuation of the degenerate secondary Hopf bifurcation DHF2b in Fig. 8.8 into Y, Θ space shows saddle-nodes in Θ and Y.

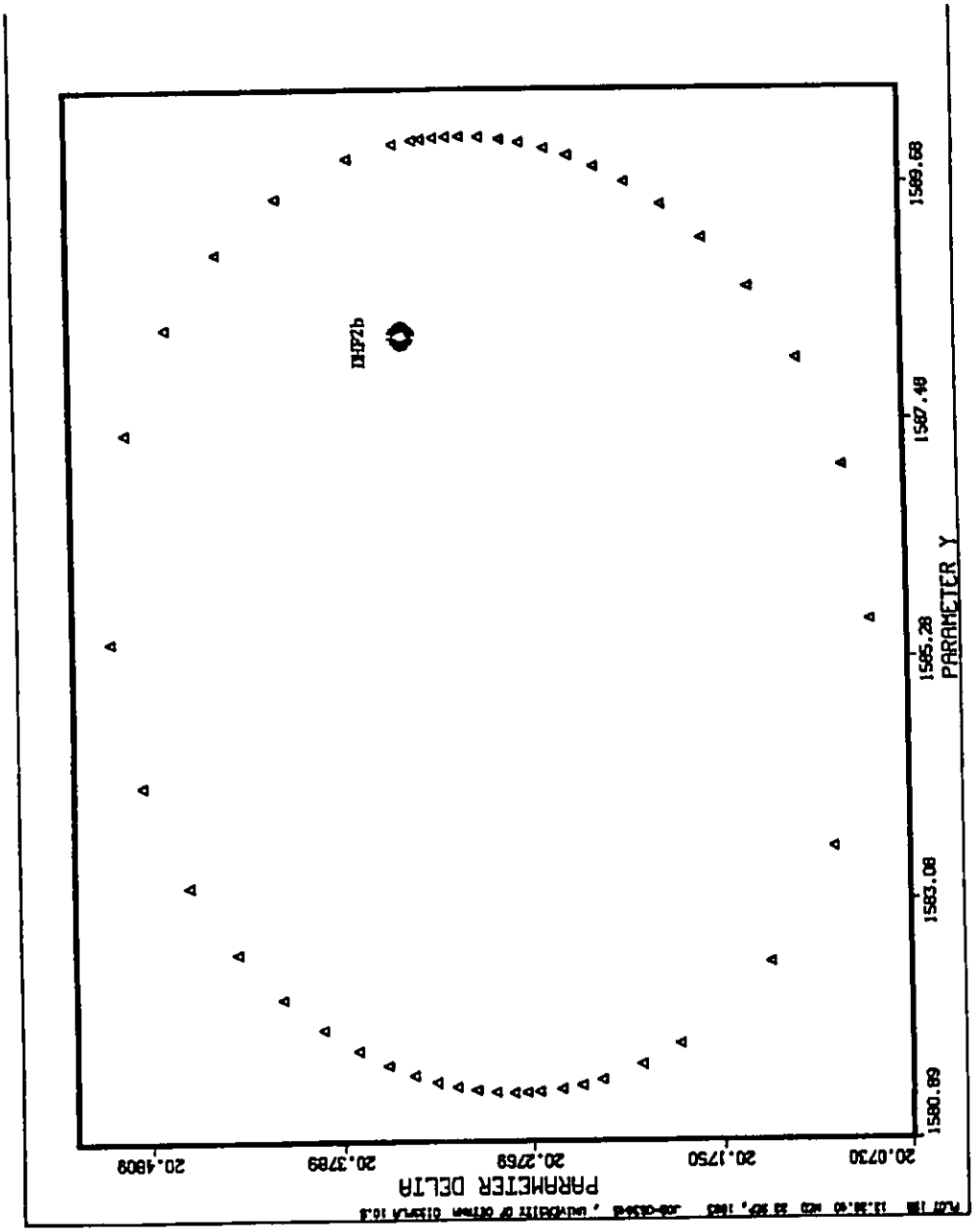

Figure 8.20: For $\Theta = -33.87543762$ the detached Hopf loop has almost shrunken to a single point. It is still surrounded by a saddle-node loop that in turn will shrink to a point and vanish at $\Theta = -33.878828571$. At this value of Θ the whole of Fig. 7.1 disappears.

Conclusion

This thesis was devoted to the numerical analysis and control of nonhyperbolic periodic solutions of autonomous ordinary differential equations.

In the first part, we reviewed theoretical formulae to characterize and distinguish among certain bifurcations involving periodic orbits. Therefore, we first introduced in great detail the pseudo-arclength continuation method as well as the Poincaré map and highlighted how, by a combination of these, one can follow a hyperbolic periodic orbit across a one-dimensional parameter space, thereby detecting and classifying its possible bifurcations. By successively augmenting this system with an additional equation which characterizes the previously found degeneracy, we set up various enlarged defining systems for the continuation of certain codimension-one and codimension-two bifurcations of periodic orbits across a two-dimensional, respectively three-dimensional, parameter space.

In the second part, we actually implemented these ideas in a collection of FORTRAN codes. Even though the formulae and systems used are well known, we think that it is only fair to say that they have mostly been applied to more or less simple and low dimensional maps. We are not aware of this approach in the context of higher order degenerate periodic solutions via the Poincaré map [167], [154]. In particular, we mention here our subroutine that evaluates the third derivative of the return time and, subsequently, of the Poincaré map with respect to phase space coordinates. We may say that our codes allow an analysis of nonhyperbolic periodic orbits as, for instance in [35], [46], [51], [54], [55], for equilibria.

Finally, in the third part, we applied the codes to periodic solutions of a two-level laser model. At first, we found that, as usual, theory and practice may differ a lot — several difficulties that can occur of course, by Murphy's law, did occur! However, after several improvements in important and subtle details were made, we believe

that our codes can successfully and efficiently treat the vast majority of problems in the class they are designed for. In fact, we computed the data of almost all of our figures in a single run.

Concerning the model, we must undoubtably conclude that it is first of all another instructive example of a relatively simple nonlinear model exhibiting exceedingly rich bifurcation patterns. Disregarding global bifurcations and bifurcations involving equilibria, our findings for certain periodic orbits alone reflect its complex dynamics. Moreover, our results in a three-dimensional parameter space largely extend the known equilibria behaviour. Additionally, with our new discovery of attractive invariant curves, we showed that the flow in this model can be governed by stationary, periodic, quasiperiodic or chaotic motions, where, indeed, several attractors of the same type may very well coexist. In particular, we have every reason to believe in the coexistence of attractive tori. We also found evidence for the existence of an attractive three-torus and doubled two-tori. These are certainly new and interesting results.

Even though all of the tori we found apparently exist only in a tiny interval about the supercritical secondary Hopf bifurcation, they might gain "volume" and more physical significance in a different parameter direction. Hence, one might think of them as initial values for a further torus continuation. This is an important point in a possible future extension of our work. Also, we have investigated only three of the occurring six model parameters. Additionally, considering global bifurcations, comparing the model with truncated versions of itself or with three-level laser models as in [51], and imposing stochastic forcing, ..., give plenty of room for further research. In fact, we claim that this model will most likely remain an "adventurous playground" for mathematicians and physicists to romp in.

From the mathematical point of view, we mention, in this context, the as yet unsatisfactory performance in branch switching when we continue degenerate period-doublings and/or degenerate secondary Hopf bifurcations. Perhaps, a deeper analysis of our combined approach based upon the Poincaré map with additionally imposed equations, the numerical differentiation only in the first iteration in the very first step, the secant predictor and Broyden's update for the corrector would reveal hidden properties that can be used in future improvements. Here one could also consider incorporating "automatic differentiation" and symbolic manipulation to ease and

speed up evaluation of higher order derivatives of the Poincaré map. At present time it is not clear to us to what extent (if at all) this is possible.

We would also like to briefly point out an extension of our work regarding optimizing a certain invariant function of the periodic solution. Suppose, for instance, we follow a periodic orbit γ which depends on the one-dimensional parameter $\xi \in \mathbb{R}$. Then, during continuation, we compute its period $T = T(\xi(s))$ and also, without any additional effort, the variation of T with respect to arclength as in (5.6.8):

$$\frac{\partial T}{\partial s}(x(s),\xi(s)) = T_x(x(s),\xi(s))U\dot{x}(s) + T_\xi(x(s),\xi(s))\dot{\xi}(s). \tag{8.5.4}$$

Thus and we may locate a (local) extremum in the period by observing a change in the sign of (8.5.4) and, subsequently, by applying the secant scheme. If the solution branch of the continuation leads to a closed loop, then we can even find global maxima and minima of the period. Let us then assume $T = T(\xi_0)$ is the maximal period of γ with respect to ξ. For $\lambda = (\xi,\nu) \in \mathbb{R}^2$ we can then free the second parameter $\nu \in \mathbb{R}$ and continue this extremal period by solving: $g(y_{N+1}) :=$

$$\begin{cases} S(\bar{x}_{N+1},\lambda_{N+1}) - \bar{x}_{N+1} & = 0 \\ \left(\frac{\partial T}{\partial x}(x_{N+1},\lambda_{N+1})\right)^T U\dot{\bar{x}}_{N+1} + \frac{\partial T}{\partial \xi}(x_{N+1},\lambda_{N+1})\dot{\xi}_{N+1} & = 0 \\ S_{\bar{x}}(\bar{x}_{N+1},\lambda_{N+1})\dot{\bar{x}}_{N+1} + S_{\bar{\xi}}(\bar{x}_{N+1},\lambda_{N+1})\dot{\xi}_{N+1} & = 0 \\ \|\dot{\bar{x}}_{N+1}\|^2 + |\dot{\xi}_{N+1}| - 1 & = 0 \\ (\bar{x}_{N+1} - \bar{x}_N)^T\dot{\bar{x}}_N + (\lambda_{N+1} - \lambda_N)^T\dot{\lambda}_N & \\ \quad + (\dot{\bar{x}}_{N+1} - \dot{\bar{x}}_N)^T\ddot{\bar{x}}_N + (\dot{\bar{\xi}}_{N+1} - \dot{\bar{\xi}}_N)\ddot{\bar{\xi}}_N - \delta s & = 0 \end{cases} \tag{8.5.5}$$

for the the next solution point $y_{N+1} = (\bar{x}_{N+1},\lambda_{N+1},\dot{\bar{x}}_{N+1},\dot{\bar{\xi}}_{N+1})$ on a branch of periodic orbits with extremal periods with respect to ξ. When solving (8.5.5) we may then watch for an extremal period with respect to $\lambda \in \mathbb{R}^2$ and continue this one by freeing a third variable. Since the limiting period for γ, when approaching a homoclinic or heteroclinic orbit, is $+\infty$, this idea could be useful in detecting global bifurcation.

A related system continues a maximal Floquet multiplier. Suppose the continuation in ξ yields a (simple and real) extremal Floquet multiplier $k_0 = k(\xi_0)$. Then, from (5.3.20):

$$\dot{\kappa}_0 = w^T(S_{\bar{x}\bar{x}}(\bar{x}_0,\xi_0)\dot{\bar{x}}_0 + S_{\bar{x}\xi}(\bar{x}_0,\xi_0)\dot{\xi}_0)v = 0. \tag{8.5.6}$$

We may therefore continue this occurrence, after having rescaled the time as in (5.5.6),

by solving: $g(y_{N+1}) :=$

$$\begin{cases} S(\overline{x}_{N+1}, \lambda_{N+1}) - \overline{x}_{N+1} & = 0 \\ \left(S_{\overline{x}}(\overline{x}_{N+1}, \lambda_{N+1}) - \beta_{N+1}\,\mathrm{id}\right) z_{N+1} - & \\ \left(S_{\overline{x}\overline{x}}(\overline{x}_{N+1}, \lambda_{N+1})\dot{\overline{x}}_{N+1} + S_{\overline{x}\xi}(\overline{x}_{N+1}, \lambda_{N+1})\dot{\xi}_{N+1}\right) v_{N+1} & = 0 \\ \left(S_{\overline{x}}(\overline{x}_{N+1}, \lambda_{N+1}) - \beta_{N+1}\,\mathrm{id}\right) v_{N+1} & = 0 \\ v_{N+1}^T v_N & = 0 \\ v_{N+1}^T z_{N+1} - 1 & = 0 \\ S_{\overline{x}}(\overline{x}_{N+1}, \lambda_{N+1})\dot{\overline{x}}_{N+1} + S_{\overline{\xi}}(\overline{x}_{N+1}, \lambda_{N+1})\dot{\xi}_{N+1} & = 0 \\ \|\dot{\overline{x}}_{N+1}\|^2 + |\dot{\xi}_{N+1}| - 1 & = 0 \\ (\overline{x}_{N+1} - \overline{x}_N)^T \dot{\overline{x}}_N + (\lambda_{N+1} - \lambda_N)^T \dot{\lambda}_N + (\beta_{N+1} - \beta_N)\dot{\beta}_N & \\ + (z_{N+1} - z_N)^T \dot{z}_N + (v_{N+1} - v_N)^T \dot{v}_N + (\dot{\overline{x}}_{N+1} - \dot{\overline{x}}_N)^T \ddot{\overline{x}}_N & \\ + (\dot{\xi}_{N+1} - \dot{\xi}_N)\ddot{\xi}_N - \delta s & = 0 \end{cases} \tag{8.5.7}$$

for $y_{N+1} = (\overline{x}_{N+1}, \lambda_{N+1}, \beta_{N+1}, z_{N+1}, v_{N+1}, \dot{\overline{x}}_{N+1}, \dot{\xi}_{N+1})$. Hence, we may systematically continue an unstable periodic orbit into a parameter region where it gains stability. Also, a very large Floquet multiplier can indicate a global bifurcation nearby and the continuation of (8.5.7) may be useful in finding the bifurcation value.

As a final outlook we propose a system that continues a special point of $\overline{x}$ of γ, namely one with extremal distance to an assumed equilibrium. For simplicity, let $f(0, \lambda) = 0$. For any periodic orbit γ with $x^* \in \gamma$ we can apply a simple iteration scheme to find $x_0 = \phi(t^*, x^*) \in \gamma$ such that $\|x_0\|_2 = \|\phi(0, x_0, \lambda)\|_2$ minimizes the distance to the origin, i.e. $< \phi(t^*, x^*), f(\phi(t^*, x^*)) >= 0$. Now free ξ and solve: $g(y_{N+1} :=$

$$\begin{cases} S(\overline{x}_{N+1}, \xi_{N+1}) - \overline{x}_{N+1} & = 0 \\ < \phi(t, U\overline{x} + x_{\text{orig}}, \xi_{N+1}), f(\phi(t, U\overline{x} + x_{\text{orig}}, \xi_{N+1}), \xi_{N+1}) > & = 0 \\ (\overline{x}_{N+1} - \overline{x}_N)^T \dot{\overline{x}}_N + (\xi_{N+1} - \xi_N)^T \dot{\xi}_N + (t_{N+1} - t_N)\dot{t}_N - \delta s & = 0 \end{cases} \tag{8.5.8}$$

with $x_{\text{orig}} = \phi(t_N, x_N, \xi_N)$ or $x_{\text{orig}} = x_N$ for $y_{N+1} = (\overline{x}_{N+1}, \xi_{N+1}, t_{N+1})$. Of course, if the fixed point(s) depend(s) on the parameters as well, then one must couple (8.5.8) with a system that continues equilibria. The continuation may then lead to the detection of bifurcations of periodic orbits involving equilibria, for instance Hopf bifurcations or, again, global bifurcations.

We hope that our results contribute to a better understanding of Haken's laser model and stimulate further investigations of it. We are especially curious about the

development of our tori — can one continue them into different parameter regions? What bifurcations will they undergo? And will they grow?

Moreover, we also hope that our codes get a second chance to prove their power and usefulness and that the problems we encountered will be attacked in the future. In particular, a fast and efficient evaluation of higher order derivatives of the Poincaré map should significantly push our ideas forward.

Anyway, we are sure that continuation methods will remain a fascinating subject — worthwhile to continue!

Bibliography

[1] R. H. Abraham and C. D. Shaw (1982) *Dynamics: The geometry of behavior, Part one, Periodic behavior*, Aerial Press, Santa Cruz, Ca.

[2] R. H. Abraham and C. D. Shaw (1983) *Dynamics: The geometry of behavior, Part two, Chaotic behavior*, Aerial Press, Santa Cruz, Ca.

[3] R. H. Abraham and C. D. Shaw (1985) *Dynamics: The geometry of behavior, Part three, Global behavior*, Aerial Press, Santa Cruz, Ca.

[4] E. Allgower and K. Georg (1990), *Numerical continuation methods*, Springer Series in Computational Mathematics **13**, Springer, Berlin.

[5] E. Allgower and P. H. Schmidt (1985), *An algorithm for piecewise-linear approximation of an implicitly defined manifold*, SIAM J. Numer. Anal. **22**, 322–346.

[6] M. Aluko and H.-C. Chang (1984), *PEFLOQ: An algorithm for the bifurcation analysis of periodic solutions of autonomous systems*, Computers and Chemical Engineering 8, 355–365.

[7] H. Amann (1983) *Gewöhnliche Differentialgleichungen*, de Gruyter, Berlin.

[8] O. Arino, D. Axelrod, and M. Kimmel (1992), *Mathematical population dynamics*, Dekker, New York, NY.

[9] D. Armbruster and R. Rand (1987), *Perturbation methods, bifurcation theory, and computer algebra*, Applied Mathematical Sciences, **65**, Springer-Verlag, New York, NY.

[10] V. Arnold (1983), *Geometrical methods in the theory of ordinary differential equations*, Springer, New York, NY.

[11] J. Aronson (1990), *Chaos: A SUN-based program for analyzing chaotic systems*, Computers in Physics 4(4), 408–417.

[12] A. Back, J. Guckenheimer, M. Myers, F. Wicklin, and P. Worfolk (1992), *DSTOOL: Computer assisted exploration of dynamical systems*, Notices of the Amer. Math. Soc. **39**(4), 303–309.

[13] H. Bai-Lin (1990), *Chaos II*, World Scientific, Singapore.

[14] G. L. Baker and J. P. Gollub (1990), *Chaotic dynamics — an introduction*, Cambridge University Press, Cambridge.

[15] R. E. Bank (1988), *PLTMG User's Guide - Edition 5.0*, University of California, La Jolla, CA.

[16] R. E. Bank and H. D. Mittelmann (1989), *Stepsize selection in continuation procedures and damped Newton's method*, in: H. D. Mittelmann and D. Roose (eds.) (1989), Continuation Techniques and Bifurcation Problems, Reprint from the Journal of Computational and Applied Mathematics Vol. 26 (1989) no. 1 and 2, **ISNM 92**, Birkhäuser, Basel, pp. 67–78.

[17] H.-U. Bauer (1991), *Nichtlineare Dynamik rückgekoppelter neuronaler Netze*, Reihe Physik Bd. 9, Verlag Harri Deutsch, Frankfurt/M.

[18] P. Bergé, Y. Pommeau, and C. Vidal (1984), Order and chaos: Towards a deterministic approach to turbulence, Wiley-Interscience, New York, NY.

[19] H. W. Broer, F. Dumortier, S. J. van Strien, and F. Takens (1991), *Finite-dimensional deterministic studies*, Noth-Holland, Amsterdam.

[20] H. W. Broer and F. Takens (eds.) (1992), *Geometry and analysis in nonlinear dynamics*, Proceedings of the workshop on chaotic dynamics and bifurcations held at the University of Groningen March 1989, Pitman Reaserch Notes in Mathematics Series **222**, Wiley, New York, NY.

[21] C. G. Broyden (1965), *A class of methods for solving nonlinear simultaneous equations*, Math. Comput. **19**, 577–593.

[22] T. Bessoir and A. Wolf (1991), *CHAOS SIMULATIONS, combined graphical and numerical methods for exploring deterministic chaos in both physical systems and mathematical models*, The American Institute of Physics in cooperation with the American Physical Society and the American Association of Physics Teachers, Woodbury, New York, NY.

[23] J. Carr (1983), *Applications of center manifold theory*, Applied Mathematical Sciences, **35**, Springer-Verlag, New York, NY.

[24] B. Chirikov and H. Flaschka (eds.) (1988), *Progress in chaotic dynamics*, North-Holland, Amsterdam.

[25] S. N. Chow and J. Hale (1982), *Methods of bifurcation theory*, Springer, New York, NY.

[26] L. O. Chua and T. S. Parker (1989), *Practical numerical algorithms for chaotic systems*, Springer-Verlag, Berlin.

[27] E. A. Coddington and N. Levinson (1955), *Theory of ordinary differential equations*, McGraw-Hill, New York, NY.

[28] Z. Coelho and E. Shiels (eds.) (1990), *Workshop on dynamical systems*, Proceedings of the workshop in honor of the sixty-fifth birthday of René Thom held in Trieste September 1988, Pitman Reaserch Notes in Mathematics Series **221**, Longman Scientific and Technical, Harlow, Wiley, New York.

[29] M. G. Crandall and P. H. Rabinowitz (1971), *Bifurcation fron simple eigenvalues*, J. Functional Analysis **8**, 321–340.

[30] J. Crutchfield, D. Farmer, N. Packard, R. Shaw, G. Jones, and R. J. Donnelly (1980), *Power spectral analysis of a dynamical system*, Phys. Lett. **76A**, 1–4.

[31] J. H. Curry (1979), *An algorithm for finding closed orbits*, in: Z. Nitecki and C. Robinson (eds.) Global Theory of Dynamical Systems, Lecture Notes in Mathematics **819**, Springer-Verlag, Berlin, pp. 111–120.

[32] G. Danglmayr and M. Wegelin (1991), *On a codimension-four bifurcation occurring in optical bistability*, in: Papers from the symposium held at the University of Warwick, Coventry 1988–1989, Lecture Notes in Mathematics **1463**, Springer, Berlin, pp. 107–121.

[33] G. Danglmayr and M. Wegelin (1990) *Determining an organizing center for passive optical systems*, in: D. Roose, B. De Dier, and A. Spence (eds.) Continuation and Bifurcations: Numerical Techniques and Applications, NATO ASI Series **C313**, Kluwer Academic Publishers, Dordrecht, pp. 335–348.

[34] B. De Dier (1989) *An investigation of a reaction-diffusion model exhibiting dissipative structures*, Ph.D. thesis, University of Leuven, Leuven.

[35] B. De Dier, D. Roose, and P. Van Rompay (1989), *Interaction between fold and Hopf curves leads to new bifurcation phenomena*, J. Comp. Appl. Math. **26**(1–2), 171–186.

[36] J. E. Dennis Jr. (1978), *A brief introduction to quasi-Newton methods*, in: Numerical Analysis, Proceedings of Symposia in Applied Mathematics **22**, Amer. Math. Soc., Providence, RI, pp. 19–53.

[37] J. E. Dennis and J. J. Moré (1977), *Quasi-Newton methods, motivation, and theory*, SIAM Review **19**, 46–89.

[38] P. Deuflhard (1979), *A stepsize control for continuation methods and its special application to multiple shooting techniques*, Numer. Math. **33**, 115-146.

[39] P. Deuflhard (1984), *Computation of periodic solutions of nonlinear ODE's*, BIT **24**, 456–466.

[40] R. L. Devaney (1992), *A first course in chaotic dynamical systems — theory and experiments*, Addison-Wesley, Redwood City, CA.

[41] J. Dieudonné (1960), *Foundations of modern analysis*, Academic Press, New York, NY.

[42] E. J. Doedel (1986), *AUTO: Software for continuation and bifurcation problems in ordinary differential equations*, Report Cal. Inst. of Techn., Pasadena, CA.

[43] E. J. Doedel (1992), *Private communication*, Department of Computer Science, Concordia University, Montreal.

[44] E. J. Doedel, A. D. Jepson, and H. B. Keller (1984), *Numerical methods for Hopf bifurcation and continuation of periodic solution paths*, in: R. Glowinski and

J.-L. Lions (eds.), Computing Methods in Applied Sciences and Engineering, North-Holland, Amsterdam.

[45] B. Ermentrout (1990), *Phase plane: The dynamical systems tool*, Brooks/Cole, New York, NY.

[46] W. W. Farr and R. Aris (1986), *Degenerate Hopf bifurcations in the CSTR with reactions* $A \rightarrow B \rightarrow C$, in: Proceedings of the 1986 Annual Semianr Held July 13–25, 1986, CMS Conference Proceedings, Vol. 8, Amer. Math. Soc., Providence, RI, pp. 397–418.

[47] U. Feudel and W. Jansen (1992), *CANDYS/QA: A software system for the qualitative analysis of nonlinear dynamical systems*, Int. J. Bifurcation and Chaos **2**(4), 773–794.

[48] M. Field and M. Golubitsky (1992), *Symmetry in chaos: a search for pattern in mathematics, art and nature*, Oxford University Press, Oxford.

[49] V. Franceschini (1983), *Bifurcation of tori and phase locking in a dissipative system of differential equations*, Physica D **6**, 285–304.

[50] E. Freire, E. Gamero, and E. Ponce (1990), *Symbolic computation and bifurcation methods*, in: D. Roose, B. De Dier, and A. Spence (eds.), Continuation and Bifurcations: Numerical Techniques and Applications, NATO ASI Series **C313**, Kluwer Academic Publishers, Dordrecht, pp. 105–122.

[51] W. Forysiak, J. V. Moloney and R. G. Harrison (1991), *Bifurcations of an optically pumped three-level laser model*, Physica D **53**, pp. 162–186.

[52] J. Froyland and K. Alfsen (1984), *Lyapunov-exponent spectra for the Lorenz model*, Phys. Rev. A. **29**(5), 2928–2931.

[53] J. Falzarano, A. Steindl, A. Troesch and H. Troger (1991), *Rolling motion of ships treated as bifurcation problems*, in: R. Seydel, F. W. Schneider, T. Küpper, and H. Troger (eds.) (1991), Bifurcation and Chaos: Analysis, Algorithms, Applications, **ISNM 97**, Birkhäuser, Basel, pp. 117–121.

[54] H. Gang, C.-Z. Ning, and H. Haken (1990), *Codimension-two bifurcations in single-mode optical bistable systems*, Phys. Rev. A **41**(5), 2702–2711.

[55] H. Gang, C.-Z. Ning, and H. Haken (1990), *Distribution of subcritical Hopf bifurcations and regular and chaotic attractors in optical bistable systems*, Phys. Rev. A **41**(7), 3975–3984.

[56] A. V. Gaponov-Grekhov and M. I. Rabinovich (1992), *Nonlinearities in action. Oscillations, Chaos, Structures, Fractals*, Springer, Berlin.

[57] K. Gatermann and A. Hohmann (1991), *SYMCON: Symbolic exploitation of symmetry in numerical pathfollowing*, Impact of Computing in Science and Engineering **3**, 330–365.

[58] J. Gleick (1987), *Chaos: Making a new science*, Viking, New York, NY.

[59] P. Glendinning (1992), *Robust new routes to chaos in differential equations*, Phys. Lett. A **168**(1), 40–46.

[60] P. Glendinning (1993), *Stability, instability and chaos*, Cambridge Texts in Applied Mathematics, **11**(1), Cambridge University Press, Cambridge.

[61] M. Golubitsky and D. G. Schaeffer (1985), *Singularities in bifurcation theory*, Applied Mathematical Sciences, **51**, Springer-Verlag, New York, NY.

[62] M. Golubitsky and D. G. Schaffer (1980), *A singularity theory approach to steady-state bifurcation theory*, in: R. L. Sternberg, A. J. Kalinowski, and J. S. Papadakis (eds.), Nonlinear Partial Differential Equations in Engineering and Applied Sciences, Dekker, New York, NY.

[63] R. Goodwin (1990), *Chaotic economic dynamics*, Clarendon Press, Oxford.

[64] D. Grobgeld, E. Pollak, and J. Zakrzewski (1991), *A numerical method for locating stable periodic orbits in chaotic systems*, Physica D **56**, 368–380.

[65] J. Guckenheimer (1991), *Computational environments for exploring dynamical systems*, Int. J. Bifurcation and Chaos **1**(2), 269–276.

[66] J. Guckenheimer and P. Holmes (1983), *Nonlinear oscillations, dynamical systems and bifurcations of vector fields*, Applied Mathematical Sciences, **42**, Springer-Verlag, New York, NY.

[67] J. Guckenheimer and S. Kim (1990), *The two-dimensional torus: numerical explorations and mathematical conjectures*, in: D. K. Campbell (ed.), CHAOS/XAOC Soviet-American Perspectives on Nonlinear Science, American Institute of Physics, New York, NY, pp.145–152.

[68] J. Guckenheimer and S. Kim (1990), *Kaos*, Mathematical Sciences Institute Technical Report, Cornell University, Ithaca, NY.

[69] H. Haken (1983), *Advanced synergetics*, Springer, Berlin.

[70] J. Hale and H. Koçak (1991), *Dynamics and bifurcations*, Texts in Applied Mathematics **3**, Springer-Verlag, New York, NY.

[71] P. Hartman (1982), *Ordinary differential equations*, Birkhäuser, Basel.

[72] B. D. Hassard (1980), *BIFOR2: Analysis of Hopf bifurcation in an ordinary differential system*, Computer Program, State University of New York at Buffalo, Buffalo, NY.

[73] M. E. Henderson (1987), *An application of complex bifurcation to a problem in computer graphics*, in: T. Küpper, R. Seydel, and H. Troger (1987), Bifurcation: Analysis, Algorithms, Applications, Proceedings of the Conference at the University of Dortmund, Aug. 18–22, 1986, **ISNM 79**, Birkhäuser, Basel, pp. 114–121.

[74] M. W Hirsch and S. Smale (1974), *Differential equations, dynamical systems and linear algebra*, Academic Press, New York, NY.

[75] M. Holodniok and M. Kubiček (1984), *DERPER: An algorithm for the continuation of periodic solutions in ordinary differential equations*, J. Comp. Phys. **55**(2), 254–267.

[76] M. Holodniok and M. Kubiček (1984), *Continuation of periodic solutions in ordinary differential equations — numerical algorithm and application to Lorenz model*, in: T. Küpper, H. D. Mittelmann, and H. Weber (1984), Numerical Methods for Bifurcation Problems, Proceedings of the Conference at the University of Dortmund, Aug. 22–26, 1983, **ISNM 70**, Birkhäuser, Basel, pp. 181–194.

[77] E. Hopf (1942), *Abzweigung einer periodischen Lösung von einer stationären Lösung eines Differentialsystems*, Berichte der Math. Phys. Akademie der Wissenschaften Leipzig **XCIV**, 1–22.

[78] J. Hubbard and B. West (1992), *MacMath, a dynamical systems software package for Macintosh*, Springer-Verlag, New York, NY.

[79] J. Hubbard and B. West (1991), *Differential equations: A dynamical systems approach, Part I: Ordinary differential equations*, Texts in Applied Mathematics **5**, Springer-Verlag, New York, NY.

[80] R. L. Ingraham (1992), *A survey of nonlinear dynamics "Chaos theory"*, World Scientific, River Edge, NJ.

[81] G. Iooss and D. D. Joseph (1980), *Elementary stability and bifurcation theory*, 2nd ed., Springer-Verlag, New York, NY.

[82] G. Iooss and W. F. Langford (1980), *Conjectures on the routes to turbulence via bifurcations*, in: R. H. G. Helleman (ed.) (1980), Nonlinear Dynamics, Annals of the New York Academy of Science **357**, New York Academy of Sciences, New York, NY, pp. 489–505.

[83] E. Isaacson and H. B. Keller (1966), *Analysis of numerical methods*, Wiley, New York, NY.

[84] E. A. Jackson (1990), *Perspectives of nonlinear dynamics*, Vol. 1 and Vol. 2, corrected reprint of the 1989 editions, Cambridge University Press, Cambridge.

[85] A. D. Jepson and H. B. Keller (1984), *Steady state and periodic solution paths: their bifurcations and computations*, in: T. Küpper, H. D. Mittelmann, and H. Weber (1984), Numerical Methods for Bifurcation Problems, Proceedings of the Conference at the University of Dortmund, Aug. 22–26, 1983, **ISNM 70**, Birkhäuser, Basel, pp. 219–246.

[86] A. D. Jepson and A. Spence (1984), *Singular points and their computation*, in: T. Küpper, H. D. Mittelmann, and H. Weber (1984), Numerical Methods for Bifurcation Problems, Proceedings of the Conference at the University of Dortmund, Aug. 22–26, 1983, **ISNM 70**, Birkhäuser, Basel, pp. 195–209.

[87] C. Kaas-Petersen (1989), *Technique to trace bifurcation points of periodic solutions*, in: P. L. Christiansen and R. D. Parmentier (eds.), Structure, Coherence and Chaos in Dynamical Systems, Proceedings in Nonlinear Science, Manchester University Press, Manchester, pp. 491–495.

[88] C. Kaas-Petersen (1987), *Computation, continuation, and bifurcation of torus solutions for dissipative maps and ordinary differential equations*, Pysica **25D**, 288–306.

[89] C. Kaas-Petersen (1987), *Path — User's guide*, Centre for Nonlinear Studies, University of Leeds, Leeds.

[90] H. B. Keller (1987), *Lectures on numerical methods in bifurcation problems*, Tata Institute of Fundamental Research, T.I.F.R.-I.I.Sc. Programme in Applications of Mathematics, Springer-Verlag, Berlin.

[91] H. B. Keller (1977), *Numerical solution of bifurcation and nonlinear eigenvalue problems*, in: P. H. Rabinowitz (ed.), Applications of Bifurcation Theory, Academic Press, New York, NY, pp. 359–384.

[92] H. B. Keller (1980), *Isolas and perturbed bifurcation theory*, in: R. L. Sternberg, A. J. Kalinowski, and J. S. Papadakis (eds.), Nonlinear Partial Differential Equations in Engineering and Applied Sciences, Dekker, New York, NY.

[93] H. B. Keller (1992), *A numerical approach to Hilbet's sixteenth problem*, in: D. S. Broomhead and A. Iserles (eds.) (1992), The Dynamics of Numerics and the Numerics of Dynamics, Proceedings of the IMA conference held at the University of Bristol, July 31th–Aug. 2nd, 1990, The Institute of Mathematics and its Applications Conference Series. New Series **34**, Clarendon Press, Oxford University Press, New York, NY, pp. 127–135.

[94] J. A. Kempf, R. K. Mehra, and E. F. Wood (1984), *BISTAB: A portable bifurcation and stability analysis package*, Appl. Math. Comp. **15**, 343–355.

[95] R. Ketzmerick (1992), *Chaos, fraktale Spektern und Quantendynamik in Halbleiter-Mikrostrukturen*, Verlag Harri Deutsch, Frankfurt/M.

[96] I. G. Kevrekidis, R. Aris, L. D. Schmidt, and S. Pelikan (1985), *Numerical computation of invariant circles of maps*, Physica D **16**, 243–251.

[97] A. I. Khibnik (1990) *LINLBF: A program for continuation and bifurcation analysis of equilibria up to codimension three*, in: D. Roose, B. De Dier, and A. Spence (eds.), Continuation and Bifurcations: Numerical Techniques and Applications, NATO ASI Series **C313**, Kluwer Academic Publishers, Dordrecht.

[98] J. H. Kim and J. Stringer (1992), *Applied chaos*, Wiley, New York, NY.

[99] U. Kirchgraber (1992), *Mathematik im Chaos. Ein Zugang auf dem Niveau der Sekundarstufe II*, Math. Semesterber. **39**(1), 43–68.

[100] M. Kleczka, W. Kleczka, and E. Kreuzer (1990), *Bifurcation analysis: a combined numerical and analytical approach*, in: D. Roose, B. De Dier, and A. Spence (eds.) Continuation and Bifurcations: Numerical Techniques and Applications, NATO ASI Series **C313**, Kluwer Academic Publishers, Dordrecht, pp. 123–138.

[101] W. Kleczka, E. Kreuzer, and C. Wilmers (1991), *Combined analytical-numerical analysis of nonlinear dynamical systems*, in: R. Seydel, F. W. Schneider, T. Küpper, and H. Troger (eds.) (1991), Bifurcation and Chaos: Analysis, Algorithms, Applications, **ISNM 97**, Birkhäuser, Basel, pp. 199–204.

[102] H. Koçak (1989), *Differential and difference equations through computer experiments (incl. Software package Phaser)*, 2nd ed., Springer-Verlag, New York. NY.

[103] M. Kubiček (1976), *Algorithm 502: Dependence of solutions of nonlinear systems on a parameter*, ACM Trans. of Math. Software **2**, 98–107.

[104] M. Kubiček and M. Marek (1983), *Computational methods in bifurcation theory and dissipative structures*, Springer-Verlag, New York, NY.

[105] M. Kubiček, I. Stuchl, and M. Marek (1982), *"Isolas" in solution diagrams*, J. Comp. Phys. **48**, 106–112.

[106] M. Küper (1987), *External forcing in a glycolytic model*, in: T. Küpper, R. Seydel, and H. Troger (1987), Bifurcation: Analysis, Algorithms, Applications, Proceedings of the Conference at the University of Dortmund, Aug. 18–22, 1986, **ISNM 79**, Birkhäuser, Basel, pp. 172–176.

[107] T. Küpper, H. D. Mittelmann, and H. Weber (1984), *Numerical methods for bifurcation problems*, Proceedings of the Conference at the University of Dortmund, Aug. 22–26, 1983, **ISNM 70**, Birkhäuser, Basel.

[108] T. Küpper, R. Seydel, and H. Troger (1987), *Bifurcation: Analysis, Algorithms, Applications* , Proceedings of the Conference at the University of Dortmund, Aug. 18–22 1986, **ISNM 79**, Birkhäuser, Basel.

[109] W. F. Langford (1984), *Numerical studies of torus bifurcations*, in: T. Küpper, H. D. Mittelmann, and H. Weber (1984), Numerical Methods for Bifurcation Problems, Proceedings of the Conference at the University of Dortmund, Aug. 22–26, 1983, **ISNM 70**, Birkhäuser, Basel, pp. 285–295.

[110] W. Lauterborn and J. Holzfuss (1991), *Acoustic chaos*, Int. J. Bifurcation and Chaos **1**(1), 13–26.

[111] A. J. Lichtenberg and M. A. Lieberman (1992), *Regular and chaotic dynamics*, 2nd ed., Applied Mathematical Sciences, **38**, Springer-Verlag, New York, NY.

[112] W. Liebert (1991), *Chaos und Herzdynamik*, Reihe Physik Bd. **4**, Verlag Harri Deutsch, Frankfurt/M.

[113] E. Lindtner, A. Steindl, and H. Troger (1989), *Generic one-parameter bifurcations in the motion of a simple robot*, in: H. D. Mittelmann and D. Roose (eds.) (1989), Continuation Techniques and Bifurcation Problems, Reprint from the Journal of Computational and Applied Mathematics, Vol. 26 (1989), nos. 1 and 2, **ISNM 92**, Birkhäuser, Basel, pp. 199–218.

[114] A. A. Lokshin and E. A. Sagomonyan (1992), *Nonlinear waves in inhomogeneous and hereditary media*, Springer, Berlin.

[115] L. A. Lugiato and L. M. Narducci (1985), *Single-mode and multimode instabilities in lasers and related optical systems*, Phys. Rev. A **32**, 1576–1587.

[116] L. A. Lugiato and L. M. Narducci (1988), *Optical instabilities*, in: G. Caglioti, H. Haken, and L. A. Lugiato (eds.) (1988), Synergetics and Dynamic Instabilities, North-Holland, Amsterdam, pp. 51–71.

[117] E. N. Lorenz (1963), *Deterministic nonperiodic flow*, J. Atmospheric Sci. **20**, 130–141.

[118] J. L. McCanley (1993), *Chaos, dynamics and fractals. An algorithmic approach to deterministic chaos*, Cambridge Nonlinear Science Series **3**, Cambridge University Press, Cambridge.

[119] M. Marek and I. Schreiber (1989) *Chaotic behaviour of deterministic dissipative systems*, Cambridge University Press, Cambridge, Academia Press, Prague.

[120] J. E. Marsden and M. McCracken (1976), *The Hopf bifurcation and its applications*, Applied Mathematical Sciences, **19**, Springer-Verlag, New York, NY.

[121] S. B. Margolis and B. J. Matkowsy (1983), *Nonlinear stability and bifurcation in the transition from laminar to turbulent flame propagation*, Combustion Science and Technology **34**, 45–77.

[122] A. I. Mees (1981), *Dynamics of feedback systems*, Wiley, New York, NY.

[123] R. G. Melhelm and W. Rheinboldt (1982), *A comparison of methods for determining turning points of nonlinear equations*, Computing **29**, 201–226.

[124] R. Menzel and G. Pönisch (1984), *A quadratically convergent method for computing simple singular roots and its application to determining simple bifurcation points*, Computing, **32**, 127–138.

[125] R. Meyer-Spasche and H. B. Keller (1985), *Some bifurcation diagrams for Taylor vortex flows*, Phys. Fluids, **28**(5), 1248–1252.

[126] H. D. Mittelmann and D. Roose (eds.) (1989), *Continuation techniques and bifurcation problems*, Reprint from the Journal of Computational and Applied Mathematics, Vol. 26 (1989) nos. 1 and 2, **ISNM 92**, Birkhäuser, Basel.

[127] H. D. Mittelmann and H. Weber (1980), *Numerical methods for bifurcation problems — a survey and classification*, in: H. D. Mittelmann and H. Weber (eds.) (1980), Bifurcation Problems and Their Numerical Solution, Workshop on bifurcation problems and their numerical solution, Dortmund, Jan. 15–17, 1980, **ISNM 54**, Birkhäuser, Basel, pp. 1–45.

[128] F. C. Moon (1992), *Chaotic and fractal dynamics: an introduction for applied scientists and engineers*, Wiley, New York, NY.

[129] G. Moore and A. Spence (1980), *The calculation of turning points of nonlinear equations*, SIAM J. Numer. Anal. **17**, 567–576.

[130] I. Moret (1992), *A method for the computation of nonsimple turning points corresponding to cusps*, J. Comput. Appl. Math. **40**(3), pp. 269–284.

[131] T. Nagashima and I. Shimada (1979), *A numerical approach to ergodic problems of dissipative dynamical systems*, Prog. Theor. Phys. **61**(6), 1605–1616.

[132] K. Nakamura (1993), *Quantum chaos. A new paradigm of nonlinear dynamics*, Cambridge Nonlinear Science Series **2**, Cambridge University Press, Cambridge.

[133] K.-G. Nolte (1991), *Universal appearance of periodic orbits in the Lorenz equations*, C. R. Math. Rep. Acad. Sci. Canada, **XIII**(4), 125–130.

[134] K.-G. Nolte (1990), *Co-existing periodic attractors in the Lorenz equations*, C. R. Math. Rep. Acad. Sci. Canada, **XII**(6), 229–234.

[135] L. A. Orozco, H. J. Kimble, A. T. Rosenberger, L. A. Lugiato, M. L. Asquini, M. Brambilla and L. M. Narducci (1989), *Single-mode instability in optical bistability*, Phys. Rev. A **39**, 1235–1252.

[136] J. M. Ortega and W. Rheinboldt (1970), *Iterative solution of non-linear equations in several variables*, Academic Press, New York, NY.

[137] A. M. Ostrowski (1966), *Solutions of equations and systems of equations*, 2nd ed., Academic Press, New York, NY.

[138] D. Ostrusska (1992), *Systemdynamik nichtlinearer Marktreaktionsmodelle*, Physica Verlag, Heidelberg.

[139] J. Palis and F. Takens (1993) *Hyperbolicity, stability and chaos at homoclinic bifurcations*, Cambridge University Press, Cambridge.

[140] S. Parker and L. O. Chua (1987), *INSITE: A software toolkit for the analysis of nonlinear dynamical systems*, Proceedings of the IEEE, **75**(8), 1081–1089, and: INSITE Software, P.O. Box 9662, Berkeley, CA 94709-9662.

[141] T. S. Parker and L. O. Chua (1987), *Chaos: a tutorial for engineers*, Proceedings of the IEEE, **75**(8), 982–1008.

[142] K. Pawelzik (1991), *Nichtlineare Dynamik und Hirnaktivität*, Reihe Physik Bd. **6**, Verlag Harri Deutsch, Frankfurt/M.

[143] L. Perko (1991), *Differential equations and dynamical systems*, Texts in Applied Mathematics **7**, Springer-Verlag, New York, NY.

[144] G. Pönisch and H. Schwetlick (1981), *Computing turning points of curves implicitly defined by nonlinear equations depending on a parameter*, Computing **26**, 107–121.

[145] E. J. Ponce-Nuñez and E. Gamero (1991), *Generating Hopf bifurcation formula with MAPLE*, in: R. Seydel, F. W. Schneider, T. Küpper, and H. Troger (eds.) (1991), Bifurcation and Chaos: Analysis, Algorithms, Applications, **ISNM 97**, Birkhäuser, Basel, pp. 295–300.

[146] P. Rabinowitz (ed.) (1970), *Numerical methods for nonlinear algebraic equations*, Gordon and Breach, London.

[147] S. N. Rasband (1990), *Chaotic dynamics of nonlinear systems*, Wiley, New York, NY.

[148] E. Reithmeier (1991), *Periodic solutions of nonlinear dynamical systems: Numerical computation, stability, bifurcation and transition to chaos*, Lecture Notes in Mathematics, **1483**, Springer, Berlin.

[149] W. Rheinboldt (1986), *Numerical analysis of parametrized nonlinear equations*, University of Arkansas Lecture Notes in the Mathematical Sciences, **7**, Wiley-Interscience, New York, NY.

[150] W. Rheinboldt (1987), *On a moving frame algorithm and the triangulation of equilibrium manifolds*, in: T. Küpper, R. Seydel, and H. Troger (1987), Bifurcation: Analysis, Algorithms, Applications, Proceedings of the Conference at the University of Dortmund, Aug. 18–22, 1986, **ISNM 79**, Birkhäuser, Basel, pp. 256–267.

[151] W. Rheinboldt (1981), *Numerical analysis of continuation methods for nonlinear structural problems*, Computers & Structures **13**, 103–113.

[152] W. Rheinboldt and J. Burkhardt (1983), *A locally parametrized continuation process*, ACM Trans. Math. Software **9**, 215–235.

[153] W. Rheinboldt, D. Roose, and R. Seydel (1990), *Aspects of continuation software*, in: D. Roose, B. De Dier, and A. Spence (eds.), Continuation and Bifurcations: Numerical Techniques and Applications, NATO ASI Series **C313**, Kluwer Academic Publishers, Dordrecht, pp. 261–268.

[154] D. Roose (1993), *Private communication*, Department of Computer Science, Katholieke Universiteit Leuven, Leuven, Leuven.

[155] D. Roose (1987), *Numerical computation of origins for Hopf bifurcation in a two-parameter problem*, in: T. Küpper, R. Seydel, and H. Troger (1987), Bifurcation: Analysis, Algorithms, Applications, Proceedings of the Conference at the University of Dortmund, Aug. 18–22, 1986, **ISNM 79**, Birkhäuser, Basel, pp. 268–276.

[156] D. Roose (1985), *An algorithm for the computation of Hopf bifurcation points in comparison with other methods*, J. Comput. Appl. Math. **12/13**, 517–529.

[157] D. Roose and R. Caluwaerts (1984), *Direct methods for the computation of a nonsimple turning point corresponding to a cusp*, in: T. Küpper, H. D. Mittelmann, and H. Weber (1984), Numerical Methods for Bifurcation Problems, Proceedings of the Conference at the University of Dortmund, Aug. 22–26 1983, **ISNM 70**, Birkhäuser, Basel, pp. 426–440.

[158] D. Roose and V. Hlavacek (1985), *A direct method for the computation of Hopf bifurcation points*, SIAM J. Appl. Math. **45**, 879–894.

[159] D. Roose and R. Piessens (1985), *Numerical computation of nonsimple turning points and cusps*, Numer. Math. **46**(2), 189–211.

[160] P. Rosendorf, J. Orsag, I. Schreiber, and M. Marek (1989), *Interactive system for studies in nonlinear dynamics*, Prague Institute of Chemical Technology, Prague.

[161] D. Ruelle (1980), *Stange attractors*, Mathematical Intelligencer **2**, 126–137.

[162] H. Schuster (ed.) (1991), *Nonlinear dynamics and neuronal networks*, Proceedings of the 63rd W.E. Heraeus Seminar Friedrichsdorf 1990, Verlag Chemie, Weinheim.

[163] R. Seydel (1988) *From equilibrium to chaos: practical bifurcation and stability analysis*, Elsevier, New York, NY.

[164] R. Seydel (1983), *BIFPACK: A program package for calculating bifurcations*, Report Dept. of Mathematics, State University of New York at Buffalo, Buffalo, NY.

[165] R. Seydel (1991), *Tutorial on continuation*, Int. J. Bifurcation and Chaos **1**(1), 3–11.

[166] R. Seydel (1984), *A continuation algorithm with step control*, in: T. Küpper, H. D. Mittelmann, and H. Weber (1984), Numerical Methods for Bifurcation Problems, Proceedings of the Conference at the University of Dortmund, Aug. 22–26, 1983, **ISNM 70**, Birkhäuser, Basel, pp. 480–494.

[167] R. Seydel (1993), *Private communication*, Abteilung für Angewandte Mathematik, Universität Ulm, Ulm.

[168] R. Seydel (1991), *On detecting stationary bifurcations*, Int. J. Bifurcation and Chaos **1**(2), 335–337.

[169] R. Seydel (1983), *Berechnung von periodischen Lösungen bei gewöhnlichen Differentialgleichungen*, ZAMM **63** T98–T99.

[170] R. Seydel, F. W. Schneider, T. Küpper and H. Troger (eds.) (1991), *Bifurcation and chaos: Analysis, algorithms, applications*, **ISNM 97**, Birkhäuser, Basel.

[171] K. Shiraiawa (ed.) (1991), *Dynamical systems and related topics*, Proceedings of the International Conference Held in Nagoya, Sept. 3–7, 1990, Advanced Series in Dynamical Systems **9**, World Scientific, River Edge, NJ.

[172] Y. G. Sinai (ed.) (1991), *Dynamical systems*, Advanced Series in Nonlinear Dynamics **1**, World Scientific, Teaneck, NJ.

[173] C. Sparrow (1982), *The Lorenz equations: Bifurcations, chaos, and strange attractors*, Applied Mathematical Sciences, **41**, Springer-Verlag, New York, NY.

[174] A. Spence, K. A. Cliffe, and A. D. Jepson (1989), *A note on the calculation of paths of Hopf bifurcations*, in: H. D. Mittelmann and D. Roose (eds.) (1989), Continuation Techniques and Bifurcation Problems, Reprint from the Journal of Computational and Applied Mathematics, Vol. 26 (1989) nos. 1 and 2, **ISNM 92**, Birkhäuser, Basel, pp. 125–132.

[175] A. Spence and A. D. Jepson (1984), *The numerical calculation of cusps, bifurcation points and isola formation points in two parameter problems*, in: T. Küpper, H. D. Mittelmann, and H. Weber (1984), Numerical Methods for Bifurcation Problems, Proceedings of the Conference at the University of Dortmund, Aug. 22–26, 1983, **ISNM 70**, Birkhäuser, Basel.

[176] A. Spence and B. Werner (1982), *Non-simple turning points and cusps*, IMA J. Numer. Anal. **2**, 413–427.

[177] W. H. Steeb and A. Kunick (1986), *Chaos in dynamischen Systemen*, B.I.-Wissenschaftsverlag, Mannheim.

[178] A. Steindl and H. Troger (1991), *Nonlinear stability and bifurcation theory*, Springer, Wien.

[179] I. Stewart (1992) *Bifurcation theory old and new*, in: D. S. Broomhead and A. Iserles (eds.) (1992), The Dynamics of Numerics and the Numerics of Dynamics, Proceedings of the IMA conference held at the University of Bristol, July 31th–Aug. 2nd, 1990, The Institue of Mathematics and its Applications Conference Series. New series **34**, The Clarendon Press, Oxford University Press, New York, NY, pp. 31–67.

[180] H. B. Stewart and J. M. T. Thompson (1986), *Nonlinear dynamics and chaos: Geometrical methods for engineers and scientists*, Wiley, Chichester.

[181] H. L. Swinney and J. P. Gollub (eds.) (1981), *Hydrodynamic instabilities and the transition to turbulence*, Springer, Berlin.

[182] G. Tsarouhas and J. Pade (1986), *The Hopf bifurcation in the Lorenz model by the 2-timing method*, Physica **138A**, 507–517.

[183] N. V. Tu (1992), *Dynamical systems. An introduction with applications in economics and biology*, Springer, Berlin.

[184] M. Urabe (1967), *Nonlinear autonomous oscillations*, Academic Press, New York, NY.

[185] Y.-H. Wan (1978), *Computation of the stability condition for the Hopf bifurcation of diffeomorphisms on* $\mathbb{R}^2$, SIAM J. Appl. Math. **34**(1), 167–175.

[186] S. Wiggins (1990), *Introduction to applied nonlinear dynamical systems and chaos*, Springer-Verlag, Berlin.

[187] A. Wolf, J. Swift, H. Swinney, and J. Vastano (1985), *Determining Lyapunov exponents from a time series*, Physica D **16**, 285–317.

[188] J. Yorke (1989), *Dynamics: A program for IBM PC clones*, University of Maryland, (AIP), New York, NY.